# Novel formulation principles for bioavailability enhancement of poorly water-soluble and poorly permeable drugs

Dissertation zur Erlangung des naturwissenschaftlichen Doktorgrades der

Julius-Maximilians-Universität Würzburg

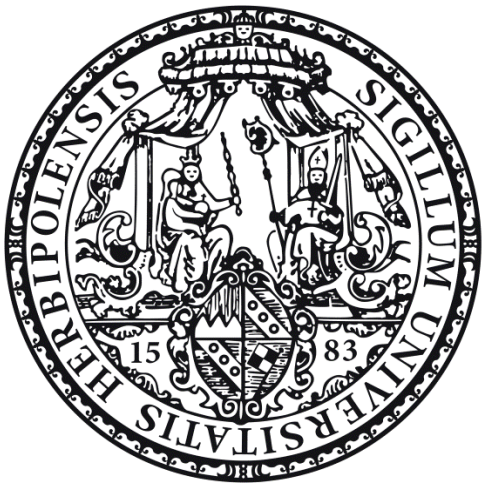


vorgelegt von

**Nina Kristin Petra Schüßler**

aus Erlenbach am Main

Würzburg 2017

Eingereicht bei der Fakultät für Chemie und Pharmazie am

_____

Gutachter der schriftlichen Arbeit

1. Gutachter: _____

2. Gutachter: _____

Prüfer des öffentlichen Promotionskolloquiums

1. Prüfer: _____

2. Prüfer: _____

3. Prüfer: _____

Datum des öffentlichen Promotionskolloquiums

_____

Doktorurkunde ausgehändigt am

_____

Die vorliegende Arbeit wurde in der Zeit von November 2012 bis Dezember 2017

am Institut für Pharmazie und Lebensmittelchemie

der Bayerischen Julius-Maximilians-Universität Würzburg unter der Anleitung von

**Herrn Prof. Dr. Dr. Lorenz Meinel**

mit finanzieller Unterstützung der bayerischen Forschungsstiftung

und der ACC GmbH Analytical Clinical Concepts angefertigt.

Die Wissenschaft fängt eigentlich erst da an interessant zu werden, wo sie aufhört.

*Justus von Liebig (1803-1873)*

# TABLE OF CONTENTS

# SUMMARY

Since four decades, high-throughput screenings have been conducted in drug discovery, fuelling the identification of potential new drug candidates. This approach, however, often promotes the detection of compounds with undesired physico-chemical properties like poor aqueous solubility or low membrane permeability. Indeed, dissolution and absorption of a drug are prerequisites for systemic exposure and therapeutic effects. Therefore, innovative strategies to optimize unfavourable performance of new drug candidates are in great demand in order to increase drug concentrations at the site of action whilst simultaneously reducing drug variability.

In **chapter I** of this research work, hydrophobic ion pairing (HIP) is discussed as a promising strategy to improve the bioavailability of BCS class III compounds, which have high aqueous solubility and low permeability. The review points out the limitations of poorly absorbable drugs and details the approach of pairing these APIs with hydrophobic counterions. Apart from the motivation to tailor physico-chemical, biopharmaceutical and toxicological properties of BCS class III compounds, the hydrophobic ion pairing facilitates their formulation into drug delivery systems. Besides advantageous effects, disadvantages of the ion pair formation, such as the decreased aqueous solubility of the ions pair, are critically outlined. Finally, the review covers an overview of non-invasive administration routes permitted after ion pair formation, including oral/enteral, buccal, nasal, ocular and transdermal drug administration. Overall, the HIP approach offers substantial benefits regarding the bioavailability enhancement of BCS class III compounds.

**Chapter II** concerns GHQ168 developed by Holzgrabe et al., a BCS class II compound characterized by low aqueous solubility and high permeability. GHQ168 was developed for the treatment of human African trypanosomiasis (HAT), a tropical disease for which novel active compounds are urgently needed. This lead compound was found to be very active against *trypanosoma brucei brucei* and *trypanosoma brucei rhodesiense* in cell

culture assays, however, the low aqueous solubility prevented further preclinical development. To target this drawback, two different approaches were selected, including (I) the chemical modification and (II) the spray drying of GHQ168. The newly synthesized set of derivatives as well as the spray dried GHQ168 were subjected to a physico-chemical and microbiological characterization. It turned out that both approaches successfully improved aqueous solubility, however, for the derivatives of GHQ168 at the expense of activity. Furthermore, the pharmacokinetic parameters of GHQ168 and of the most active derivatives, GHQ242 and GHQ243, were evaluated. Elimination half-lives between 1.5 to 3.5 h after intraperitoneal administration and modest to strong serum albumin binding for GHQ243 (45%) and GHQ168 (80%) and very high binding (> 99%) for GHQ242 were detected. The spray dried formulation of GHQ168, as well as GHQ242 and GHQ243 were investigated in two *in vivo* studies in mice infected with *t. b. rhodesiense* (STIB900), referred to as (I) stringent model and (II) early-treatment model. In the stringent model (2 applications/day on day 3-6 after infection) the mean survival duration (MSD) of mice treated with spray dried GHQ168 exceeded the MSD of the untreated control group (17 days versus 9 days), a difference that was statistically significant. In contrast, no statistical difference was observed for GHQ242 (14 days) and GHQ243 (12 days). GHQ168 was further assessed in the early-treatment model (2 applications/day on day 1-4 after infection) and again a statistically significant improvement of MSD (32 days (end of observation period) versus 7 days) was observed. Finally, exciting antitrypanosomal efficacy for the spray dried formulation of GHQ168 was demonstrated.

NADPH oxidases (NOX) were found to be the main source of endothelial reactive oxygen species (ROS) formation. **Chapter III** reports on the formulation studies on triazolopyrimidine derivatives from the VAS library, a set of NADPH oxidase inhibitors. These were developed for the treatment of elevated ROS levels, which contribute to the development of cardiovascular diseases. Although *in vitro* results from numerous studies indicated promising efficacy and selectivity for the VAS-compounds, the low water

solubility impeded the *in vivo* translation and further preclinical development. For this reason, three derivatives, VAS2870, VAS3947, and VAS4024 were physico-chemically characterized and VAS3947, the most soluble compound, was selected for further formulation studies. These approaches included (I) spray drying, (II) microemulsification and (III) complexation with cyclodextrins in order to develop formulations for oral and parenteral application. Solubility improvement of VAS3947 was successfully demonstrated for all preparations as expressed by supersaturation ratios in comparison to the solubility of the unformulated compound. For seven spray dried formulations, the ratio ranged from 3-9, and the ratio for four microemulsions was 8-19 after 120 min, respectively. The six cyclodextrin formulations achieved the highest supersaturation ratio between 3 and 174 after 20 hours. NMR measurements elucidated the inclusion of VAS3947 within the CD's cavity as well as the interaction with its outer surface. Ultimately, NOX inhibitors were opened for oral and parenteral administration for the first time.

After successful solubility improvement of VAS3947, further investigations towards *in vivo* studies were conducted including stability studies with a focus on stability in solution and in plasma as presented in **chapter IV**. Furthermore, permeability and cytotoxicity assays were performed for the first time. It turned out that VAS3947 was instable in buffer and when exposed to light. Moreover, the compound showed decomposition in the presence of mouse microsomes and in human plasma. The VAS compounds contain an oxazol moiety linked to the triazolopyrimidine skeleton via a thioether. This structural element is responsible for the efficacy of the compound class, however it is susceptible to hydrolysis and to further degradation reactions. Moreover, VAS3947 harmed membrane integrity in the cell permeability assays and cytotoxicity investigations in HEK-293 and HEP-G2 cells revealed $IC_{50}$ values in the same concentration range as reported for efficacy assays. Summarized, it was demonstrated that substances from the VAS library were no appropriate model compounds for ROS investigations nor suitable candidates for further preclinical development.

# ZUSAMMENFASSUNG

Seit vier Jahrzehnten werden Hochdurchsatz-Screenings in der Arzneimittelforschung durchgeführt, was die Erkennung von potentiellen Wirkstoffkandidaten vorantreibt. Diese Vorgehensweise begünstigt jedoch häufig die Identifizierung von Substanzen mit unerwünschten physikochemischen Eigenschaften wie geringer Wasserlöslichkeit oder geringer Membranpermeabilität. Der Bioverfügbarkeitstheorie zufolge sind die Auflösung und die Absorption eines Arzneistoffs Voraussetzung für die systemische Verfügbarkeit und die therapeutische Wirkung. Daher werden innovative Strategien, die die ungünstigen Eigenschaften neuer Wirkstoffkandidaten optimieren, dringend benötigt, um die Arzneistoffkonzentration am Wirkort zu erhöhen und gleichzeitig Wirkstoffschwankungen zu reduzieren.

In **Kapitel I** dieser Forschungsarbeit wird die hydrophobe Ionenpaarbildung als vielversprechende Strategie diskutiert, um die Bioverfügbarkeit von BCS Klasse III Substanzen zu verbessern, die sich durch hohe Wasserlöslichkeit und geringe Permeabilität auszeichnen. Der Review zeigt die Grenzen von schlecht absorbierbaren Arzneistoffen auf und stellt den Ansatz vor, diese mit hydrophoben Gegenionen zu kombinieren. Abgesehen von der Motivation, die physikochemischen, biopharmazeutischen und toxikologischen Eigenschaften von BCS Klasse III Substanzen positiv zu beeinflussen, wird die Formulierung der hydrophoben Ionenpaare in Trägersysteme erleichtert. Neben den Vorteilen werden auch die Nachteile der hydrophoben Ionenpaarbildung, wie beispielsweise die geringere Wasserlöslichkeit der Ionenpaare, kritisch dargestellt. Abschließend gibt der Review eine Übersicht über die verschiedenen nicht-invasiven Applikationsrouten, die nach hydrophober Ionenpaarbildung realisierbar sind, was die orale/enterale, bukkale, nasale, okulare und transdermale Arzneistoffgabe umfasst. Insgesamt bietet dieser Formulierungsansatz wesentliche Vorteile im Hinblick auf die Verbesserung der Bioverfügbarkeit von BCS Klasse III Substanzen.

**Kapitel II** befasst sich mit GHQ168, entwickelt von Holzgrabe et al., einer BCS Klasse II Substanz mit geringer Wasserlöslichkeit und hoher Permeabilität. GHQ168 wurde zur Behandlung der afrikanischen Schlafkrankheit entwickelt, einer tropischen Erkrankung, für die neue Arzneistoffe dringend benötigt werden. Diese Leitsubstanz bewies in Zellkulturversuchen sehr hohe Aktivität gegen *Trypanosoma brucei brucei* und *Trypanosoma brucei rhodesiense*, die geringe Wasserlöslichkeit verhinderte jedoch die weitere präklinische Entwicklung. Um diese Herausforderung anzugehen, wurden zwei verschiedene Ansätze gewählt, zum einen (I) die chemische Modifikation und zum anderen (II) die Sprühtrocknung von GHQ168. Die neu synthetisierten Derivate und das sprühgetrocknete GHQ168 wurden physikochemisch und mikrobiologisch charakterisiert. Beide Ansätze verbesserten erfolgreich die Wasserlöslichkeit, im Fall der Derivate von GHQ168 jedoch zu Lasten der Aktivität. Weiterhin wurden die pharmakokinetischen Eigenschaften von GHQ168 und den aktivsten Derivaten, GHQ242 und GHQ243, untersucht. Nach intraperitonealer Applikation resultierten Halbwertszeiten zwischen 1.5 und 3.5 Stunden und eine mittlere bis hohe Plasmaproteinbindung für GHQ243 (45%) und GHQ168 (80%) und eine sehr hohe Plasmaproteinbindung für GHQ242 (> 99%). Die sprühgetrocknete Formulierung von GHQ168 sowie GHQ242 und GHQ243 wurden in zwei *in vivo* Studien in Mäusen, die mit *t. b. rhodesiense* (STIB900) infiziert waren, untersucht, die Modelle werden als (I) *stringent model* und (II) *early-treatment model* bezeichnet. Im *stringent model* (2x tägliche Gabe an Tag 3-6 nach Infektion) war die durchschnittliche Überlebensdauer von Mäusen, die mit sprühgetrocknetem GHQ168 behandelt worden waren, statistisch signifikant höher als die der unbehandelten Kontrollgruppe (17 gegenüber 9 Tagen). Im Gegensatz hierzu wurde kein statistisch signifikanter Unterschied für GHQ242 (14 Tage) und GHQ243 (12 Tage) festgestellt. GHQ168 wurde im *early-treatment model* (2x tägliche Gabe an Tag 1-4 nach Infektion) weiter untersucht und erneut wurde eine statistisch signifikante Verbesserung der durchschnittlichen Überlebensdauer (32 Tage (Ende der Beobachtungsphase) gegenüber

7 Tagen) bewiesen. Letztendlich konnte für die sprühgetrocknete Formulierung von GHQ168 eine erstaunliche Aktivität gegenüber Trypanosomen gezeigt werden.

NADPH-Oxidasen (NOX) wurden als Hauptproduzenten von endothelialem reaktivem Sauerstoff erkannt. **Kapitel III** befasst sich mit Formulierungsstudien von Triazolopyrimidinderivaten aus der VAS-Substanzbibliothek, einer Reihe von NADPH-Oxidase-Inhibitoren. Diese Substanzen wurden zur Behandlung erhöhter reaktiver Sauerstoffspezies Werte entwickelt, denn diese tragen zur Entstehung von kardiovaskulären Erkrankungen bei. Obwohl die *in vitro* Ergebnisse zahlreicher Studien auf die vielversprechende Wirksamkeit und Selektivität der VAS-Substanzen hinweisen, verhinderte die geringe Wasserlöslichkeit den Übertrag auf *in vivo* Studien sowie die weitere präklinische Entwicklung. Daher wurden drei Derivate, VAS2870, VAS3947 und VAS4024, physikochemisch charakterisiert und VAS3947, die wasserlöslichste Substanz, wurde für weitere Formulierungsentwicklungen ausgewählt. Die Formulierungsansätze umfassten (I) die Sprühtrocknung, (II) die Herstellung von Mikroemulsionen und (III) die Komplexierung mit Cyclodextrinen, um Formulierungen für die orale und parenterale Verabreichung zu entwickeln. Die Löslichkeitsverbesserung von VAS3947 konnte für alle Ansätze erfolgreich gezeigt werden und wurde als Übersättigungsrate im Vergleich zur Löslichkeit der unformulierten Substanz dargestellt. Für sieben sprühgetrocknete Formulierungen und für vier Mikroemulsionen ergab sich eine Übersättigungsrate von 3-9, beziehungsweise von 8-19 nach 120 Minuten. Die sechs Cyclodextrin-Formulierungen erreichten mit 3-174 nach 20 Stunden die höchste Übersättigungsrate. Der Einschluss von VAS3947 in die Kavität der Cyclodextrine sowie die Interaktion mit deren Außenseite wurde mittels NMR aufgeklärt. Schließlich wurde erstmals die Möglichkeit der oralen und parenteralen Gabe der NOX-Inhibitoren eröffnet.

Nach erfolgreicher Löslichkeitsverbesserung von VAS3947 wurden weitere Untersuchungen mit dem Ziel von *in vivo* Studien durchgeführt, was Stabilitätsuntersuchungen mit besonderem Schwerpunkt auf Stabilität in Lösung und in

Plasma einschließt, wie im **Kapitel IV** aufgezeigt. Weiterhin wurden erstmals Permeabilitäts- und Zytotoxizitätsstudien durchgeführt. Es stellte sich heraus, dass VAS3947 in Puffer und bei Lichtexposition instabil war. Zudem wurde die Substanz in Gegenwart von Maus-Mikrosomen und in menschlichem Plasma abgebaut. Die VAS-Substanzen enthalten eine Oxazol-Ringstruktur, die über einen Thioether mit dem Triazolopyrimidin-Gerüst verbunden ist. Diese Strukturelemente sind für die Wirksamkeit der Substanzklasse verantwortlich, sind jedoch auch hydrolyseempfindlich und anfällig für weitere Abbaureaktionen. Zudem schädigte VAS3947 die Membranintegrität in den Permeabilitätsversuchen und die Zytotoxizitätsuntersuchungen in HEK-293 und HEP-G2 Zellen ergaben $IC_{50}$-Werte im gleichen Konzentrationsbereich wie in Aktivitätsuntersuchungen berichtet. Zusammenfassend wurde aufgezeigt, dass die VAS-Substanzen weder ein geeignetes Modell für die Untersuchung reaktiver Sauerstoffspezies sind, noch geeignet für die weitere präklinische Entwicklung.

# CHAPTER I

## HYDROPHOBIC ION PAIRING TO IMPROVE BIOAVAILABILITY OF BCS CLASS III COMPOUNDS

Nina Schüßler[1], Javier O. Morales[2], Lorenz Meinel[1,*]

[1]University of Würzburg, Institut für Pharmazie und Lebensmittelchemie, Am Hubland, DE-97074, Würzburg, Germany

[2]Department of Pharmaceutical Science and Technology, School of Chemical and Pharmaceutical Sciences, University of Chile, Santiago 8380494, Chile

*Unpublished manuscript.*

## Abstract

According to the biopharmaceutical classification system, BCS class III substances are characterized by high aqueous solubility and low permeability with the transport across membranes being the rate controlling step of the drug absorption process. Ion pair formation between BCS class III substances and large lipophilic counterions was reported to overcome poor absorption through masking polar surface of the drug by the counterion. Besides increased membrane transport, the ion pairing with suitable counterions allows for tailored physico-chemical, biopharmaceutical and toxicological properties of an API or facilitates the formulation into drug delivery systems. This review summarizes strategies for ion pairing and their application for bioavailability improvement of BCS class III substances. It critically assesses advantages and disadvantages with a focus on non-invasive delivery through the oral/enteral, buccal, nasal, ocular or transdermal administration route.

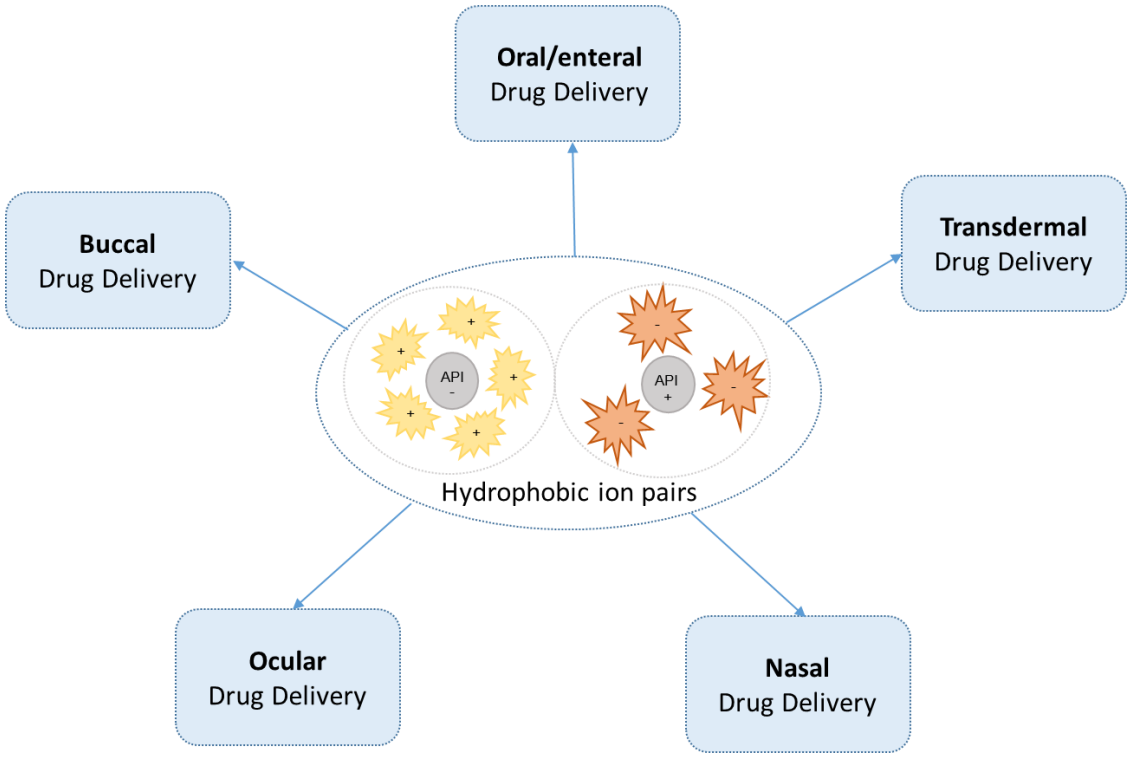

# 1. Introduction

Since the early 1980s, combinatorial chemistry and high throughout screenings have identified an increasing number of drug candidates with undesired physico-chemical properties, such as low permeability across physiological membranes or low aqueous solubility [1]. Permeability and solubility of a drug are key parameters in determining the rate and extent of drug absorption and are therefore directly related to the compound's bioavailability [2], which is why both parameters are reflected within the biopharmaceutical classification system (BCS). BCS categorizes pharmaceutical compounds into four different groups (class I – IV) [3-5]. Drugs with high solubility (i.e. the highest dose strength is soluble in < 250 mL of aqueous media over the pH range of 1-6.8 [6]) in combination with low permeability (i.e. the extent of absorption in humans is determined to be < 85% of an administered dose, based on mass-balance or in comparison to an intravenous reference dose [6]) are classified into BCS class III. The often hydrophilic or ionic nature of BCS class III compounds is responsible for their favorable aqueous solubility but potentially jeopardizes the transport across lipophilic biological membranes [7]. Strategies addressing these challenges are needed to open or improve therapies with BCS III compounds [8]. Literature reports several successful approaches for increasing the permeability of hydrophilic drugs, such as chemical modifications by synthesizing prodrugs [9-11], resulting in novel chemical entities driving a train of complex and costly activities including novel safety assessments. Other studies focus on technological strategies through which the API structure is maintained and uptake is facilitated e.g. by supplemented absorption enhancers [12-14]. Another focus is on impacting influx and efflux transporters [15, 16] or enzymes [17] for the improvement of gastrointestinal absorption. Along these lines, "ion pairing" of hydrophilic drugs with hydrophobic counterions - the topic of this review article - has been attracting interest for more than four decades in pharmaceutical sciences [18-21]. The term "hydrophobic ion pairing" (HIP) was introduced in 1998 by Meyer and Manning [22] and describes complexes of

oppositely charged ions, i.e. a positively or negatively charged, hydrophilic drug molecule coupled to a (often bulky) hydrophobic counterion of opposite charge. Drug and counterion are associated by hydrophobic and electrostatic interactions. To the outside, the ion pair acts as a neutral or nearly neutral entity with increased lipophilicity as compared to the free drug molecule, which is easily assessed in vitro by the determination of partitioning coefficients between an aqueous and a lipid phase [23-26] or in cell culture permeability assays [27, 28]. These investigations serve as predictive data for the API transport across natural barriers including eukaryotic cell membranes or bacterial surfaces.

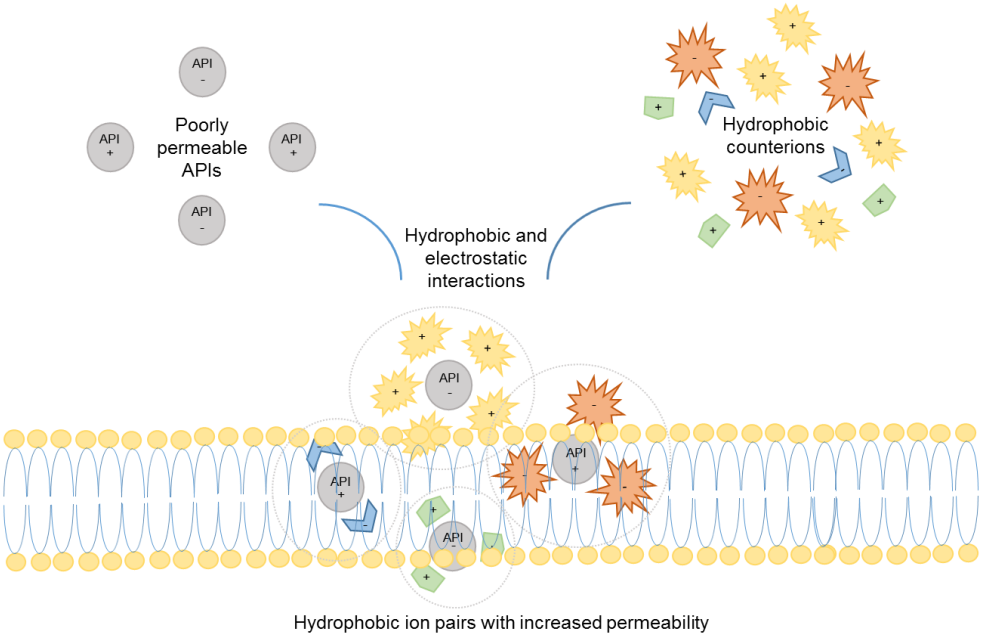


**Figure 1**: Mechanism of the hydrophobic ion pairing.

This review reports on ion pair formation relating to poorly permeable BCS class III substances and critically discusses the advantages and drawbacks of this formulation strategy with a focus on the oral/enteral, buccal, nasal, ocular, and transdermal drug delivery.

## 2. Ion pair formation of BCS class III compounds

Systemic absorption of a compound is a prerequisite for its systemic effects. Many drugs, however, have poor membrane permeability at physiological pH frequently attributed to their charged nature and high polarity thereby reducing their bioavailability while driving inter-subject variability [2, 29]. For this reason, the administration of BCS class III compounds is often restricted to routes that avoid resorption processes (i.e. the parenteral route), or to the administration at the target site directly (i.e. intra-cardial, intrathecal), which is more costly, inconvenient, and risky as compared to non-invasive administration [30, 31]. The motivation for hydrophobic ion pair formation of BCS class III compounds is, therefore, based on the maximization of bioavailability. Up to date, numerous studies demonstrated the usefulness of lipophilicity enhancement for the purpose of higher drug transport across biological membranes [32] in vitro and in vivo as well for eukaryotic [33-36] and for prokaryotic cells [37, 38]. It turned out that efficiently designed ion pairs of BCS class III compounds and counterions can increase the drug concentration at the site of action, but overall, it has to be critically stated that promising in vitro results do not necessarily reflect successful in vivo outcomes. Moreover, the impact of successful ion pairing is beyond uptake considerations, as the release from formulations is impacted [36], or the ion pair is affecting enterohepatic circulation as compared to the free drug or its conventional salts [30]. Interestingly, other studies reported systemic effects of ion pairing in reduced binding of drugs to plasma lipoproteins suggesting incomplete dissociation even in circulation [33]. For example, an improvement of pharmacokinetic (PK) parameters was demonstrated after intravenous administration in mice for doxorubicin-cholesteryl hemisuccinate ion pairs that were incorporated into liposomes [33] as well as for doxorubicin oleic acid nanoparticles [34].

The incorporation of BCS class III compounds into lipid drug delivery systems is challenged by their hydrophilic nature and low solubility in the lipid layer resulting in low drug loading, stability challenges during manufacture and/or storage and uncontrolled

release after administration [39, 40]. The amphiphilic or neutral surface of ion pairs, however, may facilitate the formulation of polar APIs into liposomes [33], nanoparticles [30, 31, 41-45], nanoemulsions [34], microparticles [46] solid lipospheres [47] or self-emulsifying drug delivery systems (SEDDS) [24, 39] and building off the targeted lining of polar API structures by the counterion thereby hydrophobizing the overall ion pair. Consequently, drug loading and entrapment efficiency of formerly hydrophilic drugs are optimized for their hydrophobic ion pairs into lipid formulations [36, 38, 48, 49]. As the chemical structure of the drug is not altered by the ion pairing approach, it may be expected that toxicity remains unchanged. It was reported, however, that the possibility of embedding ion pairs into lipid drug delivery systems indeed affected their toxicological profile. For example, doxorubicin accumulation within the heart, kidney and lung following intravenous injection of ion pair complexes was improved as compared to the free drug [34, 43].

One exciting emerging field for hydrophobic ion pairing are biologicals in an effort to open the oral route for their delivery by deploying protecting formulations after the API was paired with hydrophobic counterions [50-54]. For example, insulin ion pairs were incorporated into nanoparticles and self-nanoemulsifying drug delivery systems, thereby protecting the peptide from degradation [30, 31, 55]. Low molecular weight heparins were protected from acidic conditions by ion pairing of the polyanion with dodecylamine and subsequent incorporation of the complex into SEDDS [39]. The incorporation of the hydrophobic ion pair of desmopressin/sodium docusate into SEDDS successfully preserved desmopressin from degradation in the presence of glutathione and displayed protective effects against α-chymotrypsin [24]. Similarly, the acylation of octreotide under acidic conditions was less than 7% after 55 days due to the masking of the amine groups with dextran sulfate A and B and subsequent embedding into PLGA nanoparticles as compared to about 60% acylated octreotide for the marketed Sandostatin LAR® depot [46]. In conclusion, hydrophobic ion pairing is a beneficial strategy to retain protein

stability during delivery from formulations. Moreover, the ion pairing approach offers an uncomplicated and cost effective strategy for the lipophilicity enhancement of BCS class III substances. The properties and the formation efficacy are tunable through the counterion structure, e.g. by its aliphatic chain length (whereas longer chains lead to higher lipophilicity), or its polar/apolar characteristics and by the drug/counterion ratio [24, 25, 56-58].

Aside these advantages, hydrophobic ion pairing comes along with some challenges one of which is decreased aqueous solubility [25, 30, 36, 37, 56]. Moreover, the altered physico-chemical features can influence the stability or pharmacokinetics (plasma protein binding, distribution, elimination) of a drug and ultimately its bioequivalence. Occasionally, ion pair complexes fail to facilitate permeability resulting in loss of activity. This has been attributed to the (often bulky) structure of the counterions and increased hydrodynamic diameter of the resulting ion pairs. Thereby, the increase in lipophilicity is over-compensated by the increase in size and reducing the ion pair's bioavailability. Similarly, it was hypothesized that large counterions, such as quaternary ammonium cations for instance, are sterically or thermodynamically hindered and thus lower attractive forces are present between the drug and the counterion [58, 59]. Possibly, suboptimal counterion concentrations are responsible for the observed lack of absorption [60]. Nevertheless, these disadvantageous features are tunable by tailored counterion design [61] and as recently demonstrated for ionic liquids [62]. These examples illustrate the need for tailored counterion design for hydrophobic ion pairing with the ultimate goal to improve bioavailability.

Safety is another reason for careful counterion selection [63]. The list of "generally recognized as safe" (GRAS) substances provided by the FDA may guide formulation scientists in selection, as introducing novel structures triggers regulatory constraints. In general, natural derived oils and triglycerides are suitable as non-toxic ion pairing reagents whereas surfactants like sodium dodecyl sulfate (SDS) can cause detrimental

effects due to various membrane interactions [28]. In this regard, the viability of Caco-2 cells was significantly reduced after one and four hours of incubation with enoxaparin-dodecylamine, which was linked to counterion toxicity [39] and other studies demonstrated counterions' dose dependent toxicity [24, 64]. Ultimately, the intended administration route of the final formulation has to be taken into account as certain counterions are not qualified for some administration routes [65].

## 3. Non-invasive administration of hydrophobic ion pairs of BCS class III compounds

### 3.1. Oral/enteral drug administration

The oral route is the most common route for drug administration and preferred by the patients. As mentioned above, promising results were reported after oral administration of an insulin-sodium deoxycholate ion pair [30, 31]. The subsequent encapsulation of the nanoparticles into hydroxypropyl methyl cellulose phthalate (HP55) further lowered the blood glucose level and raised the relative bioavailability, which was attributed to the absorption enhancing features of the ion pair [31]. Similarly, the enoxaparin dodecylamine ion pair incorporated into SEDDS reached the blood compartment after oral administration in rats, whereas the aqueous enoxaparin solution failed. Firstly, the protein was prevented from degradation in the stomach and secondly, it successfully crossed the gastrointestinal barrier [39]. Recently, two ion pairs consisting of atenolol/brilliant blue and atenolol/bromophenol blue were studied for colon permeability in rats. Both formulations had improved permeability values (Papp) as compared to atenolol alone [26]. In another study, the effect of ion pair formation between trospium chloride and the counterions glycochenodeoxycholate (GCDC) and taurodeoxycholate (TDOC) was investigated ex vivo using rat jejunum in the Ussing chamber model. It was demonstrated that bile salt concentrations of 0.5 M lead to a permeation increase of the API (factor 1.5 and 1.25,

respectively), suggesting higher passive diffusion due to the ion pair formation. However, higher concentrations of GCDC and TDOC (2 mM to 8 mM) did not further improve the permeation of trospium chloride, which was explained by the almost complete masking of API charges by the counterions at the concentration 0.5 M already [23]. The poorly permeable antiviral agents guanidino oseltamivir (GO) and zanamivir heptyl ester (ZHE) were ion paired with 1-hydroxy-2-naphthoic acid (HNAP) and investigated in the rat jejunum perfusion assay. No significant improvement of Peff was observed for the GO ion pair, whereas the ZHE ion pair resulted in significantly higher Peff for 4 mM and 10 mM HNAP [66]. These findings were attributed to the higher association constant of ZHE-HNAP as compared to GO-HNAP, that makes the ion pair more resistant towards dissociation. A PK/PD study investigating an insulin-deoxycholyl-L-lysyl-methylester ion pair revealed equal PK profiles after intrajejunal administration in rats as compared to the subcutaneous administration of insulin, advancing further investigations towards the oral delivery of insulin [67].

### 3.2. Buccal drug administration

Buccal administration is an emergent alternative to intravenous injection as well as to oral application, especially for peptides and proteins or other drugs that undergo degradation or suffer from first pass effects [68-70]. This stratified epithelium does not present tight junctions and thus ion pair permeability would be largely dependent on its physico-chemical properties and interactions through the lipid-rich interstitium and lipid cell membranes [71]. To date, however, limited data is available on the buccal administration of ion pairs of BCS class III substances. Only one study reports the ion pairing of insulin with basic amino acids (arginine, histidine, lysine), acidic amino acids (glutamic acid, aspartic acid) and sodium deoxycholate (SDC) [64]. Besides arginine, any amino acid (concentration 10 µg/ml) significantly enhanced insulin permeability across TR146 buccal cells while simultaneously being non-toxic as assessed by TEER values and MTT assay.

At 200 µg/ml, histidine and lysine ion pairs induced disruptive effects on the cell layer, whereas the acidic amino acids maintained cell integrity. Contrary to these findings, none of the SDC concentrations was effective and safe at the same time. Additionally, the authors confirmed the active transport for the neutral insulin-glutamic acid ion pair.

### 3.3. Nasal drug administration

Due to the high porosity of the nasal membrane and the low enzymatic concentrations [72, 73] the nasal cavity is particularly suitable for the delivery of BCS class III proteins. Accordingly, the attempt to shield the anionic charge of enoxaparin with the help of 25 kDa, 750 kDa and 1000 kDa polyethylenimines (PEI) enhanced nasal absorption of enoxaparin [61]. Comparably, the AUC0-480 min and the absolute bioavailability were higher for all ion pair formulations as compared to the administration of pure enoxaparin. In fact, there was no concentration dependent increase in the absorption rate of drug with increasing PEI concentrations, possibly due to self-aggregation of the counterion resulting in greater particle sizes or related to unfavorable drug/counterion ratios. Similar results were published for ion pairs of methotrexate with increasing ratios of L-arginine after in vitro permeation experiments through freshly excised nasal mucosa from rabbits [74]. The authors attributed the absorption plateau for arginine ratios ≥ 1:3 to low thermodynamic driving forces in the permeation system. Methotrexate is classified into BCS class III [3], however, it is important to mention that active transport mechanisms contribute to its absorption, which might influence the results of the ion pairing study.

### 3.4. Ocular drug administration

Due to the physiological structure of the eye, drugs should exhibit both, hydrophilic as well as lipophilic properties [75, 76]. Therefore, ion pairing approaches have been considered for ocular drug administration of hydrophobic drugs [77, 78], as amphiphilic entities of drug and counterion are predestined to reach the anterior and posterior segments of the eye to elicit therapeutic responses. For example, ocular administration of a tobramycin-

hexadecylphosphate ion pair (1:2) embedded in solid lipid nanoparticles permitted the penetration of tobramycin into both vitreous and aqueous humor in rabbits [79]. In contrast, any tobramycin was detected in the vitreous humor after ocular administration of the reference product Tobral® eye drops and fivefold lower concentrations were found in the aqueous humor after three hours. Comparable observations were made in the vitreous and aqueous humor after intravenous administration of the ion pair as compared to Tobramycin solution. The ocular administration of carteolol ion paired with sorbate caused a 2.6 times higher AUC in the aqueous humor as compared to an equally concentrated solution of the pure compound [57]. In contrast, there was no difference in the plasma levels, suggesting no systemic absorption improvement by the ion pair.

### 3.5. Transdermal drug administration

Human and animal skin acts as a selective barrier towards the permeation of substances. The immanent lipophilicity of the outer skin layers exceedingly reduces the penetration of charged and polar compounds like BCS class III substances. Instead, the skin mainly permits the absorption of uncharged molecules exhibiting favorable hydrophilic/lipophilic balance, meaning aqueous as well as lipid solubility [80, 81] and requires a molecular weight < 500 Da [82, 83]. Ion pair complexes partition into the lipid stratum corneum as neutral entity and subsequently dissociate into charged species in aqueous environment [84]. Accordingly, salicylate complexed with different alkylamines (5-9 C-atoms) was administered on rat and snake skin and data suggested the existence of ion pairs as explanation for successful permeation increase [85]. This was contrary to the observations made by another in vitro study investigating salicylate complexed with alkylamines (1-12 C-atoms) through human epidermis, as slightly lower permeability coefficients as compared to the pure salicylate were found [60]. The later epidermal application of the respective ion pairs in rats, however, clearly increased the recovery of salicylate in dermis, subcutaneous tissue and top muscles as compared to pure salicylate and the respective

sodium salt, which was attributed to lower clearance rates of the more lipophilic pairs from these tissues [60]. Likewise, corresponding plasma concentration levels increased more rapidly after ion pair administration and remained constant over 8 hours, suggesting equilibrium between plasma and tissue concentrations. An investigation studying ion pairs of lignocaine with different counterions showed an increased apparent partition coefficient, however, the steady state flux through a polydimethylsiloxane (PDMS) membrane model as well as through human epidermis was not significantly improved [86]. In this study, mainly small counterions (bromide, nitrate, sulfonate, and benzoate) with low lipophilicity were investigated, suggesting only weak ability to promote the absorption of lignocaine.

## 4. Conclusion

The number of pharmaceutical compounds with unfavorable properties, such as poor intestinal absorption, has risen in recent decades and is challenging pharmacists to date. Traditional formulation approaches often fail to transport these drugs to the target site in a suitable concentration, or require uncomfortable administration routes. Therefore, the development of novel drug delivery options is of crucial importance to overcome the bioavailability limitations of pharmacologically effective agents. The ion pairing of new drug candidates or marketed drugs with hydrophobic counterions is widely used in pharmaceutical technology. To date, numerous studies reported the beneficial effects of the ion pairing approach, rendering this strategy a valuable tool to optimize physico-chemical, biopharmaceutical, pharmacokinetic and toxicological drug properties of BCS class III compounds. Embedding of the ion pairs into lipid drug delivery systems further supports the optimization of bioavailability and enhances therapeutic efficacy by protecting the drugs against enzymatic or hydrolytic degradation and offering controlled release kinetics. As pointed out, ion pairing is a versatile drug development strategy that

should be considered when formulating BCS class III substances for oral/enteral buccal, nasal, ocular, or transdermal application.

## Acknowledgements

We thank the Bayerische Forschungsstiftung (grant „Antibiotisch-osmoprotektive Ionische Flüssigkeiten“; AZ-1204-16) for financial support.

## References

[1] R.O. Williams III, A.B. Watts, D.A. Miller, Formulating Poorly Water Soluble Drugs Springer-Verlag, 2012.

[2] G.L. Amidon, H. Lennernas, V.P. Shah, J.R. Crison, A theoretical basis for a biopharmaceutic drug classification: the correlation of *in vitro* drug product dissolution and *in vivo* bioavailability, Pharm Res, 12 (1995) 413-420.

[3] M. Lindenberg, S. Kopp, J.B. Dressman, Classification of orally administered drugs on the World Health Organization Model list of Essential Medicines according to the biopharmaceutics classification system, Eur J Pharm Biopharm, 58 (2004) 265-278.

[4] N.A. Kasim, M. Whitehouse, C. Ramachandran, M. Bermejo, H. Lennernas, A.S. Hussain, H.E. Junginger, S.A. Stavchansky, K.K. Midha, V.P. Shah, G.L. Amidon, Molecular properties of WHO essential drugs and provisional biopharmaceutical classification, Mol Pharm, 1 (2004) 85-96.

[5] T. Takagi, C. Ramachandran, M. Bermejo, S. Yamashita, L.X. Yu, G.L. Amidon, A provisional biopharmaceutical classification of the top 200 oral drug products in the United States, Great Britain, Spain, and Japan, Mol Pharm, 3 (2006) 631-643.

[6] Waiver of *In Vivo* Bioavailability and Bioequivalence Studies for Immediate-Release Solid Oral Dosage Forms Based on a Biopharmaceutics Classification System, Food and Drug Administration (2015).

[7] M.N. Martinez, G.L. Amidon, A mechanistic approach to understanding the factors affecting drug absorption: a review of fundamentals, J Clin Pharmacol, 42 (2002) 620-643.

[8] V.S. Dave, D. Gupta, M. Yu, P. Nguyen, S. Varghese Gupta, Current and evolving approaches for improving the oral permeability of BCS Class III or analogous molecules, Drug Dev Ind Pharm, 43 (2017) 177-189.

[9] V. Stella, R. Borchardt, M. Hageman, R. Oliyai, H. Maag, J. Tilley, Prodrugs: challenges and rewards, Springer-Verlag, 2007.

[10] H.K. Han, G.L. Amidon, Targeted prodrug design to optimize drug delivery, AAPS PharmSci, 2 (2000) 48-58.

[11] P. Ettmayer, G.L. Amidon, B. Clement, B. Testa, Lessons learned from marketed and investigational prodrugs, J Med Chem, 47 (2004) 2393-2404.

[12] B.J. Aungst, Absorption enhancers: applications and advances, AAPS J, 14 (2012) 10-18.

[13] E. Scott Swenson, W.J. Curatolo, Intestinal permeability enhancement for proteins, peptides and other polar drugs: mechanisms and potential toxicity, Advanced Drug Delivery Reviews, 8 (1992) 39-92.

[14] C. Yewale, S. Patil, A. Kolate, G. Kore, A. Misra, Oral Absorption Promoters: Opportunities, Issues, and Challenges, Crit Rev Ther Drug Carrier Syst, 32 (2015) 363-387.

[15] M.V. Varma, C.M. Ambler, M. Ullah, C.J. Rotter, H. Sun, J. Litchfield, K.S. Fenner, A.F. El-Kattan, Targeting intestinal transporters for optimizing oral drug absorption, Curr Drug Metab, 11 (2010) 730-742.

[16] A. Dahan, G.L. Amidon, Segmental dependent transport of low permeability compounds along the small intestine due to P-glycoprotein: the role of efflux transport in the oral absorption of BCS class III drugs, Mol Pharm, 6 (2009) 19-28.

[17] D. Fleisher, B.H. Stewart, G.L. Amidon, Design of prodrugs for improved gastrointestinal absorption by intestinal enzyme targeting, Methods Enzymol, 112 (1985) 360-381.

[18] R. Neubert, Ion pair transport across membranes, Pharm Res, 6 (1989) 743-747.

[19] J.H. Jonkman, C.A. Hunt, Ion pair absorption of ionized drugs-fact or fiction?, Pharm Weekbl Sci, 5 (1983) 41-48.

[20] B. Lippold, Ion pairs-their synthesis, determination and significance, Pharmazie, 28 (1973) 713-720.

[21] S. Lee, S. Kim, Hydrophobization of ionic drugs for transport through membranes, J Control Release, 6 (1987) 3-13.

[22] J.D. Meyer, M.C. Manning, Hydrophobic ion pairing: altering the solubility properties of biomolecules, Pharm Res, 15 (1998) 188-193.

[23] C.A. Heinen, S. Reuss, G.L. Amidon, P. Langguth, Ion pairing with bile salts modulates intestinal permeability and contributes to food-drug interaction of BCS class III compound trospium chloride, Mol Pharm, 10 (2013) 3989-3996.

[24] O. Zupancic, G. Leonaviciute, H.T. Lam, A. Partenhauser, S. Podricnik, A. Bernkop-Schnurch, Development and *in vitro* evaluation of an oral SEDDS for desmopressin, Drug Deliv, 23 (2016) 2074-2083.

[25] H. Zhou, C. Lengsfeld, D.J. Claffey, J.A. Ruth, B. Hybertson, T.W. Randolph, K.Y. Ng, M.C. Manning, Hydrophobic ion pairing of isoniazid using a prodrug approach, J Pharm Sci, 91 (2002) 1502-1511.

[26] I. Lozoya-Agullo, I. Gonzalez-Alvarez, M. Gonzalez-Alvarez, M. Merino-Sanjuan, M. Bermejo, Development of an ion-pair to improve the colon permeability of a low permeability drug: Atenolol, Eur J Pharm Sci, 93 (2016) 334-340.

[27] P. Shah, V. Jogani, T. Bagchi, A. Misra, Role of Caco-2 cell monolayers in prediction of intestinal drug absorption, Biotechnol Prog, 22 (2006) 186-198.

[28] E.K. Anderberg, P. Artursson, Epithelial transport of drugs in cell culture. VIII: Effects of sodium dodecyl sulfate on cell membrane and tight junction permeability in human intestinal epithelial (Caco-2) cells, J Pharm Sci, 82 (1993) 392-398.

[29] E.T. Hellriegel, T.D. Bjornsson, W.W. Hauck, Interpatient variability in bioavailability is related to the extent of absorption: Implications for bioavailability and bioequivalence studies, Clin Pharmacol Ther, 60 (1996) 601-607.

[30] S. Sun, N. Liang, Y. Kawashima, D. Xia, F. Cui, Hydrophobic ion pairing of an insulin-sodium deoxycholate complex for oral delivery of insulin, Int J Nanomedicine, 6 (2011) 3049-3056.

[31] S. Sun, N. Liang, X. Gong, W. An, Y. Kawashima, F. Cui, P. Yan, Multifunctional Composite Microcapsules for Oral Delivery of Insulin, Int J Mol Sci, 18 (2016) 54.

[32] P.K. Suresh, S.D. Paul, Ion-paired Drug Delivery: An Avenue for Bioavailability Improvement, Sierra Leone J Biomed Res, 3 (2011) 70-76.

[33] H. Xu, L. Zhang, L. Li, Y. Liu, Y. Chao, X. Liu, Z. Jin, Y. Chen, X. Tang, H. He, Q. Kan, C. Cai, Membrane-Loaded Doxorubicin Liposomes Based on Ion-Pairing Technology with High Drug Loading and pH-Responsive Property, AAPS PharmSciTech, 18 (2017) 2120-2130.

[34] X. Zhang, X. Sun, J. Li, X. Zhang, T. Gong, Z. Zhang, Lipid nanoemulsions loaded with doxorubicin-oleic acid ionic complex: characterization, *in vitro* and *in vivo* studies, Pharmazie, 66 (2011) 496-505.

[35] A.C. de Verdiere, C. Dubernet, F. Nemati, E. Soma, M. Appel, J. Ferte, S. Bernard, F. Puisieux, P. Couvreur, Reversion of multidrug resistance with polyalkylcyanoacrylate nanoparticles: towards a mechanism of action, Br J Cancer, 76 (1997) 198-205.

[36] T. Zhang, Y. Zheng, Q. Peng, X. Cao, T. Gong, Z. Zhang, A novel submicron emulsion system loaded with vincristine-oleic acid ion-pair complex with improved anticancer effect: *in vitro* and *in vivo* studies, Int J Nanomedicine, 8 (2013) 1185-1196.

[37] R. Pignatello, A. Mangiafico, L. Basile, B. Ruozi, P.M. Furneri, Amphiphilic ion pairs of tobramycin with lipoamino acids, Eur J Med Chem, 46 (2011) 1665-1671.

[38] R. Pignatello, A. Mangiafico, B. Ruozi, G. Puglisi, P.M. Furneri, Amphiphilic erythromycin-lipoamino acid ion pairs: characterization and *in vitro* microbiological evaluation, AAPS PharmSciTech, 12 (2011) 468-475.

[39] O. Zupancic, J.A. Griebetainger, J. Rohrer, I. Pereira de Sousa, L. Danninger, A. Partenhauser, N.E. Sundermann, F. Laffleur, A. Bernkop-Schnurch, Development, *in vitro* and *in vivo* evaluation of a self-emulsifying drug delivery system (SEDDS) for oral enoxaparin administration, Eur J Pharm Biopharm, 109 (2016) 113-121.

[40] S. Vrignaud, J.P. Benoit, P. Saulnier, Strategies for the nanoencapsulation of hydrophilic molecules in polymer-based nanoparticles, Biomaterials, 32 (2011) 8593-8604.

[41] A.D. Holmkvist, A. Friberg, U.J. Nilsson, J. Schouenborg, Hydrophobic ion pairing of a minocycline/Ca2+/AOT complex for preparation of drug-loaded PLGA nanoparticles with improved sustained release, Int J Pharm, 499 (2016) 351-357.

[42] S. Sun, N. Liang, H. Yamamoto, Y. Kawashima, F. Cui, P. Yan, pH-sensitive poly(lactide-co-glycolide) nanoparticle composite microcapsules for oral delivery of insulin, Int J Nanomedicine, 10 (2015) 3489-3498.

[43] G.P. Zara, R. Cavalli, A. Fundaro, A. Bargoni, O. Caputo, M.R. Gasco, Pharmacokinetics of doxorubicin incorporated in solid lipid nanospheres (SLN), Pharmacol Res, 40 (1999) 281-286.

[44] H.S. Yoo, H.K. Choi, T.G. Park, Protein-fatty acid complex for enhanced loading and stability within biodegradable nanoparticles, Journal of Pharmaceutical Sciences, 90 (2001) 194-201.

[45] Y.H. Song, E. Shin, H. Wang, J. Nolan, S. Low, D. Parsons, S. Zale, S. Ashton, M. Ashford, M. Ali, D. Thrasher, N. Boylan, G. Troiano, A novel in situ hydrophobic ion paring (HIP) formulation strategy for clinical product selection of a nanoparticle drug delivery system, J Control Release, 229 (2016) 106-119.

[46] R.D. Vaishya, A. Mandal, M. Gokulgandhi, S. Patel, A.K. Mitra, Reversible hydrophobic ion-paring complex strategy to minimize acylation of octreotide during long-term delivery from PLGA microparticles, Int J Pharm, 489 (2015) 237-245.

[47] R. Cavalli, O. Caputo, M.R. Gasco, Solid Lipospheres of Doxorubicin and Idarubicin, International Journal of Pharmaceutics, 89 (1993) R9-R12.

[48] A.A. Attama, M.A. Momoh, P.F. Builders, Lipid Nanoparticulate Drug Delivery Systems: A Revolution in Dosage Form Design and Development, Intech, 2012.

[49] S. Matschiner, R. Neubert, W. Wohlrab, Optimization of topical erythromycin formulations by ion pairing, Skin Pharmacol, 8 (1995) 319-325.

[50] S. Mitragotri, P.A. Burke, R. Langer, Overcoming the challenges in administering biopharmaceuticals: formulation and delivery strategies, Nat Rev Drug Discov, 13 (2014) 655-672.

[51] J. Wang, V. Yadav, A.L. Smart, S. Tajiri, A.W. Basit, Toward oral delivery of biopharmaceuticals: an assessment of the gastrointestinal stability of 17 peptide drugs, Mol Pharm, 12 (2015) 966-973.

[52] P. Fonte, F. Araujo, S. Reis, B. Sarmento, Oral insulin delivery: how far are we?, J Diabetes Sci Technol, 7 (2013) 520-531.

[53] N. Yin, M. Brimble, P. Harris, J. Wen, Enhancing the Oral Bioavailability of Peptide Drugs by using Chemical Modification and Other Approaches, Med chem, 4 (2014) 763-769.

[54] D. QuintanarGuerrero, E. Allemann, H. Fessi, E. Doelker, Applications of the ion-pair concept to hydrophilic substances with special emphasis on peptides, Pharm Res, 14 (1997) 119-127.

[55] T. Karamanidou, K. Karidi, V. Bourganis, K. Kontonikola, O. Kammona, C. Kiparissides, Effective incorporation of insulin in mucus permeating self-nanoemulsifying drug delivery systems, Eur J Pharm Biopharm, 97 (2015) 223-229.

[56] S.K. You, H.H. Kwon, J.M. Lee, S.C. Shin, C.W. Cho, Studies on the formation of hydrophobic ion-pairing complex of alendronate, Arch Pharm Res, 32 (2009) 1055-1060.

[57] M. Higashiyama, T. Tajika, K. Inada, A. Ohtori, Improvement of the ocular bioavailability of carteolol by ion pair, J Ocul Pharmacol Ther, 22 (2006) 333-339.

[58] S.A. Megwa, S.E. Cross, H.A.E. Benson, M.S. Roberts, Ion-pair formation as a strategy to enhance topical delivery of salicylic acid, J. Pharm. Pharmacol., 52 (2000) 919-928.

[59] R. Neubert, T. Dittrich, Ampicillin ion pair transport in comparison with the transport of other penicillins, Pharmazie, 44 (1989) 67-68.

[60] S. Megwa, S. Cross, M. Whitehouse, H. Benson, M. Roberts, Effect of ion pairing with alkylamines on the *in-vitro* dermal penetration and local tissue disposition of salicylates, J Pharm Pharmacol., 52 (2000) 929-940.

[61] T. Yang, A. Hussain, S. Bai, I.A. Khalil, H. Harashima, F. Ahsan, Positively charged polyethylenimines enhance nasal absorption of the negatively charged drug, low molecular weight heparin, J Control Release, 115 (2006) 289-297.

[62] J. Wiest, M. Saedtler, A. Balk, B. Merget, T. Widmer, H. Bruhn, M. Raccuglia, E. Walid, F. Picard, H. Stopper, W. Dekant, T. Lühmann, C. Sotriffer, B. Galli, U. Holzgrabe, L. Meinel, Mapping the pharmaceutical design space by amorphous ionic liquid strategies, J. Control. Release (2017).

[63] B.J. Aungst, Intestinal Permeation Enhancers, J. Pharm. Sci., 89 (2000) 429-442.

[64] A. Iyire, M. Alayedi, A.R. Mohammed, Pre-formulation and systematic evaluation of amino acid assisted permeability of insulin across *in vitro* buccal cell layers, Sci Rep, 6 (2016) 32498.

[65] R.G. Strickley, Solubilizing Excipients in Oral and Injectable Formulations, Pharm Res, 21 (2004) 201-230.

[66] J.M. Miller, A. Dahan, D. Gupta, S. Varghese, G.L. Amidon, Enabling the intestinal absorption of highly polar antiviral agents: ion-pair facilitated membrane permeation of zanamivir heptyl ester and guanidino oseltamivir, Mol Pharm, 7 (2010) 1223-1234.

[67] F. Mahmud, O.C. Jeon, T.A. Al-Hilal, S. Kweon, V.C. Yang, D.S. Lee, Y. Byun, Absorption Mechanism of a Physical Complex of Monomeric Insulin and Deoxycholyl-l-lysyl-methylester in the Small Intestine, Mol Pharm, 12 (2015) 1911-1920.

[68] T. Caon, L. Jin, C.M. Simoes, R.S. Norton, J.A. Nicolazzo, Enhancing the buccal mucosal delivery of peptide and protein therapeutics, Pharm Res, 32 (2015) 1-21.

[69] J.O. Morales, D.J. Brayden, Buccal delivery of small molecules and biologics: of mucoadhesive polymers, films, and nanoparticles, Curr Opin Pharmacol, 36 (2017) 22-28.

[70] J.O. Morales, J.T. McConville, Novel strategies for the buccal delivery of macromolecules, Drug Dev Ind Pharm, 40 (2014) 579-590.

[71] C.A. Squier, M.J. Kremer, Biology of oral mucosa and esophagus, J Natl Cancer Inst Monogr (2001) 7-15.

[72] S. Turker, E. Onur, Y. Ozer, Nasal route and drug delivery systems, Pharm World Sci, 26 (2004) 137-142.

[73] L. Illum, Nasal drug delivery - recent developments and future prospects, J Control Release, 161 (2012) 254-263.

[74] V.D. Ivaturi, S.K. Kim, Enhanced permeation of methotrexate in vitro by ion pair formation with L-arginine, J Pharm Sci, 98 (2009) 3633-3639.

[75] E. Mutschler, G. Geisslinger, H.K. Kroemer, P. Ruth, M. Schäfer-Korting, Mutschler Arzneimittelwirkungen, Wissenschaftliche Verlagsgesellschaft Stuttgart, 2008.

[76] I.P. Kaur, M. Kanwar, Ocular preparations: the formulation approach, Drug Dev Ind Pharm, 28 (2002) 473-493.

[77] S.S. Davis, E. Tomlinson, C.G. Wilson, J. Crossland, The effect of ion-association on the transcorneal transport of drugs [proceedings], Br J Pharmacol, 64 (1978) 444P.

[78] A. Kato, S. Iwata, In vitro study on corneal permeability to bunazosin, J Pharmacobiodyn, 11 (1988) 115-120.

[79] P. Chetoni, S. Burgalassi, D. Monti, S. Tampucci, V. Tullio, A.M. Cuffini, E. Muntoni, R. Spagnolo, G.P. Zara, R. Cavalli, Solid lipid nanoparticles as promising tool for intraocular tobramycin delivery: Pharmacokinetic studies on rabbits, Eur J Pharm Biopharm, 109 (2016) 214-223.

[80] P. Langguth, E. Mutschler, Lipophilisation of hydrophilic compounds. Consequences on transepidermal and intestinal transport of trospium chloride, Arzneimittelforschung, 37 (1987) 1362-1366.

[81] B.W. Barry, Dermatological Formulations: Percutaneous Absorption, Dekker, New York, 1983.

[82] J.D. Bos, M.M. Meinardi, The 500 Dalton rule for the skin penetration of chemical compounds and drugs, Exp. Dermatol., 9 (2000) 165-169.

[83] M.R. Prausnitz, R. Langer, Transdermal drug delivery, Nat Biotechnol, 26 (2008) 1261-1268.

[84] B.W. Barry, Novel mechanisms and devices to enable successful transdermal drug delivery, Eur J Pharm Sci, 14 (2001) 101-114.

[85] M. Kadono, K. Kubo, H. Miyazaki, N. Tojyo, S. Nakagawa, K. Miyashita, T. Imanishi, J. Rytting, T. Mayumi, Enhanced in vitro percutaneous penetration of salicylate by ion pair formation with alkylamines., Biol Pharm Bull., 21 (1998) 599-603.

[86] C. Valenta, U. Siman, M. Kratzel, J. Hadgraft, The dermal delivery of lignocaine: influence of ion pairing, Int J Pharm, 197 (2000) 77-85.

# CHAPTER II

## QUINOLONE AMIDES AS ANTITRYPANOSOMAL LEAD COMPOUNDS WITH *IN VIVO* ACTIVITY

Georg Hiltensperger[1], Nina Hecht[1], Marcel Kaiser[2,3], Jens-Christoph Rybak[1], Alexander Hoerst[1], Nicole Dannenbauer[4], Klaus Müller-Buschbaum[4], Heike Bruhn[5], Harald Esch[1], Leane Lehmann[1], Lorenz Meinel[1], Ulrike Holzgrabe[1,*]

[1]Universität Würzburg, Institut für Pharmazie und Lebensmittelchemie, Würzburg, Germany

[2]Swiss Tropical and Public Health Institute, Parasite Chemotherapy, Basel, Switzerland

[3]Universität Basel, Basel, Switzerland

[4]Universität Würzburg, Institut für Anorganische Chemie, Germany

[5]Universität Würzburg, Institut für Molekulare Infektionsbiologie, Würzburg, Germany

This originally chapter is published in Antimicrob Agents Chemother, 60 (2016) 4442-4452; doi: 10.1128/AAC.01757-15; 

## Abstract

Human African trypanosomiasis (HAT) is a major tropical disease for which few drugs for treatment are available, driving the need for novel active compounds. Recently, morpholino-substituted benzyl amides of the fluoroquinolone-type antibiotics were identified to be compounds highly active against *Trypanosoma brucei brucei*. Since the lead compound GHQ168 was challenged by poor water solubility in previous trials, the aim of this study was to introduce structural variations to GHQ168 as well as to formulate GHQ168 with the ultimate goal to increase its aqueous solubility while maintaining its *in vitro* antitrypanosomal activity. The pharmacokinetic parameters of spray-dried GHQ168 and the newly synthesized compounds GHQ242 and GHQ243 in mice were characterized by elimination half-lives ranging from 1.5 to 3.5 h after intraperitoneal administration (4 mice/compound), moderate to strong human serum albumin binding for GHQ168 (80%) and GHQ243 (45%), and very high human serum albumin binding (> 99%) for GHQ242. For the lead compound, GHQ168, the apparent clearance was 112 ml/h and the apparent volume of distribution was 14 liters/kg of body weight (BW). Mice infected with *T. b. rhodesiense* (STIB900) were treated in a stringent study scheme (2 daily applications between days 3 and 6 postinfection). Exposure to spray-dried GHQ168 in contrast to the control treatment resulted in mean survival durations of 17 versus 9 days, respectively, a difference that was statistically significant. Results that were statistically insignificantly different were obtained between the control and the GHQ242 and GHQ243 treatments. Therefore, GHQ168 was further profiled in an early-treatment scheme (2 daily applications at days 1 to 4 postinfection), and the results were compared with those obtained with a control treatment. The result was statistically significant mean survival times exceeding 32 days (end of the observation period) versus 7 days for the GHQ168 and control treatments, respectively. Spray-dried GHQ168 demonstrated exciting antitrypanosomal efficacy.

## Introduction

Human African trypanosomiasis (HAT), also known as sleeping sickness, is caused by *Trypanosoma brucei rhodesiense* and *T. b. gambiense*. It is widespread in eastern and southern Africa (*T. b. rhodesiense*) and in western and central Africa (*T. b. gambiense*). In spite of currently decreasing numbers of new infections in humans, these regions are threatened by a large reservoir of the parasites in cattle, horses, and other nonmammalian species, creating an imminent risk of the next outbreak of HAT [1]. In addition, the rapid development of resistance can be observed [2]. Moreover, as the available drugs, such as suramin, pentamidine, melarsoprol, or eflornithine, either are active against only one of the two stages of HAT, the acute or chronic form, or exhibit dangerous adverse events, new anti-HAT drugs are urgently needed. Thus, it is important and perhaps indispensable to rigorously expand the arsenal of potent and safe antiparasitic compounds with demonstrated efficacy against HAT [3]. Currently, two new drugs, i.e., the 5-nitroimidazole fexinidazole (phase II/III trials) and the oxaborole SCYX-6759 (phase I trials), are in clinical trials, in which they have shown promising initial results ([4]; http://www.dndi.org/diseases-projects/diseases/hat.html). However, significant hurdles remain to be overcome before these new drug candidates may become commercially available.

By means of a medium-throughput screening campaign, we recently discovered a new group of antitrypanosomal compounds derived from the fluoroquinolones, the latter of which are active against most Gram-positive and Gram-negative bacterial species but not against *T. b. brucei* [5-8]. The replacement of the carboxylic acid functionality, which is important for the inhibitory activity toward many classes of bacterial topoisomerases, by a benzyl amide group resulted in a library of novel compounds. The newly synthesized compounds are active against *T. b. brucei* and *T. b. rhodesiense* at nanomolar concentrations [9] without cell toxicity, as assessed in macrophages. Structure-activity studies revealed that the quinolone carrying a butyl chain in position N-1, an *N*-benzyl

group at the amido function in position 3, and a morpholino ring in position 7 was the most active and is referred to as GHQ168 (**Figure 1**).

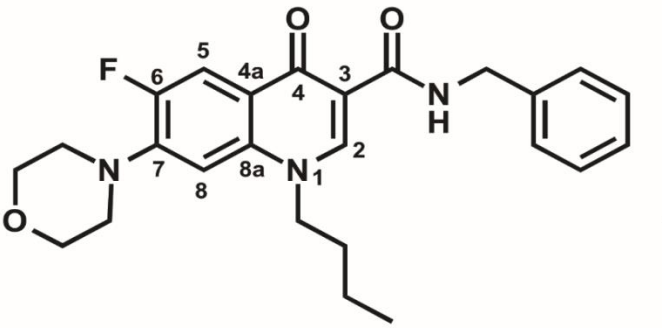


Activity:

$IC_{50}$ (*T. b. brucei*, 72 h) = 47 nM
$IC_{50}$ (BSF *T. b. brucei*, 48 h) = 23 nM
$IC_{50}$ (*T. b. rhodesiense*, 72 h) = 9 nM

Toxicity:

$IC_{50}$ (*J774.1 macrophages*) = 57 µM

**Figure 1**: Structure and activity/toxicity data for GHQ168, the most active compound from the novel quinolone amide library.

Initial biological studies hinted at the influence of the active compound GHQ168 (compound 29 in reference [9]) on the morphology of the mitochondria and its ability to hinder segregation of the kinetoplast [9]. In contrast to quinolone carboxylic acids, which are active against the trypanosomal topoisomerase II (from *T. b. brucei*) [6, 7, 10], we could show that the corresponding amides do not affect the topoisomerase in trypanosomes [9]. Taken together, these findings indicate that the mode of action of GHQ168 remains to be elucidated.

Even though GHQ168 has favorable structural properties that predict oral bioavailability [10] (a favorable octanol-water partition coefficient (logP) is ≤ 5 and the logP for GHQ168 is 3.8, a favorable molecular mass is ≤ 500 g/mol and the molecular mass of GHQ168 is 437.5 g/mol, a favorable structure has 5 hydrogen bond donors represent and GHQ168 has 1, and a favorable structure has 10 hydrogen bond acceptors and GHQ168 has 7), this compound showed very poor aqueous solubility. Thus, in order to overcome the solubility problem in experiments with mice, the compound was administered

intraperitoneally (i.p.) as a lipid formulation. However, these previous experiments had to be stopped due to low tolerance of the vehicle by the test animals [9].

In this study, we aimed to develop by chemical modification fluoroquinolone amide compounds with improved solubility. Furthermore, we developed a formulation of GHQ168 with the same goal of meeting the necessary solubility requirements. The compounds were characterized with regard to their physicochemical properties, *in vitro* antitrypanosomal activity, and *in vitro* toxicity. Three of the synthesized compounds were selected and analysed with regard to intestinal absorption (Caco-2 cell model) for assessment of the feasibility of the development and use of oral dosage forms in the future. Furthermore, the three compounds were profiled for their *in vivo* pharmacokinetics (PK) and *in vivo* antitrypanosomal activity in infected mice.

# Materials and Methods

### Materials

Reference substances (used for the determination of lipophilicity, permeability, *in vitro* activity, and metabolism), excipients, and reagents were purchased from Sigma-Aldrich, Taufkirchen, Germany, and were of analytical or pharmaceutical grade, unless noted otherwise. Poly(methacrylic acid-comethyl methacrylate) (Eudragit L100; approximate $M_w$ = 125000 g/mol) for formulation preparation was from Evonik, Essen, Germany. Liquid chromatography (LC) columns were obtained from Phenomenex, Aschaffenburg, Germany (Synergi MAX-RP, Kinetex, Luna) and from MZ-Analytical, Mainz, Germany (Inertsil ODS-2). A PLTK4710 ultrafiltration membrane for albumin binding was purchased from Millipore, Schwalbach, Germany. Caco-2 cells were from ATCC; the polyethylene terephthalate (PET) membrane was from Greiner Bio-One, Frickenhausen, Germany; and Dulbecco's modified Eagle medium (DMEM), high glucose, with l-glutamine, nonessential amino acids, and penicillin-streptomycin solution was from Gibco, Life Technologies, Darmstadt, Germany. For cytotoxicity assays, all cells were purchased from ATCC, Wesel, Germany; RPMI medium was from Gibco, Life Technologies, Darmstadt, Germany; and fetal calf serum (FCS) was from GE Healthcare Europe GmbH, Freiburg, Germany. For metabolism and mutagenesis experiments, NADP sodium salt was obtained from Applichem, Darmstadt, Germany; mass spectrometry (MS)-grade solvents were from VWR, Ismaning, Germany; and all other chemicals, including cell culture medium and supplements, were from Sigma-Aldrich, Taufkirchen, Germany, or Roth, Karlsruhe, Germany, unless specified otherwise. For metabolic stability testing, the S9 fraction was purchased from MP Biomedicals, Illkirch-Graffenstaden, France; the Bradford reagent was from Bio-Rad, Munich, Germany. For mutagenicity testing, fetal calf serum was purchased from Invitrogen, Karlsruhe, Germany, and culture flasks and tissue culture dishes were from Greiner Bio-One, Frickenhausen, Germany. For plasma stability

assessment, human plasma was obtained from Bayerisches Rotes Kreuz, Munich, Germany. For the analysis of blood samples, solvents were purchased from Fisher Scientific, Schwerte, Germany.

**Synthesis**

The synthesis of GHQ168 was performed as described previously [9]. The synthesis of the other related salt compounds presented herein (GHQ237, GHQ242, GHQ243, GHQ250, GHQ232, GHQ215) can be found in the supplemental material. The stoichiometry of the substances and the respective counterion was determined using CHN analysis.

**Formulation**

A solid dispersion was produced using a nanospray dryer (B-90; Büchi, Essen, Germany). GHQ168 (0.2%, wt/vol) and Eudragit L100 (2.0%, wt/vol) were dissolved in methanol, resulting in a 1:10 (wt/wt) spray-dried formulation. Spray drying was performed with the head in the vertical position and with the formulation sprayed through a mesh with a 7-µm mesh size at an airflow set at 150 liters/min, an inlet temperature of 60 °C, an outlet temperature of 34 °C, a pressure of $5.2 \times 10^3$ Pa, and a spray rate of 100%. The resulting white, amorphous nanoparticles were stored in a desiccator over silica gel at room temperature.

**Solubility**

A preliminary determination for the fast and approximate assessment of kinetic solubility was achieved by diluting dimethyl sulfoxide (DMSO) stock solutions of the desired compounds (1 mM, 20 mM) in phosphate-buffered saline (PBS) buffer (pH 7.4) in order to give aqueous solutions with concentrations of 10, 100, 500, 1000, 1500, 2000, 2500, 3000, 4000, and 5000 µM (one experiment was performed with each concentration).

Precipitation was detected microscopically (SZ-PT microscope; Olympus, Shinjuku, Japan).

In addition, a more precise determination of kinetic solubility was conducted for those compounds applied in the efficacy studies. “Kinetic solubility” refers to the apparent solubility of a compound in a metastable state, at which, in spite of the fact that the chemical potential of the compound in solution exceeds the chemical potential of the solid compound, precipitation is so slow that a (kinetic) solubility exceeding the equilibrium solubility may be observed.

As described above, dilution series were prepared for each compound but with closer concentration steps (GHQ168, 5, 10, 15, 20, 25, 30, and 35 µg/ml; GHQ242, 150, 200, 250, 300, 350, 400, 450, and 500 µg/ml; GHQ243, 50, 100, 125, 150, 175, 200, 250, and 300 µg/ml; $n$ = 3 each) to end with a maximum of 2.5% residual DMSO content. Detection was accomplished nephelometrically (NEPHEOLOstar BMG, Ortenberg, Germany) using 96-well plates with a flat bottom (Greiner Bio-One, Frickenhausen, Germany). The temperature was set to 37 °C, the laser intensity was 80%, and the laser beam focus was 2.20 mm. The gain was adjusted to 60 (GHQ168, GHQ242) and 75 (GHQ243), and the measurement time per well was 0.1 s. The mean result for three dilution series was determined. Two replicate measurements of the same solutions were performed (time frame, 30 min), and the standard deviation (SD) was calculated from the means of three replicate measurements over time.

In contrast to the kinetic solubility, the thermodynamic solubility (also called “equilibrium solubility”) describes a thermodynamically stable state that might take its time to be generated but that is maintained when environmental conditions remain unchanged. The determination of the thermodynamic solubility of GHQ168 was conducted by dosing solid substance (in excess) into 2-ml Eppendorf vials, followed by dissolution in PBS buffer (pH 7.4). Throughout the assay, continuous shaking (800 rpm) and a constant temperature (37 °C) were maintained (Eppendorf Thermomixer; Eppendorf AG, Hamburg,

Germany). Samples were taken after 10, 30, 60, 120, and 1,200 min, followed by centrifugation (13000 rpm, 1 min; Micro 2416; VWR International, Darmstadt, Germany) and high-performance liquid chromatography (HPLC)-UV (Jasco, Groß-Umstadt, Germany) analysis of the supernatant (Synergi MAX-RP column; 80 Å; 4 µm; 150 by 4.6 mm; mobile phase, acetonitrile-water (72/28); temperature, 40 °C; flow rate, 1.2 ml/min; injection volume, 20 µl; detection wavelength, 280 nm). Solubility determination was performed in triplicate.

**X-ray diffractometry**

X-ray powder diffractograms were recorded on an X-ray powder diffraction (XRPD) apparatus (D8 Discover; Bruker, Karlsruhe, Germany) using a copper tube operating at 40 kV and 40 mA. A focusing Goebel mirror was installed in the primary beam path (slit, 0.6 mm; axial Soller slit, 2.5°). For the secondary beam path, no slit was applied and the axial Soller slit was set to 2.5°. Detection was done using a LynxEye one-dimensional detector (Bruker AXS). The investigation was performed in coupled two theta/theta mode with a 2-Θ range of 5 to 45°, a step width of 0.025°, and a 1.0 s measurement time per step. Data collection and processing were conducted with the software packages DIFFRAC.Suite (v2 2.2.690; Bruker AXS 2009-2011) and DIFFRAC.EVA (version 3.0; Bruker AXS 2010-2013). Details on the method used for single crystal structure analysis can be found in the supplemental material.

**SEM**

Scanning electron microscopy (SEM) (JSM-7500F SEM microscope; JEOL, Japan) was performed with an accelerating voltage of 2.0 kV and a ×1000 magnification at a working distance of 8.6 mm. Prior to examination, the samples were sputter coated with gold.

**Physicochemical parameters**

LogP data were recorded using HPLC-UV ($C_{18}$ reversed-phase Inertsil ODS-2 column; 5 µm; 150 by 4.6 mm; mobile phase, phosphate buffer (10 mM; pH 7.4)-methanol (containing 0.02% *N,N*-dimethylhexylamine), 30/70; temperature, 30 °C; flow rate, 1.5 ml/min; injection volume, 40 µl; detection wavelength, 254 nm) as described previously [9]. Compounds with known logP values (2-phenylethanol, benzene, *N,N*-dimethylaniline, toluene, chlorobenzene, ethylbenzene, biphenyl, and anthracene) served as reference substances. The capacity factor (k′) that correlates with logP values can be derived from the retention time ($t_R$) and dead time ($t_0$) of the compounds by the following equation: $k' = (t_R - t_0)/t_0$.

Experimental determination of $pK_a$ was conducted for GHQ168, GHQ242, and GHQ243 on a Sirius T3 instrument (Sirius, Forest Row, United Kingdom). Due to its low aqueous solubility, determination of the $pK_a$ of GHQ168 was conducted from a DMSO stock solution (10 µM) using the assay type fast UV-metric $pK_a$ (in which $pK_a$ assessment is accomplished by the identification of changes in the absorption profile due to sample ionization). For GHQ242 and GHQ243, the solid compounds (weight, 0.43 mg to 0.56 mg) were dosed into the instrument and the assay type pH-metric $pK_a$ (in which the potentiometric $pK_a$ is assessed using a pH electrode) was applied. Potassium chloride solution (1.5 ml, 0.15 M) was added to the compounds, and the temperature was maintained at 25 °C throughout the assay. The titrations were conducted over the pH range of 2 to 12, starting at low pH values (acidification prior to titration with 0.5 M hydrochloric acid; titration with 0.5 M potassium hydroxide solution).

**DSC**

Melting point determinations were performed using a differential scanning calorimetry (DSC) 8000 instrument (PerkinElmer, Waltham, MA, USA). The scanning rate was set to 20 °C/min over the range of −50 °C to 300 °C.

**Serum albumin binding**

In principle, albumin binding was determined *in vitro* by means of the continuous titration methods described herein [11]. In brief, the self-made instrument consists of a low-pressure HPLC pump (Bischoff, Leonberg, Germany), an injection valve (Rheodyne, Alsbach, Germany) for injection of the human serum albumin (HSA) solution into the system, an ultrafiltration cell, and a UV detector (Knauer, Berlin, Germany). The ultrafiltration cell contains the PLTK4710 ultrafiltration membrane with a molecular mass cutoff of 30 kDa. HSA and the test compounds were dissolved in 0.03 M phosphate buffer (pH 7.4) containing 0.1 M NaCl for the simulation of physiological conditions. In the case of GHQ168, the substance was dissolved in dimethylformamide (1 mg/ml), and 420 µl of this solution was diluted with 2 mM polysorbate 20 in buffer to 100.0 ml. The concentration of the drug solutions was within the range of 10 to 20 mg/liter. Initially, the drug solution was continuously pumped through the cell and the curves of the measured absorption versus time were plotted. The system was rinsed with buffer, and subsequently, the albumin solution (40 mg/ml) was injected into the system. The ultrafiltration membrane retains the protein in the cell. The drug solution was again pumped through the ultrafiltration cell and the absorbance was measured again. The interaction between drug and HSA present in the cell leads to a shift of the second curve to the right compared to the location of the first recorded curve. The size of the area between the two drug curves is proportional to the amount of drug bound to the HSA.

**Permeation through Caco-2 cell monolayers**

The evaluation of permeation was performed in principle as reported previously [12]. In brief, Caco-2 cells at passage number 51 were thawed, passaged four times, and seeded at $1.3 \times 10^5$ cells/cm$^2$ on 24-well cell culture inserts with a PET membrane (pore size, 0.4 µm). The cells were cultivated in DMEM, high glucose, with l-glutamine, nonessential amino acids, and penicillin-streptomycin solution for 23 days at 37 °C in 5% $CO_2$. Transepithelial electric resistance (TEER) in DMEM was monitored three times a week during the medium change (EVOM$^2$ electrode; World Precision Instruments, USA). Prior to the permeability experiment, the cells were washed twice with Hanks balanced salt solution (HBSS), 25 mM HEPES, pH 7.4, and TEER was measured in order to assess the integrity of the monolayer (cells with TEER values of < 200 Ω · cm$^2$ were excluded from the experiment). For permeation testing, 150 µl of 20 µM GHQ168, GHQ242, and GHQ243 in HBSS–0.5% DMSO was added to the apical compartment and 600 µl of HBSS was added to the basolateral compartment, followed by gentle shaking for 1 h at 37 °C in 5% $CO_2$. The cells were washed with HBSS, and the integrity of the monolayer was reconfirmed by TEER measurement. Fluorescein isothiocyanate-dextran was used as a nonpermeant negative control, and propranolol HCl was used as a positive control with high levels of permeation. For each compound, at least three independent Caco-2 cell assays were conducted within 1 day. The concentration of fluorescein isothiocyanate-dextran was determined fluorimetrically (excitation wavelength, 490 nm; emission wavelength, 514 nm; LS50B luminescence spectrometer; PerkinElmer). All other compounds were analyzed by LC/MS/MS using the analytical method described in “Pharmacokinetics” below.

***In vitro* activity**

The methods described by Räz et al. [13], Baltz et al. [29], Papadopoulou et al. [14], Larson et al. [15], and Muth et al. [16] were applied for determination of *in vitro* activity.

**Cytotoxicity**

The methods used to determine cytotoxicity are described in the supplemental material.

**Metabolism and mutagenesis**

Phase I metabolism of GHQ168 by cytochrome P450-dependent monooxygenase was investigated in rat liver microsomes. Microsomes were prepared by ultracentrifugation (100000 × g, 60 min, 4 °C) from a commercially available S9 fraction from Aroclor 1254-treated male Sprague-Dawley rats. After resuspension in HEPES buffer (25 mM HEPES, 100 mM NaCl, 1.5 mM disodium EDTA, 1 mM dithiothreitol, 10% glycerol, pH 7.4), the protein concentration was determined with the Bradford reagent, yielding 7 mg/ml, and the microsomes were stored at −80 °C until use.

Microsomal incubation mixtures (final volume, 500 µl) contained GHQ168 (100 µM, 1% DMSO), microsomal protein (1 mg/ml), 0.1 M phosphate buffer (pH 7.4), and an NADPH-generating system and were incubated at 37 °C for 30, 60, and 90 min. The NADPH-generating system was prepared from isocitrate (10 mM), isocitrate dehydrogenase (0.05 U), $MgCl_2$ (4 mM), and NADP (1 mM) and was preincubated for 5 min at 37 °C prior to addition to the incubation system. Control incubations were carried out under the same conditions with heat-deactivated microsomes.

After the incubation period, the reaction was stopped by addition of ethyl acetate. Then, 7-(4-acetylpiperazin-1-yl)-*N*-(2,4-dichlorobenzyl)-6-fluoro-1-(2-fluorophenyl)-4-oxo-1,4-dihydroquinoline-3-carboxamide, which is structurally similar to GHQ168, was added as an internal standard and the reaction mixture was extracted three times with ethyl acetate. After evaporation of the solvent, the residues were dissolved in 100 µl acetonitrile and subjected to HPLC with photodiode array detection (LaChrome; Merck Hitachi, Darmstadt, Germany) to determine the rate of GHQ168 decrease (Kinetex column; 2.6 µm; $C_{18}$; 100 by 3 mm; mobile phase A, water, 0.5% formic acid; mobile phase B, acetonitrile, 0.5% formic acid; gradient, 38% mobile phase B for 6 min, gradually increasing to 60% mobile

phase B within 44 min; room temperature; flow rate, 0.2 ml/min; injection volume, 10 µl; detection wavelength, 282 nm). The m/z ratios of the metabolites were obtained by HPLC-mass spectrometry (Agilent LC/MSD G1946D single quadrupole mass spectrometer; Agilent Technologies, Waldbronn, Germany) in full scan mode using positive ionization, a fragmentor voltage of 70 V, a capillary voltage of 4000 V, and full scan range of m/z 100 to 500.

Three independent microsomal incubations were performed (with a new vial of microsomes and a fresh solution of test compound for each test).

The mutagenicity of GHQ168 was assessed in a hypoxanthine-guanine phosphoribosyltransferase (HPRT) assay in cells of the V79 Chinese hamster fibroblast cell line [17]. V79 cells were cultured in DMEM supplemented with 100 U/ml penicillin, 100 µg/ml streptomycin, and 10% FCS, referred to as DMEM complete. The HPRT assay was performed as described previously [18]. Briefly, $1.5 \times 10^6$ V79 cells were seeded in 175-$cm^2$ cell culture flasks containing 20 ml DMEM complete. After 24 h, the medium was changed (day 0) and the cells were treated with different concentrations of GHQ168, 1 µM 4-nitroquinoline-*N*-oxide (NQO; positive control), or 1% DMSO (negative control) for 24 h. A total of $1 \times 10^6$ cells were subcultured in fresh medium directly after treatment (day 1) and again on day 4.

On days 1, 4, and 6, the numbers of viable cells and cells with a disintegrated cell membrane were counted with a CASY model DT electronic cell counter (Schaerfe, Reutlingen, Germany) as a reference point for cytotoxicity and proliferation.

On day 6, cells with mutations at the Hprt gene locus were selected by growing cells in DMEM complete and 7 µg 6-thioguanine (6-TG)/ml using three tissue culture-treated dishes (diameter, 145 mm) with $1 \times 10^6$ cells per dish. To determine the plating efficiency (PE) on days 1 and 6, cells were grown in the absence of 6-TG (500 cells per 100-mm dish, three dishes). After 1 week, the cells were fixed with ethanol and stained with methylene blue (0.5% in methanol). The colonies were counted, and the PE, i.e., the

number of colonies per number of seeded cells, and the mutant frequency, i.e., the number of colonies/(number of seeded cells × PE on day 6), were calculated. Three independent HPRT tests were performed (with a new batch of cells and a fresh solution of test compound for each test).

**Plasma stability**

A plasma stability assay was performed as described by Di et al. [19]. In brief, a 1 mM DMSO stock solution of the selected compound was added to human plasma, and this mixture was diluted 1:2 with PBS buffer (pH 7.4) to achieve a final compound concentration of 10 µM. The mixture was incubated at 37 °C for 2 h. Within that time, aliquots of 100 µl were taken at time zero (reference), 30, 60, and 120 min. All samples were diluted with 300 µl acetonitrile and centrifuged (3000 rpm for 15 min), and the supernatant (200 µl) was analyzed by means of HPLC (Synergi MAX-RP column; 80 Å; 4 µm; 150 by 2 mm; mobile phase, acetonitrile (ACN), 10 mM ammonium acetate buffer (pH 4); gradient, 10% ACN, increasing to 90% in 7 min, 90% ACN for 2 min, 90% ACN decreasing to 10% ACN in 2 min, 10% ACN for 2 min; temperature, 40 °C; flow rate, 0.4 ml/min; injection volume, 30 µl; detection wavelength, 281 nm (GHQ242) or 278 nm (GHQ243)). The resulting peak areas of each aliquot were divided by the peak area of the reference sample (time zero) to calculate the percent decrease. The stability of each compound was measured in duplicate.

**PBPK modeling and pharmacokinetics**

Prior to the *in vivo* efficacy studies, *in silico* physiologically based pharmacokinetic (PBPK) modeling [20] was conducted using the Simcyp software package (Simcyp, Sheffield, United Kingdom) in order to identify a suitable dose and study design. The study design (e.g., duration, dosing interval) and the prediction of the plasma levels were performed with a mouse model. The parameters calculated experimentally to enable determination of a relevant PK study design took into account molar mass, $pK_a$, logP, and the fraction

unbound in plasma. The volume of distribution (V) was calculated by the software according to the corrected Poulin and Theil method [21-24]. Clearance (CL) was calculated from the predicted volume of distribution normalized per kilogram of body weight (V) according to the formula CL = V × $k_{el}$ × weight of the mouse, where $k_{el}$ is the elimination rate constant derived experimentally from *in vitro* metabolic stability assays. The weight of a mouse was set to be 25 g, and simulations were conducted assuming first-order elimination kinetics.

Analysis of mouse blood samples was performed using a Triple Quad 5500 LC/MS/MS system from AB Sciex (Darmstadt, Germany) (Luna column; 3 µm; C18(2); 100 Å; 75- by 3-mm reversed-phase column; mobile phase, methanol (800 ml), LC/MS-grade water (200 ml), ammonium formate (0.636 g), and concentrated formic acid (1.25 ml) (pH 4.5); room temperature; injection volume, 3 µl; detection masses, 438.1 Da to 331.0 Da (GHQ168), 439.1 Da to 331.0 Da (GHQ242), 453.1 Da to 72.0 Da (GHQ243), and 494.2 Da to 368.9 Da (glibenclamide; internal standard); turbospray ionization in the positive mode). The dwell time was set to 150 ms. Nitrogen was used both as the nebulizing and the drying gas (validation data on the analytical method are provided in **Table S3A to F** and **Figure S6A to C** in the supplemental material).

### *In vivo* efficacy studies

The *T. b. rhodesiense* STIB900 strain is a derivative of the STIB704 strain isolated from a patient in Ifakara, Tanzania, in 1982 [25]. The mouse model of acute STIB900 infection mimics the first stage of the disease, in which the trypanosomes are localized in the hemolymphatic system. Prior to the efficacy studies, a donor female NMRI mouse was inoculated intraperitoneally with 1 × $10^4$ bloodstream forms of STIB900. In the efficacy studies, four female NMRI mice were used per experimental group. Each mouse was inoculated i.p. with $10^4$ bloodstream forms of STIB900. For that, heparinized blood from the donor mouse with a level of parasitemia of approximately 5 × $10^6$/ml was suspended

in phosphate-saline-glucose (PSG) to obtain a trypanosome suspension of $4 \times 10^4$ trypanosomes/ml. Each mouse used for the experiments was injected with 0.25 ml trypanosome suspension. Two efficacy studies were conducted: in the first study, compound administration began on day 3 postinfection (stringent model; test compounds, GHQ168, GHQ242, and GHQ243), and in the second study, compound administration began 1 day postinfection (early-treatment model; test compound, GHQ168). Other than this difference, both studies were designed equally (route of administration, i.p.; dosing interval, 12 h; study duration, 4 days; single doses of GHQ168 at 3.5 mg/kg of body weight, GHQ242 at 22.9 mg/kg, or GHQ243 at 21.9 mg/kg; fluid intake with dose, 0.1 ml/10 g body weight).

For *in vivo* administration, GHQ168 spray-dried particles and crystalline GHQ242 and GHQ243 were dissolved in the following delivery vehicles prior to i.p. application: for GHQ168, 5% (wt/vol), glucose, 1% (wt/vol) polysorbate 80, and PBS buffer (pH 7.4); for GHQ242 and GHQ243, 5% (wt/vol) glucose, 1% (wt/vol) polysorbate 80, 10% (vol/vol) DMSO, and PBS buffer (pH 7.4).

Four mice served as infected, untreated controls. They were not injected with the vehicle alone, since it was established in the lab that these vehicles do not affect parasitemia or the mice (data not shown). All mice were monitored for parasitemia by microscopic examination of tail blood twice a week until day 32 postinfection and afterwards once per week until day 60. The time to parasite relapse was recorded to calculate the mean relapse duration (MRD; in days) after infection. Mice were euthanized after detection of a relapse of parasitemia (at least 2 trypanosomes per field of view). The mean survival duration (MSD; in days) of the treated groups and the MSD of the control group were compared using an unpaired t-test; the level of significance was defined at an α level of 0.05 (Minitab software, version 17.2.1). Data for mice that died during the treatment but without parasites in the blood were excluded from the calculation of MSD and MRD, as the cause of death was not related to parasitemia. Mice that survived to and that were

aparasitemic at day 60 (stringent model) or at day 32 (early-treatment model) were considered cured (which was endpoint of the model) and euthanized.

During the efficacy study with the stringent mouse model, blood samples were collected from tail blood for subsequent LC/MS/MS analysis at predetermined time points (1 h and 4 h after the 7th treatment and 16 h after the 8th treatment) in order to assess pharmacokinetics (see **Table S4** in the supplemental material). *In vivo* efficacy studies in mice were conducted at the Swiss Tropical and Public Health Institute (Basel, Switzerland) according to the rules and regulations for the protection of animal rights (Tierschutzverordnung) of the Swiss Bundesamt für Veterinärwesen. They were approved by the veterinary office of the Canton Basel-Stadt, Switzerland.

**Statistics**

Statistical tests (in metabolism and mutagenesis studies) were performed using OriginPro software (version 9.1; OriginLab Corp., Northampton, MA, USA). Multiple data sets were analyzed by analysis of variance with *post hoc* comparison by the Scheffé test. Pairwise comparisons were performed by Student's t-test. The evidence was postulated to have statistical significance if the P-value was $< 0.05$.

# Results

### Solubility in water

The thermodynamic solubility of GHQ168 was 0.005 ± 0.001 µg/ml, as assessed after equilibration for 20 h in PBS buffer and under the conditions described above in Methods and Materials. The kinetic solubility was 15 ± 1 µg/ml; i.e., the kinetic solubility exceeded the thermodynamic solubility by a factor of 3000. Therefore, GHQ168 was practically insoluble in water [22], driving the need for solubility improvement before *in vivo* efficacy studies commenced. Solubility improvement was addressed by (i) formulation approaches and (ii) structural modification.

The formulation strategy was fueled by the coplanar stacking of GHQ168 within its crystal (**Figure 2**), with the crystalline nature being corroborated by XRPD (see **Figure S1A** in the supplemental material).

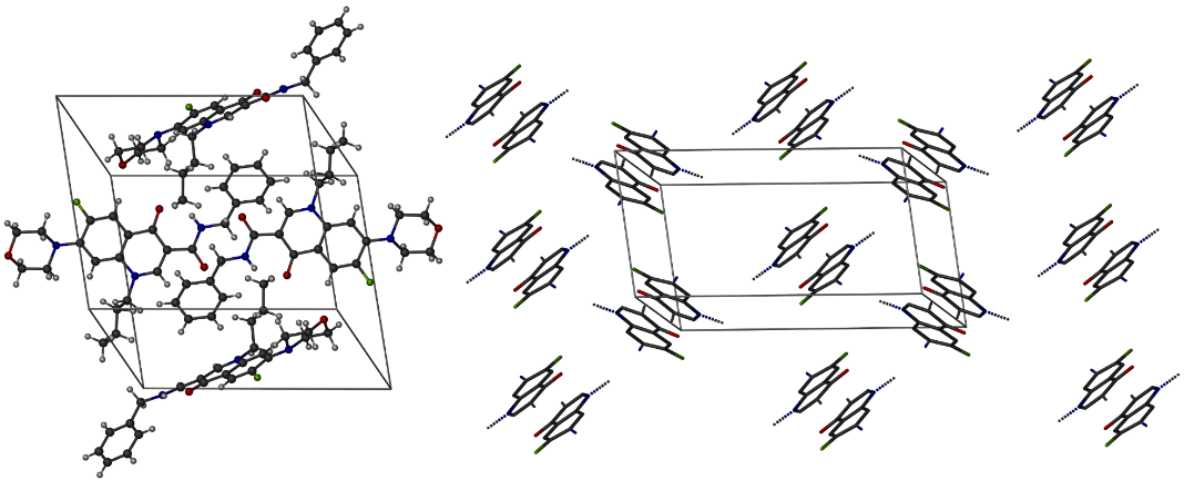

**Figure 2**: Crystal structure of GHQ168. (Left) View of the unit cell with four molecules of GHQ168; (right) view from another direction with a restricted depiction of the quinolone backbone of the molecule only, illustrating the arrangement of GHQ168 molecules as coplanar dimers in the crystal structure. Black, C atoms; white, H atoms; green, F atoms; blue, N atoms; red, O atoms.

These highly ordered structures may allow a low free enthalpy state, consequently demanding high levels of work for molecular escape from the crystal. The resulting high melting point of the crystal (171 °C) reflects these patterns and favors the low solubility of GHQ168. Consequently, a formulation strategy pushing GHQ168 to free enthalpy states higher than the state of the crystal was deployed. For that, GHQ168 was spray dried into a polymer, thereby embedding the drug in an amorphous state (see **Figure S1B** in the supplemental material) within microparticles (see the scanning electron micrographs in **Figure S2** in the supplemental material). In addition to the amorphous presentation, the spray-dried formulation massively increased the surface area of the compound compared to the compact arrangement within the crystal, typically increasing the dissolution rate on the basis of simple Fickian diffusion considerations. The methacrylic acid polymer used for embedding the compound was selected to readily dissolve at a pH exceeding approximately 5.5, thereby gradually releasing the molecularly dispersed drug when its exposed to a pH that is at or that exceeds this pH threshold [26]. Stability studies demonstrated the physical stability of this formulation for 1 year of storage by the absence of (re-)crystallization (the formulation was not assessed at later time points; see **Figure S1B** in the supplemental material). Spray drying of GHQ168 resulted in white nanoparticles of a size ranging below 350 nm, which was confirmed by subsequently performed dynamic light scattering (DLS) experiments (see **Figure S3** in the supplemental material) in order to monitor the pattern in solution over time. Furthermore, a smooth surface, spherical form, and narrow size distribution were illustrated with the help of scanning electron micrographs (see **Figure S2** in the supplemental material). The overall spray-drying process yielded an efficacy of about 90%. The maximum solubility (supersaturated state) in PBS buffer was determined to be 32.9 ± 1.6 µg/ml after 30 min, and this decreased to 7.3 ± 0.7 µg/ml after 6 h (**Figure 3**), thereby transiently exceeding the thermodynamic solubility of GHQ168 by a factor > 6000. Physical mixtures of GHQ168 with the methacrylic acid polymer did not impact the solubility profile, indicating that

amorphization is essential to improve the solubility and corroborating the formulation hypothesis, in that breaking the crystalline forces by amorphization is instrumental to increasing the pharmaceutical properties of GHQ168 (**Figure 3**).

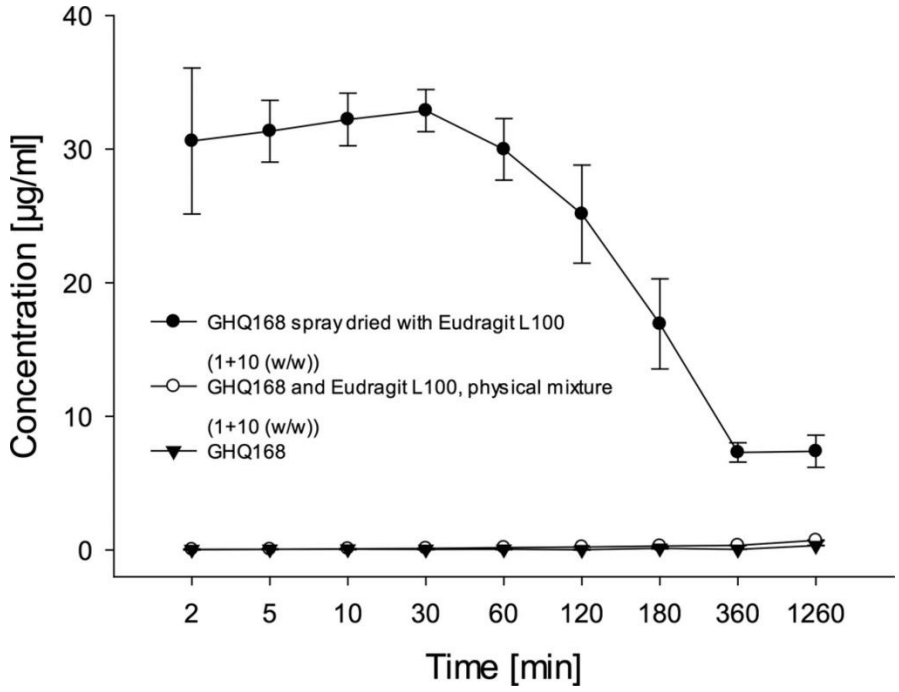


**Figure 3**: Solubility profile of the GHQ168 spray-dried formulation in comparison to that of the physical mixture of crystalline GHQ168 with Eudragit L100 and that of the crystalline raw substance.

The chemical strategy targeted solubility improvement by structural modification of GHQ168 (**Figure 4**) as follows (i). The introduction of basic moieties (tertiary amines) allowed salt formation, and the resulting GHQ243 and GHQ250 were presented as oxalate salts with a stoichiometry (active pharmaceutical ingredient (API) to oxalate) of 1:1 and 1:1.5, respectively. (ii) The introduction of a polar substituent, i.e., the replacement of a phenyl moiety with a pyridine ring, resulted in GHQ242 and GHQ237, again presented as oxalate salts with a stoichiometry (API to oxalate) of 1:1.5 and 1:0.5, respectively. (iii) The formation of the amidine of GHQ168 resulted in GHQ232, presented as a hydrochloride. (iv) The introduction of an additional carbonyl group in position 2 resulted in GHQ215, an acidic moiety.

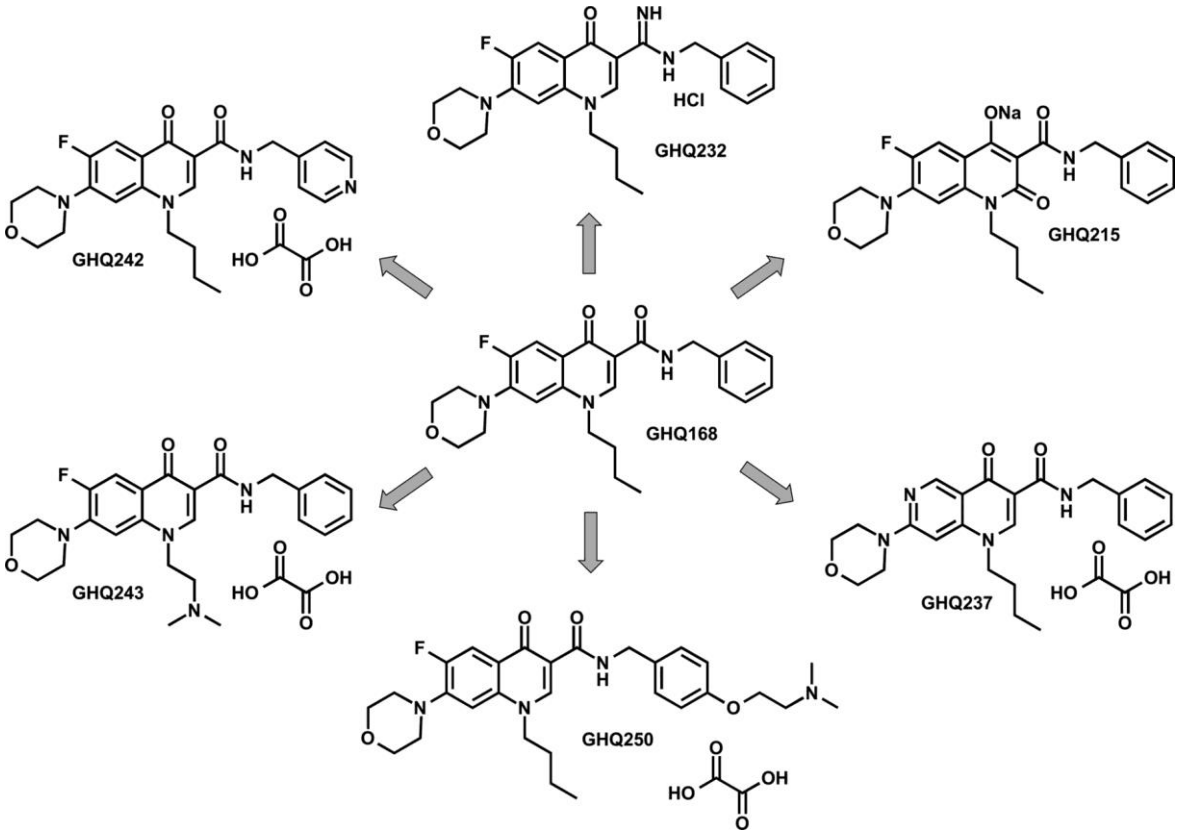


**Figure 4**: Structures of salt compounds newly synthesized for solubility enhancement.

Details of the synthesis pathways (including the experimental details) are described in the supplemental material. The introduction of a basic functionality in position 7, which is essential for the activity of the topoisomerase inhibitors in clinical treatment [24], always resulted in a substantially decreased activity against *T. b. brucei* and a lower selectivity index (SI; calculated as the 50% cytotoxic concentration for Vero cells divided by the 50% inhibitory concentration ($IC_{50}$) of the compound for T. cruzi cells) [9]. Thus, this position was not considered for the introduction of a basic substituent.

With the exception of GHQ215, the solubility of the compounds was enhanced by structure variations, particularly for the oxalate salts GHQ242, GHQ243, and GHQ250, as preliminarily assessed by light microscopy (**Table 1**). However, all new compounds were less active against *T. b. brucei* and, therefore, displayed a decreased selectivity index (**Table 1**), which was already reported previously [9]. The potentiometric determination of

the $pK_a$ of GHQ168 did not result in a measurable value between pH 2 and pH 12. After introduction of basic moieties, the $pK_a$ values of GHQ242 and GHQ243, the candidates chosen for use in *in vivo* efficacy studies, were 5.25 ± 0.05 and 6.86 ± 0.06, respectively (data not shown). We detailed the preliminary, microscopic assessment of solubility (**Table 1**) nephelometrically, with GHQ242 and GHQ243 having aqueous kinetic solubilities of 274 ± 18 µg/ml and 152 ± 1 µg/ml, respectively. Both had a statistically significant and improved kinetic solubility compared to that of GHQ168 (15 ± 1 µg/ml).

.

| Compound | Mol wt (g/mol) | LogP | Preliminary kinetic solubility (µM) | Melting point (°C) | Albumin binding (%) | $IC_{50}$ (µM) at | | $CC_{50}$[a] (µM) | | | |
|---|---|---|---|---|---|---|---|---|---|---|---|
| | | | | | | 48 h/72 h for *T. b. brucei* | 72 h for *T. b. rhodesiense* | L6 | J774.1A | HEK 293T | HepG2 |
| GHQ168[b] | 437.5 | 3.67 | < 19 | 171.4 | 80.5 | 0.047 ± 0.00/ 0.05 ± 0.01 | 0.001 ± 0.0006 | 47.2 ± 9.7 | 57 | 26.30 ± 5.35 | 47.04 ± 3.04 |
| GHQ237 | 420.5 | 3.05 | 100 | 178.1 | 67.6 ± 4.53 | 0.55 ± 0.08/ 1.02 ± 0.33 | 0.012 ± 0.0025 | > 95.2 | > 100 | > 160 | > 160 |
| GHQ242 | 438.5 | 1.74 | > 5000 | 149.0 | 99.95 ± 0.02 | 0.29 ± 0.26/ 0.76 ± 0.77 | 0.002 ± 0.0004 | 24.3 ± 4.2 | > 100 | 86.81 ± 6.43 | 153.31 ± 9.47 |
| GHQ243 | 452.5 | 2.67 | 1000 | 198.2, 223.0 | 45.9 ± 4.19 | 0.54 ± 0.01/ 0.63 ± 0.01 | 0.018 ± 0.0094 | 30.7 ± 7.4 | 42.3 | 48.03 ± 1.94 | 48.84 ± 0.12 |
| GHQ250 | 524.6 | 3.41 | > 5000 | 172.3 | 79.1 ± 7.42 | 2.89 ± 0.62/ 3.37 ± 0.29 | ND[c] | ND | 39.9 | 10.25 ± 1.56 | 13.12 ± 0.03 |
| GHQ232 | 436.5 | 3.47 | 100 | > 300 | 85.8 ± 5.27 | 9.08 ± 0.12/ 15.05 ± 1.79 | ND | ND | 39.1 | 13.98 ± 0.64 | 19.34 ± 2.91 |
| GHQ215 | 453.5 | 5.53 | 10 | > 300 | ND | 3.08 ± 0.69/ 5.73 ± 0.91 | ND | ND | > 100 | 26.59 ± 5.29 | > 160 |

[a]$CC_{50}$, 50% cytotoxic concentration

[b]Most of the data for GHQ168 were already reported in reference [9] (see compound 29)

[c]ND, not determined

**Table 1**: Physicochemical and microbiological data for quinolone amide compounds.

**Albumin binding, metabolism, plasma stability, mutagenicity, and transepithelial transport**

Albumin binding was determined by a continuous titration method [11, 27]. Whereas GHQ168 and GHQ243 were 81% and 46% bound to albumin, respectively, GHQ242 was completely bound to albumin at a level exceeding 99% (**Table 1**). Since GHQ168 was found to be the most active compound *in vivo* (see below), the oxidative metabolism of GHQ168 was studied. The HPLC-MS full scan analysis revealed 4 peaks (at m/z 454, at m/z 412, and twice at m/z 348) not observed in control reactions. The m/z results suggested metabolites resulting from ring hydroxylation, β-oxidation, and *N*-dearylation, respectively. Although linear NADPH generation and the activity of microsomal enzymes for 90 min were assessed (data not shown), the decrease in the GHQ168 concentration did not differ significantly after 30, 60, and 90 min (4.7% ± 0.9%), indicating enzyme inhibition by GHQ168 or one of its metabolites. Concerning stability in plasma, no degradation was observed throughout 2 h for GHQ168, GHQ242, and GHQ243.

The mutagenicity of GHQ168 in cultured V79 cells was assessed in the HPRT assay. In light of the GHQ168-mediated inhibition of microsomal enzyme activity and the absence of metabolites with a structural alert for mutagenicity (such as catechols), the HPRT assay was performed in the absence of a metabolically activating system. GHQ168 was tested at concentrations ranging from 2 to 47 µM, and it significantly decreased the plating efficiency and cell numbers at 47 µM and 16 to 47 µM, respectively, as determined by previously described protocols [28]. Whereas the known mutagen NQO caused a significant increase in the mutant frequency to 186 ± 42 compared to that for control cells (9 ± 3), the mutant frequency was not affected by treatment with any concentration of GHQ168.

In light of future profiling of the compounds, GHQ168, GHQ242, and GHQ243 were tested for transepithelial transport. GHQ168, GHQ242, and GHQ243 had a flux through Caco-2 cell monolayers (as an *in vitro* model for intestinal absorption) comparable to that for the

positive control, propranolol HCl (see **Figure S4** and **Table S2** in the supplemental material). On the basis of the previously demonstrated low solubility and the good permeation observed with the Caco-2 cell monolayer assay, in the absence of information from *in vivo* studies, GHQ168 can only preliminarily be categorized as Biopharmaceutics Classification System (BCS) class II (low solubility, high permeation).

**Cell toxicity and *in vitro* efficacy**

GHQ168 as well as the new derivatives were characterized for their physicochemical properties (logP, kinetic solubility, melting point) as well as albumin binding, their activity against *T. b. brucei* and *T. b. rhodesiense* (72 h), and their cytotoxicity (muscle cells, macrophages, kidney cells, and hepatocytes), which are displayed in **Table 1**. On the basis of the solubility results and demonstrated *in vitro* efficacy, spray-dried GHQ168 and the oxalate salts of GHQ242 and GHQ243 were selected for use in *in vivo* efficacy studies.

**Pharmacokinetics**

During the efficacy study with the stringent mouse model, blood samples were collected from the surviving mice at three time points and analyzed by LC/MS/MS (**Figure 5**; see also **Figure S7** in the supplemental material). Blood concentrations were about 10-fold higher for GHQ168 (delivered from the spray-dried formulation) and GHQ243 than for GHQ242. An unusual time response of the blood concentration of GHQ242 was observed among the mice. Two of the four mice tested within the GHQ242 group had higher blood concentrations at a subsequent time point than a previous one (see **Figure S7** in the supplemental material; data for these 2 mice are highlighted by arrows). The half-lives of GHQ168 and GHQ243 were comparable, ranging from approximately 1.5 to 3.5 h (**Table 2**). The pharmacokinetic outcome for GHQ242 was more heterogeneous (see above), such that we cannot decide whether the blood concentrations analyzed 16 h after application were due to metabolism of the compound or due to flip-flop

kinetics. In fact, the half-life reported for GHQ242 may reflect metabolism or may reflect another step, such as drug release from a precipitate formed during i.p. injection. As the data obtained were insufficient to clarify this question (data obtained after intravenous (i.v.) administration would be required), we did not calculate the apparent clearance or the apparent volume of distribution for GHQ242, as in the absence of a clear assignment of the terminal half-life to elimination for this compound, possible conclusions may very well be prone to misinterpretation. However, the apparent clearance and the apparent volume of distribution were similar for GHQ168 and GHQ243 (**Table 2**).

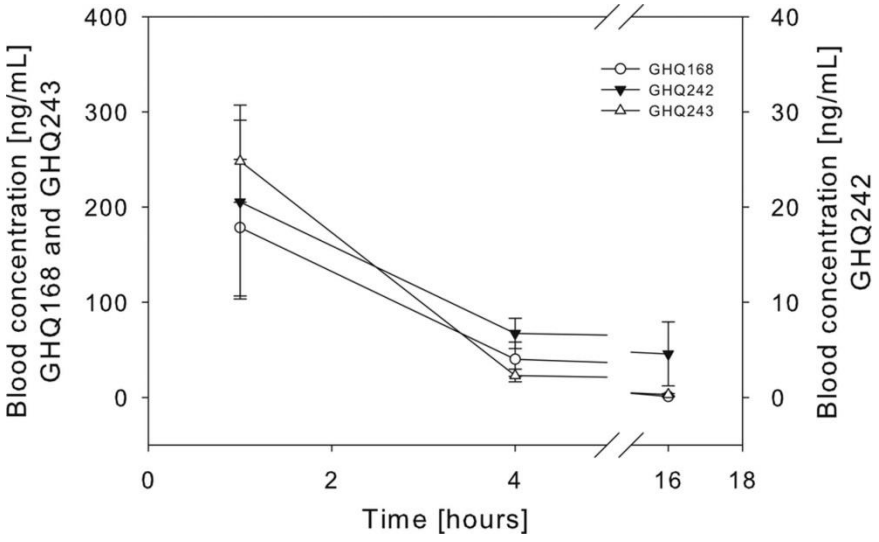


**Figure 5**: Mean blood concentration-versus-time profile ± SD.

| Compound | Mouse no. | $t_{1/2}$ (h) | CL (ml/h) | *V* (liters/kg BW) | $AUC_{0-\infty}$ (ng · h/ml) |
|---|---|---|---|---|---|
| GHQ168 | 1 | 1.6 | 93 | 8 | 945 |
| | 2 | 2.3 | 118 | 15 | 742 |
| | 3 | 2.6 | 125 | 19 | 701 |
| GHQ242 | 1 | * | * | * | * |
| | 2 | 3.7 | 4792 | 1014 | 120 |
| | 3 | 23 | 4232 | 5608 | 135 |
| | 4 | 2.3 | 2.686 | 357 | 213 |
| GHQ243 | 1 | 2.4 | 402 | 55 | 1350 |
| | 2 | 3.1 | 819 | 148 | 663 |
| | 3 | 2.3 | 693 | 92 | 784 |
| | 4 | 1.8 | 830 | 86 | 6542 |

[a] $t_{1/2}$, half-life; CL, clearance; *V*, volume of distribution; BW, body weight; $AUC_{0-\infty}$, area under the concentration-time curve from time zero to infinity

*calculation of PK parameters was not possible due to flip-flop kinetics

**Table 2**: PK parameters for GHQ168, GHQ242, and GHQ243[a].

### *In vivo* efficacy studies

The dose and its regimen were simulated through PBPK modeling prior to *in vivo* studies (see **Figure S5A to C** in the supplemental material). Two *in vivo* models were used and are referred to as the stringent mouse model, in which 8 doses were administered twice daily throughout days 3 to 6 postinfection, and the early-treatment model, in which 8 doses were administered twice daily throughout days 1 to 4. Treatment with all three compounds tested, especially GHQ168, showed *in vivo* activity, whereas no treatment did not (**Figure 6A**). All infected mice treated with compound GHQ168 were free of parasites for 10 days (tail blood examinations; microscopy test) and relapsed on day 14. One mouse treated with GHQ168 died after the 5th treatment without parasitemia. Test animals treated with compounds GHQ242 and GHQ243 did not show parasitemia on day 7 but relapsed on day 10 (GHQ242) and day 14 (GHQ243) postinfection. The mean survival durations (MSDs) of mice in the study with the stringent mouse model and medicated with GHQ168, GHQ242, GHQ243, and the control treatment were 17, 14, 12, and 9 days, respectively (**Table 3**), meaning that statistically significant differences were

observed for GHQ168 versus the control ($P < 0.001$), whereas insignificant results were obtained for GHQ242 and GHQ243 versus the control.

| **Study model** | **Compound** | **Treatment period (days) postinfection** | **Dose (mg/kg b.i.d.[a])** | **No. of mice cured/ no. infected** | **MSD[b]** | **MRD[c]** |
|---|---|---|---|---|---|---|
| Stringent | Control | | | 0/4 | 9 | |
| | GHQ168 | 3–6 | 3.5 | 0/4[d] | 17 | 14 |
| | GHQ242 | 3–6 | 22.9 | 0/4 | 14 | 10 |
| | GHQ243 | 3–6 | 21.7 | 0/4 | 12 | 11 |
| Early treatment | Control | | | 0/4 | 7 | |
| | GHQ168 | 1–4 | 3.5 | 3/6[e] | > 32 | > 32 |

[a]b.i.d., twice a day

[b]MSD, mean survival duration (days postinfection)

[c]MRD, mean relapse duration (days), where relapse is defined as the presence of parasites in blood

[d]One mouse died during the treatment but did not have parasites in its blood. Data for mice that died during the treatment but without parasites were excluded from the calculation of MSD and MRD, as the cause of death was unrelated to parasitemia

[e]Three mice died during and after the treatment but did not have parasites in their blood. Data for mice that died during the treatment but without parasites were excluded from the calculation of MSD and MRD, as the cause of death was unrelated to parasitemia

**Table 3**: Trial design and results of the *in vivo* efficacy studies.

On the basis of this outcome and corroboration of the results with those of the *in vitro* microbiological assays, GHQ168 was further profiled in the early-treatment model (**Figure 6B**). GHQ168 administration prevented parasitemia in all animals (**Figure 6B**). However, one mouse died after the 5th dose and two mice died after the 8th dose but showed no external signs of toxicity or parasitemia. The MSDs for the three remaining mice were > 32 days (end of study; all surviving mice were free of parasites, as determined by tests of tail blood). This resulted in statistically significant differences in the MSD for GHQ168 versus that for the control ($P < 0.001$). A similar efficacy of melarsoprol (2 mg/kg) and

pentamidine isethionate (5 mg/kg) was reported in previous studies for surviving mice [28]. However, in this study, the mice were infected with *T. b. brucei*.

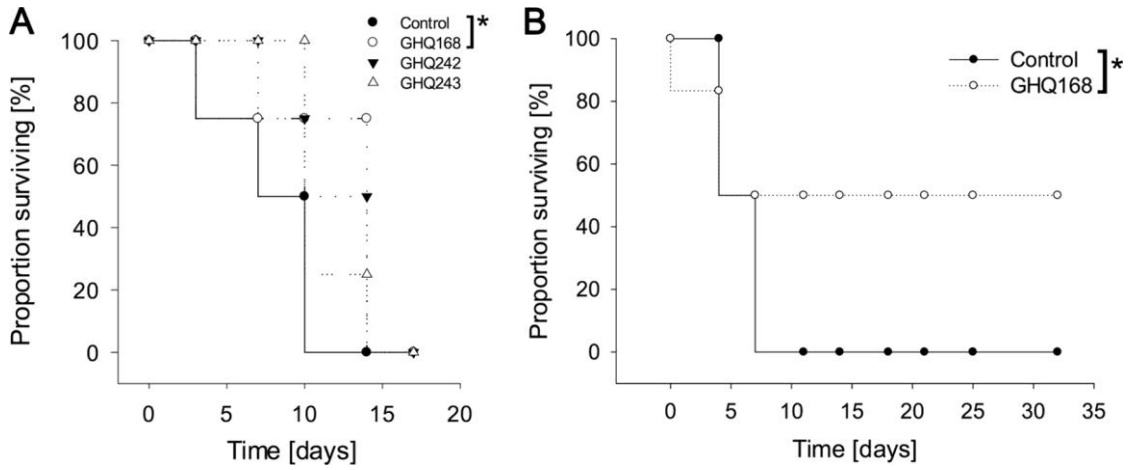


**Figure 6A**: Activities of GHQ168, GHQ242, and GHQ243 in the stringent mouse model (n = 4). Statistically significant differences in MSD between the group treated with GHQ168 (17 days) and the control group (9 days) were observed ($P < 0.001$).

**Figure 6B**: Mice treated with GHQ168 in the easy-to-cure mouse model (n = 6). Again, statistically significant differences in MSD were observed between the two groups ($P < 0.001$).

## Discussion

In a previous study, a morpholino-substituted quinolone amide (**Figure 1**) was identified to be highly active against *T. b. brucei* and *T. b. rhodesiense* [9]. However, this substance was practically insoluble in aqueous media (**Table 1**), thereby making *in vivo* studies challenging. Thus, the aim of the study reported here was to overcome the solubility limitations and to characterize the compound class concerning physicochemical and biological properties as well as profiling these in *in vivo* pharmacokinetic and efficacy experiments for the first time.

The solubility could be enhanced by using an appropriate formulation (**Figure 3**) as well as by making structural variations to the hit/lead compound (**Figure 4**). The introduction of amino functions as well as the replacement of phenyl rings with pyridine rings especially resulted in compounds with lower lipophilicities and, hence, increased solubilities, and the oxalate salts of the active bases particularly increased the solubility. However, the solubility enhancement by these structural modifications was achieved at the expense of activity, i.e., a decrease of the $IC_{50}$s of at least 10-fold toward *T. b. brucei* (**Table 1**). Since the cytotoxicity, determined in L6 cells, macrophages, kidney cells, and hepatocytes (**Table 1**), was found to be almost equal to or even higher than that of the lead compound, the selectivity deteriorated. Nevertheless, compounds GHQ242 and GHQ243 were considered for use in *in vivo* studies because both substances showed (i) rather high levels of activity against *T. b. rhodesiense* ($IC_{50}$s, 2 nM and 18 nM for GHQ242 and GHQ243, respectively, after 72 h), (ii) low cytotoxicity, and (iii) sufficient solubility, as determined by PBPK modeling. Since GHQ168 still ranked among the most active compounds with an $IC_{50}$ value (72 h) of 1 nM against *T. b. rhodesiense*, a formulation improving the kinetic solubility by a factor of 6000 was developed (**Figure 3**), thereby opening this promising compound to efficacy studies. The spray-drying technology has been applied industrially for decades, and in the meantime, spray drying has become

a well-understood process that is easily scaled up from developmental batch sizes. The spray drying of GHQ168 was a robust and efficient process, facilitating the amorphization of the drug substance while maintaining its stability in Eudragit L100. In order to avoid the use of blood concentration-time levels beyond the therapeutic window, the corresponding doses for the *in vivo* studies for intraperitoneal administration as well as the study design were predicted by means of PBPK simulations.

Since pharmacokinetic properties govern the activities of drugs, the most important properties were evaluated. Whereas GHQ168 and GHQ243 exhibited high and moderate levels of human serum albumin binding (81% and 46%), an almost exhaustive albumin binding was found for GHQ242. Therefore, the fraction unbound was very low for GHQ242, and provided that the dissociation kinetics (which were not determined) are slow, this pattern may potentially challenge the use of this compound in the future, at least for parenteral use. Interestingly, the pharmacokinetic profile of GHQ242 reflected observations analogous to those found for albumin binding. In spite of the fact that the same dose (in moles) of GHQ242 as GHQ168 and GHQ243 was applied, PK concentrations were roughly 10-fold lower upon i.p. administration. Possible explanations for this low PK concentration profile include (i) local precipitation upon i.p. injection (suggested by the fluctuating PK profile [see below]) or (ii) extensive binding to the extracellular matrix and other surfaces at the site of injection and/or at other sites (suggested by the albumin binding (see above)), or (iii) both. One may speculate that the initially paradox observation that following GHQ242 administration some blood concentrations exceeded those in previous samples reflects slow drug release from precipitated drug following i.p. injection. Further studies, including analysis of pharmacokinetic profiles following i.v. administration, are required to detail these findings. However, in light of the possibility of GHQ242 precipitation at the injection site, the half-life calculated from the pharmacokinetic profile (**Figure 5**; see also **Figure S7** in the supplemental material) might not reflect metabolism (i.e., the elimination half-life) but

might reflect the slow release of molecules from the GHQ242 precipitate at the injection site (the half-life of molecules being released from the precipitate). With that in mind, we did not calculate the apparent clearance and apparent volume of distribution for GHQ242 because, since data from i.v. profiles were missing, we were unable to clearly assign the terminal half-life to metabolism or drug release kinetics from a possible precipitate formed upon administration. These pharmacokinetic data sets indicated that the successful development of GHQ242 as a parenteral form is more risky than the development of GHQ168 or GHQ243 as a parenteral form. However, GHQ242 may be successfully presented as an oral formulation, thereby overcoming the possibility of local precipitation upon injection. The possible successful use of GHQ242 as an oral formulation was also suggested by the permeation results from the Caco-2 cell monolayer studies (see **Figure S4** in the supplemental material).

The target site of these compounds is still unknown. Previously performed studies point to the kinetoplast as a possible target, as these quinolone amide derivatives impact kinetoplast segregation [9]. However, sensitivity measurements with acriflavine-induced dyskinetoplastic *T. b. brucei* revealed a decrease of the $IC_{50}$, but the $IC_{50}$ was still in the low micromolar range (data not shown), indicating that the compounds are still highly active and may address another lethal target. This remains to be elucidated.

GHQ168 and its related molecules differ from the available quinolones marketed today, in that the free carboxyl group of the marketed quinolones is derivatized and therefore does not address the topoisomerase target in trypanosomes. Due to the absence of the carboxyl group in GHQ168, this compound might be associated with fewer or no side effect issues due to the complexation of $Mg^{2+}$ and $Ca^{2+}$; this will need to be experimentally confirmed in future studies.

The small number of animals exposed to these novel quinolones is a limitation of this study. Therefore, positive trends may be assumed from the data sets, but larger studies need to be performed to corroborate the findings and to obtain a final conclusion.

As pointed out above, no final conclusion regarding the pharmacokinetic profile for GHQ242 can be drawn, as flip-flop kinetics may have occurred due to the possible precipitation of the i.p. administered molecule. Lastly, the solubility challenges for GHQ168 observed during the serum albumin binding studies render the outcome of this experiment for this compound questionable.

The *in vivo* studies suggested a statistically significant impact of GHQ168 on the mean survival time compared to that for the untreated controls in both efficacy studies (**Figure 6A and B**). However, statistical calculations based on the small data set are critical and require careful interpretation. Future studies need to confirm the evidence provided here. Following i.p. administration of GHQ168, this test substance kept the mice free of parasites over a period of 14 days, on average (stringent mouse model), and over more than 32 days (easy-to-cure model). However, some mice without parasitemia died during the treatment period. Although no external signs of toxicity were observed in the efficacy studies (and in the PK studies), future studies need to detail the cause of these events. GHQ242 and GHQ243 had a positive trend on the MSD, but the outcome was not significantly different from that for the control (**Figure 6A**). This observation suggests that GHQ242's 10 times higher *in vitro* activity against *T. b. rhodesiense* than that of GHQ243 (**Table 1**) compensated for its 10 times lower exposure than that of GHQ243 (**Table 2**, area under the concentration-time curve).

In conclusion, the quinolone amide skeleton was found to be a promising starting point for the development of highly active antitrypanosomal compounds. This study identified a lead compound with promising pharmacokinetic properties and efficacy, in that curing of *T. b. rhodesiense*-infected mice was achieved. The development of even more active compounds and compounds with greater solubility by variation of the skeleton is in progress, as is the search for the detailed mode of action.

## Acknowledgements

We thank Elena Katzowitsch and Tobias Ölschläger (Institute for Molecular Infection Biology, University of Würzburg) for the cytotoxicity screening, Jennifer Rath and Antje Fuss (Medical Mission Institute, Würzburg, Germany) for testing the compounds against *T. b. brucei*, Alena Zikova (University of South Bohemia, Czech Budejovice, Czech Republic) for the dyskinetoplast experiments, Annette Albrecht (Institute of Pharmacy and Food Chemistry, University of Würzburg) for testing GHQ168 in the HPRT assay, Marius Gareis (Institute of Pharmacy and Food Chemistry, University of Würzburg) for performing the studies on the oxidative metabolism of GH168, and Lena Lauber for support with the Caco-2 cell assays. V79 cells were kindly provided by H. Glatt, German Institute of Human Nutrition, Potsdam, Germany.

We gratefully acknowledge the Deutsche Forschungsgemeinschaft (SFB 630) and the Bayerische Forschungsstiftung (grant Springs and Parachutes) for financial support, as well as ACC GmbH (Analytical Clinical Concepts GmbH, Leidersbach, Germany) for financial support, support with statistics (Volker Guth), and support with analytical work (Martin Barkworth).

We declare no conflict of interest.

## Funding Information

This work, including the efforts of Nina Hecht, was funded by ACC GmbH. This work, including the efforts of Heike Bruhn, Alexander Hoerst, and Georg Hiltensperger, was funded by Deutsche Forschungsgemeinschaft (DFG) (SFB 630). This work, including the efforts of Nina Hecht and Jens-Christoph Rybak, was funded by Bayerische Forschungsstiftung (Bavarian Research Foundation) (Springs and Parachutes).

Financial support (consumables) and equipment were received from the funding sources.

## References

[1] Franco JR, Simarro PP, Diarra A, Jannin JG. 2014. Epidemiology of human African trypanosomiasis. Clin Epidemiol 6:257–275. http://dx.doi.org/10.2147/CLEP.S39728.

[2] Stich A, Ponte-Sucre A, Holzgrabe U. 2013. Do we need new drugs against human African trypanosomiasis? Lancet Infect Dis 13:733–734. http://dx.doi.org/10.1016/S1473-3099(13)70191-9.

[3] Pena I, Pilar Manzano M, Cantizani J, Kessler A, Alonso-Padilla J, Bardera AI, Alvarez E, Colmenarejo G, Cotillo I, Roquero I, de Dios-Anton F, Barroso V, Rodriguez A, Gray DW, Navarro M, Kumar V, Sherstnev A, Drewry DH, Brown JR, Fiandor JM, Julio Martin J. 2015. New compound sets identified from high throughput phenotypic screening against three kinetoplastid parasites: an open resource. Sci Rep 5:8771. http://dx.doi.org/10.1038/srep08771.

[4] Maser P, Wittlin S, Rottmann M, Wenzler T, Kaiser M, Brun R. 2012. Antiparasitic agents: new drugs on the horizon. Curr Opin Pharmacol 12:562–566. http://dx.doi.org/10.1016/j.coph.2012.05.001.

[5] Bringmann G, Hoerr V, Holzgrabe U, Stich A. 2003. Antitrypanosomal naphthylisoquinoline alkaloids and related compounds. Pharmazie 58:343–346.

[6] Nenortas E, Kulikowicz T, Burri C, Shapiro TA. 2003. Antitrypanosomal activities of fluoroquinolones with pyrrolidinyl substitutions. Antimicrob Agents Chemother 47:3015–3017. http://dx.doi.org/10.1128/AAC.47.9.3015-3017.2003.

[7] Keiser J, Burri C. 2001. Evaluation of quinolone derivatives for antitrypanosomal activity. Trop Med Int Health 6:369–389. http://dx.doi.org/10.1046/j.1365-3156.2001.00713.x.

[8] Ma X, Zhou W, Brun R. 2009. Synthesis, *in vitro* antitrypanosomal and antibacterial activity of phenoxy, phenylthio or benzyloxy substituted quinolones. Bioorg Med Chem Lett 19:986–989. http://dx.doi.org/10.1016/j.bmcl.2008.11.078.

[9] Hiltensperger G, Jones NG, Niedermeier S, Stich A, Kaiser M, Jung J, Puhl S, Damme A, Braunschweig H, Meinel L, Engstler M, Holzgrabe U. 2012. Synthesis and structure-activity relationships of new quinolonetype molecules against Trypanosoma brucei. J Med Chem 55:2538–2548. http://dx.doi.org/10.1021/jm101439s.

[10] Lipinski CA, Lombardo F, Dominy BW, Feeney PJ. 2001. Experimental and computational approaches to estimate solubility and permeability in drug discovery and development settings. Adv Drug Deliv Rev 46:3–26. http://dx.doi.org/10.1016/S0169-409X(00)00129-0.

[11] Heinze A, Holzgrabe U. 2006. Determination of the extent of protein binding of antibiotics by means of an automated continuous ultrafiltration method. Int J Pharm 311:108 –112. http://dx.doi.org/10.1016/j.ijpharm.2005.12.022.

[12] Hubatsch I, Ragnarsson EG, Artursson P. 2007. Determination of drug permeability and prediction of drug absorption in Caco-2 monolayers. Nat Protoc 2:2111–2119. http://dx.doi.org/10.1038/nprot.2007.303.

[13] Räz B, Iten M, Grether-Buhler Y, Kaminsky R, Brun R. 1997. The Alamar Blue assay to determine drug sensitivity of African trypanosomes (*T. b. rhodesiense* and *T. b. gambiense*) *in vitro*. Acta Trop 68:139–147. http://dx.doi.org/10.1016/S0001-706X(97)00079-X.

[14] Papadopoulou MV, Bloomer WD, Lepesheva GI, Rosenzweig HS, Kaiser M, Aguilera-Venegas B, Wilkinson SR, Chatelain E, Ioset JR. 2015. Novel 3-nitrotriazole-based amides and carbinols as bifunctional antichagasic agents. J Med Chem 58:1307–1319. http://dx.doi.org/10.1021/jm5015742.

[15] Larson EM, Doughman DJ, Gregerson DS, Obritsch WF. 1997. A new, simple, nonradioactive, nontoxic *in vitro* assay to monitor corneal endothelial cell viability. Invest Ophthalmol Vis Sci 38:1929–1933.

[16] Muth M, Hoerr V, Glaser M, Ponte-Sucre A, Moll H, Stich A, Holzgrabe U. 2007. Antitrypanosomal activity of quaternary naphthalimide derivatives. Bioorg Med Chem Lett 17:1590–1593. http://dx.doi.org/10.1016/j.bmcl.2006.12.088.

[17] Bradley MO, Bhuyan B, Francis MC, Langenbach R, Peterson A, Huberman E. 1981. Mutagenesis by chemical agents in V79 Chinese hamster cells: a review and analysis of the literature. A report of the Gene-Tox Program. Mutat Res 87:81– 142.

[18] Schumacher DM, Metzler M, Lehmann L. 2005. Mutagenicity of the mycotoxin patulin in cultured Chinese hamster V79 cells, and its modulation by intracellular glutathione. Arch Toxicol 79:110–121. http://dx.doi.org/10.1007/s00204-004-0612-x.

[19] Di L, Kerns EH, Hong Y, Chen H. 2005. Development and application of high throughput plasma stability assay for drug discovery. Int J Pharm 297:110–119. http://dx.doi.org/10.1016/j.ijpharm.2005.03.022.

[20] Jones HM, Gardner IB, Watson KJ. 2009. Modelling and PBPK simulation in drug discovery. AAPS J 11:155–166. http://dx.doi.org/10.1208/s12248-009-9088-1.

[21] Poulin P, Theil FP. 2002. Prediction of pharmacokinetics prior to *in vivo* studies. II. Generic physiologically based pharmacokinetic models of drug disposition. J Pharm Sci 91:1358–1370. http://dx.doi.org/10.1002/jps.10128.

[22] Poulin P, Theil FP. 2002. Prediction of pharmacokinetics prior to *in vivo* studies. 1. Mechanism-based prediction of volume of distribution. J Pharm Sci 91:129–156. http://dx.doi.org/10.1002/jps.10005.

[23] Berezhkovskiy LM. 2004. Volume of distribution at steady state for a linear pharmacokinetic system with peripheral elimination. J Pharm Sci 93:1628–1640. http://dx.doi.org/10.1002/jps.20073.

[24] Berezhkovskiy LM. 2004. Determination of volume of distribution at steady state with complete consideration of the kinetics of protein and tissue binding in linear pharmacokinetics. J Pharm Sci 93:364–374. http://dx.doi.org/10.1002/jps.10539.

[25] Brun R, Schumacher R, Schmid C, Kunz C, Burri C. 2001. The phenomenon of treatment failures in human African trypanosomiasis. Trop Med Int Health 6:906– 914. http://dx.doi.org/10.1046/j.1365-3156.2001.00775.x.

[26] Williams RO, III, Watts AB, Miller DA. 2012. Formulating poorly water soluble drugs. Springer, New York, NY.

[27] Ponte-Sucre A, Gulder T, Wegehaupt A, Albert C, Rikanovic C, Schaeflein L, Frank A, Schultheis M, Unger M, Holzgrabe U, Bringmann G, Moll H. 2009. Structure-activity relationship and studies on the molecular mechanism of leishmanicidal N,C-coupled arylisoquinolinium salts. J Med Chem 52:626–636. http://dx.doi.org/10.1021/jm801084u.

[28] Milliken GA, Johnson DE. 2009. Analysis of messy data: designed experiments. Chapman & Hall/CRC, Boca Raton, FL.

[29] Baltz T, Baltz D, Giroud C, Crockett J. 1985. Cultivation in a semidefined medium of animal infective forms of *Trypanosoma brucei, T. equiperdum, T. evansi, T. rhodesiense* and *T. gambiense*. EMBOJ 4:1273–1277.

# Supplementing Information

## Syntheses

The compounds A, B, C, D, GHQ168, H, I, J, P, Q, R have already been published and can be found in refs 1, 2, 3, 4, 5, 6, 7, and 8.

### Synthesis of *N*-Benzyl-1-butyl-6-fluoro-7-morpholino-4-oxo-1,4-dihydroquinoline-3-carboxamide (GHQ168)

*Synthesis of Diethyl 2-(((3-chloro-4-fluorophenyl)amino)methylene)malonate (A)* [1]

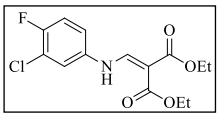

A solution of 5.00 g (34.4 mmol) 3-chloro-4-fluoroaniline, 8.91 g (41.2 mmol, 8.33 ml) diethyl ethoxymethylenemalonate and 5 Weflon®-discs were heated to 110 °C under microwave irradiation (heat-up rate: in 3 min to 110 °C, 800 W). After 1 h at 110 °C the solvent was removed under reduced pressure and the remaining oil was dissolved in 50 ml *n*-hexane. After storing the solution at -20 °C overnight the white precipitate was filtered off, washed with cold *n*-hexane and dried in vacuo.

Yield: 10.8 g (34.2 mmol, 99%), mp: 60 - 62 °C (*n*-hexane).

Spectroscopical data were consistent with literature [1].

*Synthesis of Ethyl 7-chloro-6-fluoro-4-hydroxyquinoline-3-carboxylate (B)* [1]

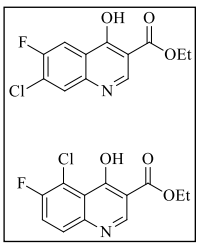

10.0 g (31.7 mmol) of diethyl 2-(((3-chloro-4-fluorophenyl)-amino)methylene)malonate (A) were dissolved in 5 ml $Ph_2O$. After addition of 3 Weflon®-discs the mixture was heated to 210 °C for 15 min under microwave irradiation (heat-up rate: in 5 min to 210 °C, 800 W). The resulting suspension was cooled to rt, diluted with 100 ml $Et_2O$ and stirred for 1 h. The light grey solid was filtered off, washed with $Et_2O$ and dried in vacuo to give the desired regioisomer in a 10:1 ratio.

Yield: 5.26 g (19.5 mmol, 62%), mp: 315 - 318 °C ($Ph_2O$).

Spectroscopical data were consistent with literature [1].

*Synthesis of 1-Butyl-7-chloro-6-fluoro-4-oxo-1,4-dihydroquinoline-3-carboxylic acid (C)* [2]

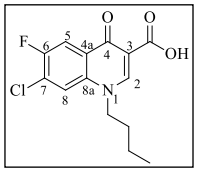

1.00 g (3.71 mmol) ethyl 7-chloro-6-fluoro-4-hydroxyquinoline-3-carboxylate (B) and 2.56 g (18.5 mmol) $K_2CO_3$ were suspended in 20 ml anhydrous DMF and heated to 60 °C for 1 h. 3.05 g (22.3 mmol, 2.38 ml) 1-bromobutane and a catalytic amount of KI were added and the mixture was stirred at 100 °C for 24 h. The solvent was removed in vacuo and the residue was partitioned between 60 ml water and 50 ml EA. After separation the aqueous layer was extracted with EA (3 x 50 ml). The combined organic layers were dried over $Na_2SO_4$, concentrated in vacuo and the crude ester was purified by normal phase column chromatography on silica gel ($CHCl_3$/*i*PrOH 150:1, $R_f$: 0.33). The resulting white solid was suspended in 45 ml of aqueous KOH-solution (3 M) and 5 ml EtOH and refluxed for 20 h. After cooling to rt the clear solution was acidified (pH = 3 - 4) with aqueous HCl-solution (2 M). The white precipitate was filtered off and recrystallized from EtOH.

Yield: 960 mg (3.23 mmol, 87%), mp: 233 - 235 (EtOH).

Spectroscopical data were consistent with literature [2].

*Synthesis of 1-Butyl-6-fluoro-7-morpholino-4-oxo-1,4-dihydroquinoline-3-carboxylic acid (D)* [2]

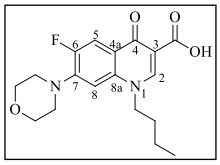

200 mg (672 µmol) 1-butyl-7-chloro-6-fluoro-4-oxo-1,4-dihydroquinoline-3-carboxylic acid (C) were dissolved in 10 ml morpholine and heated to 110 °C for 4 h under microwave irradiation (heat-up rate: in 4 min to 110 °C, 600 W). The mixture was diluted with 30 ml water and acidified (pH = 5) with aqueous HCl-solution (2 M). The precipitate was collected by filtration and recrystallized form EtOH/$CHCl_3$ to give a light yellow solid.

Yield: 160 mg (459 µmol, 68%), mp: 242 - 243 °C (EtOH/$CHCl_3$).

Spectroscopical data were consistent with literature [2].

*Synthesis of N-Benzyl-1-butyl-6-fluoro-7-morpholino-4-oxo-1,4-dihydroquinoline-3-carboxamide (GHQ168)* [2]

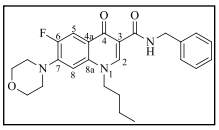

To a cooled solution (0 °C) of 150 mg (431 µmol) 1-butyl-6-fluoro-7-morpholino-4-oxo-1,4-dihydroquinoline-3-carboxylic acid (D) and 218 mg (2.15 mmol, 237 µl) NMM in 10 ml anhydrous DMF 235 mg (1.72 mmol, 223 µl) isobutyl chloroformate were added dropwise under argon atmosphere. After 1 h at 0 °C 185 mg (2.90 mmol, 188 µl) benzylamine were added and stirring at rt was continued for 45 min. The solvent was removed in vacuo and the crude product was purified via normal phase column chromatography on silica gel ($CHCl_3$/MeOH 100:1, $R_f$: 0.79) followed by recrystallization from EA.

Yield: 135 mg (309 µmol, 72%), mp: 157 - 159 (EA).

Spectroscopical data were consistent with literature [2].

**Synthesis of N-Benzyl-1-butyl-6-fluoro-7-morpholino-4-oxo-1,4-dihydroquinoline-3-carboximidamide hydrochloride (GHQ232)**

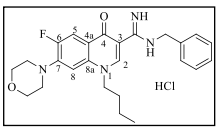

200 mg (457 µmol) *N*-Benzyl-1-butyl-6-fluoro-7-morpholino-4-oxo-1,4-dihydroquinoline-3-carboxamide (GHQ168) were dissolved in 4 ml $POCl_3$ and warmed to 40 °C for 24 h. The solution was diluted with 20 ml toluene and concentrated to dryness in vacuo. The residue was dissolved in 10 ml anhydrous ACN under argon atmosphere and cooled to 0 °C. A separately prepared solution of 49 mg (914 µmol) $NH_4Cl$ and 118 mg (914 µmol, 159 µl) DIPEA dissolved in 5 ml anhydrous ACN, which was stirred at rt for 30 min under argon atmosphere, was added dropwise and the combined mixture was stirred at 0 °C for 3 h. After dilution with 20 ml water the pH value was adjusted to 8 - 9 using conc. $NH_3$-solution and the aqueous mixture was

extracted with DCM (4 x 30 ml). The combined organic layers were dried over $Na_2SO_4$ and concentrated in vacuo. The crude product was purified by means of normal phase column chromatography on silica gel ($CHCl_3$/MeOH/conc. $NH_3$ 100:10:1, $R_f$: 0.31). The obtained solid was dissolved in 10 ml THF and treated with 1 ml of isopropanolic HCl-solution in order to achieve the corresponding hydrochloride salt. The resulting precipitate was filtered off and recrystallized from ACN/MeOH to give the desired product as a light yellow solid.

Yield: 56 mg (118 µmol, 26%), mp: 311 - 312 °C (ACN/MeOH),

**IR** (ATR, $\tilde{\nu}$ [$cm^{-1}$]): 3223 (w), 3113 (w), 3060 (w), 2965 (w), 2872 (w), 1644 (s), 1626 (m), 1557 (m), 1509 (s), 1449 (m), 1370 (m), 1255 (s), 1118 (m), 929 (m), 823 (m), 737 (w), 694 (m).

**$^1$H-NMR** (DMSO-$d_6$, δ [ppm], *J* [Hz]): 9.93 (s, 1H, CN**H**$_2$NHR$^+$), 9.67 (t, 1H, $^3J$ = 5.6, $CNH_2N$**H**$R^+$), 9.47 (s, 1H, CN**H**$_2$NHR$^+$), 9.34 (s, 1H, **H**-2), 8.56 (d, 1H, $^3J_{\mathbf{H,F}}$ = 15.0, **H**-5), 7.42-7.25 (m, 5H, benzyl-C**H**$_{arom.}$), 7.20 (d, 1H, $^4J_{\mathbf{H,F}}$ = 7.7, **H**-8), 4.59 (t, 2H, $^3J$ = 7.4, NC**H**$_2CH_2CH_2CH_3$), 4.51 (d, 2H, $^3J$ = 5.6, benzyl-C**H**$_2$), 3.82-3.80 (m, 4H, morpholino-C**H**$_2$-O-C**H**$_2$), 3.41-3.38 (m, 4H, morpholino-C**H**$_2$-N-C**H**$_2$), 1.86 (quint, 2H, $^3J$ = 7.4, $NCH_2C$**H**$_2CH_2CH_3$), 1.41 (sext, 2H, $^3J$ = 7.4, $NCH_2CH_2C$**H**$_2CH_3$), 0.95 (t, 3H, $^3J$ = 7.4, $NCH_2CH_2CH_2C$**H**$_3$).

**$^{13}$C-NMR** (DMSO-$d_6$, δ [ppm], *J* [Hz]): 165.3 (1C, **C**$NH_2NHR^+$), 155.7 (d, 1C, $^4J_{\mathbf{C,F}}$ = 2.7, **C**-4), 152.8 (d, 1C, $^1J_{\mathbf{C,F}}$ = 251.7, **C**-6), 146.4 (1C, **C**-2), 145.6 (d, 1C, $^2J_{\mathbf{C,F}}$ = 10.0, **C**-7), 138.8 (1C, benzyl-**C**$_q$), 135.7 (1C, **C**-8a), 128.3 (2C, benzyl-**C**H$_{arom.}$), 127.5 (2C, benzyl-**C**H$_{arom.}$), 126.9 (1C, benzyl-**C**H$_{arom.}$), 111.6 (d, 1C, $^3J_{\mathbf{C,F}}$ = 9.6, **C**-4a), 111.4 (d, 1C, $^2J_{\mathbf{C,F}}$ = 25.4, **C**-5), 105.0 (d, 1C, $^3J_{\mathbf{C,F}}$ = 4.6, **C**-8), 103.0 (1C, **C**-3), 65.7 (2C, morpholino-**C**$H_2$-O-**C**$H_2$), 54.2 (1C, N**C**$H_2CH_2CH_2CH_3$), 49.5 (2C, $^4J_{\mathbf{C,F}}$ = 4.6, morpholino-**C**$H_2$-N-**C**$H_2$), 42.5 (1C, benzyl-**C**$H_2$), 30.1 (1C, $NCH_2$**C**$H_2CH_2CH_3$), 19.1 (1C, $NCH_2CH_2$**C**$H_2CH_3$), 13.4 (1C, $NCH_2CH_2CH_2$**C**$H_3$).

**Synthesis of Sodium 3-(benzylcarbamoyl)-1-butyl-6-fluoro-7-morpholino-2-oxo-1,2-dihydroquinoline-4-olate (GHQ215)**

*Synthesis of 2-(Butylamino)-4-chloro-5-fluorobenzoic acid (E)*

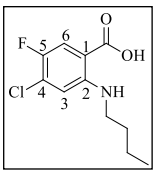


2.00 g (9.57 mmol) 2,4-Dichloro-5-fluorobenzoic acid, 1.32 g (9.57 mmol) $K_2CO_3$ and 608 mg (9.57 mmol) cupper powder were suspended in 20 ml anhydrous DMF under argon atmosphere and stirred at rt for 10 min. After addition of 1.40 g (19.1 mmol, 1.89 ml) *n*-butylamine the mixture was heated to 80 °C for 5 h. The solvent was removed in vacuo and the residue was dissolved in 50 ml water. After the pH value was adjusted to 4 using aqueous HCl-solution (2 M) the suspension was extracted with DCM (4 x 50 ml). The combined organic layers were dried over $Na_2SO_4$ and concentrated under reduced pressure. The crude product was purified by normal phase column chromatography on silica gel ($CHCl_3$/FA 100:1, $R_f$: 0.65) to give the desired product as light yellow solid.

Yield: 1.74 g (7.08 mmol, 74%), mp: 138 - 139 °C ($CHCl_3$/FA).

**IR** (ATR), $\tilde{\nu}$ [$cm^{-1}$]: 3380 (m), 2954 (m), 2929 (w), 2869 (m), 1660 (s), 1570 (s), 1510 (s), 1478 (m), 1406 (m), 1223 (s), 1191 (s), 997 (m), 840 (m).

**$^1$H-NMR** (DMSO-$d_6$, δ [ppm], *J* [Hz]): 11.7 (s, 1H, COO**H**), 7.74 (d, 1H, $^3J_{\mathbf{H,F}}$ = 9.9, **H**-6), 7.45 (s, 1H, N**H**), 6.71 (d, 1H, $^4J_{\mathbf{H,F}}$ = 6.1, **H**-3), 3.18 (t, 2H, $^3J$ = 7.3, NC**H**$_2$CH$_2$CH$_2$CH$_3$), 1.71 (quint, 2H, $^3J$ = 7.3, NCH$_2$C**H**$_2$CH$_2$CH$_3$), 1.49 (sext, 2H, $^3J$ = 7.3, NCH$_2$CH$_2$C**H**$_2$CH$_3$), 1.02 (t, 3H, $^3J$ = 7.3, NCH$_2$CH$_2$CH$_2$C**H**$_3$).

**$^{13}$C-NMR** (DMSO-$d_6$, δ [ppm], *J* [Hz]): 172.6 (d, 1C, $^4J_{\mathbf{C,F}}$ = 2.2, **C**OOH), 148.9 (1C, **C**-2), 148.1 (d, 1C, $^1J_{\mathbf{C,F}}$ = 236.3, **C**-5), 129.6 (d, 1C, $^2J_{\mathbf{C,F}}$ = 18.9, **C**-4), 118.6 (d, 1C, $^2J_{\mathbf{C,F}}$ = 22.8, **C**-6), 112.7 (1C, **C**-3), 106.8 (d, 1C, $^3J_{\mathbf{C,F}}$ = 5.3, **C**-1), 43.0 (1C, N**C**H$_2$CH$_2$CH$_2$CH$_3$), 31.0 (1C, NCH$_2$**C**H$_2$CH$_2$CH$_3$), 20.3 (1C, NCH$_2$CH$_2$**C**H$_2$CH$_3$), 13.8 (1C, NCH$_2$CH$_2$CH$_2$**C**H$_3$).

*Synthesis of Ethyl 1-butyl-7-chloro-6-fluoro-4-hydroxy-2-oxo-1,2-dihydroquinoline-3-carboxylate (F)*

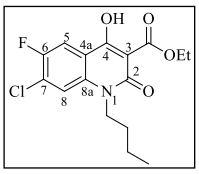


To a cooled solution (0 °C) of 628 mg (2.12 mmol) triphosgene in 10 ml anhydrous $CHCl_3$, 400 mg (1.63 mmol) 2-(butylamino)-4-chlor-5-fluorobenzoic acid (E) dissolved in 5 ml anhydrous $CHCl_3$ were added dropwise under argon atmosphere. After 20 h of stirring at rt 5 ml sat. $NaHCO_3$-solution were added carefully and the biphasic system was stirred at rt for further 5 min. The organic layer was separated and the aqueous layer was extracted with $CHCl_3$ (2 x 30 ml). The combined organic layers were dried over $Na_2SO_4$ and concentrated in vacuo to give the crude isatoic anhydrid derivative. Under argon atmosphere 98 mg (2.45 mmol) sodium hydride (60% dispersion in mineral oil) were suspended in 15 ml anhydrous DMF followed by addition of 522 mg (3.26 mmol, 493 µl) diethyl malonate. After stirring for 15 min at rt the mixture was cooled to 0 °C and the crude isatoic anhydride dissolved in 5 ml anhydrous DMF was added dropwise. After complete addition the solution was stirred at rt for 16 h followed by evaporation under reduced pressure. The residue was dissolved in 20 ml water, the pH value was adjusted to 4 using aqueous HCl-solution (2 M) and the resulting precipitate was collected via filtration. The crude product was purified via normal phase column chromatography on silica gel ($CHCl_3$, $R_f$: 0.94) to give a white solid.

Yield: 310 mg (907 µmol, 56%), mp: 119 - 120 °C ($CHCl_3$).

**IR** (ATR), $\tilde{\nu}$ [$cm^{-1}$]: 3079 (w), 2965 (m), 2934 (m), 2874 (w), 1666 (s), 1629 (s), 1593 (m), 1555 (m), 1500 (s), 1467 (m), 1410 (m), 1318 (s), 1207 (s), 1042 (m), 898 (m), 807 (m).

**$^1$H-NMR** ($CDCl_3$, δ [ppm], *J* [Hz]): 14.2 (s, 1H, O**H**), 7.90 (d, 1H, $^3J_{\mathbf{H,F}}$ = 8.9, **H**-5), 7.31 (d, 1H, $^4J_{\mathbf{H,F}}$ = 5.9, **H**-8), 4.50 (q, 2H, $^3J$ = 7.1, OC**H**$_2$CH$_3$), 4.14 (t, 2H, $^3J$ = 7.5, NC**H**$_2$CH$_2$CH$_2$CH$_3$), 1.67 (quint, 2H, $^3J$ = 7.5, NCH$_2$C**H**$_2$CH$_2$CH$_3$), 1.49 (sext, 2H, $^3J$ = 7.5, NCH$_2$CH$_2$C**H**$_2$CH$_3$), 1.47 (t, 3H, $^3J$ = 7.1, OCH$_2$C**H**$_3$), 1.00 (t, 3H, $^3J$ = 7.5, NCH$_2$CH$_2$CH$_2$C**H**$_3$).

**$^{13}$C-NMR** ($CDCl_3$, δ [ppm], *J* [Hz]): 172.9 (1C, **C**$O_2$Et), 170.6 (d, 1C, $^4J_{\mathbf{C,F}}$ = 2.8, **C**-4), 159.2 (1C, **C**-2), 153.5 (d, 1C, $^1J_{\mathbf{C,F}}$ = 245.8, **C**-6), 137.9 (d, 1C, $^4J_{\mathbf{C,F}}$ = 1.8, **C**-8a), 128.9 (d, 1C, $^2J_{\mathbf{C,F}}$ = 19.6, **C**-7), 116.6 (1C, **C**-8), 114.9 (d, 1C, $^3J_{\mathbf{C,F}}$ = 7.3, **C**-4a), 112.6 (d, 1C, $^2J_{\mathbf{C,F}}$ = 23.6, **C**-5), 99.1 (1C, **C**-3), 63.1 (1C, O**C**$H_2CH_3$), 43.1 (1C, N**C**$H_2CH_2CH_2CH_3$), 29.9 (1C, $NCH_2$**C**$H_2CH_2CH_3$), 20.7 (1C, $NCH_2CH_2$**C**$H_2CH_3$), 14.7 (1C, $OCH_2$**C**$H_3$), 14.2 (1C, $NCH_2CH_2CH_2$**C**$H_3$).

*Synthesis of N-Benzyl-1-butyl-7-chloro-6-fluoro-4-hydroxy-2-oxo-1,2-dihydroquinoline-3-carboxamide (G)*

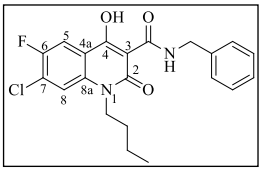


To a solution of 280 mg (819 µmol) ethyl 1-butyl-7-chloro-6-fluoro-4-hydroxy-2-oxo-1,2-dihydroquinoline-3-carboxylate (F) in 100 ml toluene 220 mg (2.05 mmol, 223 µl) benzylamine were added and the mixture was refluxed for 1 h. Within that time 3 x 10 ml toluene were distilled of (Dean-Stark-apparatus) and replaced by an equal amount of fresh toluene. Afterwards the solvent was concentrated to a volume of about 5 ml. Upon cooling to rt the desired product crystallized as white solid which was dried in vacuo.

Yield: 264 mg (655 µmol, 80%), mp: 111 - 112 °C (toluene).

**IR** (ATR), $\tilde{\nu}$ [$cm^{-1}$]: 3210 (w), 2957 (m), 2925 (w), 2867 (w), 1638 (s), 1585 (m), 1542 (s), 1498 (s), 1457 (m), 1397 (m), 1335 (m), 1218 (m), 1031 (m), 885 (m), 801 (m), 693 (m).

**$^1$H-NMR** (DMSO-$d_6$, δ [ppm], *J* [Hz]): 10.6 (t, 1H, $^3J$ = 6.0, CON**H**R), 7.87 (d, 1H, $^4J_{\mathbf{H,F}}$ = 4.8, **H**-8), 7.85 (d, 1H, $^3J_{\mathbf{H,F}}$ = 8.2, **H**-5), 7.37-726 (m, 5H, benzyl-C$\mathbf{H}_{arom.}$), 4.58 (d, 2H, $^3J$ = 6.0, benzyl-C$\mathbf{H}_2$), 4.17 (t, 2H, $^3J$ = 7.3, NC$\mathbf{H}_2CH_2CH_2CH_3$), 1.54 (quint, 2H, $^3J$ = 7.3, $NCH_2$C$\mathbf{H}_2CH_2CH_3$), 1.37 (sext, 2H, $^3J$ = 7.3, $NCH_2CH_2$C$\mathbf{H}_2CH_3$), 0.91 (t, 3H, $^3J$ = 7.3, $NCH_2CH_2CH_2$C$\mathbf{H}_3$).

**$^{13}$C-NMR** (DMSO-$d_6$, δ [ppm], *J* [Hz]): 170.1 (1C, **C**ONHR), 169.8 (d, 1C, $^4J_{\mathbf{C,F}}$ = 2.5, **C**-4), 161.0 (1C, **C**-2), 152.3 (d, 1C, $^1J_{\mathbf{C,F}}$ = 244.8, **C**-6), 137.8 (1C, benzyl-$\mathbf{C}_q$), 135.9 (d, 1C, $^4J_{\mathbf{C,F}}$ = 1.3, **C**-8a), 128.5 (2C, benzyl-**C**$H_{arom.}$), 127.5 (2C, benzyl-**C**$H_{arom.}$), 127.2 (1C,

benzyl-**C**H$_{arom.}$), 126.6 (d, 1C, $^{2}J_{\mathbf{C,F}}$ = 19.8, **C**-7), 117.4 (1C, **C**-8), 115.0 (d, 1C, $^{3}J_{\mathbf{C,F}}$ = 6.8, **C**-4a), 110.9 (d, 1C, $^{2}J_{\mathbf{C,F}}$ = 22.7, **C**-5), 96.4 (1C, **C**-3), 42.3 (1C, benzyl-**C**H$_2$), 41.7 (1C, N**C**H$_2$CH$_2$CH$_2$CH$_3$), 29.2 (1C, NCH$_2$**C**H$_2$CH$_2$CH$_3$), 19.4 (1C, NCH$_2$CH$_2$**C**H$_2$CH$_3$), 13.6 (1C, NCH$_2$CH$_2$CH$_2$**C**H$_3$).

*Synthesis of Sodium 3-(benzylcarbamoyl)-1-butyl-6-fluoro-7-morpholino-2-oxo-1,2-dihydroquinoline-4-olate (GHQ215)*

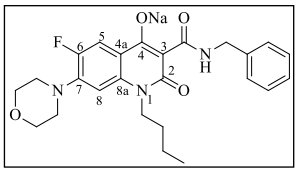


420 mg (1.04 mmol) *N*-benzyl-1-butyl-7-chloro-6-fluoro-4-hydroxy-2-oxo-1,2-dihydroquinoline-3-carboxamide (G) were dissolved in 15 ml morpholine and heated to 110 °C for 4 h under microwave irradiation (heat-up rate: in 3 min to 110 °C, 600 W). The solution was diluted with 50 ml water and the pH value was adjusted to 6 using aqueous HCl-solution (2 M). The aqueous solution was extracted with EA (4 x 50 ml), the combined organic layers were dried over $Na_2SO_4$ and the solvent was evaporated under reduced pressure followed by purified via normal phase column chromatography on silica gel (PE/EA 3:1, $R_f$: 0.57). In order to achieve the corresponding sodium salt the isolated white solid was suspended in 10 ml EtOH and treated with 114 µl (1.14 mmol) aqueous NaOH-solution (10 M). After temporary dissolution the desired sodium salt started to precipitate. After 15 min of stirring at rt the precipitate was filtered off, washed with a mixture of water and EtOH (1:1) and dried in vacuo to give a white solid.

Yield: 112 mg (236 µmol, 23%), mp: 317 - 318 °C (water).

**IR** (ATR), $\tilde{\nu}$ [cm$^{-1}$]: 2956 (w), 2852 (w), 1617 (s), 1573 (m), 1496 (s), 1455 (m), 1406 (m), 1259 (m), 1122 (m), 909 (m), 807 (m), 697 (s).

**$^{1}$H-NMR** (DMSO, δ [ppm], *J* [Hz]): 11.5 (t, 1H, $^{3}J$ = 5.4, CON**H**R), 7.68 (d, 1H, $^{3}J_{\mathbf{H,F}}$ = 13.9, **H**-5), 7.32-7.21 (m, 5H, benzyl-C**H**$_{arom.}$), 6.64 (d, 1H, $^{4}J_{\mathbf{H,F}}$ = 7.0, **H**-8), 4.46 (d, 2H, $^{3}J$ = 5.4, benzyl-C**H**$_2$), 4.10 (br, 2H, NC**H**$_2$CH$_2$CH$_2$CH$_3$), 3.77 (br, 4H, morpholino-C**H**$_2$-O-C**H**$_2$), 3.12

(br, 4H, morpholino-C**H**$_2$-N-C**H**$_2$), 1.56 (quint, 2H, $^3J$ = 7.2, NCH$_2$C**H**$_2$CH$_2$CH$_3$), 1.37 (sext, 2H, $^3J$ = 7.2, NCH$_2$CH$_2$C**H**$_2$CH$_3$), 0.95 (t, 3H, $^3J$ = 7.2, NCH$_2$CH$_2$CH$_2$C**H**$_3$).

**$^{13}$C-NMR** (DMSO, δ [ppm], *J* [Hz]): 173.7 (d, 1C, $^4J_{C,F}$ = 1.5, **C**-4), 169.1 (1C, **C**ONHR), 164.0 (1C, **C**-2), 149.6 (d, 1C, $^1J_{C,F}$ = 239.9, **C**-6), 141.9 (d, 1C, $^2J_{C,F}$ = 9.6, **C**-7), 140.8 (1C, benzyl-**C**$_q$), 136.0 (1C, **C**-8a), 128.1 (2C, benzyl-**C**H$_{arom.}$), 127.2 (2C, benzyl-**C**H$_{arom.}$), 126.3 (1C, benzyl-**C**H$_{arom.}$), 117.4 (d, 1C, $^3J_{C,F}$ = 7.2, **C**-4a), 111.9 (d, 1C, $^2J_{C,F}$ = 20.5, **C**-5), 102.8 (1C, **C**-8), 97.7 (1C, **C**-3), 66.0 (2C, morpholino-**C**H$_2$-O-**C**H$_2$), 50.1 (2C, $^4J_{C,F}$ = 3.5, morpholino-**C**H$_2$-N-**C**H$_2$), 41.6 (1C, benzyl-**C**H$_2$), 40.2 (1C, N**C**H$_2$CH$_2$CH$_2$CH$_3$), 22.3 (1C, NCH$_2$**C**H$_2$CH$_2$CH$_3$), 19.7 (1C, NCH$_2$CH$_2$**C**H$_2$CH$_3$), 13.7 (1C, NCH$_2$CH$_2$CH$_2$**C**H$_3$).

**Synthesis of *N*-Benzyl-1-butyl-7-morpholino-4-oxo-1,4-dihydro-1,6-naphthyridine-3-carboxamide oxalate (GHQ237)**

*Synthesis of Ethyl 4,6-dihydroxynicotinate (H)* [3]

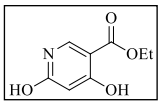


7.00 g (34.6 mmol) Diethyl 1,3-acetonedicarboxylate and 5.13 g (34.6 mmol, 5.70 ml) triethyl orthoformate were dissolved in 7.07 g (69.2 mmol, 6.55 ml) acetic anhydride and heated to reflux for 3 h. Excess of acetic anhydride was removed in vacuo and the residue was dissolved in 15 ml conc. $NH_3$-solution. The mixture was stirred at rt for 15 h followed by acidification (pH = 2) with aqueous HCl-solution (2 M). The yellow precipitate was filtered off, washed with water and dried in vacuo.

Yield: 4.68 g (26.5 mmol, 77%), mp: 214 - 215 °C (water).

Spectroscopical data were consistent with literature [3].

*Synthesis of Ethyl 4,6-dichloronicotinate (I)* [4]

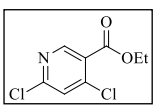


2.50 g (13.7 mmol) ethyl 4,6-dihydroxynicotinate (H) were dissolved in 21.0 g (0.14 mol, 12.6 ml) $POCl_3$ and heated to 80 °C for 24 h. After cooling to rt the dark brown solution was poured into 150 g ice and the aqueous mixture was extracted with EA (4 x 40 ml). The combined organic layers were washed with 50 ml

$Na_2CO_3$-solution (10%) and 50 ml brine. After drying over $Na_2SO_4$ the solvent was evaporated under reduced pressure and the crude product was purified via normal phase column chromatography on silica gel ($CHCl_3$/PE 2:1) to give a light yellow oil.

Yield: 2.14 g (9.73 mmol, 71%).

Spectroscopical data were consistent with literature [4].

*Synthesis of 4,6-dichloronicotinic acid (J)* [5]

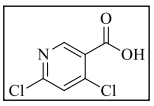

A solution of 441 mg (10.5 mmol) LiOH dissolved in 15 ml water was added dropwise to 1.93 g (8.77 mmol) ethyl 4,6-dichloronicotinate (I) dissolved in 15 ml THF. The mixture was stirred at rt for 15 h followed by evaporation of THF under reduced pressure. The remaining aqueous solution was acidified (pH = 3) using aqueous HCl-solution (2 M) and the resulting precipitate was collected by filtration. The solid was washed with water and dried in vacuo to give the desired product as a white solid.

Yield: 1.28 g (6.67 mmol, 76%), mp: 151 - 152 (water).

Spectroscopical data were consistent with literature [5].

*Synthesis of Ethyl 1-butyl-7-chloro-4-oxo-1,4-dihydro-1,6-naphthyridine-3-carboxylate (K)*

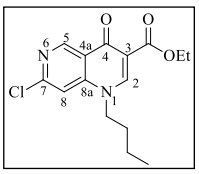

900 mg (4.69 mmol) 4,6-dichloronicotinic acid (J) were dissolved in 15 ml $SOCl_2$ and heated to 80 °C for 2 h. Afterwards excess of $SOCl_2$ was distilled off under reduced pressure and the residue was dissolved in 10 ml anhydrous toluene under argon atmosphere. 1.21 g (9.38 mmol, 1.63 ml) DIPEA and 1.01 g (7.03 mmol) Ethyl 3-(*N*,*N*-dimethylamino)acrylate were added and the mixture was heated to 90 °C for 2 h. After removing the solvent in vacuo the acrylate intermediate was purified by normal phase column chromatography on silica gel (EA/PE 2:1). The intermediate was dissolved in 40 ml EtOH and 20 ml $Et_2O$ and 398 mg (5.45 mmol, 538 µl) *n*-butylamine were added. After 10 min of stirring at rt the mixture was evaporated to dryness under reduced pressure. The crude mixture was dissolved in 10 ml anhydrous DMF under argon atmosphere, 1.00 g (7.26 mmol) $K_2CO_3$ were added and the

suspension was heated to 100 °C for 1 h. The solvent was removed in vacuo and the residue was partitioned between 50 ml water and 40 ml DCM. The organic layer was separated and the aqueous layer was extracted with DCM (3 x 40 ml). The combined organic layers were dried over $Na_2SO_4$, concentrated under reduced pressure and the resulting light brown solid was recrystallized from EA to give the desired product as a light yellow solid.

Yield: 862 mg (2.79 mmol, 77%), mp: 161 - 162 °C (EA).

**IR** (ATR), $\tilde{\nu}$ [$cm^{-1}$]: 3071 (w), 2956 (w), 2933 (m), 2872 (w), 1724 (s), 1634 (m), 1577 (s), 1466 (s), 1318 (m), 1225 (m), 1190 (s), 1072 (s), 928 (m), 890 (m), 808 (m).

**$^1$H-NMR** ($CDCl_3$, δ [ppm], *J* [Hz]): 9.36 (s, 1H, **H**-2), 8.40 (s, 1H, **H**-5), 7.27 (s, 1H, **H**-8), 4.37 (q, 2H, $^3J$ = 7.1, OC**H**$_2$$CH_3$), 4.09 (t, 2H, $^3J$ = 7.4, NC**H**$_2$$CH_2CH_2CH_3$), 1.85 (quint, 2H, $^3J$ = 7.4, $NCH_2$C**H**$_2$$CH_2CH_3$), 1.44 (sext, 2H, $^3J$ = 7.4, $NCH_2CH_2$C**H**$_2$$CH_3$), 1.39 (t, 3H, $^3J$ = 7.1, $OCH_2$C**H**$_3$), 1.01 (t, 3H, $^3J$ = 7.4, $NCH_2CH_2CH_2$C**H**$_3$).

**$^{13}$C-NMR** ($CDCl_3$, δ [ppm], *J* [Hz]): 173.1 (1C, **C**-4), 164.5 (1C, **C**$O_2$Et), 154.4 (1C, **C**-7), 152.3 (1C, **C**-5), 150.3 (1C, **C**-2), 145.8 (1C, **C**-8a), 122.8 (1C, **C**-4a), 114.6 (1C, **C**-3), 109.2 (1C, **C**-8), 61.3 (1C, O**C**$H_2$$CH_3$), 53.3 (1C, N**C**$H_2$$CH_2CH_2CH_3$), 30.6 (1C, $NCH_2$**C**$H_2$$CH_2CH_3$), 19.8 (1C, $NCH_2CH_2$**C**$H_2$$CH_3$), 14.3 (1C, $NCH_2CH_2CH_2$**C**$H_3$), 13.5 (1C, $OCH_2$**C**$H_3$).

*Synthesis of 1-Butyl-7-morpholino-4-oxo-1,4-dihydro-1,6-naphthyridine-3-carboxylic acid hydrochloride (M)*

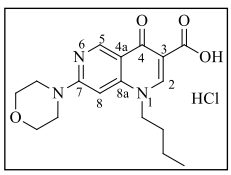


Under microwave irradiation 400 mg (1.30 mmol) ethyl 1-butyl-7-chloro-4-oxo-1,4-dihydro-1,6-naphthyridine-3-carboxylate (K) dissolved in 15 ml morpholine were heated to 85 °C for 1.5 h (heat-up rate: in 2 min to 85 °C, 600 W). The mixture was diluted with 30 ml water and extracted with DCM (4 x 50 ml). The combined organic layers were dried over $Na_2SO_4$ and concentrated in vacuo. The residue was suspended in 5 ml EtOH and 5 ml HCl-solution

(6 M) and refluxed for 3 h. Afterwards the suspension was evaporated to dryness under reduced pressure and the crude product was recrystallized from EA/MeOH to give a yellow, crystalline solid.

Yield: 356 mg (968 µmol, 75%), mp: 257 - 259 °C (EA/MeOH).

**IR** (ATR), $\tilde{\nu}$ [$cm^{-1}$]: 2962 (w), 2856 (w), 2497 (br), 1710 (m), 1607 (s), 1525 (m), 1467 (s), 1418 (m), 1112 (m), 967 (m), 821 (m), 806 (m).

**$^{1}$H-NMR** (DMSO-$d_6$, δ [ppm], *J* [Hz]): 15.0 (s, 1H, COO**H**), 9.06 (s, 1H, **H**-5), 8.84 (s, 1H, **H**-2), 6.89 (s, 1H, **H**-8), 4.41 (t, 2H, $^{3}J$ = 7.3, NC**H**$_2$CH$_2$CH$_2$CH$_3$), 3.73 (s, 8H, morpholino-C**H**$_2$), 1.72 (quint, 2H, $^{3}J$ = 7.3, NCH$_2$C**H**$_2$CH$_2$CH$_3$), 1.33 (sext, 2H, $^{3}J$ = 7.3, NCH$_2$CH$_2$C**H**$_2$CH$_3$), 1.01 (t, 3H, $^{3}J$ = 7.3, NCH$_2$CH$_2$CH$_2$C**H**$_3$).

**$^{13}$C-NMR** (DMSO-$d_6$, δ [ppm], *J* [Hz]): 177.2 (1C, **C**-4), 165.6 (1C, **C**OOH), 160.7 (1C, **C**-7), 151.2 (1C, **C**-2), 149.9 (1C, **C**-5), 146.1 (1C, **C**-8a), 112.2 (1C, **C**-4a), 107.6 (1C, **C**-3), 88.7 (1C, **C**-8), 65.7 (2C, morpholino-**C**H$_2$-O-**C**H$_2$), 52.1 (1C, N**C**H$_2$CH$_2$CH$_2$CH$_3$), 44.8 (2H, morpholino-**C**H$_2$-N-**C**H$_2$), 30.1 (1C, NCH$_2$**C**H$_2$CH$_2$CH$_3$), 19.0 (1C, NCH$_2$CH$_2$**C**H$_2$CH$_3$), 14.4 (1C, NCH$_2$CH$_2$CH$_2$**C**H$_3$).

*Synthesis of N-Benzyl-1-butyl-7-morpholino-4-oxo-1,4-dihydro-1,6-naphthyridine-3-carboxamide oxalate (GHQ237)*

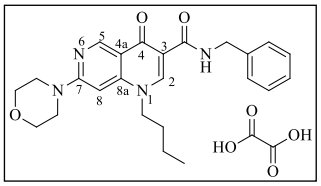

To a cooled solution (0 °C) of 200 mg (544 µmol) 1-butyl-7-morpholino-4-oxo-1,4-dihydro-1,6-naphthyridine-3-carboxylic acid hydrochloride (M) and 275 mg (2.72 mmol, 299 µl) NMM in 10 ml anhydrous DMF 298 mg (2.18 mmol, 285 µl) isobutyl chloroformate were added dropwise under argon atmosphere. After 1 h at 0 °C 234 mg (2.18 mmol, 238 µl) benzylamine were added and stirring at rt was continued for 45 min. The solvent was removed in vacuo and the crude product was purified via normal phase column chromatography on silica gel ($CHCl_3$/EtOH 20:1, $R_f$: 0.49). The resulting solid was

dissolved in 4 ml ACN and a solution of 245 mg (2.72 mmol) oxalic acid in 6 ml ACN was added dropwise. At -20 °C the oxalic salt precipitated and was recrystallized from ACN.

Yield: 217 mg (465 µmol, 85%), mp: 178 - 179 °C (ACN).

CHN: *calculated* C: 64.50, H: 6.28, N: 12.04, O: 17.18 (for **API**/**Ox** 1:0.5), *found* C: 64.42, H: 6.29, N: 11.98.

Stoichiometry: **API**/**Ox** 1:0.5.

**IR** (ATR), $\tilde{\nu}$ [$cm^{-1}$]: 3171 (w), 3056 (m), 2954 (m), 2911 (m), 2867 (m), 2603 (w), 1734 (m), 1645 (s), 1610 (s), 1552 (s), 1467 (m), 1454 (m), 1440 (m), 1363 (m), 1192 (s), 1118 (m), 813 (m), 736 (m), 682 (m).

**$^{1}$H-NMR** (DMSO-$d_6$, δ [ppm], *J* [Hz]): 10.2 (t, 1H, $^{3}J$ = 5.8, CON**H**R), 9.02 (s, 1H, **H**-5), 8.70 (s, 1H, **H**-2), 7.37-7.24 (m, 5H, benzyl-C**H**$_{arom.}$), 6.63 (s, 1H, **H**-8), 4.53 (d, 2H, $^{3}J$ = 5.8, benzyl-C**H**$_2$), 4.34 (t, 2H, $^{3}J$ = 7.3, NC**H**$_2$CH$_2$CH$_2$CH$_3$), 3.73-3.63 (m, 8H, morpholino-C**H**$_2$), 1.72 (quint, 2H, $^{3}J$ = 7.3, NCH$_2$C**H**$_2$CH$_2$CH$_3$), 1.31 (sext, 2H, $^{3}J$ = 7.3, NCH$_2$CH$_2$C**H**$_2$CH$_3$), 0.91 (t, 3H, $^{3}J$ = 7.3, NCH$_2$CH$_2$CH$_2$C**H**$_3$).

**$^{13}$C-NMR** (DMSO-$d_6$, δ [ppm], *J* [Hz]): 175.4 (1C, **C**-4), 163.7 (1C, **C**ONHR), 160.8 (1C, **C**-7), 160.5 (Oxalat), 149.9 (1C, **C**-5), 149.7 (1C, **C**-2), 146.0 (1C, **C**-8a), 139.2 (1C, benzyl-**C**$_q$), 128.4 (2C, benzyl-**C**H$_{arom.}$), 127.3 (2C, benzyl-**C**H$_{arom.}$), 126.8 (1C, benzyl-**C**H$_{arom.}$), 114.2 (1C, **C**-4a), 111.4 (1C, **C**-3), 88.5 (1C, **C**-8), 65.7 (2C, morpholino-**C**H$_2$-O-**C**H$_2$), 51.6 (1C, N**C**H$_2$CH$_2$CH$_2$CH$_3$), 44.8 (2H, morpholino-**C**H$_2$-N-**C**H$_2$), 42.1 (1C, benzyl-**C**H$_2$), 30.1 (1C, NCH$_2$**C**H$_2$CH$_2$CH$_3$), 19.0 (1C, NCH$_2$CH$_2$**C**H$_2$CH$_3$), 13.5 (1C, NCH$_2$CH$_2$CH$_2$**C**H$_3$).

**Synthesis of N-Benzyl-1-(2-(dimethylamino)ethyl)-6-fluoro-7-morpholino-4-oxo-1,4-dihydroquinoline-3-carboxamide oxalate (GHQ243)**

*Synthesis of Ethyl 7-chloro-1-(2-(dimethylamino)ethyl)-6-fluoro-4-oxo-1,4-dihydroquinoline-3-carboxylate (N)*

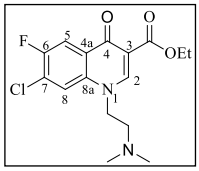

1.00 g (3.71 mmol) ethyl 7-chloro-6-fluoro-4-hydroxychinolin-3-carboxylate (B) and 769 mg (5.57 mmol) $K_2CO_3$ were suspended in 15 ml anhydrous DMF under argon atmosphere and stirred at rt for 30 min. A catalytic amount of KI and 588 mg (4.08 mmol) 2-chloro-*N*,*N*-dimethylethylamine hydrochloride were added and the mixture was heated to 100 °C for 16 h. The solvent was removed in vacuo and the residue was partitioned between 50 ml water and 50 ml EA. The organic layer was separated and the aqueous layer was extracted with EA (2 x 50 ml). After drying the combined organic layers over $Na_2SO_4$ and evaporating the solvent under reduced pressure the crude product was purified via normal phase column chromatography on silica gel ($CHCl_3$/MeOH/conc. $NH_3$ 150:10:1, $R_f$: 0.43) to give a white solid.

Yield: 480 mg (1.41 mmol, 38%), mp: 140 - 141 °C ($CHCl_3$/MeOH/conc. $NH_3$).

**IR** (ATR), $\tilde{\nu}$ [$cm^{-1}$]: 2981 (w), 2933 (w), 2871 (w), 2840 (w), 2776 (w), 1716 (s), 1611 (m), 1594 (m), 1548 (m), 1487 (s), 1460 (m), 1384 (m), 1313 (m), 1209 (m), 1160 (s), 1040 (m), 893 (m), 800 (m), 770 (m).

**$^1$H-NMR** (DMSO-$d_6$, δ [ppm], *J* [Hz]): 8.61 (s, 1H, **H**-2), 8.18 (d, 1H, $^4J_{\mathbf{H,F}}$ = 6.0, **H**-8), 8.03 (d, 1H, $^3J_{\mathbf{H,F}}$ = 9.4, **H**-5), 4.47 (t, 2H, $^3J$ = 5.7, NC**H**$_2$CH$_2$N(CH$_3$)$_2$), 4.23 (q, 2H, $^3J$ = 7.1, OC**H**$_2$CH$_3$), 2.58 (t, 2H, $^3J$ = 5.7, NCH$_2$C**H**$_2$N(CH$_3$)$_2$), 2.18 (s, 6H, NCH$_2$CH$_2$N(C**H**$_3$)$_2$), 1.28 (t, 3H, $^3J$ = 7.1, OCH$_2$C**H**$_3$).

**$^{13}$C-NMR** (DMSO-$d_6$, δ [ppm], *J* [Hz]): 171.2 (d, 1C, $^4J_{\mathbf{C,F}}$ = 2.3, **C**-4), 164.3 (1C, **C**OOEt), 154.2 (d, 1C, $^1J_{\mathbf{C,F}}$ = 246.9, **C**-6), 150.5 (1C, **C**-2), 135.9 (d, 1C, $^4J_{\mathbf{C,F}}$ = 1.8, **C**-8a), 128.6 (d, 1C, $^3J_{\mathbf{C,F}}$ = 5.4, **C**-4a), 125.3 (d, 1C, $^2J_{\mathbf{C,F}}$ = 20.0, **C**-7), 120.1 (1C,**C**-8), 112.4 (d, 1C,

$^{2}J_{\mathbf{C,F}}$ = 22.4, **C**-5), 109.1 (1C, **C**-3), 59.8 (1C, O**C**$H_2CH_3$), 56.9 (1C, N**C**$H_2CH_2N(CH_3)_2$), 50.4 (1C, $NCH_2$**C**$H_2N(CH_3)_2$), 45.2 (2C, $NCH_2CH_2N$(**C**$H_3)_2$), 14.2 (1C, $OCH_2$**C**$H_3$).

*Synthesis of 1-(2-(Dimethylamino)ethyl)-6-fluoro-7-morpholino-4-oxo-1,4-dihydroquinoline-3-carboxylic acid hydrochloride (O)*

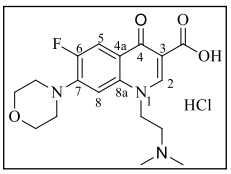


670 mg (1.97 mmol) ethyl 7-chloro-1-(2-(dimethylamino)ethyl)-6-fluoro-4-oxo-1,4-dihydroquinoline-3-carboxylate (N) were suspended in 5 ml EtOH and 5 ml aqueous HCl-solution (6 M) and heated to reflux for 4 h. The suspension was evaporated to dryness under reduced pressure and the residue was dissolved in 15 ml morpholine. The solution was heated to 100 °C for 4 h under microwave irradiation (heat-up rate: in 3 min to 100 °C, 600W). Excess of morpholine was removed in vacuo and the remaining oil was dissolved in 10 ml MeOH. After addition of 1.5 ml isopropanolic HCl-solution (6 M) the precipitate was filtered off and recrystallized from MeOH/water in order to give the desired product as hydrochlorid salt.

Yield: 276 mg (690 µmol, 35%), 298 - 299 °C (MeOH/water).

**IR** (ATR), $\tilde{\nu}$ [$cm^{-1}$]: 3246 (w), 3046 (w), 2968 (w), 2903 (w), 2864 (m), 2373 (br), 1700 (s), 1622 (s), 1523 (m), 1488 (s), 1468 (m), 1385 (m), 1267 (s), 1118 (s), 1036 (m), 884 (m), 807 (m), 752 (m).

**$^{1}$H-NMR** (DMSO-$d_6$, δ [ppm], *J* [Hz]): 15.2 (s, 1H, COO**H**), 11.5 (br, 1H, N**H**$^{+}$), 9.03 (s, 1H, **H**-2), 7.94 (d, 1H, $^{3}J_{\mathbf{H,F}}$ = 13.4, **H**-5), 7.26 (d, 1H, $^{4}J_{\mathbf{H,F}}$ = 7.1, **H**-8), 5.03 (t, 2H, $^{3}J$ = 7.2, NC**H**$_2CH_2N(CH_3)_2$), 3.79 (br, 4H, morpholino-C**H**$_2$-O-C**H**$_2$), 3.53 (br, 2H, $NCH_2$C**H**$_2N(CH_3)_2$), 3.40 (br, 4H, morpholino-C**H**$_2$-N-C**H**$_2$), 2.83 (s, 6H, $CH_2CH_2N$(C**H**$_3)_2$).

**$^{13}$C-NMR** (DMSO-$d_6$, δ [ppm], *J* [Hz]): 176.3 (d, 1C, $^{4}J_{\mathbf{C,F}}$ = 2.3, **C**-4), 165.7 (1C, **C**OOH), 152.7 (d, 1C, $^{1}J_{\mathbf{C,F}}$ **=** 249.5, **C**-6), 149.7 (1C, **C**-2), 145.5 (d, 1C, $^{2}J_{\mathbf{C,F}}$ = 9.9, **C**-7), 137.3 (1C, **C**-8a), 119.1 (d, 1C, $^{3}J_{\mathbf{C,F}}$ = 7.8, **C**-4a), 111.3 (d, 1C, $^{2}J_{\mathbf{C,F}}$ = 23.1, **C**-5), 107.3 (1C, **C**-3), 105.5 (d, 1C, $^{3}J_{\mathbf{C,F}}$ = 3.3, **C**-8), 65.8 (2C, morpholino-**C**$H_2$-O-**C**$H_2$), 53.0 (1C,

N**C**$H_2CH_2N(CH_3)_2$), 50.0 (2C, $^4J_{\mathbf{C,F}}$ = 4.8, morpholino-**C**$H_2$-N-**C**$H_2$), 47.6 (1C, $NCH_2$**C**$H_2N(CH_3)_2$), 42.2 (2C, $NCH_2CH_2N$(**C**$H_3)_2$).

*Synthesis of N-Benzyl-1-(2-(dimethylamino)ethyl)-6-fluoro-7-morpholino-4-oxo-1,4-dihydroquinoline-3-carboxamide oxalate (GHQ243)*

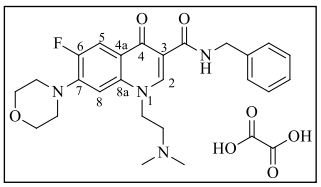

To a cooled solution (0 °C) of 250 mg (625 µmol) 1-(2-(dimethylamino)ethyl)-6-fluoro-7-morpholino-4-oxo-1,4-dihydroquinoline-3-carboxylic acid hydrochloride (O) and 506 mg (2.50 mmol, 273 µl) NMM in 10 ml anhydrous DMF 342 mg (2.50 mmol, 326 µl) isobutyl chloroformate were added dropwise under argon atmosphere. After 1 h at 0 °C 268 mg (2.50 mmol, 273 µl) benzylamine were added and stirring at rt was continued for 45 min. The solvent was removed in vacuo and the crude product was purified via normal phase column chromatography on silica gel ($CHCl_3$/MeOH/conc. $NH_3$ 100:10:1, $R_f$: 0.65). The resulting solid was dissolved in 4 ml ACN and a solution of 281 mg (3.13 mmol) oxalic acid in 6 ml ACN was added dropwise. After 30 min of agitating at rt the oxalic salt precipitated which was recrystallized from MeOH.

Yield: 145 mg (267 µmol, 43%), mp: 227 - 228 °C (MeOH).

CHN: *calculated* C: 59.77, H: 5.76, F: 3.50, N: 10.33, O: 20.64 (for **API**/**Ox** 1:1), *found* C: 59.62, H: 5.62, N: 10.36.

Stoichiometry: **API**/**Ox** 1:1.

**IR** (ATR), $\tilde{\nu}$ [$cm^{-1}$]: 3175 (w), 3056 (m), 2981 (w), 2885 (w), 2815 (w), 2716 (br), 1717 (br), 1635 (s), 1572 (s), 1490 (s), 1450 (m), 1360 (m), 1251 (m), 1171 (m), 1122 (m), 1001 (m), 932 (m), 745 (m), 694 (m).

**$^1$H-NMR** (DMSO-$d_6$, δ [ppm], *J* [Hz]): 10.3 (t, 1H, $^3J$ = 5.8, CON**H**R), 8.86 (s, 1H, **H**-2), 7.88 (d, 1H, $^3J_{\mathbf{H,F}}$ = 13.6, **H**-5), 7.35-7.23 (m, 5H, benzyl-C$\mathbf{H}_{arom.}$), 7.12 (d, 1H, $^4J_{\mathbf{H,F}}$ = 7.0, **H**-8), 4.79 (t, 2H, $^3J$ = 6.8, NC$\mathbf{H}_2CH_2N(CH_3)_2$), 4.56 (d, 2H, $^3J$ = 5.8, benzyl-C$\mathbf{H}_2$), 3.79 (br,

4H, morpholino-C**H**$_2$-O-C**H**$_2$), 3.28 (br, 6H, morpholino-C**H**$_2$-N-C**H**$_2$, NCH$_2$C**H**$_2$N(CH$_3$)$_2$), 2.68 (s, 6H, NCH$_2$CH$_2$N(C**H**$_3$)$_2$).

**$^{13}$C-NMR** (DMSO-$d_6$, δ [ppm], *J* [Hz]): 174.2 (d, 1C, $^4J_{C,F}$ = 2.2, **C**-4), 163.9 (1C, **C**ONHR), 163.8 (Oxalat), 152.4 (d, 1C, $^1J_{C,F}$ = 247.5, **C**-6), 148.5 (1C, **C**-2), 144.6 (d, 1C, $^2J_{C,F}$ = 9.9, **C**-7), 139.3 (1C, benzyl-**C**$_q$), 136.6 (1C, **C**-8a), 128.3 (2C, benzyl-**C**H$_{arom.}$), 127.3 (2C, benzyl-**C**H$_{arom.}$), 126.8 (1C, benzyl-**C**H$_{arom.}$), 121.2 (d, 1C, $^3J_{C,F}$ = 7.1, **C**-4a), 111.5 (d, 1C, $^2J_{C,F}$ = 22.9, **C**-5), 110.4 (1C, **C**-3), 105.2 (d, 1C, $^3J_{C,F}$ = 2.3, **C**-8), 65.9 (2C, morpholino-**C**H$_2$-O-**C**H$_2$), 54.2 (1C, NCH$_2$**C**H$_2$N(CH$_3$)$_2$), 49.9 (2C, $^4J_{C,F}$ = 4.4, morpholino-**C**H$_2$-N-**C**H$_2$), 48.2 (1C, N**C**H$_2$CH$_2$N(CH$_3$)$_2$), 43.3 (2C, NCH$_2$CH$_2$N(**C**H$_3$)$_2$), 42.1 (1C, benzyl-**C**H$_2$).

**Synthesis of 1-Butyl-*N*-(4-(2-(dimethylamino)ethoxy)benzyl)-6-fluoro-7-morpholino-4-oxo-1,4-dihydroquinoline-3-carboxamide oxalate (GHQ250)**

*Synthesis of tert-Butyl-4-hydroxybenzylcarbamate (P)* [6]

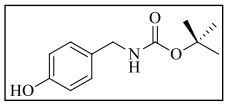

905 mg (7.35 mmol) 4-hydroxybenzylamine, 2.41 g (11.0 mmol) di-*tert*-butyl dicarbonate and 1.24 g (14.7 mmol) NaHCO$_3$ were suspended in 20 ml MeOH and stirred at rt for 16 h. The solvent was removed in vacuo, the residue was dissolved in 20 ml water and extracted with DCM (4 x 50 ml). After drying the combined organic layers over Na$_2$SO$_4$ and concentrating under reduced pressure the crude product was purified by normal phase column chromatography on silica gel (PE/EA 2:1, R$_f$: 0.69) to give a colorless oil.

Yield: 1.20 g (5.37 mmol, 73%).

Spectroscopical data were consistent with literature [6].

*Synthesis of 2-(4-(Aminomethyl)phenoxy)-N,N-dimethylethanamine (Q)* [7]

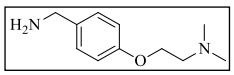

Under argon atmosphere 600 mg (2.69 mmol) *tert*-butyl-4-hydroxybenzylcarbamate (P) were added potionwise to a cooled suspension (0 °C) of 215 mg (5.38 mmol) sodium hydride (60% dispersion in mineral oil)

in 10 ml anhydrous DMF. After 30 min at 0 °C 465 mg (3.23 mmol) 2-chloro-*N*,*N*-dimethylethylamine hydrochloride dissolved in 10 ml anhydrous DMF were added dropwise and the resulting solution was stirred at rt for 15 h. The solvent was removed in vacuo and the residue was partitioned between 50 ml water and 50 ml DCM. The organic layer was separated and the aqueous layer was extracted with DCM (3 x 50 ml). The combined organic layers were dried over $Na_2SO_4$, the solvent was evaporated under reduced pressure and the residue was purified by means of normal phase column chromatography on silica gel ($CHCl_3$/methanolic $NH_3$ (6 M) 40:1, $R_f$: 0.85). For deprotection the intermediate was dissolved in 10 ml DCM and 4 ml TFA were added. After stirring the mixture for 2 h at rt the solvent was removed in vacuo and the residue was dissolved in 50 ml water. The pH was adjusted to 9 - 10 using aqueous NaOH-solution (2 M) and the mixture was extracted with DCM (4 x 50 ml). The combined organic layers were dried over $Na_2SO_4$ and concentrated under reduced pressure to give the desired product as colorless oil.

Yield: 193 mg (995 µmol, 37%).

**IR** (ATR), $\tilde{\nu}$ [$cm^{-1}$]: 3361 (w), 3275 (w), 2940 (m), 2863 (m), 2821 (m), 2770 (m), 1610 (m), 1583 (m), 1510 (s), 1463 (m), 1239 (s), 1031 (m), 811 (m).

**$^1$H-NMR** ($CDCl_3$, δ [ppm], *J* [Hz]): 7.21 (d, 2H, $^3J$ = 8.6, benzyl-C**H**$_{arom.}$), 6.89 (d, 2H, $^3J$ = 8.6, benzyl-C**H**$_{arom.}$), 4.06 (t, 2H, $^3J$ = 5.8, OC**H**$_2$$CH_2N$), 3.80 (s, 2H, benzyl-C**H**$_2$), 2.72 (t, 2H, $^3J$ = 5.8, $OCH_2$C**H**$_2$N), 2.33 (s, 6H, N(C**H**$_3$)$_2$), 1.54 (s, 2H, N**H**$_2$).

**$^{13}$C-NMR** ($CDCl_3$, δ [ppm], *J* [Hz]): 157.8 (1C, benzyl-$C_q$), 135.7 (1C, benzyl-$C_q$), 128.2 (2C, benzyl-$CH_{arom.}$), 114.6 (2C, benzyl-$CH_{arom.}$), 66.1 (1C, $OCH_2CH_2N$), 58.3 (1C, $OCH_2CH_2N$), 45.9 (1C, benzyl-$CH_2$), 45.8 (2C, $N(CH_3)_2$).

*Synthesis of 1-Butyl-N-(4-(2-(dimethylamino)ethoxy)benzyl)-6-fluoro-7-morpholino-4-oxo-1,4-dihydroquinoline-3-carboxamide oxalate (GHQ250)*

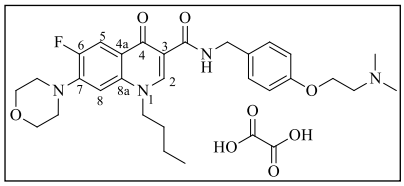

To a cooled solution (0 °C) of 100 mg (287 µmol) 1-butyl-6-fluoro-7-morpholino-4-oxo-1,4-dihydroquinoline-3-carboxylic acid (D) and 116 mg (1.15 mmol, 125 µl) NMM in 10 ml anhydrous DMF 118 mg (862 µmol, 112 µl) isobutyl chloroformate were added dropwise under argon atmosphere. After 1 h at 0 °C 168 mg (862 µmol) 2-(4-(aminomethyl)phenoxy)-*N*,*N*-dimethylethanamine (Q) were added and stirring at rt was continued for 45 min. The solvent was removed in vacuo and the crude product was purified via normal phase column chromatography on silica gel ($CHCl_3$/MeOH/ conc. $NH_3$ 100:10:1, $R_f$: 0.81). The resulting solid was dissolved in 4 ml ACN and a solution of 129 mg (1.44 mmol) oxalic acid in 6 ml ACN were added dropwise. At -20 °C the oxalic salt precipitated which was recrystallized from ACN.

Yield: 103 mg (156 µmol, 54%), mp: 172 - 173 °C (ACN).

CHN: *calculated* C: 58.26, H: 6.11, F: 2.88, N: 8.49, O: 24.25 (for **API**/**Ox** 1:1.5), *found* C: 58.57, H: 6.33, N: 8.71.

Stoichiometry: **API**/**Ox** 1:1.5.

**IR** (ATR), $\tilde{\nu}$ [$cm^{-1}$]: 3175 (w), 3034 (w), 2956 (w), 2925 (w), 2853 (w), 2593 (w), 1732 (br), 1645 (s), 1558 (m), 1490 (s), 1376 (w), 1241 (m), 1179 (m), 1117 (m), 934 (m), 802 (m), 681 (m).

**$^1$H-NMR** (DMSO-$d_6$, δ [ppm], *J* [Hz]): 10.3 (t, 1H, $^3J$ = 5.7, CON**H**R), 8.77 (s, 1H, **H**-2), 7.85 (d, 1H, $^3J_{\mathbf{H,F}}$ = 13.6, **H**-5), 7.29 (d, 2H, $^3J$ = 8.6, benzyl-C**H**$_{arom.}$), 7.08 (d, 1H, $^4J_{\mathbf{H,F}}$ = 7.2, **H**-8), 6.96 (d, 2H, $^3J$ = 8.6, benzyl-C**H**$_{arom.}$), 4.48-4.46 (m, 4H, benzyl-C**H**$_2$, NC**H**$_2$CH$_2$CH$_2$CH$_3$), 4.29 (t, 2H, $^3J$ = 5.0, OC**H**$_2$CH$_2$N(CH$_3$)$_2$), 3.79-3.77 (m, 4H, morpholino-C**H**$_2$-O-C**H**$_2$), 3.44 (t, 2H, $^3J$ = 5.0, OCH$_2$C**H**$_2$N(CH$_3$)$_2$), 3.25-2.24 (m, 4H, morpholino-C**H**$_2$-N-C**H**$_2$), 2.80 (s, 6H, OCH$_2$CH$_2$N(C**H**$_3$)$_2$), 1.75 (quint, 2H, $^3J$ = 7.3,

$NCH_2C\mathbf{H}_2CH_2CH_3$), 1.30 (sext, 2H, $^3J$ = 7.3, $NCH_2CH_2C\mathbf{H}_2CH_3$), 0.91 (t, 3H, $^3J$ = 7.3, $NCH_2CH_2CH_2C\mathbf{H}_3$).

**$^{13}$C-NMR** (DMSO-$d_6$, δ [ppm], *J* [Hz]): 174.1 (d, 1C, $^4J_{\mathbf{C},F}$ = 2.5, **C**-4), 164.0 (1C, **C**ONHR), 163.4 (Oxalat), 156.6 (1C, benzyl-$\mathbf{C}_q$), 152.5 (d, 1C, $^1J_{\mathbf{C},F}$ = 247.5, **C**-6), 147.8 (1C, **C**-2), 144.4 (d, 1C, $^2J_{\mathbf{C},F}$ = 10.3, **C**-7), 136.6 (1C, **C**-8a), 132.3 (1C, benzyl-$\mathbf{C}_q$), 128.8 (2C, benzyl-$\mathbf{C}H_{arom.}$), 121.5 (d, 1C, $^3J_{\mathbf{C},F}$ = 7.0, **C**-4a), 114.7 (2C, benzyl-$\mathbf{C}H_{arom.}$), 111.4 (d, 1C, $^2J_{\mathbf{C},F}$ = 22.4, **C**-5), 110.0 (1C, **C**-3), 105.6 (d, 1C, $^3J_{\mathbf{C},F}$ = 3.1, **C**-8), 65.9 (2C, morpholino-$\mathbf{C}H_2$-O-$\mathbf{C}H_2$), 62.4 (1C, $O\mathbf{C}H_2CH_2N(CH_3)_2$), 55.3 (1C, $OCH_2\mathbf{C}H_2N(CH_3)_2$), 52.9 (1C, $N\mathbf{C}H_2CH_2CH_2CH_3$), 49.8 (2C, $^4J_{\mathbf{C},F}$ = 4.4, morpholino-$\mathbf{C}H_2$-N-$\mathbf{C}H_2$), 42.8 (2C, $OCH_2CH_2N(\mathbf{C}H_3)_2$), 41.6 (1C, benzyl-$\mathbf{C}H_2$), 30.3 (1C, $NCH_2\mathbf{C}H_2CH_2CH_3$), 19.2 (1C, $NCH_2CH_2\mathbf{C}H_2CH_3$), 13.5 (1C, $NCH_2CH_2CH_2\mathbf{C}H_3$).

**Synthesis of 1-Butyl-6-fluoro-7-morpholino-4-oxo-*N*-(pyridin-4-ylmethyl)-1,4-dihydroquinoline-3-carboxamide oxalate (GHQ242)**

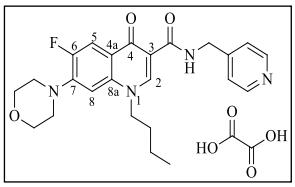

To a cooled solution (0 °C) of 150 mg (431 µmol) 1-butyl-6-fluoro-7-morpholino-4-oxo-1,4-dihydroquinoline-3-carboxylic acid (D) and 218 mg (2.16 mmol, 237 µl) NMM in 10 ml anhydrous DMF 235 mg (1.72 mmol, 224 µl) isobutyl chloroformate were added dropwise under argon atmosphere. After 1 h at 0 °C 186 mg (1.72 mmol, 175 µl) 4-(aminomethyl)pyridine were added and stirring at rt was continued for 45 min. The solvent was removed in vacuo and the crude product was purified via normal phase column chromatography on silica gel ($CHCl_3$/PE 100:1, $R_f$: 0.49). The resulting solid was dissolved in 4 ml ACN and a solution of 194 mg (2.16 mmol) oxalic acid in 6 ml ACN was added dropwise. After 30 min of agitating at rt the oxalic salt precipitated which was recrystallized from ACN.

Yield: 87 mg (151 µmol, 35%), mp: 191 - 192 °C (ACN).

CHN: *calculated* C: 56.54, H: 5.27, F: 3.31, N: 9.77, O: 25.06 (for **API**/**Ox** 1:1.5), *found* C: 56.46, H: 5.28, N: 9.70.

Stoichiometry: **API**/**Ox** 1:1.5.

**IR** (ATR), $\tilde{\nu}$ [$cm^{-1}$]: 3235 (w), 3073 (w), 2957 (m), 2931 (w), 2871 (w), 2614 (br), 1905 (br), 1728 (br), 1660 (s), 1629 (s), 1530 (m), 1489 (s), 1451 (m), 1376 (w), 1258 (s), 1198 (m), 1114 (m), 932 (m), 799 (m), 692 (m).

**$^{1}$H-NMR** (DMSO-$d_6$, δ [ppm], $J$ [Hz]): 10.5 (t, 1H, $^{3}J$ = 5.8, CON**H**R), 8.78 (s, 1H, **H**-2), 8.55 (d, 2H, $^{3}J$ = 5.2, Py-C**H**), 7.90 (d, 1H, $^{3}J_{\mathbf{H,F}}$ = 13.5, **H**-5), 7.39 (d, 2H, $^{3}J$ = 5.2, Py-C**H**), 7.10 (d, 1H, $^{4}J_{\mathbf{H,F}}$ = 7.2, **H**-8), 4.62 (d, 2H, $^{3}J$ = 5.8, C**H**$_2$), 4.48 (t, 2H, $^{3}J$ = 7.3, NC**H**$_2$CH$_2$CH$_2$CH$_3$), 3.80 (br, 4H, morpholino-C**H**$_2$-O-C**H**$_2$), 3.26 (br, 4H, morpholino-C**H**$_2$-N-C**H**$_2$), 1.77 (quint, 2H, $^{3}J$ = 7.3, NCH$_2$C**H**$_2$CH$_2$CH$_3$), 1.32 (sext, 2H, $^{3}J$ = 7.3, NCH$_2$CH$_2$C**H**$_2$CH$_3$), 0.92 (t, 3H, $^{3}J$ = 7.3, NCH$_2$CH$_2$CH$_2$C**H**$_3$).

**$^{13}$C-NMR** (DMSO-$d_6$, δ [ppm], $J$ [Hz]): 174.1 (d, 1C, $^{4}J_{\mathbf{C,F}}$ = 1.8, **C**-4), 164.5 (1C, **C**ONHR), 161.0 (Oxalat), 152.5 (d, 1C, $^{1}J_{\mathbf{C,F}}$ = 248.0, **C**-6), 149.9 (1C, Py-**C**$_q$), 148.6 (2C, Py-**C**H), 147.8 (1C, **C**-2), 144.3 (d, 1C, $^{2}J_{\mathbf{C,F}}$ = 10.4, **C**-7), 136.6 (1C, **C**-8a), 122.4 (2C, Py-**C**H), 121.4 (d, 1C, $^{3}J_{\mathbf{C,F}}$ = 6.6, **C**-4a), 111.4 (d, 1C, $^{2}J_{\mathbf{C,F}}$ = 22.7, **C**-5), 109.7 (1C, **C**-3), 105.5 (d, 1C, $^{3}J_{\mathbf{C,F}}$ = 2.0, **C**-8), 65.8 (2C, morpholino-**C**H$_2$-O-**C**H$_2$), 52.8 (1C, N**C**H$_2$CH$_2$CH$_2$CH$_3$), 49.8 (d, 2C, $^{4}J_{\mathbf{C,F}}$ = 4.4, morpholino-**C**H$_2$-N-**C**H$_2$), 41.2 (1C, **C**H$_2$), 30.2 (1C, NCH$_2$**C**H$_2$CH$_2$CH$_3$), 19.1 (1C, NCH$_2$CH$_2$**C**H$_2$CH$_3$), 13.4 (1C, NCH$_2$CH$_2$CH$_2$**C**H$_3$).

**References**

[1] de la Cruz A EJ, Goya P, Martinez A., Pfleiderer W. 1992. Tautomerism and Acidity in 4-Quinolone-3-carboxylic Acid Derivatives. Tetrahedron 48: 6135-6150.

[2] Hiltensperger G, Jones NG, Niedermeier S, Stich A, Kaiser M, Jung J, Puhl S, Damme A, Braunschweig H, Meinel L, Engstler M, Holzgrabe U. 2012. Synthesis and structure-activity relationships of new quinolone-type molecules against Trypanosoma brucei. J Med Chem 55:2538-2548.

[3] Kellenberger JLD, J.; Reinelt, S. B. 2009. Preparation of Clarithromycin Macrolide Derivatives as Antiinflammatory Agents.

[4] Kohlmann A, Zech SG, Li F, Zhou T, Squillace RM, Commodore L, Greenfield MT, Lu X, Miller DP, Huang WS, Qi J, Thomas RM, Wang Y, Zhang S, Dodd R, Liu S, Xu R, Xu Y, Miret JJ, Rivera V, Clackson T, Shakespeare WC, Zhu X, Dalgarno DC. 2013. Fragment growing and linking lead to novel nanomolar lactate dehydrogenase inhibitors. J Med Chem 56:1023-1040.

[5] Brunette SRK, J. M.; Lemieux, R. M.; Tschantz, M. A. 2006. Preparation of Pyridine Derivatives Useful as Inhibitors of PKC-Theta for Treating Various Diseases.

[6] Chichak KS, Peters AJ, Cantrill SJ, Stoddart JF. 2005. Nanoscale borromeates. J Org Chem 70:7956-7962.

[7] Löber OB, C.; Ebel, K.; Johann, P. 2004. Verfahren zur Herstellung von Aminoalkoxybenzylaminen und Aminoalkoxybenzonitrilen als Zwischenprodukte.

## Physicochemical characterization

### X-ray analysis

For single crystal structure analysis of GHQ168, a suited crystal with a size of 0,072 x 0, 112 x 0.19 $mm^3$ was selected. Data collection was carried out on a BRUKER AXS Apex II diffractometer (Mo-Kα radiation; λ=71.07 pm) at 100 K with Helios-mirror using the BRUKER AXS Apex Suite Software package [1]. Data processing was done with the Olex2 software package [2]. Structure solution was carried out with olex.solve [3] using charge flipping methods. The model was refined with the olex2.refine refinement package using Gauss-Newton minimization [4]. Integrity of symmetry was checked using PLATON [5]. Non-hydrogen atoms were refined anisotropically by least square techniques, hydrogen atoms were refined with geometrical constraints regarding their positions. Crystallographic data are summarized in **Table S1**.

### References

[1] Bruker. SMART Apex Suite 2001, Bruker AXS Inc., Madison, Wisconsin, USA.

[2] Bourhis LJ, Dolomanov OV, Gildea RJ, Howard JA, Puschmann H. 2015. The anatomy of a comprehensive constrained, restrained refinement program for the modern computing environment- Olex2 dissected. Acta Crystallogr A Found Adv 71:59-75.

[3] L. J. Bourhis OVD, R. J. Gildea, J. A. K. Howard, H. Puschmann. 2011. olex.solve.

[4] L. J. Bourhis OVD, R. J. Gildea, J. A. K. Howard, H. Puschmann. 2011. olex.refine.

[5] A. L. Spek. 2003. Single-crystal structure validation with the program *PLATON.* J. Appl. Cryst. 2003, 36:7-13.

| | GHQ168 |
|---|---|
| Formula sum | $C_{25}H_{28}FN_3O_3$ |
| Formula wgt /gmol$^{-1}$ | 437.514 |
| *a* /pm | 842.8(2) |
| *b* /pm | 1708.3(3) |
| *c* /pm | 1753.3(4) |
| *α* /° | 61.06(3) |
| *β* /° | 83.56(3) |
| *γ* /° | 83.83(3) |
| *V* /10$^6$pm$^3$ | 2191(1) |
| Crystal system | Triclinic |
| Space group | $P\bar{1}$ |
| Z | 4 |
| $d_{calcd}$ /gcm$^{-3}$ | 1.3156 |
| *μ* /cm$^{-1}$ | 0.93 |
| *T* /K | 173 |
| Data range /° | 1.33 ≤ 2Θ ≤ 26.59 |
| X-ray radiation | Mo-Kα, λ = 71.073 pm |
| Diffractometer | Bruker APEX-II CCD |
| Reflections | 21713 |
| Unique reflections | 9082 |
| *R*(int) | 0.0756 |
| No. parameters ref. | 575 |
| $R_1$[a)] for *n* reflections with $F_o>4\sigma$ ($F_o$), *n* | 0.0732 |
| $R_1$(all) | 0.1652 |
| *w*$R_2$[b)](all) | 0.2304 |
| S[c)] | 1.0637 |
| Rem. elec. density /10$^{-6}$epm | 0.9876/-0.7158 |

a) $R_1 = \sum||F_o|-|F_c||/\sum|F_o|$

b) $wR_2 = [\sum(w(F_o^2-F_c^2)^2)/\sum(w(F_o^2)^2)]^{1/2}$

c) GooF = $S = [\sum(w(F_o^2-F_c^2)^2)/(n-p)]^{1/2}$ with $F_o$, $F_c$ = observed and calculated structure factors, *n* = number of observed reflections

**Table S1**: Crystallographic data of single crystal X-ray diffraction of GHQ168. Deviations are given in brackets.

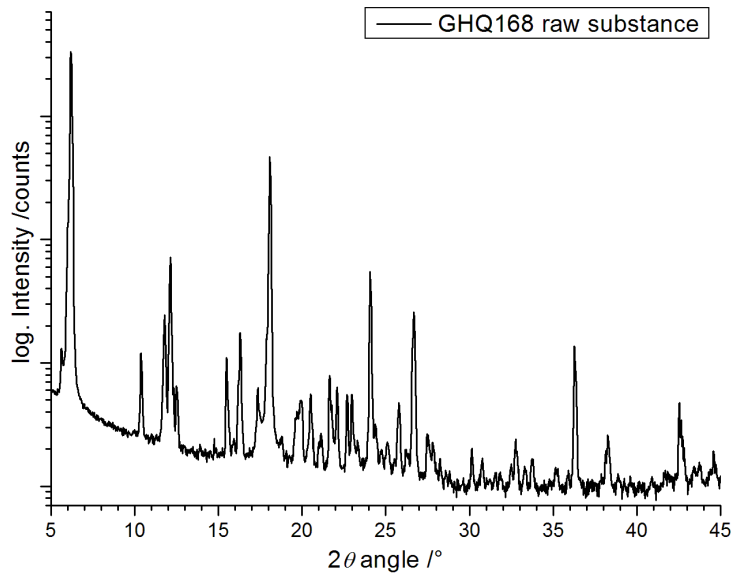


**Figure S1A**: XRPD (Bruker D8 Discover, Billerica, USA) data show characteristic crystal reflexes for GHQ168.

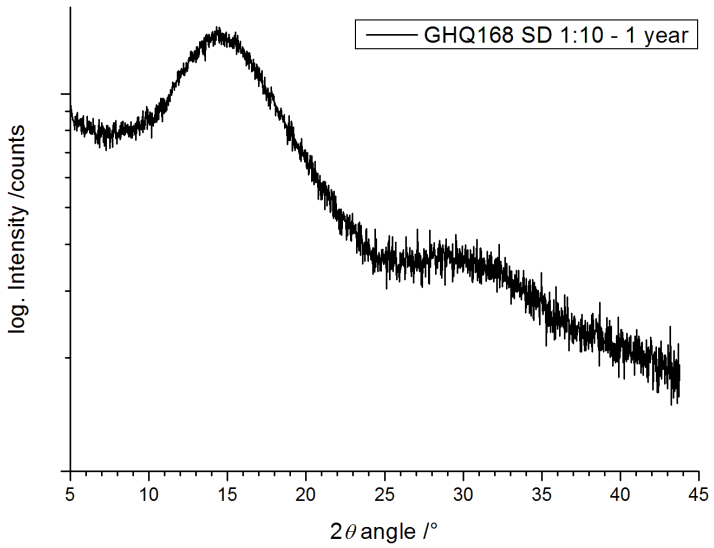


**Figure S1B**: The spray dried formulation of GHQ168 and Eudragit L100 shows a broad amorphous signal. No recrystallization events occurred after 12 months.

**Scanning electron microscopy (SEM)**

For the characterization of particle morphology, scanning electron microscopy (JSM-7500F, Jeol, Japan) was used with an accelerating voltage of 2.0 kV and a 1000-fold magnification at a working distance of 8.6 mm.

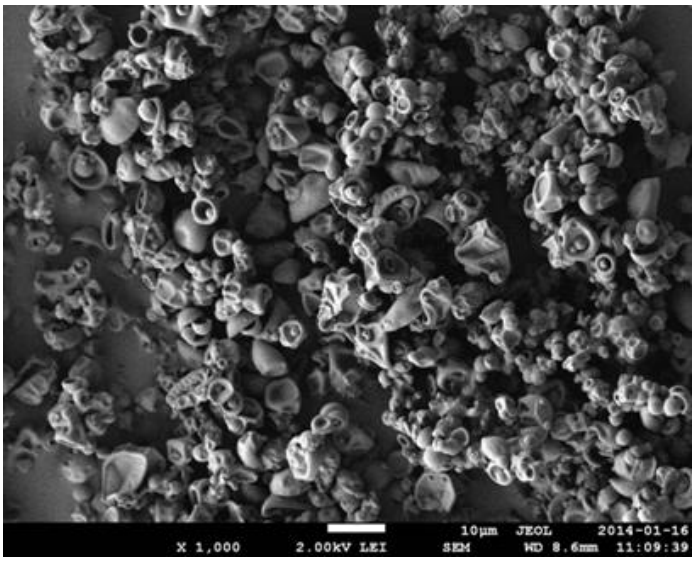


**Figure S2**: Scanning electron micrographs of spray dried particles of GHQ168 and Eudragit® L100 (1+10 w/w) revealed that the particle size distribution was within a narrow range. The morphology complies with desired specifications such as smooth surface and spherical form.

## Dynamic Light Scattering (DLS)

A solution of GHQ168 spray dried with Eudragit L100 (2 g/l) was prepared in PBS buffer and filtered using syringe filters (5 µm).

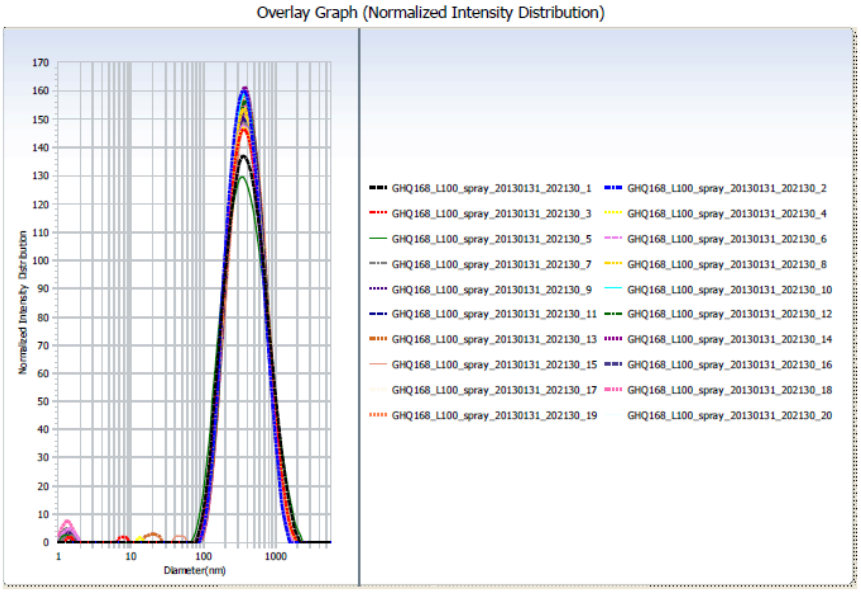


| No | Data | Repet. No | pH | Ave. Diameter(nm) | Polydispersity Index | D (10%) (nm) | D (50%) (nm) | D (90%) (nm) |
|---|---|---|---|---|---|---|---|---|
| 1 | GHQ168_L100_spray_20130131_202130_1 | 1 | NA | 331.7 | 0.236 | 164.5 | 363.8 | 842.3 |
| 2 | GHQ168_L100_spray_20130131_202130_2 | 2 | NA | 340.4 | 0.226 | 175.6 | 349.2 | 712.2 |
| 3 | GHQ168_L100_spray_20130131_202130_3 | 3 | NA | 330.3 | 0.223 | 169.7 | 359.0 | 786.7 |
| 4 | GHQ168_L100_spray_20130131_202130_4 | 4 | NA | 330.1 | 0.226 | 171.4 | 360.5 | 785.9 |
| 5 | GHQ168_L100_spray_20130131_202130_5 | 5 | NA | 317.7 | 0.256 | 150.7 | 349.3 | 859.0 |
| 6 | GHQ168_L100_spray_20130131_202130_6 | 6 | NA | 325.8 | 0.218 | 164.6 | 352.5 | 754.6 |
| 7 | GHQ168_L100_spray_20130131_202130_7 | 7 | NA | 328.5 | 0.218 | 167.4 | 357.8 | 758.6 |
| 8 | GHQ168_L100_spray_20130131_202130_8 | 8 | NA | 329.7 | 0.204 | 173.3 | 355.4 | 744.4 |
| 9 | GHQ168_L100_spray_20130131_202130_9 | 9 | NA | 331.7 | 0.212 | 171.0 | 362.8 | 743.1 |
| 10 | GHQ168_L100_spray_20130131_202130_10 | 10 | NA | 329.4 | 0.203 | 177.2 | 356.9 | 723.2 |
| 11 | GHQ168_L100_spray_20130131_202130_11 | 11 | NA | 333.0 | 0.227 | 168.9 | 349.1 | 753.6 |
| 12 | GHQ168_L100_spray_20130131_202130_12 | 12 | NA | 333.1 | 0.213 | 174.4 | 363.3 | 738.4 |
| 13 | GHQ168_L100_spray_20130131_202130_13 | 13 | NA | 332.5 | 0.214 | 176.5 | 362.5 | 734.5 |
| 14 | GHQ168_L100_spray_20130131_202130_14 | 14 | NA | 337.3 | 0.195 | 179.0 | 360.0 | 721.3 |
| 15 | GHQ168_L100_spray_20130131_202130_15 | 15 | NA | 337.8 | 0.218 | 176.0 | 374.3 | 763.3 |
| 16 | GHQ168_L100_spray_20130131_202130_16 | 16 | NA | 341.3 | 0.208 | 178.6 | 369.0 | 771.1 |
| 17 | GHQ168_L100_spray_20130131_202130_17 | 17 | NA | 341.5 | 0.204 | 179.5 | 368.1 | 768.0 |
| 18 | GHQ168_L100_spray_20130131_202130_18 | 18 | NA | 342.0 | 0.204 | 176.1 | 363.8 | 755.8 |
| 19 | GHQ168_L100_spray_20130131_202130_19 | 19 | NA | 338.4 | 0.222 | 176.2 | 374.5 | 770.5 |
| 20 | GHQ168_L100_spray_20130131_202130_20 | 20 | NA | 342.4 | 0.202 | 180.6 | 366.1 | 778.9 |

**Figure S3**: Subsequent DLS measurements were performed in order to monitor the pattern in solution (20 subsequent measurements are depicted above) and particle size did not change significantly over time.

## Caco-2 monolayers

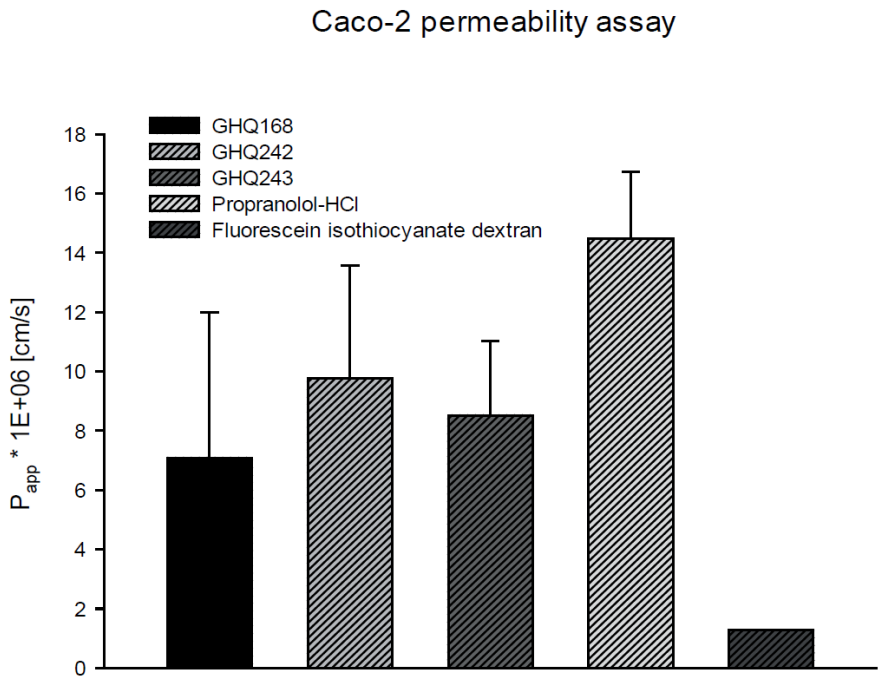


**Figure S4**: Caco-2 Cell assays illustrating the equal permeability of GHQ168, GHQ242, GHQ243, and Propranolol-HCl.

| | $P_{app}$ * 1E+06 cm/s | | | | |
|---|---|---|---|---|---|
| | Propranolol-HCl | GHQ168 | GHQ242 | GHQ243 | Fluorescein |
| MV [cm/s] | 14.47 | 7.09 | 9.77 | 8.52 | 1.27 |
| SD [cm/s] | 2.28 | 4.90 | 3.80 | 2.51 | 0.02 |
| RSD [%] | 15.75 | 69.09 | 38.96 | 29.48 | 1.70 |

**Table S2** Results for permeability testing in Caco-2 cells.

Calculation of $P_{app}$:

$$P_{app} = \frac{V_A}{\text{Area x Time}} \text{ x } \frac{[drug]_{acceptor}}{[drug]_{initial,\ donor}}$$

$V_A$ = 0.6, Area = 0.33, Time = 3600 s, $[drug]_{initial,\ donor}$ = 100

### *In vitro* activity and Cytotoxicity

#### *In vitro* activity

The anti-trypanosomal activity was recorded essentially as developed by Räz *et al.* (with some modifications, cf. Ilkay 2010). The compounds were dissolved in DMSO (20 mM). In brief, *T. b. brucei* TC 221 were incubated at a cell density of 1 x $10^5$ cells/mL in Complete Baltz medium (Baltz, 1985) with serial dilutions of the compounds at 37 °C and 5% $CO_2$ for 72 h. The final DMSO concentration was 1%. After 24 h of incubation, AlamarBlue was added to a final concentration of 1.1 mg/L and the plates were incubated further on for 48 h. Untreated cells and cells incubated with the solvent only were used as controls to check for parasite viability. The $IC_{50}$ value was calculated with respect to negative controls (without compounds) from the absorbance values measured at λ=550 nm using a microplate reader (Asys Expert 96, Biochrome, Cambridge, UK). Reference wavelength was set to λ=630 nm. *T. brucei rhodesiense* STIB 900 BSF trypomastigotes were seeded at 1 x $10^3$ cells/mL in 200 µL of growth medium (composition: Minimum Essential Medium 50 µL, 25 mM HEPES, 1g/L additional glucose, 1% MEM non-essential amino acids (100x), 0.2 mM 2-mercaptoethanol, 1 mM sodium pyruvate and 15% heat inactivated horse serum) with serial dilutions of the compounds. After incubation for 3 days at 37 °C and 5% $CO_2$, 20 µL of AlamarBlue (12.5 mg / 100 mL) were added to each well and the plates were incubated for further 16 h. After reading the plates using an excitation wavelength of 536 nm and an emission wavelength of 588 nm (Multiskan Ascent, Thermo Fisher Scientific, Braunschweig, Germany), data were analysed and the $IC_{50}$ value was calculated.

### References

[1] Räz B, Iten M, Grether-Bühler Y, Kaminsky R, Brun R. 1997. The Alamar Blue® assay to determine drug sensitivity of African trypanosomes (T.b. rhodesiense and T.b. gambiense) *in vitro*. Acta Tropica 68:139-147.

[2] Baltz T Baltz D, Giroud C, Crockett J. 1985. Cultivation in a semi-defined medium of animal infective forms of Trypanosoma brucei, T. equiperdum, T. evansi, T. rhodesiense and T. gambiense. EMBO J 4:1273-1277.

[3] Papadopoulou MV, Bloomer WD, Lepesheva GI, Rosenzweig HS, Kaiser M, Aguilera-Venegas B, Wilkinson SR, Chatelain E, Ioset J-R. 2015. Novel 3-nitrotriazole-based amides and carbinols as bifunctional antichagasic agents. Journal of medicinal chemistry 58:1307-1319.

**Cytotoxicity**

Cell viability was measured as described before (Larson 1997, Muth 2007). Briefly, the compounds were dissolved in DMSO to a concentration of 20 mM and serially diluted in DMSO. A defined number of mammalian cells (see below) were incubated in a volume of 200 µl in 96-well cell culture plates in the respective medium without phenol red with serial compound dilutions at 37 °C and 5% $CO_2$. The final concentration of DMSO was 1%. After 24 h of incubation, 10% of an AlamarBlue solution was added. The $CC_{50}$ value was calculated with respect to negative controls (without compounds) from the absorbance values measured at λ=550 nm using a microplate reader (Multiskan Ascent, Thermo Fisher Scientific, Braunschweig, Germany). The reference wavelength was set to λ=630 nm.

**References**

[1] Larson EM, Doughman DJ, Gregerson DS, Obritsch WF. 1997. A new, simple, nonradioactive, nontoxic in vitro assay to monitor corneal endothelial cell viability. Investigative Ophthalmology & Visual Science 38:1929-1933

[2] Muth M, Hoerr V, Glaser M, Ponte-Sucre A, Moll H, Stich A, Holzgrabe U. 2007. Antitrypanosomal activity of quaternary naphthalimide derivatives. Bioorganic & medicinal chemistry letters 17:1590-1593.

## PBPK Modelling

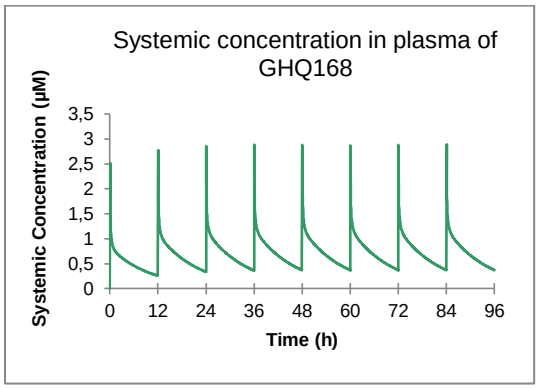


**Figure S5A**: Simcyp plasma concentration prediction for GHQ168.

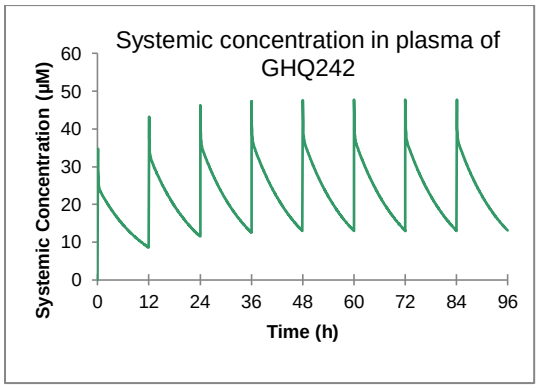


**Figure S5B**: Simcyp plasma concentration prediction for GHQ242.

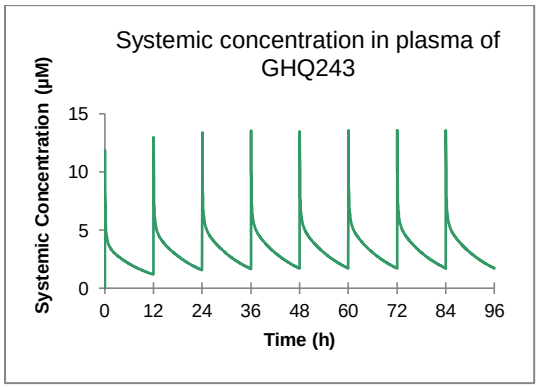


**Figure S5C**: Simcyp plasma concentration prediction for GHQ243.

## Pharmacokinetics

## Analytical Method Validation

GHQ168:

| Sample Name | Concentration [ng/ml] | Peak Area GHQ168 | Peak Area Int. standard | Ratio of Peak Areas | Weighting ($1/c^2$) | Conc. calc. [ng/ml] | RD [%] |
|---|---|---|---|---|---|---|---|
| E08 | 500.000 | 1990000 | 23400000 | 0.0850427 | 4.00E-06 | 495.08 | -1.0 |
| E07 | 400.000 | 1720000 | 24600000 | 0.0699187 | 6.25E-06 | 407.05 | 1.8 |
| E06 | 200.000 | 829000 | 23000000 | 0.0360435 | 2.50E-05 | 209.87 | 4.9 |
| E05 | 100.000 | 398000 | 22300000 | 0.0178475 | 1.00E-04 | 103.96 | 4.0 |
| E04 | 20.000 | 79200 | 22500000 | 0.0035200 | 2.50E-03 | 20.56 | 2.8 |
| E03 | 5.000 | 16300 | 22400000 | 0.0007277 | 4.00E-02 | 4.31 | -13.8 |
| E02 | 2.000 | 6820 | 21100000 | 0.0003232 | 2.50E-01 | 1.96 | -2.0 |
| E01 | 1.000 | 3590 | 21700000 | 0.0001654 | 1.00E+00 | 1.04 | 4.0 |
| **Standard curve parameters** | | Slope 0.0001718 | | Intercept -0.000012760 | | Coefficient of Correlation 0.9977 | |

**Table S3A**: Linearity data for GHQ168 in the concentration range of 1.0 - 500.0 ng/ml.

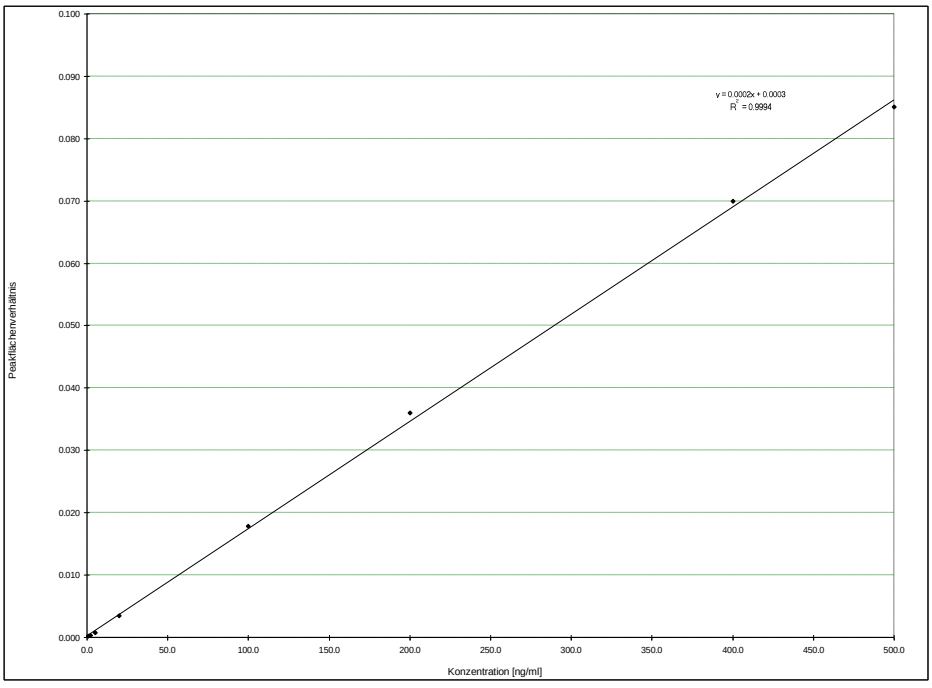


**Figure S6A**: Linearity curve of GHQ168 in the concentration range of 1.0 - 500.0 ng/ml.

| Sample Name | High conc. [ng/ml] | Peak Area GHQ168 | Peak Area Int. standard | Ratio of Peak Areas | Conc. calc. [ng/ml] | RD [%] |
|---|---|---|---|---|---|---|
| QC-H1 | 400.000 | 1620000 | 23100000 | 0.07013 | 408.281 | 2.1 |
| QC-H2 | 400.000 | 1640000 | 24000000 | 0.06833 | 397.804 | -0.5 |
| QC-H3 | 400.000 | 1650000 | 23200000 | 0.07112 | 414.044 | 3.5 |
| QC-H4 | 400.000 | 1730000 | 23300000 | 0.07425 | 432.263 | 8.1 |
| QC-H5 | 400.000 | 1730000 | 22600000 | 0.07655 | 445.651 | 11.4 |
| QC-H6 | 400.000 | 1690000 | 25200000 | 0.06706 | 390.412 | -2.4 |
| arithm. mean | | | | 0.07124 | 414.743 | |
| ±SD | | | | 0.003590 | 20.8970 | |
| CV [%] | | | | 5.0 | 5.0 | |
| RD [%] | | | | | 3.7 | |

| Sample Name | Medium conc. [ng/ml] | Peak Area GHQ168 | Peak Area Int. standard | Ratio of Peak Areas | Conc. calc. [ng/ml] | RD [%] |
|---|---|---|---|---|---|---|
| QC-M1 | 100.000 | 402000 | 24000000 | 0.01675 | 97.571 | -2.4 |
| QC-M2 | 100.000 | 368000 | 24000000 | 0.01533 | 89.306 | -10.7 |
| QC-M3 | 100.000 | 374000 | 21600000 | 0.01731 | 100.831 | 0.8 |
| QC-M4 | 100.000 | 393000 | 23000000 | 0.01709 | 99.550 | -0.5 |
| QC-M5 | 100.000 | 361000 | 21000000 | 0.01719 | 100.132 | 0.1 |
| QC-M6 | 100.000 | 362000 | 21200000 | 0.01708 | 99.492 | -0.5 |
| arithm. mean | | | | 0.01679 | 97.814 | |
| ±SD | | | | 0.000740 | 4.3070 | |
| CV [%] | | | | 4.4 | 4.4 | |
| RD [%] | | | | | -2.2 | |

| Sample Name | Low conc. [ng/ml] | Peak Area GHQ168 | Peak Area Int. standard | Ratio of Peak Areas | Conc. calc. [ng/ml] | RD [%] |
|---|---|---|---|---|---|---|
| QC-L1 | 5.000 | 15800 | 21400000 | 0.00074 | 4.382 | -12.4 |
| QC-L2 | 5.000 | 16600 | 21200000 | 0.00078 | 4.614 | -7.7 |
| QC-L3 | 5.000 | 16700 | 20500000 | 0.00081 | 4.789 | -4.2 |
| QC-L4 | 5.000 | 15900 | 21000000 | 0.00076 | 4.498 | -10.0 |
| QC-L5 | 5.000 | 15700 | 20000000 | 0.00079 | 4.673 | -6.5 |
| QC-L6 | 5.000 | 17100 | 21100000 | 0.00081 | 4.789 | -4.2 |
| arithm. mean | | | | 0.00078 | 4.624 | |
| ±SD | | | | 0.000028 | 0.1621 | |
| CV [%] | | | | 3.6 | 3.5 | |
| RD [%] | | | | | -7.5 | |

**Table S3B**: Precision data for GHQ168 at high, medium and low concentrations.

GHQ242:

| Sample Name | Concentration [ng/ml] | Peak Area GHQ168 | Peak Area Int. standard | Ratio of Peak Areas | Weighting (1/c²) | Conc. calc. [ng/ml] | RD [%] |
|---|---|---|---|---|---|---|---|
| E08 | 500.000 | 1320000 | 21500000 | 0.0613953 | 4.00E-06 | 527.61 | 5.5 |
| E07 | 400.000 | 993000 | 21400000 | 0.0464019 | 6.25E-06 | 398.80 | -0.3 |
| E06 | 200.000 | 491000 | 20500000 | 0.0239512 | 2.50E-05 | 205.92 | 3.0 |
| E05 | 100.000 | 242000 | 21400000 | 0.0113084 | 1.00E-04 | 97.31 | -2.7 |
| E04 | 20.000 | 43700 | 20100000 | 0.0021741 | 2.50E-03 | 18.83 | -5.9 |
| E03 | 5.000 | 10700 | 19400000 | 0.0005515 | 4.00E-02 | 4.89 | -2.2 |
| E02 | 2.000 | 4660 | 20900000 | 0.0002230 | 2.50E-01 | 2.07 | 3.5 |
| E01 | 1.000 | 2040 | 21000000 | 0.0000971 | 1.00E+00 | 0.99 | -1.0 |
| **Standard curve parameters** | | Slope 0.0001164 | | Intercept -0.000018075 | | Coefficient of Correlation 0.9991 | |

**Table S3C**: Linearity data for GHQ242 in the concentration range of 1.0 - 500.0 ng/ml.

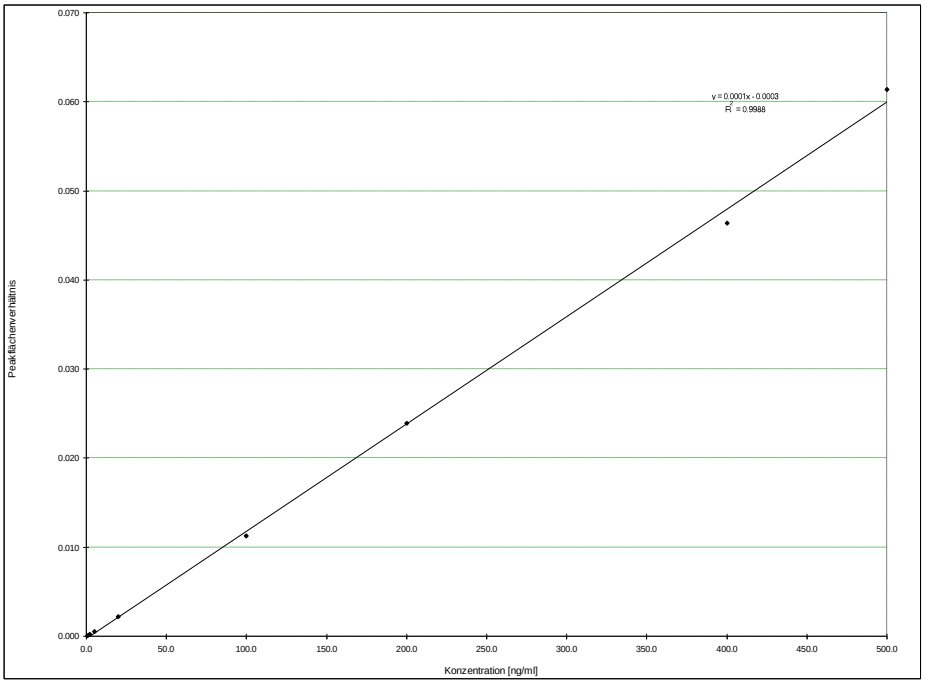


**Figure S6B**: Linearity curve of GHQ242 in the concentration range of 1.0 - 500.0 ng/ml.

| Sample Name | High conc. [ng/ml] | Peak Area GHQ168 | Peak Area Int. standard | Ratio of Peak Areas | Conc. calc. [ng/ml] | RD [%] |
|---|---|---|---|---|---|---|
| QC-H1 | 400.000 | 976000 | 20700000 | 0.04715 | 405.224 | 1.3 |
| QC-H2 | 400.000 | 1020000 | 21900000 | 0.04658 | 400.327 | 0.1 |
| QC-H3 | 400.000 | 985000 | 20700000 | 0.04758 | 408.918 | 2.2 |
| QC-H4 | 400.000 | 978000 | 20000000 | 0.04890 | 420.258 | 5.1 |
| QC-H5 | 400.000 | 1030000 | 21700000 | 0.04747 | 407.973 | 2.0 |
| QC-H6 | 400.000 | 966000 | 20600000 | 0.04689 | 402.990 | 0.7 |
| arithm. mean | | | | 0.04743 | 407.615 | |
| ±SD | | | | 0.000810 | 6.9555 | |
| CV [%] | | | | 1.7 | 1.7 | |
| RD [%] | | | | | 1.9 | |

| Sample Name | Medium conc. [ng/ml] | Peak Area GHQ168 | Peak Area Int. standard | Ratio of Peak Areas | Conc. calc. [ng/ml] | RD [%] |
|---|---|---|---|---|---|---|
| QC-M1 | 100.000 | 230000 | 19700000 | 0.01168 | 100.499 | 0.5 |
| QC-M2 | 100.000 | 231000 | 19200000 | 0.01203 | 103.506 | 3.5 |
| QC-M3 | 100.000 | 232000 | 20500000 | 0.01132 | 97.406 | -2.6 |
| QC-M4 | 100.000 | 238000 | 21000000 | 0.01133 | 97.492 | -2.5 |
| QC-M5 | 100.000 | 249000 | 21400000 | 0.01164 | 100.155 | 0.2 |
| QC-M6 | 100.000 | 238000 | 20500000 | 0.01161 | 99.898 | -0.1 |
| arithm. mean | | | | 0.01160 | 99.826 | |
| ±SD | | | | 0.000262 | 2.2544 | |
| CV [%] | | | | 2.3 | 2.3 | |
| RD [%] | | | | | -0.2 | |

| Sample Name | Low conc. [ng/ml] | Peak Area GHQ168 | Peak Area Int. standard | Ratio of Peak Areas | Conc. calc. [ng/ml] | RD [%] |
|---|---|---|---|---|---|---|
| QC-L1 | 5.000 | 11000 | 19800000 | 0.00056 | 4.966 | -0.7 |
| QC-L2 | 5.000 | 11200 | 21000000 | 0.00053 | 4.709 | -5.8 |
| QC-L3 | 5.000 | 11300 | 19900000 | 0.00057 | 5.052 | 1.0 |
| QC-L4 | 5.000 | 11000 | 20000000 | 0.00055 | 4.880 | -2.4 |
| QC-L5 | 5.000 | 10600 | 20500000 | 0.00052 | 4.623 | -7.5 |
| QC-L6 | 5.000 | 10700 | 20400000 | 0.00052 | 4.623 | -7.5 |
| arithm. mean | | | | 0.00054 | 4.809 | |
| ±SD | | | | 0.000021 | 0.1833 | |
| CV [%] | | | | 3.9 | 3.8 | |
| RD [%] | | | | | -3.8 | |

**Table S3D**: Precision data for GHQ242 at high, medium and low concentrations.

GHQ243:

| Sample Name | Concentration [ng/ml] | Peak Area GHQ168 | Peak Area Int. standard | Ratio of Peak Areas | Weighting (1/c²) | Conc. calc. [ng/ml] | RD [%] |
|---|---|---|---|---|---|---|---|
| E08 | 500.000 | 516000 | 21400000 | 0.0241121 | 4.00E-06 | 519.76 | 4.0 |
| E07 | 400.000 | 404000 | 20900000 | 0.0193301 | 6.25E-06 | 416.70 | 4.2 |
| E06 | 200.000 | 189000 | 20700000 | 0.0091304 | 2.50E-05 | 196.88 | -1.6 |
| E05 | 100.000 | 98600 | 20900000 | 0.0047177 | 1.00E-04 | 101.78 | 1.8 |
| E04 | 20.000 | 18300 | 20300000 | 0.0009015 | 2.50E-03 | 19.53 | -2.3 |
| E03 | 5.000 | 4570 | 21200000 | 0.0002156 | 4.00E-02 | 4.75 | -5.0 |
| E02 | 2.000 | 1830 | 21800000 | 0.0000839 | 2.50E-01 | 1.91 | -4.5 |
| E01 | 1.000 | 895 | 20700000 | 0.0000432 | 1.00E+00 | 1.03 | 3.0 |
| **Standard curve parameters** | | Slope 0.0000464 | | Intercept -0.000004727 | | Coefficient of Correlation 0.9991 | |

**Table S3E**: Linearity data for GHQ243 in the concentration range of 1.0 - 500.0 ng/ml.

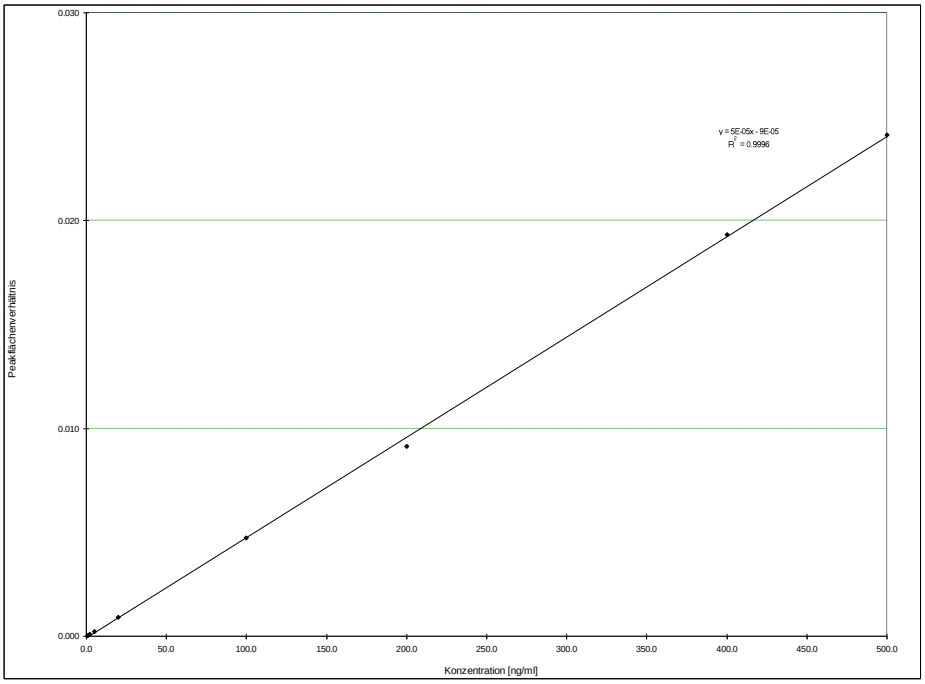


**Figure S6C**: Linearity curve of GHQ243 in the concentration range of 1.0 - 500.0 ng/ml.

| Sample Name | High conc. [ng/ml] | Peak Area GHQ168 | Peak Area Int. standard | Ratio of Peak Areas | Conc. calc. [ng/ml] | RD [%] |
|---|---|---|---|---|---|---|
| QC-H1 | 400.000 | 402000 | 21000000 | 0.01914 | 412.602 | 3.2 |
| QC-H2 | 400.000 | 401000 | 19600000 | 0.02046 | 441.050 | 10.3 |
| QC-H3 | 400.000 | 387000 | 20500000 | 0.01888 | 406.998 | 1.7 |
| QC-H4 | 400.000 | 405000 | 20900000 | 0.01938 | 417.774 | 4.4 |
| QC-H5 | 400.000 | 411000 | 20600000 | 0.01995 | 430.059 | 7.5 |
| arithm. mean | | | | 0.01956 | 421.697 | |
| ±SD | | | | 0.000639 | 13.7716 | |
| CV [%] | | | | 3.3 | 3.3 | |
| RD [%] | | | | | 5.4 | |

| Sample Name | Medium conc. [ng/ml] | Peak Area GHQ168 | Peak Area Int. standard | Ratio of Peak Areas | Conc. calc. [ng/ml] | RD [%] |
|---|---|---|---|---|---|---|
| QC-M1 | 100.000 | 102000 | 21400000 | 0.00477 | 102.904 | 2.9 |
| QC-M2 | 100.000 | 97900 | 20600000 | 0.00475 | 102.473 | 2.5 |
| QC-M3 | 100.000 | 99800 | 19800000 | 0.00504 | 108.723 | 8.7 |
| QC-M4 | 100.000 | 98200 | 20200000 | 0.00486 | 104.843 | 4.8 |
| QC-M5 | 100.000 | 96700 | 20700000 | 0.00467 | 100.748 | 0.7 |
| QC-M6 | 100.000 | 98200 | 20600000 | 0.00477 | 102.904 | 2.9 |
| arithm. mean | | | | 0.00481 | 103.766 | |
| ±SD | | | | 0.000128 | 2.7567 | |
| CV [%] | | | | 2.7 | 2.7 | |
| RD [%] | | | | | 3.8 | |

| Sample Name | Low conc. [ng/ml] | Peak Area GHQ168 | Peak Area Int. standard | Ratio of Peak Areas | Conc. calc. [ng/ml] | RD [%] |
|---|---|---|---|---|---|---|
| QC-L1 | 5.000 | 4650 | 20000000 | 0.00023 | 5.059 | 1.2 |
| QC-L2 | 5.000 | 4610 | 21600000 | 0.00021 | 4.628 | -7.4 |
| QC-L3 | 5.000 | 4290 | 21000000 | 0.00020 | 4.412 | -11.8 |
| QC-L4 | 5.000 | 4420 | 21100000 | 0.00021 | 4.628 | -7.4 |
| QC-L5 | 5.000 | 4790 | 21900000 | 0.00022 | 4.843 | -3.1 |
| QC-L6 | 5.000 | 5110 | 21400000 | 0.00024 | 5.274 | 5.5 |
| arithm. mean | | | | 0.00022 | 4.807 | |
| ±SD | | | | 0.000015 | 0.3172 | |
| CV [%] | | | | 6.8 | 6.6 | |
| RD [%] | | | | | -3.9 | |

**Table S3F**: Precision data for GHQ243 at high, medium and low concentrations.

## Blood concentration levels

| Compound | Animal | Time [h] | Conc. [ng/ml] | Conc. [µM] |
|---|---|---|---|---|
| GHQ168 | 1 | 1 | 293.0 | 0.669714 |
| | 2 | | 195.9 | 0.447771 |
| | 3 | | 46.2 | 0.105600 |
| | 1 | 4 | 17.6 | 0.040229 |
| | 2 | | 27.1 | 0.061943 |
| | 3 | | 75.7 | 0.173029 |
| | 1 | 16 | 0.3 | 0.000686 |
| | 2 | | 1.7 | 0.003886 |
| | 3 | | 1.0 | 0.002286 |
| GHQ242 | 1 | 1 | 11.7 | 0.022137 |
| | 2 | | 17.4 | 0.032921 |
| | 3 | | 3.2 | 0.006055 |
| | 4 | | 49.8 | 0.094224 |
| | 1 | 4 | 2.9 | 0.005487 |
| | 2 | | 8.4 | 0.015893 |
| | 3 | | 5.5 | 0.010406 |
| | 4 | | 10.1 | 0.019110 |
| | 1 | 16 | 14.6 | 0.027624 |
| | 2 | | 1.0 | 0.001892 |
| | 3 | | 2.2 | 0.004162 |
| | 4 | | < 1.0 | 0.000946 |
| GHQ243 | 1 | 1 | 376.1 | 0.693195 |
| | 2 | | 191.1 | 0.352219 |
| | 3 | | 223.0 | 0.411014 |
| | 4 | | 202.6 | 0.373415 |
| | 1 | 4 | 41.8 | 0.077042 |
| | 2 | | 14.3 | 0.026357 |
| | 3 | | 22.8 | 0.042023 |
| | 4 | | 13.2 | 0.024329 |
| | 1 | 16 | 4.0 | 0.007372 |
| | 2 | | 5.5 | 0.010137 |
| | 3 | | 2.0 | 0.003686 |
| | 4 | | < 1.0 | 0.000922 |

**Table S4**: Blood concentration levels of GHQ168, GHQ242 and GHQ243 in mice.

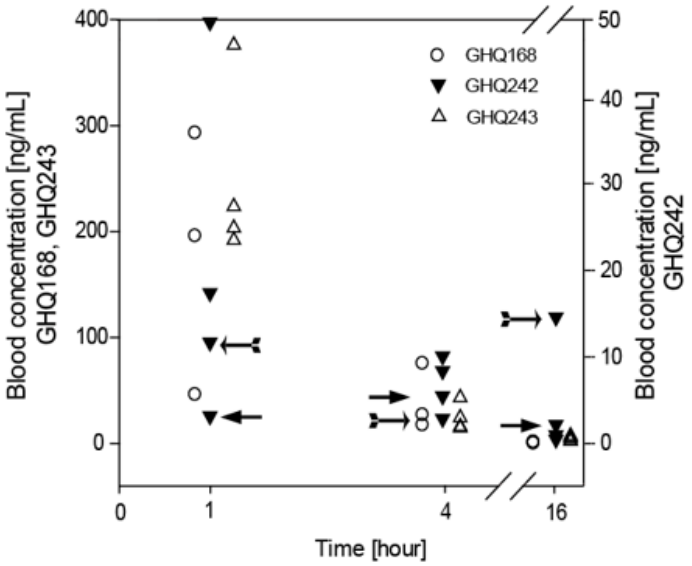


**Figure S7**: Blood concentration [ng/mL] versus time profiles [hour]. Arrows highlight two individual mice exposed to GHQ242 for which concentration results from subsequent samplings exceeded those of previous samples. The left axis is for GHQ168, and GHQ 243, the right axis for GHQ242.

# CHAPTER III

## OPENING NADPH OXIDASE INHIBITORS

## FOR *IN VIVO* TRANSLATION

Nina Hecht, Nils Terveer, Curd Schollmayer, Ulrike Holzgrabe and Lorenz Meinel*

Institute for Pharmacy and Food Chemistry, Am Hubland, University of Würzburg, DE-97074 Würzburg, Germany

This chapter is originally published in the Eur J Pharm Biopharm, 115 (2017) 206-217; doi: 10.1016/j.ejpb.2017.03.001, and appears in this thesis with permission from Elsevier. License Number: 4223270190192.

## Abstract

Triazolopyrimidine derivatives from the VAS library have been found to be efficient and selective NADPH oxidase (NOX) inhibitors *in vitro*. In spite of numerous publications on this compound class detailing efficacy for the treatment of cardiovascular diseases, *in vivo* translation is challenged by their very low water solubility which is preventing further use of these compounds and blocking clinical translation. Therefore, we addressed the challenge of water solubility for three triazolopyrimidine derivatives, VAS2870, VAS3947, and VAS4024, and developed formulations for oral or parenteral application with translational potential into preclinical and clinical studies.

Based on its physico-chemical properties, VAS3947 was selected and formulated by spray drying, microemulsification, and complexation with different cyclodextrin (CD) derivatives. The poor water solubility of VAS3947 was successfully increased in all approaches. The supersaturation ratio for seven spray dried formulations and four microemulsions ranged from 3 -9 and 8 to 19 after 120 min, respectively. For six CDs a supersaturation ratio was observed between 3 and 174 after 20 h, with an inclusion of the compound within the CD's cavity as well as interaction with its outside. In conclusion, we successfully developed formulations opening this promising compound class for oral or parenteral *in vivo* administration.

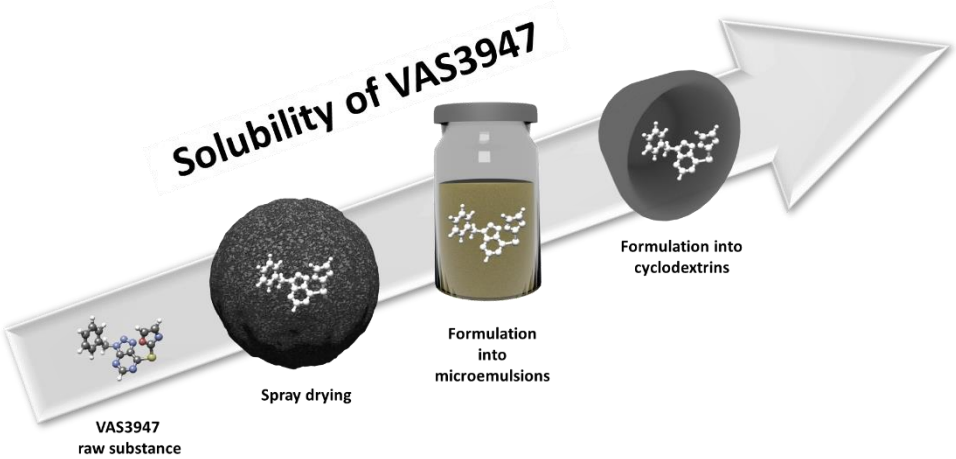

# 1. Introduction

Reactive oxygen species (ROS) mediate beneficial effects e.g. in cell signaling processes [1]. In spite of these therapeutic promises, harmful effects caused by oxidative stress clearly predominate the advantages and are among the main causes of death in industrialized countries. ROS detrimentally drive the development of cardiovascular diseases such as hypertension, atherosclerosis, as well as neurodegenerative disorders and the progression of carcinogenesis [2]. This illustrates the urgent need of effective therapeutic options for the treatment of high ROS levels, with ROS resisting control through antioxidants such as flavonoids [3]. NADPH oxidases have been identified as the main source of endothelial ROS formation [4]. Consequently, efforts focused on therapeutically targeting NADPH oxidases by NADPH oxidase inhibitors, including small molecules known as VAS2870, VAS3947, and VAS4024 (**Figure 1**), with the overall goal of reducing the high incidence of deaths resulting from endothelial dysfunctions such as myocardial and ischemic strokes. A suite of publications confirm the *in vitro* efficacy of the VAS compounds [5-7]. For example, VAS2870 blocked the oxLDL-mediated ROS formation in human endothelial cells after 2 h (101 ± 9%, $P < 0.05$ vs. oxLDL) [5]. VAS3947 inhibited the NADPH-dependent ROS production in CaCo-2 cell homogenates ($IC_{50}$ 12 µM), in HL-60 human cells ($IC_{50}$ 2 µM) and in the rat vascular cell line A7r5 ($IC_{50}$ 13 µM), which is far below the $IC_{50}$ of other known NADPH oxidase inhibitors [6]. These effects of NADPH oxidase inhibitors are comprehensively reviewed [7].

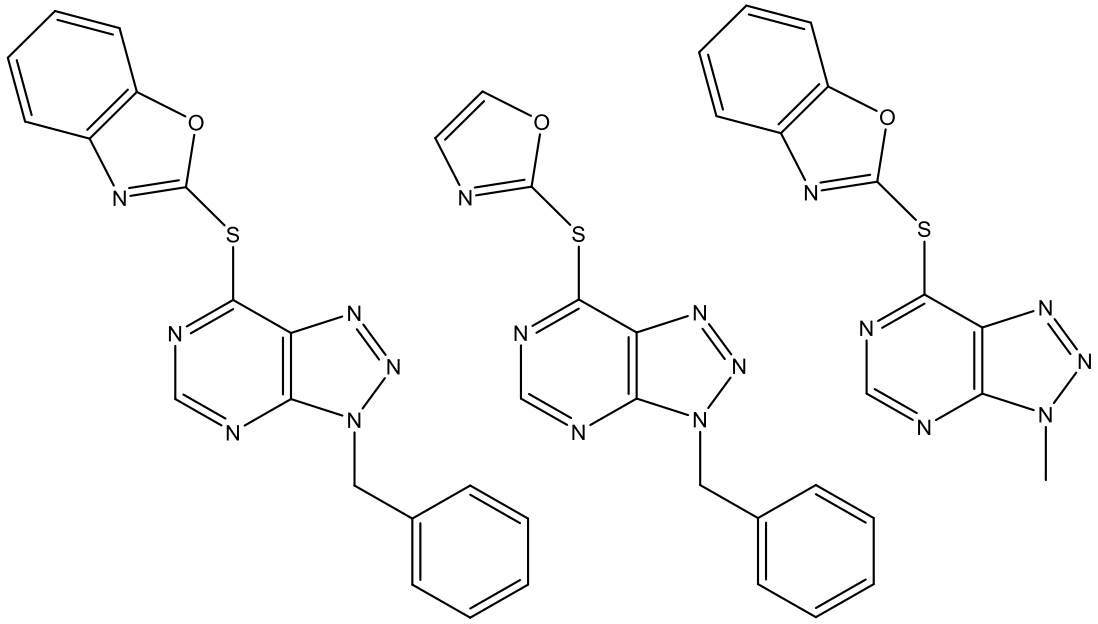

| **VAS2870** | **VAS3947** | **VAS4024** |
|---|---|---|
| LogP: 3.6 | LogP: 1.8 | LogP: 1.7 |
| MP: 165 °C | MP: 115 °C | MP: 178 °C |

**Figure 1**: Chemical structures of VAS2870, VAS3947, and VAS4024.

However, in spite of these promising effects, the clinical translation of the VAS-compounds is challenged by their improper pharmaceutical properties, more importantly low aqueous solubility. The aim of this research work was to overcome the compounds' limitations of low aqueous solubility through formulation strategies.

Following a physicochemical characterization (determination of melting points (MP), logP, kinetic and thermodynamic solubility), different formulation strategies were deployed, including spray drying [8], preparation of micro-emulsifying drug delivery systems [9], and complexing with cyclodextrins [10]. Finally, a potential formulation for oral (microemulsion) and for i.v. application (cyclodextrin formulation) is presented. Therefore, these studies lay the formulation work for the application of these promising NADPH oxidase inhibitors in studies in animals as well as the clinical application by removing the aqueous solubility hurdle which existed so far.

# 2. Materials and Methods

## 2.1. Materials

VAS2870, VAS3947, and VAS4024 were kindly supplied by Vasopharm GmbH (Würzburg, Germany). Solvents, reagents, excipients, and materials were purchased from Sigma Aldrich (Schnelldorf, Germany), unless otherwise noted. Deionized water was taken from in-house supply by a Milli-Q® system (Merck Millipore GmbH, Darmstadt, Germany) or purchased from Fisher Scientific (Schwerte, Germany). 96-well plates with flat bottom were from Greiner (Frickenhausen, Germany). Suppliers of polymers and excipients used for the spray dried formulations, microemulsions, and cyclodextrins are listed in **Tables 1, 2,** and **3**. Capryol PGMC and Labrafac Lipophile WL 1349 were from Gattefossé (Bad Krozingen, Germany). Biorelevant medium (FaSSIF) was obtained from biorelevant (London, UK). HPLC columns were purchased from Phenomenex (Aschaffenburg, Germany). 5 mm NMR tubes (S-5-900-7) and related coaxial inserts (WGS 5-BL) were purchased from Norell Inc. (Marion, NC) and deuterium oxide, deutero dimethylsulfoxide, and deutero chloroform were from Deutero GmbH (Kastellaun, Germany). Petroleum ether, ethyl acetate, and syringe filters (0.22 µm) were from VWR International GmbH (Darmstadt, Germany) and Polygram® SIL G/UV254 polyester sheets for thin layer chromatography were from Macherey-Nagel GmbH & Co. KG (Düren, Germany). All compounds were at least of analytical or pharmaceutical grade and were used without further purification.

## 2.2. Methods

### 2.2.1. Differential Scanning Calorimetry

For differential scanning calorimetry (DSC) studies a DSC 8000 instrument from Perkin Elmer (Waltham, MA) was used. The sample was weighed into an aluminum pan (2 - 5 mg) and sealed, including a small hole for pressure equilibration. Melting points were determined from the first heating cycle (heating rate: 20 K/min, nitrogen gas flow: 20 mL/min, temperature range: -50 °C to 200 °C). Subsequently, samples were cooled to -50 °C at a cooling rate of 50 K/min and then again heated at a rate of 20 K/min up to 200 °C for the determination of glass transitions temperatures and degradation events.

### 2.2.2. logP assessment

The logP value was experimentally assessed on an Agilent 1100 chromatographic system (Agilent Technologies GmbH, Waldbronn, Germany) equipped with an online degasser (G1322A), a binary pump (G1312A), an autosampler (G1313A), a thermostated column department and a diode array UV/VIS detector (G1315B). ChemStation software package was used for data handling (Agilent Technologies GmbH). HPLC-UV analysis was performed according to the method as described previously [11]. Briefly, a Phenomenex Synergi Max RP (150 x 4.6 mm; 4 µm particle size) analytical column was used. Isocratic elution was performed with a 10 mM phosphate buffer pH 7.0 (30% v/v) and methanol adjusted with 0.02% *N,N*-dimethylhexylamine (70% v/v). The column compartment was maintained at 30 °C, the flow rate was 1.0 mL/min, and 40 µL volume of every sample was injected. The stop time was 20 min. For sample preparation all substances were dissolved in methanol at a concentration of 40 µg/mL. Afterwards, each solution was transferred into a separate HPLC vial. Thiourea was used for determination of dead time. For the assessment of logP values of VAS compounds, 2-phenylethanol, benzene, *N,N*-dimethylaniline, toluene, chlorobenzene, ethylbenzene, biphenyl, and anthracene were used as reference substances with known logP values.

### 2.2.3. Solubility assessment of the unformulated compounds

For the kinetic solubility assessment, nephelometrical studies were conducted using a NEPHELOstar system from BMG Labtech GmbH (Ortenberg, Germany). A concentrated stock solution of VAS2870, VAS3947, or VAS4024 was prepared in DMSO (VAS2870 and VAS4024: 5 mM; VAS3947: 15 mM). Thereafter, dilution series in PBS buffer (pH 7.4, 5% DMSO) were performed (concentrations: VAS2870, VAS4024: 25, 50, 75, 100, 125, 150, 175, 200, 225, 250 µM; VAS3947: 75, 150, 225, 300, 375, 450, 525, 600, 675, 750 µM; n = 3/concentration). Temperature was set to 37 °C, laser intensity was 80%, and laser beam focus was 2.20 mm. The mean solubility of the compounds was determined immediately after preparation (T0) and 60 min later (T60).

The investigation of the thermodynamic solubility was performed using a heatable shaker from Eppendorf AG (Hamburg, Germany) followed by HPLC-UV analysis on a system from Jasco (Groß-Umstadt, Germany) equipped with a degasser (DG-2080-53), a gradient unit (LG-2080-02), a pump (PU-1580), an autosampler (AS-2051Plus), and a UV/VIS detector (UV-2075Plus). The column oven was from Phenomenex (Thermasphere TS-130). Galaxie chromatography software package was used for data handling (Version 1.9.3.2., Varian, Inc., CA). 3.3 mg - 3.5 mg of VAS3947 was weighed into an Eppendorf vial, PBS buffer (pH 7.4) was added, and samples were sonicated (Sonorex ultrasonic bath from Bandelin electronic GmbH, Berlin, Germany) for 5 seconds, and incubated in a heatable shaker (37 °C, 800 rpm), thereafter. 70 µL of suspension volume was taken after 2, 10, 30, 60, 120, and 240 min, respectively, and immediately centrifuged using a Mikro 22R centrifuge from Andreas Hettich GmbH (Tuttlingen, Germany) for 2 min at 13000 rpm. The supernatant was collected, diluted with acetonitrile (1/1), vortexed, and analysed by HPLC. The chromatography was done on a Phenomenex Synergi Polar RP (80 Å, 40 * 4.6 mm, 4 µm) using a mobile phase A as of $H_2O$/acetonitrile at a ratio of 90/10 and 0.05% TFA, and a mobile phase B as of $H_2O$/acetonitrile at a ratio of 10/90 and 0.05% TFA with a gradient from 0 min to 1.5 min at

80% to 60% for mobile phase A, and from 1.5 min to 4.0 min at 60% mobile phase A. Detection was at λ = 277 nm with an injection volume of 15 µL, a flow rate of 2.0 mL/min, and a column temperature at room temperature. Sample concentration were calculated from a regression line ranging from 0.1 µg/ml to 250 µg/mL (acetonitrile/PBS buffer: 1/1 (v/v)).

### 2.2.4. Preparation of spray dried formulations and physical mixtures

Physical mixtures of VAS3947 and seven different excipients (Eudragit L100, Eudragit L100-55, Eudragit RL PO, HPMC, Kollidon 30, Kollidon VA 64, and Soluplus) were prepared in a 1+10 mass ratio by mixing in a mortar and subsequent pestling for 1 min. Spray dried nanoparticles were prepared from VAS3947 and the excipients listed above in a 1+10 mass ratio using a Nano Spray Dryer B-90 from Büchi Labortechnik GmbH (Essen, Germany). Spray drying solutions were prepared for VAS3947 and excipients which were dissolved in either methanol or 2-propanol (**Table 1**) to result in 0.2% VAS3947 and 2% excipient in solution.

This solution was spray dried with the spray head in the vertical position, 7 µm mesh size, and a spray rate of 100%. The airflow ranged from 145 L/min to 154 L/min, inlet temperature was 60 °C (Eudragit L100, Eudragit L100-55, Eudragit RL PO, HPMC) or 70 °C (Kollidon 30, Kollidon VA 64, Soluplus), respectively. The outlet temperature was between 33 °C and 45 °C. The feed pump rate was 150 mL/h. The formulations were stored in white glass vials wrapped in aluminum foil and in an exsiccator with silica gel at room temperature.

| Preparation of spray dried formulations | | | Characterization of spray dried formulations after 120 min dissolution study | | |
|---|---|---|---|---|---|
| Excipient | Supplier (excipient) | Solvent | pH | Particle Size [nm] | Zeta Potential [mV] |
| 1. Eudragit L100 | Evonik Industries | Methanol | 5.95 ± 0.08 | 191.0 ± 14.5 | - 36.2 ± 1.0 |
| 2. Eudragit L100-55 | Evonik Industries | Methanol | 5.82 ± 0.01 | 185.5 ± 11.0 | - 34.9 ± 1.7 |
| 3. Eudragit RL PO | Evonik Industries | Methanol | 7.41 ± 0.01 | n.d. | + 29.6 ± 1.4 |
| 4. HPMC | Sigma Aldrich | Methanol | 7.34 ± 0.02 | 182.0 ± 18.7 | - 4.8 ± 2.0 |
| 5. Kollidon 30 | BASF | 2-Propanol | 7.32 ± 0.02 | 151.3 ± 30.5 | - 4.6 ± 1.0 |
| 6. Kollidon VA 64 | BASF | 2-Propanol | 7.37 ± 0.01 | 202.7 ± 8.2 | - 2.0 ± 2.5 |
| 7. Soluplus | BASF | 2-Propanol | 7.27 ± 0.20 | 146.5 ± 51.3 | ± 0.0 ± 1.3 |

n.d. = not determined (determination of particle size was not possible, as Eudragit RL PO particles are insoluble in PBS buffer).

**Table 1**: Preparation of spray dried formulations of VAS3947 and excipients (1+10 w/w) and characterization after 120 min dissolution study.

### 2.2.5. X-ray powder diffractometry

Powder diffractometric studies of VAS3947, spray dried (SD) formulations, and physical mixtures (PM) were performed on a Bruker Discover D8 powder diffractometer (Rheinstetten, Germany). A Cu-Kα radiation (unsplit $K\alpha_1$+$K\alpha_2$ doublet, mean wavelength λ = 154.19 pm) at a power of 40 kV and 40 mA, a focusing Goebel Mirror, and a fixed divergence slit were used. Approximately 4 mg of substances were transferred onto a silicon single crystal zero background specimen holder. For the measurements, step size was set to 0.025° and 0.25 s time per step in the range of 5 - 45°. Samples were analyzed in reflection geometry and detection was done with a LynxEye® 1D-detector (Bruker AXS) using the full detector range of 192 channels. 2.5° axial Soller Slits were mounted in the primary and secondary beam path. Data collection and processing was

done using the software packages DIFFRAC.Suite (V2 2.2.690, Bruker AXS 2009-2011) and DIFFRAC.EVA (Version 3.0, Bruker AXS 2010-2013).

### 2.2.6. Dissolution of spray-dried formulations and physical mixtures

The determination of dissolution rates of VAS3947 from spray dried formulations and physical mixtures was conducted using the dissolution conditions as described for the investigation of thermodynamic solubility. Spray dried formulation (3.2 mg - 3.8 mg) was dosed into PBS buffer and respective physical mixtures (3.2 mg - 4.0 mg) were processed likewise. Solubility determinations were performed in triplicate using the HPLC instrument and method as described in section 2.2.3. Supersaturation ratios were calculated based on the solubility of VAS3947 after 120 min (standardized to 1) in relation to the concentration resulting from the respective spray dried formulation at the same time-point.

### 2.2.7. Determination of pH, particle size, zeta potential, and crystallinity of precipitates

pH, particle size, and zeta potential were assessed after 120 min. The assessment of pH was done applying an InLab® Semi-Micro-L pH electrode from Mettler-Toledo (Greifensee, Switzerland). Particle size and zeta potential were determined using a Delsa™ Nano HC system (Beckman Coulter GmbH, Krefeld, Germany). Prior to the determination of the particle size, a filtration step was performed using Acrodisc 25 mm syringe filters with a 5 µm Versapor membrane. Afterwards, samples were diluted with PBS buffer (1:5), transferred into disposable cuvettes (1 cm path length), and particle size was determined (scattering angle: 165 °, accumulations: 50, repetitions: 3, temperature: 37 °C). Samples were further characterized regarding zeta potential after 1:4 dilution with PBS buffer (15° scattering angle, 8 accumulations, 3 repetitions, and at a temperature of 25 °C). After termination of the dissolution experiment, precipitates of spray dried formulations were evaporated to dryness and analyzed by X-ray powder diffractometry (method description *vide supra*).

### 2.2.8. Pre-formulation study for the preparation of microemulsions

In a pre-formulation study, binary mixtures of VAS3947 (approx. 2.5 mg) and 32 different lipid excipients (approx. 250 mg) were weighed into 1.5 mL vials. PBS buffer (250 mg) served as negative control. After vortex-mixing for 3 min using the mixer IKA MS 3 basic (Staufen, Germany), binary mixtures were centrifuged (2 min, 10000 rpm, 37 °C). 40 - 50 mg of the particle free supernatant was collected, diluted in 1900 µL acetonitrile, sonicated for 10 min, and again centrifuged (10 min, 10000 rpm, 37 °C). The concentration of VAS3947 (T0) in the clear supernatant was analysed by HPLC using the instrument and method as described in section 2.2.3. Afterwards, the binary mixtures were placed on a shaker (KS 15 B, Edmund Bühler GmbH, Hechingen, Germany) for 24 h (250 rpm, room temperature), then again vortexed for 3 min, and prepared as described above for the HPLC analysis (T24).

### 2.2.9. Preparation of microemulsions and particle size determination

For the preparation of microemulsions, excipients (**Table 2**) were vortexed for 30 seconds.

| Preparation of microemulsions | | | Characterization of microemulsion |
|---|---|---|---|
| Composition | Content [%] | Supplier (excipient) | Particle Size [nm] |
| Microemulsion 1 (Type II) | | | |
| Cremophor RH 40 | 44.5 | BASF | |
| Miglyol 812 | 35.5 | Caesar & Loretz GmbH | 71 ± 4 |
| Lauroglycol | 9.0 | Gattefossé | |
| Ethanol (pure) | 11.0 | Fisher Scientific | |
| Microemulsion 2 (Type IIIa) | | | |
| Cremophor RH 40 | 42.0 | BASF | |
| Labrafac PG | 25.0 | Gattefossé | 43 ± 3 |
| PEG400 | 17.0 | Caesar & Loretz GmbH | |
| Ethanol (pure) | 9.4 | Fisher Scientific | |
| Microemulsion 3 (Type IIIa) | | | |
| Cremophor RH 40 | 42.0 | BASF | |
| Capmul MCM C8 | 25.0 | ABITEC | 193 ± 10 |
| PEG400 | 17.0 | Caesar & Loretz GmbH | |
| Ethanol (pure) | 9.5 | Fisher Scientific | |
| Microemulsion 4 (Type IIIa) | | | |
| Cremophor RH 40 | 40.0 | BASF | |
| Capmul MCM C8 | 24.0 | ABITEC | 168 ± 3 |
| Propylenglycol | 16.0 | Caesar & Loretz GmbH | |
| Ethanol (pure) | 8.9 | Fisher Scientific | |

**Table 2**: Composition of microemulsions of VAS3947 and particle size assessment.

Subsequently, VAS3947 (1%) was added and vortexed for 3 min, followed by 10 min sonication at 50 °C. Microemulsions were visually controlled for the absence of crystals and precipitates. For the investigation of particle size, microemulsions were further diluted with water (1:10) and analyzed by dynamic light scattering using the instrument and method as described for the determination of particle size after dissolution of spray dried formulations.

### 2.2.10. Determination of maximum concentration of VAS3947 in microemulsions and dissolution from microemulsions

For the dissolution study, the maximum concentration of VAS3947 was incorporated into each of the four microemulsions. For this purpose, VAS3947 was added to the respective blank microemulsion and vortexed until a precipitate was observed. Subsequently, microemulsions were centrifuged (10 min, 14000 rpm, 37 °C) and the concentration of VAS3947 in the supernatant was analyzed. Therefore, 25 mg (n = 3) of the clear supernatant were diluted with 500 µL acetonitrile and vortexed for 2 min followed by centrifugation (10 min, 10000 rpm, 5 °C). Samples were further diluted with acetonitrile (1:40) and analyzed using the HPLC instrument and method as described in section 2.2.3. Dissolution of VAS3947 from microemulsions was performed based on [12]. Briefly, 200 mg of the respective microemulsion was weighed into 10 mL Falcon tubes (n = 3) and diluted with 3.6 mL pre-warmed (37 °C) digestion medium (FaSSIF; composition: sodium chloride (105.9 mM), monobasic sodium phosphate x 2 $H_2O$ (28.7 mM), sodium hydroxide (10.5 mM), sodium taurocholate (3.0 mM) and lecithin (0.75 mM)). After 10 min of incubation in a heatable shaker (37 °C, 750 rpm), 0.4 mL of freshly prepared pancreatin solution (0.2 g/mL in digestion buffer) was added to the samples. Sampling was performed at 2, 5, 10, 15, 20, 30, 45, 60, 90, and 120 min, respectively. Aliquots (0.2 mL) were taken and immediately treated with 4-bromophenylboronic acid (1 M in methanol; 3 µL) to stop further pancreatin mediated lipolysis of the formulation. Samples were

centrifuged (30 min, 14000 rpm, 37 °C), the supernatant was diluted with acetonitrile (1:10), vortexed, and centrifuged (20 min, 14000 rpm, 37 °C). HPLC analysis was performed using the instrument and method as described in section 2.2.3. Throughout the dissolution study, pH was monitored (pH Meter 744 from Metrohm, Herisau, Switzerland) and maintained at 6.5 ± 0.1 by adding 0.4 M sodium hydroxide if required. Supersaturation ratios were calculated based on the solubility of VAS3947 after 120 min (standardized to 1) in relation to the concentration of VAS3947 as released from microemulsions.

### 2.2.11. Preparation and dissolution study of cyclodextrin formulations

10 different cyclodextrins (α-CD, β-CD, γ-CD, sulfated-β-CD, methyl-β-CD, heptakis-2,6-di-methyl-β-CD, 2-hydroxypropyl-α-CD, 2-hydroxypropyl-β-CD, 2-hydroxypropyl-γ-CD, and carboxy-methyl-β-CD) were dissolved in PBS buffer (pH = 7.4) and diluted as outlined in **Table 3**, depending on the maximum solubility of the respective CD in the dilution medium.

| Cyclodextrin | Concentration (% w/w) | Supplier (excipient) |
|---|---|---|
| 1. α-CD | 0.625; 1.25; 2.5; 5; 10 | Wacker Chemie AG |
| 2. β-CD | 0.0625; 0.125; 0.25; 0.5; 1 | Wacker Chemie AG |
| 3. γ-CD | 1.25; 2.5; 5; 10; 20 | Wacker Chemie AG |
| 4. Sulfated-β-CD | 2.5; 5; 10; 20; 40 | Sigma-Aldrich |
| 5. Methyl-β-CD | 2.5; 5; 10; 20; 40 | Sigma-Aldrich |
| 6. Heptakis-2,6-di-*O*-methyl-β-CD | 2.5; 5; 10; 20; 40 | Sigma-Aldrich |
| 7. 2-Hydroxypropyl-α-CD | 2.5; 5; 10; 20; 40 | Sigma-Aldrich |
| 8. 2-Hydroxypropyl-β-CD | 1.88; 3.75; 7.5; 15; 30 | Sigma-Aldrich |
| 9. 2-Hydroxypropyl-γ-CD | 2.5; 5; 10; 20; 40 | Sigma-Aldrich |
| 10. Carboxy-methyl-β-CD | 2.5; 5; 10; 20; 40 | Sigma-Aldrich |

**Table 3**: Cyclodextrins and respective concentrations for solubility improvement of VAS3947.

2 - 5 mg of VAS3947 (in excess, depending on the CD and its concentration) was weighed into Eppendorf vials and 0.5 mL of the corresponding cyclodextrin solution was added (n = 3 / concentration of cyclodextrin). Additionally, a negative control containing a saturated solution of VAS3947 (4 mg/mL; n = 3) in PBS buffer (pH = 7.4) was prepared. Samples were incubated in a shaker for 20 h (37 °C, 800 rpm), afterwards vials were centrifuged (5 min, 13000 rpm, room temperature), and the supernatant was collected, thereafter. The quantification was performed on the HPLC system as described in section 2.2.2. The chromatography was done on a Phenomenex Synergi Max RP column (50 * 4.6 mm, 4 µm) using mobile phase A as of $H_2O$/acetonitrile at a ratio of 90/10 and 0.05% TFA, and mobile phase B as of $H_2O$/acetonitrile at a ratio of 10/90 and 0.05% TFA with the gradient from 0 min to 8 min at 100% to 20% mobile phase A, from 8 min to 9 min at 20% mobile phase A, and from 9 min to 10 min at 20% to 100% mobile phase A. Detection was at λ = 254 nm and at λ = 280 nm with an injection volume of 10 µL, the flow rate of 1.5 mL/min, and the column temperature at room temperature. Samples were diluted in a mixture of acetonitrile/PBS buffer: 15/85 (v/v) and the concentration was calculated using a regression line over the range of 1 µg/mL - 250 µg/mL (same solvent). Supersaturation ratios were calculated based on the solubility of VAS3947 after 20 h (standardized to 1) in relation to the concentration of VAS3947 as released from formulations containing 10% [w/w] of the respective CD.

### 2.2.12. $^1$H NMR investigation of 'Complexation Induced Chemical Shifts' (CICS)

$^1$H NMR measurements of VAS3947 and heptakis-2,6-di-*O*-methyl-β-CD were performed on a Bruker Avance III spectrometer operating at 400.13 MHz for $^1$H, equipped with a 5 mm BBO broadband observer with Z-gradient. $^1$H NMR spectra for the assessment of CICS were recorded with a flip angle of 30°, spectral width of 20 ppm, transmitter offset of 6.15 ppm, acquisition time of 3.99 s followed by a relaxation delay of 1.00 s. 128 scans were collected in 64000 data points resulting in a digital resolution of 0.125 Hz.

Processing parameters were set to an exponential line broadening window function of 0.3 Hz, an automatic baseline correction, and manual phasing. 20 mg of every sample were dissolved in 700 µL of $CDCl_3$ or DMSO-*d6* and transferred into a standard 5 mm NMR tube. The solvent served as the field frequency lock. The temperature was adjusted to 300 K.

For buffer preparation, 8.0 g NaCl, 0.2 g KCl, 1.42 g $Na_2HPO_4$, and 0.78 g $KH_2PO_4$ were dissolved in 800.0 mL of purified water. pH was adjusted to 4.5 by adding conc. phosphoric acid and the volume was made up to 1000 mL. The solution was sonicated for 15 min. Afterwards, 20.0 mL of this buffer was lyophilized and redissolved in 20.0 mL $D_2O$. This procedure was replicated twice.

For sample preparation, solutions with different concentrations of VAS3947 and heptakis-2,6-di-*O*-methyl-β-CD were prepared in buffer. The final concentration of VAS3947 was 5 mM, the ratio of VAS3947:cyclodextrin varied (1:5; 1:3.33; 1:1.5, 1:1; 2.5:1; 3.33:1; 5:1). Spectra were referenced to TSP (δ = 0.0 ppm), which was introduced in a coaxial insert (WGS 5-BL, Norell Inc., Morganton, NC) as external reference in $D_2O$. $^1H$ NMR spectra with a digital resolution of 0.125 Hz were analyzed concerning CICS and Δδ values were determined according to the following equation: Δδ value = δ (free VAS3947) – δ (complexes of VAS3947 and CD).

### 2.2.13. ROESY measurements

ROESY measurements were performed on a Bruker Avance III spectrometer operating at 600.13 MHz for $^1H$, equipped with a 5 mm DCH cryoProbe with Z gradient. Data processing was done with TopSpin 3.2 software. ROESY spectra were recorded using the spin lock pulse with a mixing time of 150 ms. Spectral width was set to 10 ppm with a transmitter offset of 4.7 ppm. Number of scans was adjusted to 64 and 410 increments in indirect dimension (F1) were acquired. Acquisition time was set to 0.64 s followed by a relaxation delay of 3.00 s. The experimental time was 10 h. For processing a time domain

size of 2000 was used. In both dimensions (F2 and F1) zero filling was applied, window function was set to a pure sine function, and a baseline correction was performed. An indirect dimension forward linear prediction was performed. The temperature was adjusted to 300 K.

Buffer was prepared as described in section 2.2.12. 7.8 mg of VAS3947 and 33.3 mg of heptakis-2,6-di-*O*-methyl-β-CD were dissolved in 1.0 mL of deuterated buffer. 500 µL of this solution were transferred into a NMR tube. Spectra were referenced to TSP (δ = 0.0 ppm), which was introduced in a coaxial insert as external reference in $D_2O$. ROESY spectra were analysed by normalizing the cross-signal intensities, which are represented by the 2D integrals.

### 2.2.14. Solubility of VAS3947 in a cyclodextrin formulation for i.v. application

A stock solution of VAS3947 was prepared by solubilizing VAS3947 (in excess) in 2 mL of an aqueous solution containing 40% (w/w) of 2-hydroxypropyl-β-CD (pH = 4.5; n = 3). To prepare the final formulation for i.v. application, a stock solution was diluted with 0.9% NaCl solution (1:1, n = 3). For solubility and stability assessment, samples were incubated in a heatable shaker for 24 h (400 rpm, 22 °C). After 0, 10, 30, 120 min, and 24 h, an aliquot was taken, and centrifuged (5 min, 13000 rpm). The supernatant was analyzed for content by HPLC as described previously in section 2.2.11.

### 2.2.15. Statistics

Statistical analysis were performed using Minitab® 17.2.1 (Minitab Inc., Coventry, UK). Comparisons between groups for the assessment of statistically significant differences (**Figures 2H, 3C, 4B, 4C, 6**) were performed using ANOVA and Tukey *post hoc* test with 95% CI and $p < 0.05$. Results were reported as mean ± standard deviation and measurements were carried out in triplicate unless otherwise noted.

# 3. Results

### 3.1. Physico-chemical characterization of VAS2870, VAS3947, and VAS4024

VAS2870, VAS3947, and VAS4024 structures are shown in **Figure 1**, with melting points determined by DSC at 165 °C, 115 °C, and 178 °C, respectively (**Figure S1A-S1C**). Whereas VAS2870 and VAS3947 did not recrystallize, VAS4024 had a melting point at 160 °C in the second heating run. The logP value was experimentally determined at 3.6, 1.8, and 1.7 for VAS2870, VAS3947, and VAS4024, respectively. Kinetic solubility from freshly prepared solutions (T0) resulted in 56 µg/mL for VAS2870, 91 µg/mL for VAS3947, and 51 µg/mL for VAS4024 (**Figure S2A, S2C, S2E**). Solubility was again assessed after 60 min and was 58 µg/mL, 88 µg/mL, and 61 µg/mL for VAS2870, VAS3947, and VAS4024, respectively (**Figure S2B, S2D, S2F**). Based on its favorable solubility properties, VAS3947 was selected for further formulation developmental work. For the crystalline VAS3947 the thermodynamic solubility was determined at 5.4 ± 0.8 µg/mL after 10 min and 11.4 ± 1.6 µg/mL after 240 min (**Figure 2A-2G**). Further characterization of the compounds including light stability are ongoing.

### 3.2. Characterization of spray dried formulations

VAS3947 was spray dried with seven different excipients (**Table 1**) and all spray dried formulations were amorphous as determined by XRPD (**Figure S3A-S3G**). In contrast, VAS3947 pure substance as well as physical mixtures of VAS3947 and the excipients had crystalline reflexes (**Figure S3A-S3G**). The amorphous character of VAS3947 in the spray dried formulations was confirmed by DSC with no melting point in contrast to VAS3947 and to the compound's physical mixtures with the excipients (data not shown).

### 3.3. Dissolution of VAS3947 from spray dried formulations and physical mixtures

VAS3947 dissolution from spray dried formulations with various excipients (**Table 1**) was measured over time in comparison to physical mixtures and the compound alone (**Figure 2A-2G**). Throughout all tested conditions, the physical mixtures slightly enhanced the concentration of VAS3947 as compared to the pure API. In contrast, spray drying had a profound effect for some formulations with an increasing dissolution ratio over time as of Eudragit RL PO (**Figure 2C**) < Kollidon VA 64 (**Figure 2F**) < HPMC (**Figure 2D**) < Eudragit L100-55 (**Figure 2B**) < Soluplus (**Figure 2G**). Eudragit L100 (**Figure 2A**), and Kollidon 30 (**Figure 2E**) did not preserve the metastable supersaturated state throughout the study period for 240 min.

In comparison to the compound alone, the supersaturation ratio observed after 120 min was highest for Eudragit L100 (9.1 ± 0.3 fold) and Soluplus (8.1 ± 0.9 fold). HPMC (4.9 ± 0.4 fold), Eudragit L100-55 (4.5 ± 0.1 fold), Kollidon VA 64 (3.6 ± 0.4 fold), Eudragit RL PO (3.2 ± 0.4 fold), and Kollidon 30 (2.8 ± 0.4) resulted in lower supersaturation ratios, respectively. However, all spray dried formulations significantly increased the concentration of VAS3947 after 120 min in comparison to the unformulated compound (**Figure 2H**).

After 120 min, the sample pH ranged from 7.3 - 7.4 with the exception of the samples containing the anionic polymers Eudragit L100-55 and Eudragit L100 (5.8 - 6.0; **Table 1**). Particle sizes were in the low nanomolar range for all samples as determined by dynamic light scattering (**Table 1**). Solutions containing anionic polymers exhibited negative zeta potentials (Eudragit L100, Eudragit L100-55), solutions with neutral polymers (HPMC, Kollidon 30, Kollidon VA 64, Soluplus) resulted in zeta potentials around zero and the cationic polymer Eudragit RL PO showed a positive result (**Table 1**), implying that zeta potential results are in accordance with pH.

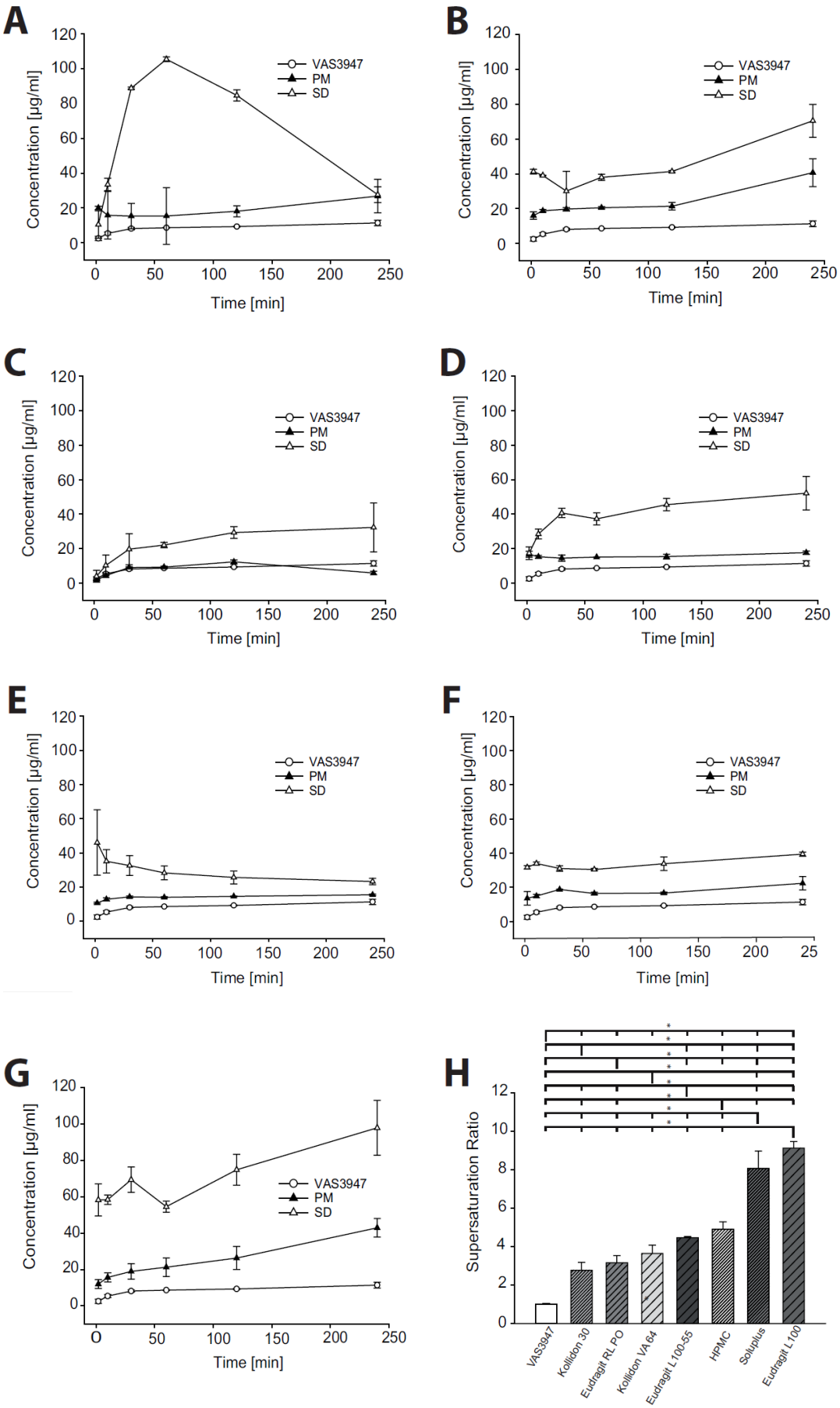
A
B
C
D
E
F
G
H
Concentration [µg/ml]
Time [min]
VAS3947
PM
SD
Supersaturation Ratio
VAS3947
Kollidon 30
Eudragit RL PO
Kollidon VA 64
Eudragit L 100-55
HPMC
Soluplus
Eudragit L 100

**Figure 2**: Dissolution profiles of VAS3947 unformulated compound (data set is shown in Fig. 2A-G, white circles) as well as from physical mixtures (PM, black triangles) and spray dried formulations (SD, white triangles) with seven different excipients (**Table 1**) in PBS buffer. The excipients were in detail: (A) Eudragit L100; (B) Eudragit L100-55; (C) Eudragit; RL PO; (D) HPMC (E) Kollidon 30; (F) Kollidon VA 64; (G) Soluplus. (H) Solubility of VAS3947 unformulated compound (standardized to 1) and respective supersaturation ratios of the spray dried formulations with seven different excipients after 120 min.

After evaporation of the dissolution medium, recrystallization was observed for the precipitates of the spray dried formulations containing Eudragit L100-55, Eudragit RL PO, HPMC, Kollidon 30, and Kollidon VA 64 but not for Eudragit L100 and Soluplus (data not shown).

In summary, formulations containing Soluplus and Eudragit L100 lead to the highest maximum solubility of VAS3947. Furthermore, Soluplus preserved the supersaturated state throughout the duration of the dissolution study and the precipitates of the formulation remained amorphous.

### 3.4. Excipient screening and characterization of microemulsions

The preformulation screening of 32 liquid and semisolid excipients and surfactants (**Figure 3A**) in binary combinations with VAS3947 revealed high solubilizing capacity for benzyl alcohol, Capmul MCM C8, Capryol PGMC, Labrafac Lipophile WL 1349, Labrafac PG, Lauroglycol, Linalool, Miglyol 812, PEG 300, PEG 400, and Triacetin after 24 h (i. e. 10 mg VAS3947 / g excipient (~ 1%)). The negative control (PBS buffer; pH 7.4) resulted in < 0.1 mg VAS3947 / g (< 0.01%) in solution.

The excipient screening for VAS2870 and VAS4024 resulted in comparable outcomes (data not shown). Derived from these results, microemulsions were prepared containing 1% VAS3947 (**Table 2**) fulfilling our specification as of (i) absence of phase separation for at least 4 h, (ii) absence of precipitation upon 1:10 dilution with water, and (iii) absence of recrystallization events in the formulation over a time period of 4 weeks. Dynamic light

scattering experiments were performed upon dilution of these microemulsions with water (1:10) and resulted in average diameters of 71 nm ± 4 nm, 43 nm ± 3 nm, 193 nm ± 10 nm, and 168 nm ± 3 nm for microemulsion 1, 2, 3, and 4, respectively (**Table 2**). Microemulsion 1 was an opaque solution, microemulsion 2 appeared as an ultrafine dispersion, and microemulsions 3 and 4 were transparent.

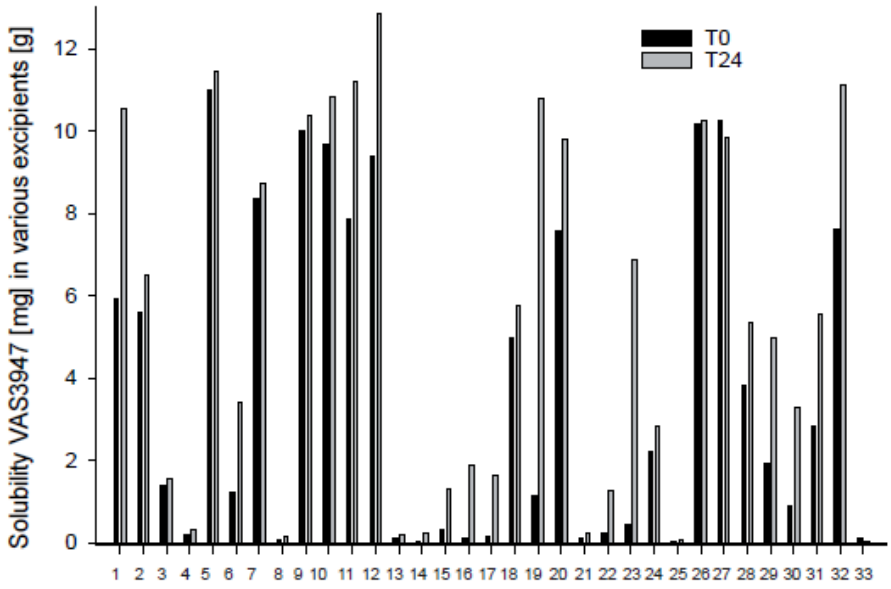


**Figure 3A**: Solubility of VAS3947 in various liquid excipients immediately after preparation (T0) and after 24 h of shaking (T24). Formulation success was defined as solubility of VAS3947 > 10 mg/g excipient. Excipients were in detail: 1 Miglyol 812; 2 Isopropylpalmitate; 3 Squalene; 4 Squalane; 5 Linalool; 6 Sesam Oil; 7 Transcutol HP; 8 Plurol Oleique; 9 Capryol PGMC; 10 Labrafac PG; 11 Labrafac Lipophile WL 1349; 12 Lauroglycol; 13 Castor Oil Refined; 14 Castor Oil Virgin; 15 Peceol; 16 Tween 20; 17 Tween 40; 18 Tween 80; 19 PEG 400; 20 PEG 300; 21 Cremophor RH 40; 22 Etocas 35; 23 Triton X; 24 Ethylenglycol; 25 Glycerol; 26 Benzyl alcohol; 27 Triacetin; 28 Propylenglycol; 29 Wheat Germ Oil; 30 Peanut Oil; 31 Corn Oil; 32 Capmul MCM C8; 33 PBS Buffer (negative control).

### 3.5. Dissolution of VAS3947 from microemulsions

The maximum drug load of VAS3947 was incorporated into the respective microemulsion and resulted in 35.3 mg/g ± 1.4 mg/g (microemulsion 1), 43.4 mg/g ± 1.1 mg/g (microemulsion 2), 39.9 mg/g ± 0.2 mg/g (microemulsion 3), and 29.2 mg/g ± 0.4 mg/g (microemulsion 4).

The dissolution profiles of VAS3947 pure API and from microemulsions were explored in FaSSIF (**Figure 3B**). The concentration of VAS3947 pure substance in FaSSIF (7.0 ± 4.4 µg/mL after 10 min) was comparable to the solubility in PBS buffer. The maximum solubility improvement was observed for microemulsion 1 (1152 µg/mL ± 168 µg/mL after 2 min) along with the longest retention of the supersaturated state (> 1 hour). For microemulsion 2, the initial solubility was elevated (834 µg/mL ± 51 µg/mL after 2 min) but decreased rapidly within 20 min to result in an equilibrium solubility around 300 µg/mL. For microemulsion 3 and 4, a short supersaturation occurred initially (211 µg/mL ± 10 µg/mL and 175 µg/mL ± 5 µg/mL after 2 min), however, no stabilization of the metastable state was observed and both microemulsions resulted in an equilibrium solubility around 120 µg/mL.

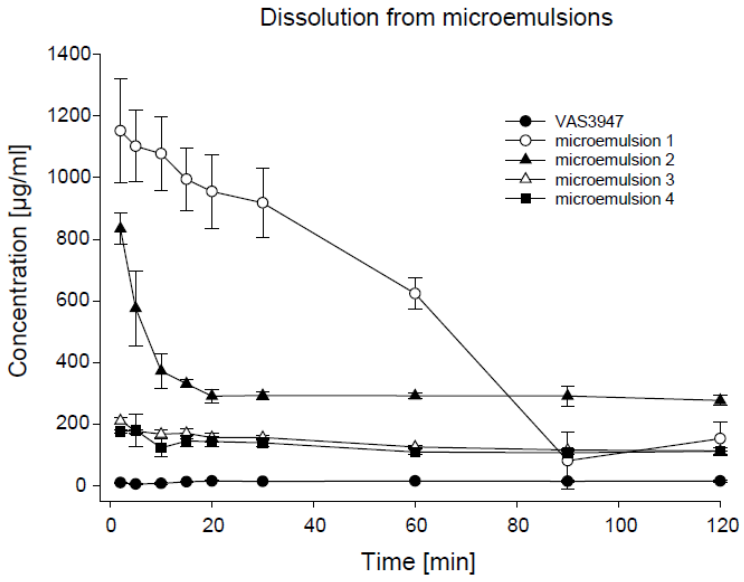


**Figure 3B**: Dissolution profiles of VAS3947 unformulated compound and from four microemulsions with different compositions (**Table 2**) in FaSSiF.

In comparison to unformulated compound, the supersaturation ratio observed after 120 min was highest for microemulsion 2 (18.8 ± 1.1 fold), followed by microemulsion 1 (10.3 ± 3.6 fold), microemulsion 3 (7.7 ± 0.0 fold), and microemulsion 4 (7.6 ± 0.7 fold; **Figure 3C**).

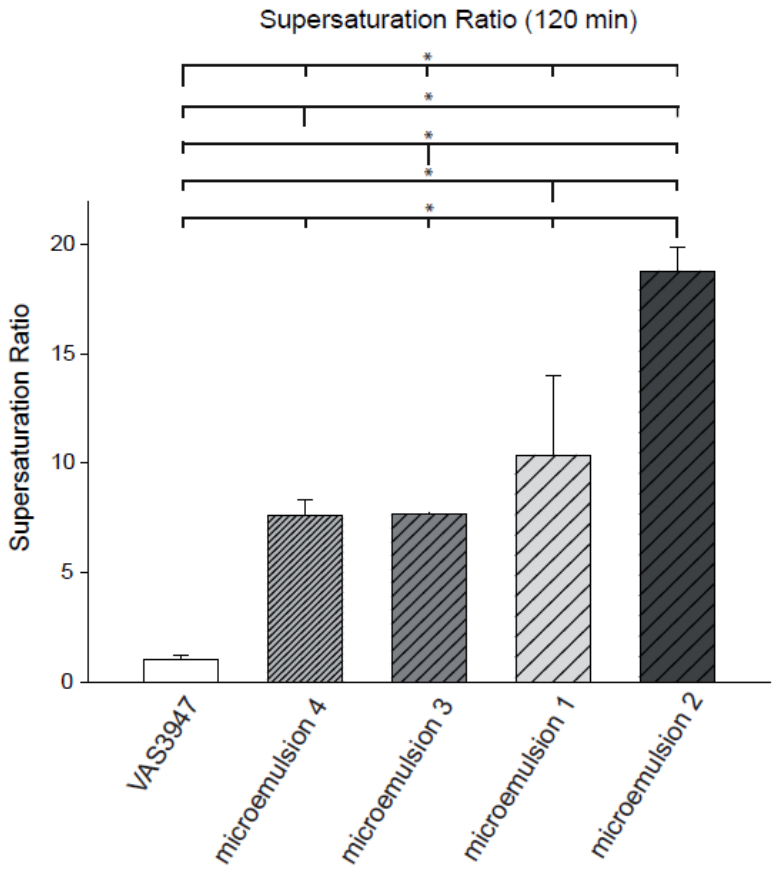


**Figure 3C**: Solubility of VAS3947 unformulated compound (standardized to 1) and respective supersaturation ratios of four microemulsions with different compositions after 120 min.

In summary, all microemulsions significantly improved the solubility of VAS3947 in FaSSiF and superseded the concentrations observed for the spray dried formulations. A rapid absorption of VAS3947 after oral administration is of importance to mitigate the observed rapid collapse of the supersaturated state for all microemulsion formulations. Studies in FeSSiF were not performed, as future *in vivo* studies are planned in fasted animals only.

### 3.6. Preparation of cyclodextrin formulations and dissolution study

10 natural and derivatized cyclodextrins were screened for their solubility improvement power for VAS3947 and studied at different concentrations up to the maximum solubility of the respective CD in PBS buffer (**Table 3**). In general, a linear increase of the VAS3947 solubility was detected with increasing concentrations of the respective cyclodextrin (**Figure 4A**).

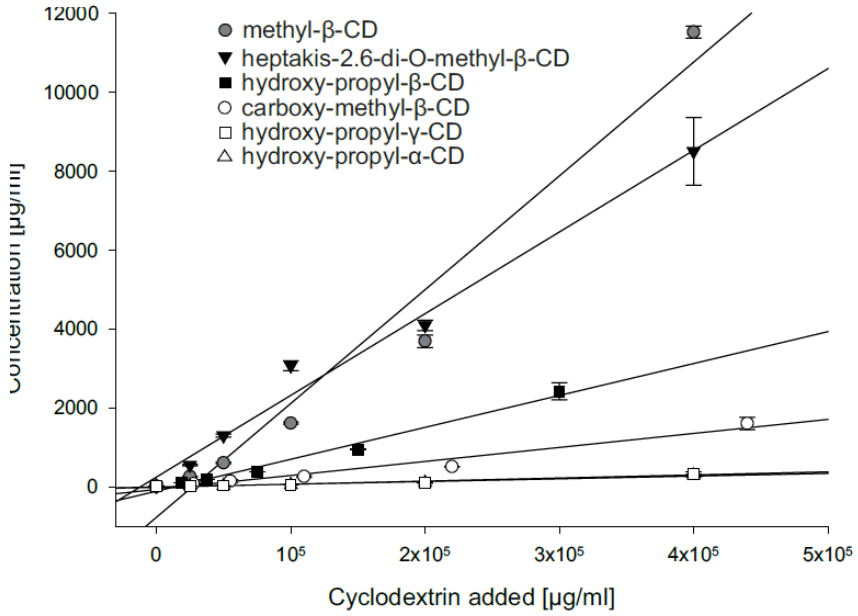


**Figure 4A**: Phase solubility plot of VAS3947 and different cyclodextrins: Solubility improvement of VAS3947 when formulated with different cyclodextrins in different concentrations.

The modified α-, β-, and γ-CDs showed a higher solubility in PBS buffer as compared to the unmodified CDs and improved the solubility of VAS3947 to a high extent (**Figure 4A**). In contrast, pilot studies excluded the unmodified α-, β-, and γ-CDs from further formulation studies as of lack of high solubility in PBS buffer and hence only minor solubility improvement of VAS3947 (data not shown in **Figure 4A** and **4B**). Sulfated-β-CD maintained a constantly low concentration of VAS3947 throughout all concentrations (data not shown in **Figure 4A** and **4B**).

In dependency on the CD, the slope of solubility improvement of VAS3947 with increasing concentrations of CD varied from 2-hydroxypropyl-α-CD (0.0007) < 2-hydroxypropyl-γ-CD (0.0008) < carboxy-methyl-β-CD (0.0035) < 2-hydroxypropyl-β-CD (0.0081) < heptakis-2,6-di-*O*-methyl-β-CD (0.0207) < methyl-β-CD (0.0288; **Figure 4B**).

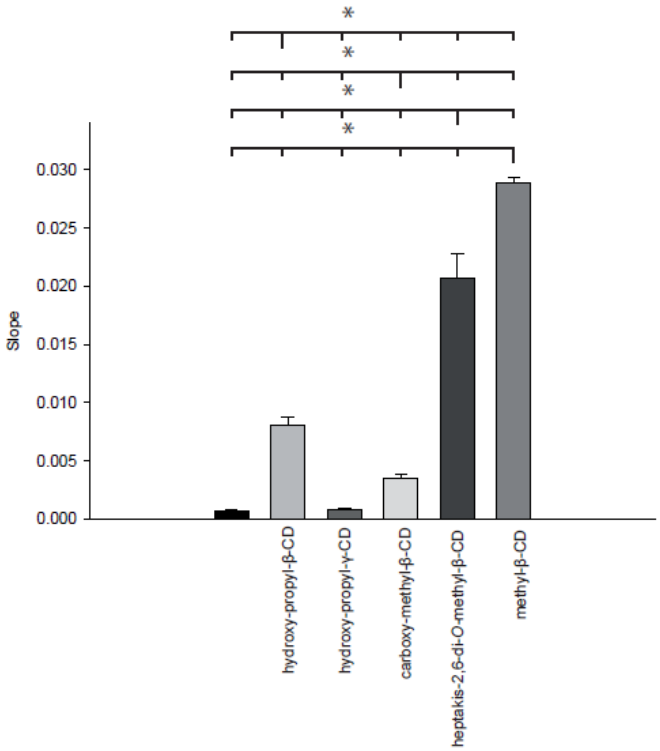


**Figure 4B**: Solubility improvement of VAS3947 when formulated with different cyclodextrins, calculated as slope over increasing cyclodextrin concentrations.

In order to compare equal conditions between CDs, the solubility of VAS3947 when formulated with 10% [w/w] of the respective CD in PBS buffer was illustrated (**Figure 4C**). The highest solubility of VAS3947 after 20 h was found for the lipophilic cyclodextrins heptakis-2,6-di-*O*methyl-β-CD (3072 µg/mL ± 124 µg/mL) and methyl-β-CD (1614 µg/mL ± 31 µg/mL), followed by 2-hydroxypropyl-γ-CD (51 µg/mL ± 5 µg/mL) and 2-hydroxypropyl-α-CD (51 µg/mL ± 1 µg/mL). Lower solubility of VAS3947 was assessed in the presence of 10% [w/w] α-CD (33 µg/mL ± 2 µg/mL), γ-CD (26 µg/mL ± 3 µg/mL), and sulfated-β-CD (12 µg/mL ± 8 µg/mL), the latter even resulting in a solubility lower than that of the VAS3947 alone (18 µg/mL ± 4 µg/mL).

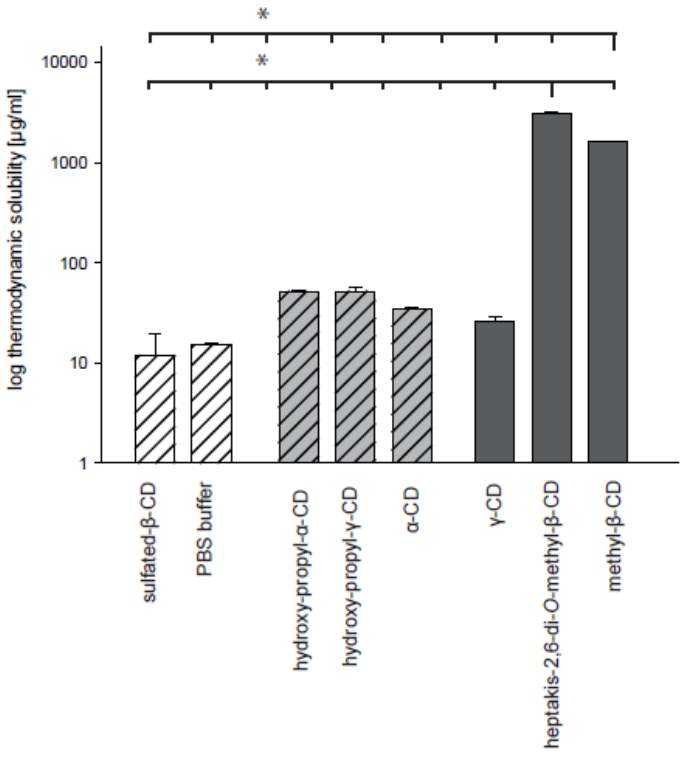


**Figure 4C**: Thermodynamic solubility of VAS3947 formulated with different cyclodextrins in the concentration 10% [w/w], respectively.

Finally, the lipophilic derivatives of β-CD led to a higher increase of solubility of VAS3947 than the derivatives of α- and γ-CD because of the more appropriate size of the cyclodextrin's cavity. In summary, the lipophilic derivatives, namely heptakis-2,6-di-*O*-methyl-β-CD and methyl-β-CD, showed the highest solubility improvement of VAS3947.

### 3.7. NMR measurements

$^{1}$H and ROESY NMR measurements were performed to detail the interaction of VAS3947 with the relatively hydrophobic heptakis-2,6-di-*O*-methyl-β-CD. A distinct shift of all proton signals of VAS3947 in comparison to the pure compound indicated the incorporation of the compound's aromatic rings into the lipophilic cavity of the cyclodextrin (**Figure 5A**).

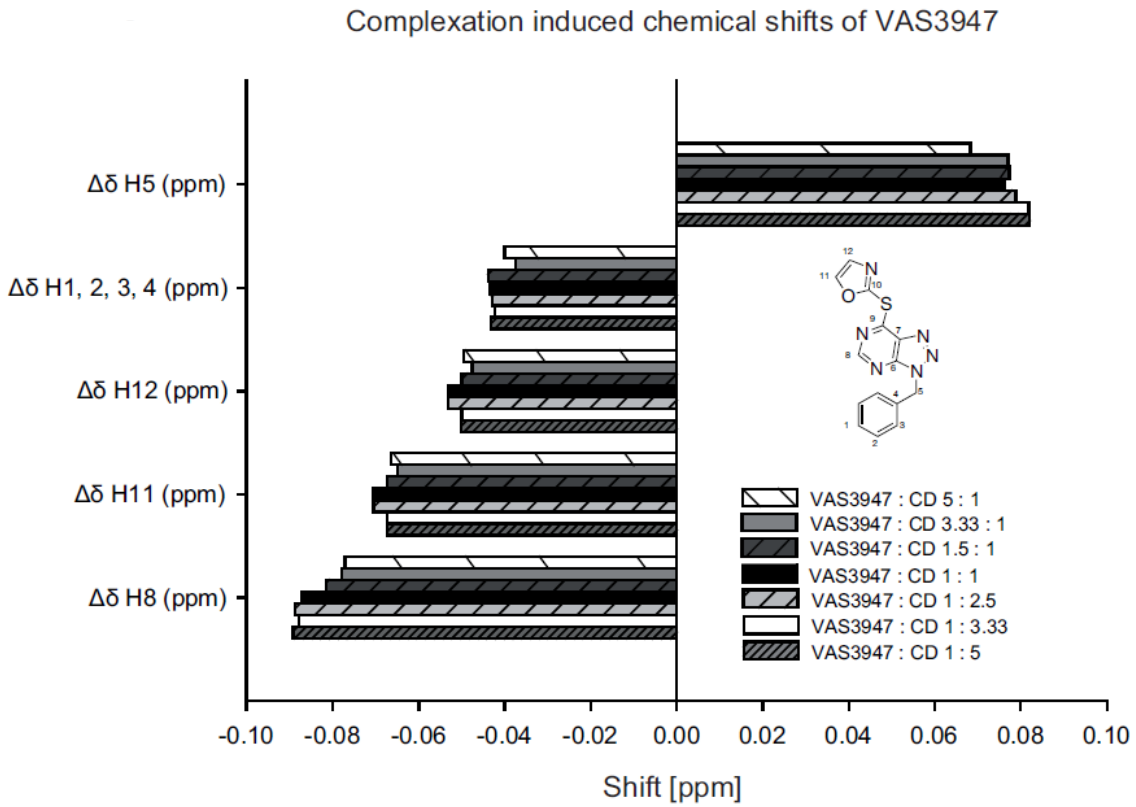


**Figure 5A**: $^{1}$H NMR investigation of complexation induced chemical shifts (CICS) of VAS3947 formulated with heptakis-2,6-di-*O*-methyl-β-CD with reference to VAS3947 unformulated compound.

These observations were corroborated by the results found for the cyclodextrin protons, with H-5' and H-6' having the strongest shifts (0.05 to 0.09 ppm) and H-1', H-2', as well as H-3' showing smaller shifts (0.01 to 0.04 ppm; **Figure 5B**).

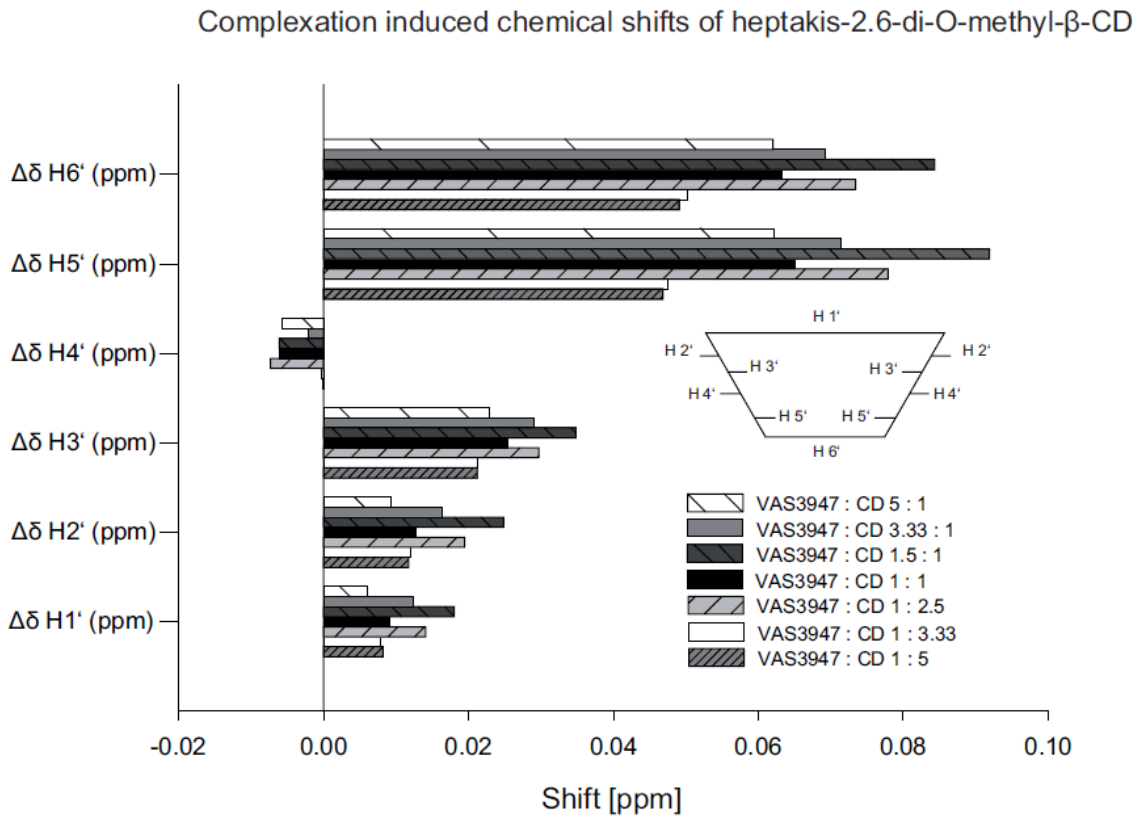


**Figure 5B**: $^{1}$H NMR investigation of complexation induced chemical shifts (CICS) of heptakis-2,6-di-*O*-methyl-β-CD formulated with VAS3947 with reference to heptakis-2,6-di-*O*-methyl-β-CD.

The ROESY spectra confirmed the strong interactions of the API protons with the cyclodextrin protons with the exception of H-1' (**Figure 5C**) as well as the penetration of the VAS compound from the narrow rim of the CD. In addition, the VAS compound seems to attach to the outside of the CD torus. Since the complexation-induced chemical shift changes correlate with the cross peaks of the ROESY measurements we can rule out that the changes are caused by non-precipitating aggregates. The higher the degree of complexation (with higher CD concentrations) the higher changes of the chemical shifts.

However, the fact that we do not observe a clear stoichiometry points to varying complex formations (stoichiometry and geometry) upon increasing the CD concentrations which might be the reason for variations of the shift changes for some CD protons. Since we have not studied this phenomenon in depth we did not discuss this in the manuscript. Nevertheless this is an often observed effect.

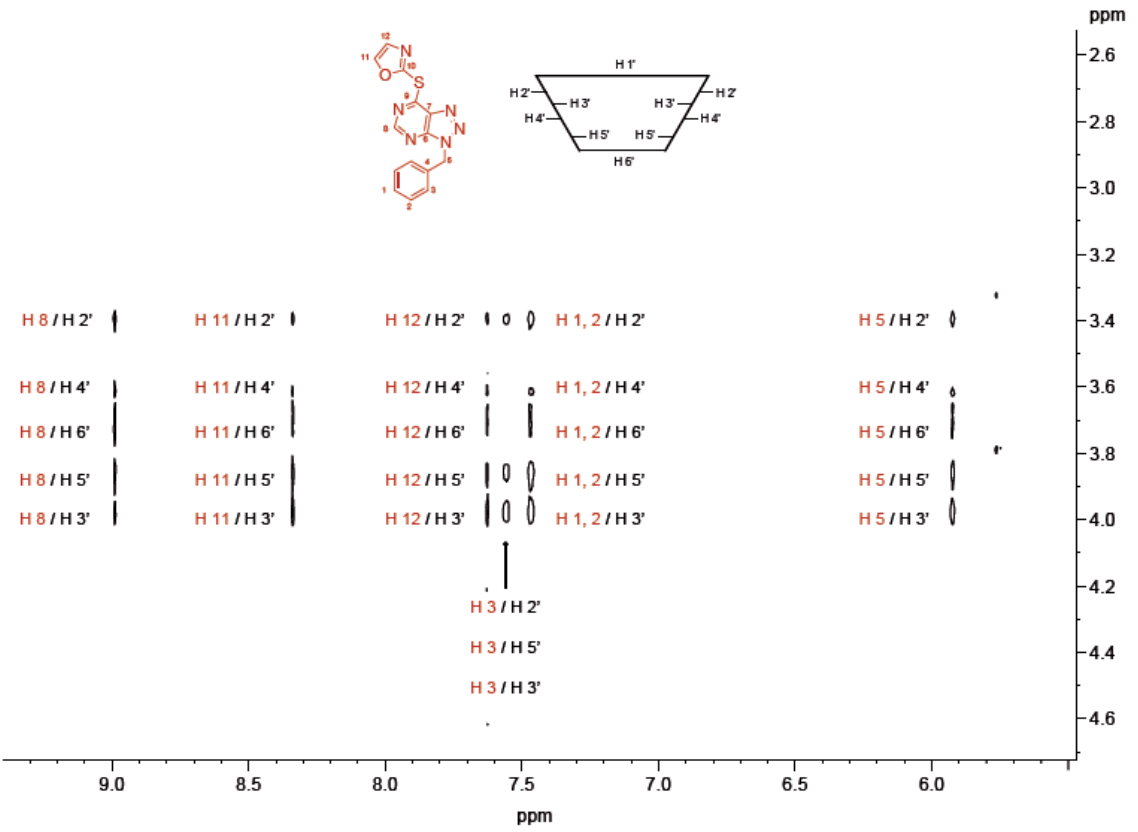


**Figure 5C**: ROESY spectrum showing the interactions of protons from VAS3947 (red) with protons from heptakis-2,6-di-O-methyl-β-CD (black).

### 3.8. VAS3947 - cyclodextrin complex solubility

One of the goals of this contribution was to provide suitable i.v. formulations based on VAS3947–cyclodextrin complexes. Therefore, we focused on 2-hydroxypropyl-β-CD (40% w/w) which is an accepted excipient for parenteral use [13]. The VAS3947–cyclodextrin complex was stable for at least 30 min and a significant decline was found at 120 min and 24 h, at which 85% of VAS3947 was still in solution (**Figure 6**). The diluted formulation (1:1 with 0.9% saline) had a higher stability, with more than 90% being in solution after 24 h (data not shown). No peaks resulting from possible degradation products of VAS3947 were observed in the chromatograms (data not shown).

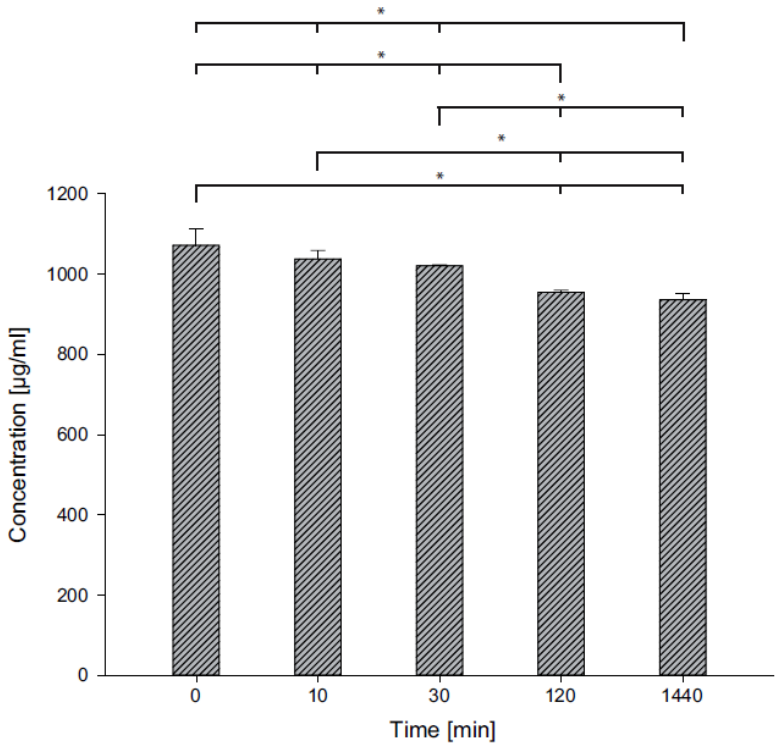


**Figure 6**: Stability assessment of an intravenous formulation of VAS3947 formulated with 2-hydroxypropyl-CD (40% w/w) in PBS buffer.

## 4. Discussion

The development of selective NOX inhibitors represents a promising therapeutic option to treat diseases resulting from elevated ROS levels. Based on the physico-chemical outcomes (MP, logP, solubility), VAS3947 was selected from the compound class of NOX inhibitors as a model substance for further formulation development. The objective of significantly improving the otherwise low aqueous solubility of VAS3947 was successfully accomplished by three different formulation approaches including spray drying with seven excipients, micro-emulsification into four vehicles and incorporation into ten cyclodextrins. Ultimately, a microemulsion for oral administration and a cyclodextrin formulation for intravenous application are suggested, opening these NOX inhibitors for preclinical and clinical assessment by oral or parenteral dosing.

In a first approach, solid dispersions were spray dried (**Table 1**), i.e. the API was dispersed in an inert carrier at solid state followed by solvent evaporation. Excipients were selected due to their chemical variety (i.e. neutral, negatively, and positively charged polymers with different chemical structure and properties) and hence multiple potential mechanisms of influencing the extent and duration of supersaturation, e.g. the ‘spring’ and ‘parachute’ properties [14]. The amorphous conversion of VAS3947 in the spray dried formulations as confirmed by XRPD (**Figure S3A-S3G**) contributed to the significant solubility improvement as compared to the respective physical mixtures (**Figure 2A-2G**) and to the unformulated compound (**Figure 2H**). This outcome was expected, as the kinetic solubility assessment is done from DMSO dissolved compounds, which is why kinetic solubility values do not represent the energy required for compound dissolution. Therefore, these values are typically higher than thermodynamic solubilities. The dissolution profiles highlight the key role of amorphization on the solubility improvement of VAS3947, however, the overall effects were only moderate (supersaturation ratios 3 - 9, **Figure 2H**). In conclusion, the spray drying approach improved the solubility of the API moderately, but none of the formulations produced a concentration of

VAS3947 > 100 µg/mL (spring) for a time period > 1 hour (parachute). An adequately high solubility is of crucial importance to achieve appropriate concentration levels of VAS3947 at the target side and a sufficient parachute time frame minimizes the risk of precipitation in the tissue or in other compartments.

To further increase the extent of the spring and the duration of the parachute, microemulsions were prepared in a second formulation approach to support oral administration. Numerous studies prove the efficiency of microemulsions, systems of water, oil, and amphiphile [9], in the development of oral formulations and in increasing the bioavailability of poorly water soluble drugs. In a pre-formulation screening, single excipients providing high solubilizing capacity for VAS3947 were identified (**Figure 3A**). The outcome of the solubility screening hinted certain standard microemulsion vehicles (**Table 2**) as carriers for VAS3947, following methodologies described before [15, 16]. The vehicles were thermodynamically stable for a sufficient time period (4 weeks) and provided high solubilizing capacities for the API (29 mg/g - 43 mg/g). A trend towards higher solubilizing capacity was observed with decreasing polarity of the formulation, which is in accordance with the logP (1.83) for VAS3947. Upon contact with water, the microemulsions formed fine dispersions in the nanomolar range (< 250 nm; data not shown), favoring dissolution rate and solubilization of the drug [17]. The supersaturation ratio calculated at the end of the study revealed significantly higher concentrations of VAS3947 in all microemulsion approaches in comparison to VAS3947 pure substance (supersaturation ratios 8 - 19, **Figure 3C**).

Previous studies detailed the $IC_{50}$ for VAS3947 between 1 µM (0.31 µg/mL) – 13 µM (4.03 µg/mL) in A7r5, Caco-2, Hl-60 cell lines [6]. The concentrations of VAS3947 after dissolution from microemulsions was greater than the solubility observed for the spray dried preparations whilst maintaining the supersaturated state for a longer time period, hence offering the more promising strategy for the oral administration of VAS3947 in future *in vivo* studies.

In an effort to open parenteral studies for the NOX inhibitors, several cyclodextrin formulations were prepared (**Table 3**). The natural cyclodextrins showed only moderate solubility improvements as compared to the unformulated compound (supersaturation ratios < 3), whereas the lipophilic methylated derivatives of β-CD (heptakis-2,6-di-*O*-methyl-β-CD, methyl-β-CD) significantly increased the concentration of VAS3947 in aqueous medium (174 and 91, respectively). We detailed the interaction of VAS3947 and heptakis-2,6-di-*O*-methyl-β-CD, which was selected as it increased the solubility of the API to the highest extent (**Figure 5A-5B**). The distinct shift of H-5', located inside the cyclodextrin cavity, indicated the presence of VAS3947 within the cyclodextrin cavity and a similar shift of H-6' confirmed a penetration of VAS3947 from the tighter side of torus. The stoichiometry was 1.5:1 (VAS3947:CD), thus deviated from 1:1 and as corroborated by H-2' and H-1' shifts, suggesting that the compound at least in part was attached to the outside of the cyclodextrin and not only within its cavity. The results derived from ROESY analysis confirmed the close contact between API and CD with the exception of H-1', whose distance to VAS3947 was found to be larger than 5 Å (**Figure 5C**). In summary, NMR measurements confirmed the formation of an interaction between API and CD which highly effectuates the solubilization of the API. It is noted that that the lipophilic cyclodextrin derivatives (e.g. heptakis-2,6-di-*O*-methyl-β-CD and methyl-β-CD) are not suitable for parenteral use [18], which is why future studies building off our characterizations and aiming for *in vivo* use may e.g. choose 2-hydroxypropyl-β-CD (40% (w/w)) in PBS buffer (pH = 4.5), a formulation which is in clinical use for other drugs [13]. This formulation stabilized VAS3947 at a concentration around 1000 µg/mL and prevented the compound from recrystallization and importantly provided chemical stability for 24 h.

## 5. Conclusion

NOX inhibitors were prevented from efficient use in animal studies due to solubility limitations. We successfully addressed this shortcoming by providing stable formulations for oral and parenteral use. Using spray drying, microemulsification and the incorporation into cyclodextrines, the thermodynamic solubility of VAS3947 was successfully enhanced for time periods allowing effective absorption *in vivo*.

## Acknowledgements

This study was funded by the Bayerische Forschungsstiftung - BFS - within the project ‘Springs and Parachutes - New Formulations for Poorly Water Soluble Drugs’. We thank Vasopharm GmbH (Würzburg) for provision of the VAS compounds and for the input of scientific knowledge. N.H. is a full-time associated of ACC GmbH, Leidersbach, and states no conflict of interest. We gratefully acknowledge ACC GmbH (Analytical Clinical Concepts GmbH, Leidersbach) for participation within the BFS project as well as instrumental support. We thank Niclas Förtig and Jonas Löffler for the support in experimental work and for plenty of fruitful discussions as well as Marcus Gutmann for the assistance in the design of the graphical abstract. We are grateful to Jens-Christoph Rybak for support in DSC and XRPD experiments.

## References

[1] E. Holzerová, H. Prokischa, Mitochondria: Much ado about nothing? How dangerous is reactive oxygen species production?, Int. J. Biochem. Cell Biol., 63 (2015) 16-20.

[2] E. Cifuentes-Pagano, D.N. Meijles, P.J. Pagano, The quest for selective nox inhibitors and therapeutics: challenges, triumphs and pitfalls, Antioxid. Redox Signal., 20 (2014) 2741-2754.

[3] A. Schramm, P. Matusik, G. Osmenda, T.J. Guzik, Targeting NADPH oxidases in vascular pharmacology, Vascul. Pharmacol., 56 (2012) 216-231.

[4] K.K. Griendling, D. Sorescu, M. Ushio-Fukai, NAD(P)H Oxidase : Role in Cardiovascular Biology and Disease, Circ. Res., 86 (2000) 494-501.

[5] C. Stielow, R.A. Catar, G. Muller, K. Wingler, P. Scheurer, H.H. Schmidt, H. Morawietz, Novel Nox inhibitor of oxLDL-induced reactive oxygen species formation in human endothelial cells, Biochem. Biophys. Res. Commun., 344 (2006) 200-205.

[6] S. Wind, K. Beuerlein, T. Eucker, H. Müller, P. Scheurer, M.E. Armitage, H. Ho, H.H. Schmidt, K. Wingler, Comparative pharmacology of chemically distinct NADPH oxidase inhibitors, Br. J. Pharmacol., 161 (2010) 885-898.

[7] S. Altenhofer, P.W. Kleikers, K.A. Radermacher, P. Scheurer, J.J. Rob Hermans, P. Schiffers, H. Ho, K. Wingler, H.H. Schmidt, The NOX toolbox: validating the role of NADPH oxidases in physiology and disease, Cell. Mol. Life Sci., 69 (2012) 2327-2343.

[8] W.L. Chiou, S. Riegelman, Pharmaceutical Applications of Solid Dispersion Systems, J. Pharm. Sci., 60 (1971) 1281-1302.

[9] I. Danielsson, B. Lindman, The definition of microemulsion, Colloids and Surfaces, 3 (1981) 391-392.

[10] T. Loftsson, P. Jarho, M. Masson, T. Järvinen, Cyclodextrins in drug delivery, Expert Opin. Drug Deliv., 2 (2005) 335-351.

[11] V. Alptüzün, M. Prinz, V. Hoerr, J. Scheiber, K. Radacki, A. Fallarero, P. Vuorela, B. Engels, H. Braunschweig, E. Erciyas, U. Holzgrabe, Interaction of (benzylidene-hydrazono)-1,4-dihydropyridines with β-amyloid, acetylcholine, and butyrylcholine esterases, Bioorg. Med. Chem., 18 (2010) 2049-2059.

[12] H.D. Williams, P. Sassene, K. Kleberg, M. Calderone, A. Igonin, E. Jule, J. Vertommen, R. Blundell, H. Benameur, A. Mullertz, C.J. Porter, C.W. Pouton, L.C. Communicated on Behalf of the, Toward the establishment of standardized *in vitro* tests for lipid-based formulations, part 4: proposing a new lipid formulation performance classification system, J. Pharm. Sci., 103 (2014) 2441-2455.

[13] R. Strickley, Solubilizing excipients in oral and injectable formulations, Pharm. Res., 21 (2004) 201-230.

[14] H.R. Guzman, M. Tawa, Z. Zhang, P. Ratanabanangkoon, P. Shaw, C.R. Gardner, H. Chen, J.P. Moreau, O. Almarsson, J.F. Remenar, Combined use of crystalline salt forms and precipitation inhibitors to improve oral absorption of celecoxib from solid oral formulations, J. Pharm. Sci., 96 (2007) 2686-2702.

[15] B. Lückel, W. Bueb, I. Ottinger, T. Reinhart, A. Ries, Microemulsion formulations comprising particular substance p antagonists, Patent application WO2005074891, 2005.

[16] C.W. Pouton, Lipid formulations for oral administration of drugs: non-emulsifying, selfemulsifying and 'self-microemulsifying' drug delivery systems., Eur. J. Pharm. Sci., 11 Suppl 2 (2000) S93-98.

[17] H.D. Williams, N.L. Trevaskis, S.A. Charman, R.M. Shanker, W.N. Charman, C.W. Pouton, C.J.H. Porter, Strategies to Address Low Drug Solubility in Discovery and Development, Pharmacol. Rev., 65 (2013) 315-499.

[18] M.E. Brewster, T. Loftsson, Cyclodextrins as pharmaceutical solubilizers, Adv. Drug Deliv. Rev., 59 (2007) 645-666.

# Supplementary Information

## DSC from VAS2870, VAS3947 and VAS4024

Method: see manuscript

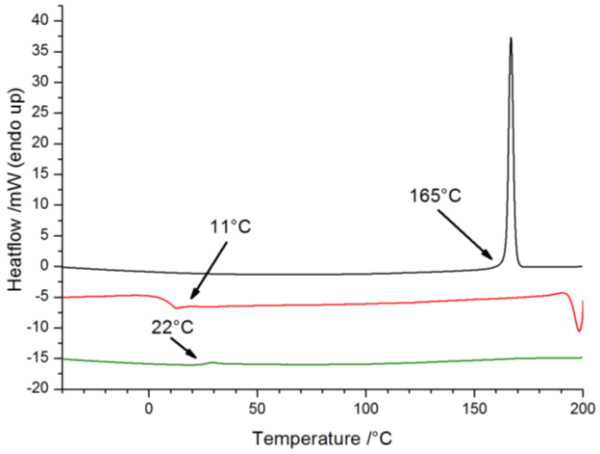


**Figure S1A**: Determination of melting point and glass transitions temperature of VAS2870 by differential scanning calorimetry (DSC). Black curve represents 1st heating run, red curve subsequent cooling run and green curve 2nd heating run.

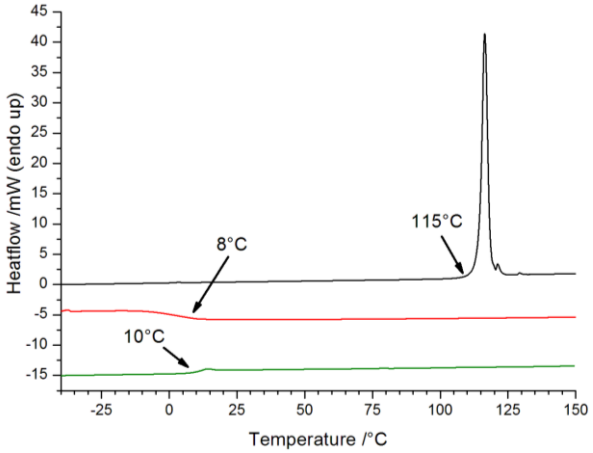


**Figure S1B**: Determination of melting point and glass transitions temperature of VAS3947 by differential scanning calorimetry (DSC). Black curve represents 1st heating run, red curve subsequent cooling run and green curve 2nd heating run.

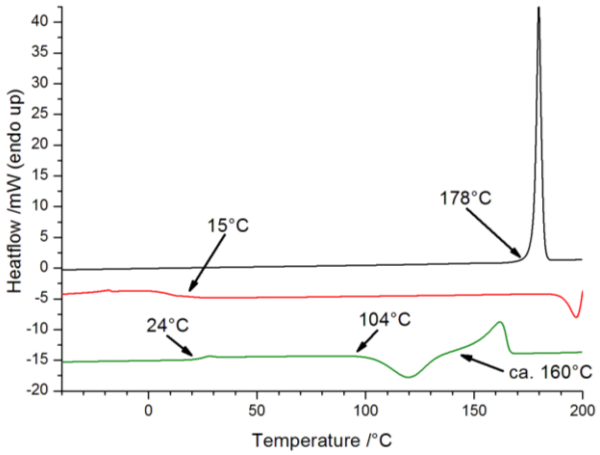


**Figure S1C**: Determination of melting point and glass transitions temperature of VAS4024 by differential scanning calorimetry (DSC). Black curve represents 1st heating run, red curve subsequent cooling run and green curve 2nd heating run.

**Nephelometric determination of kinetic solubility of VAS2870, VAS3947 and VAS4024**

Method: see manuscript

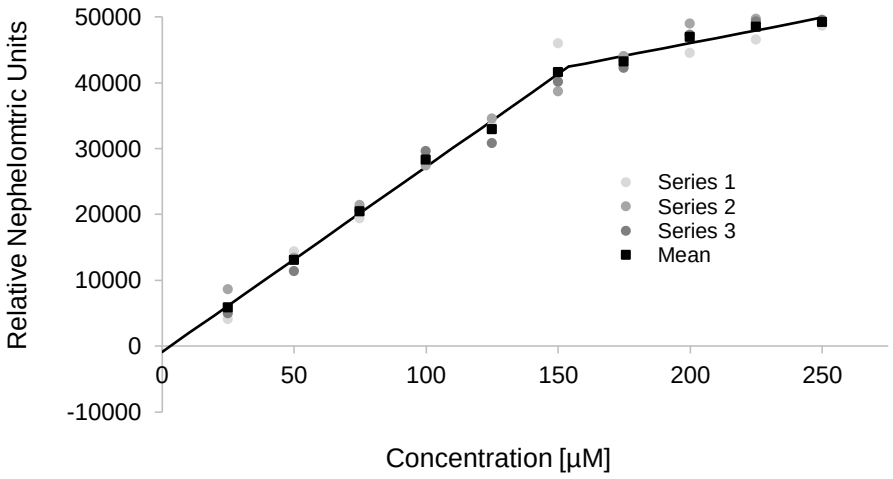


**Figure S2A:** Kinetic solubility of VAS2870 in PBS buffer (freshly prepared solutions).

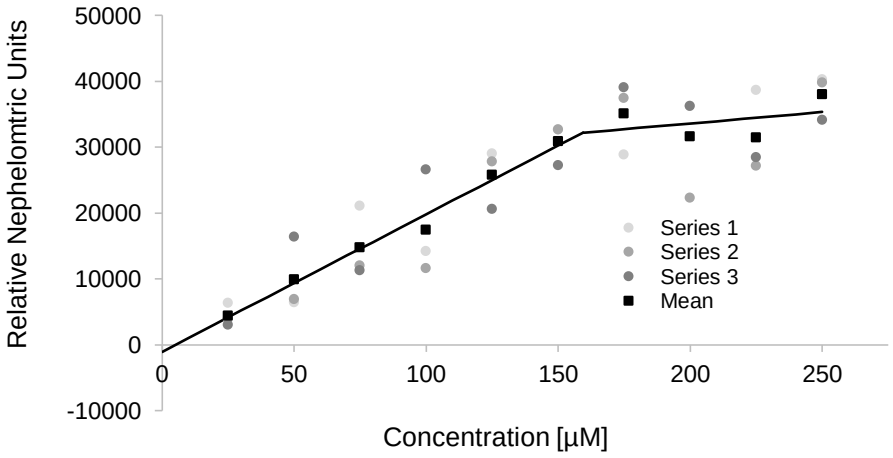


**Figure S2B**: Kinetic solubility of VAS2870 in PBS buffer after 60 minutes.

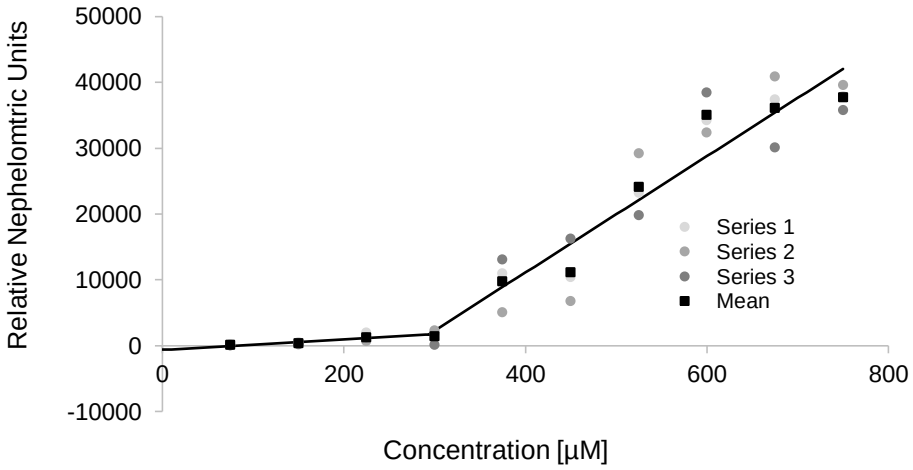


**Figure S2C**: Kinetic solubility of VAS3947 in PBS buffer (freshly prepared solutions).

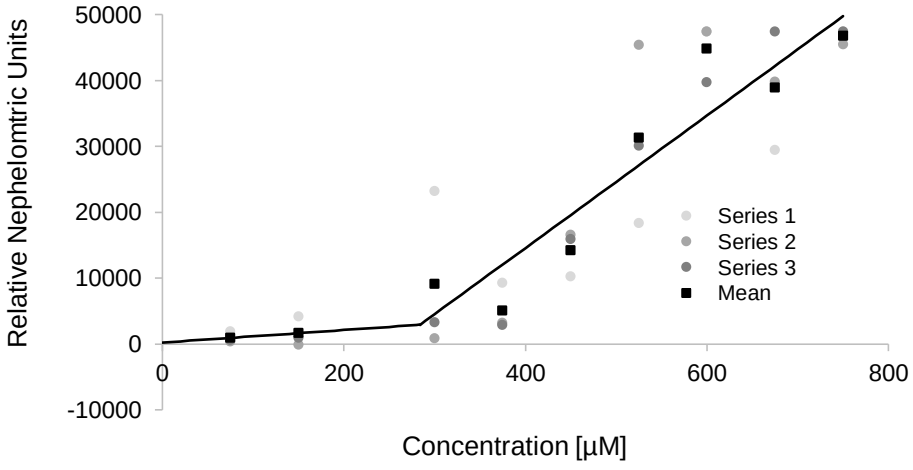


**Figure S2D**: Kinetic solubility of VAS3947 in PBS buffer after 60 minutes.

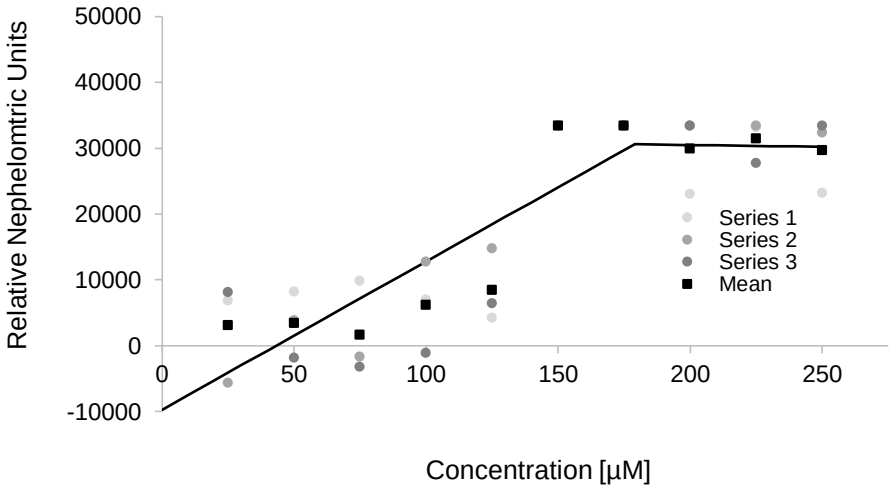


**Figure S2E**: Kinetic solubility of VAS4024 in PBS buffer (freshly prepared solutions).

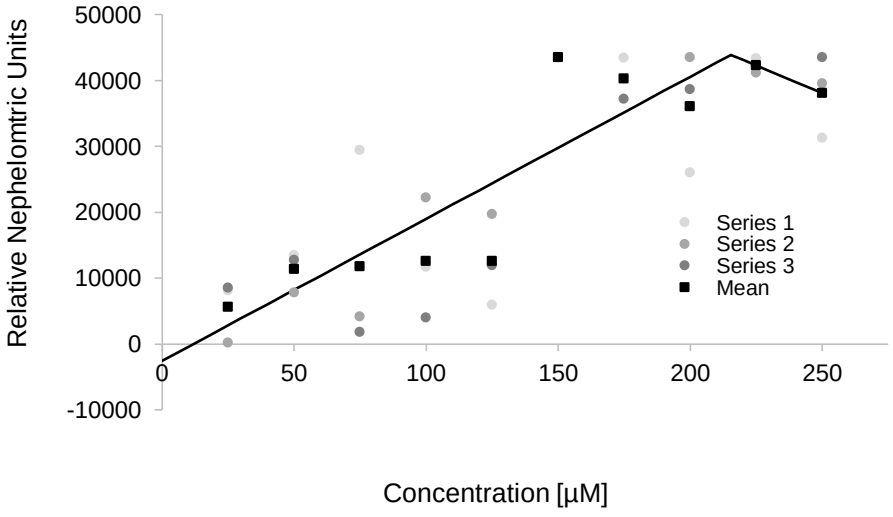


**Figure S2F**: Kinetic solubility of VAS4024 in PBS buffer after 60 minutes.

**XRPD from VAS3947, physical mixtures and spray dried formulations with different excipients**

Method: see manuscript

The amorphization of VAS3947 during the spray drying process was successfully confirmed by the absence of defined crystalline reflexes, illustrated in comparison to the physical mixtures containing crystalline VAS3947.

XRPD data for VAS3947 raw substance are shown sevenfold (**Figure S3A-S3G**).

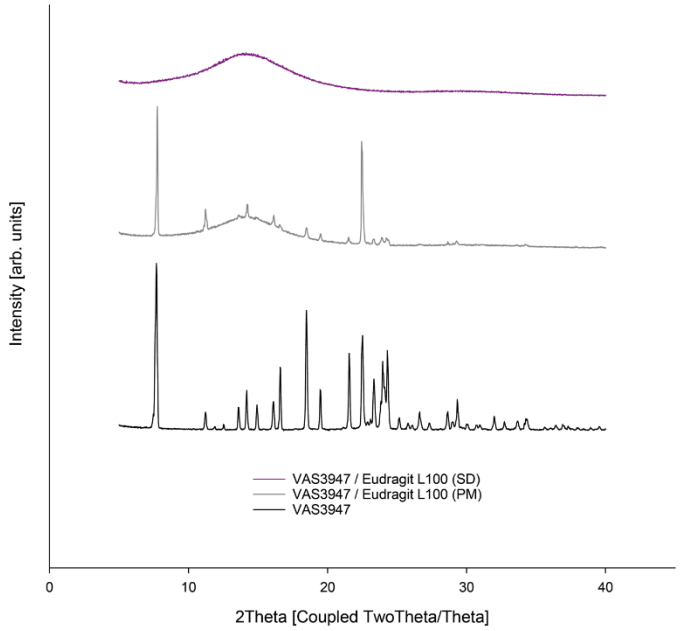


**Figure S3A**: X-ray diffraction pattern of VAS3947 (raw substance, black) and physical mixture of VAS3947 with Eudragit L100 (1+10 w/w; grey) versus respective spray dried formulation (1+10 w/w, pink).

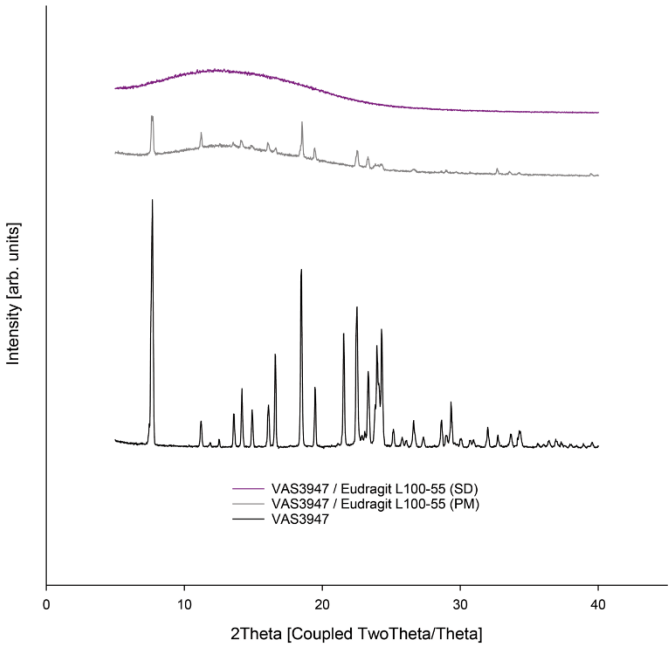


**Figure S3B**: X-ray diffraction pattern of VAS3947 (raw substance, black) and physical mixture of VAS3947 with Eudragit L100-55 (1+10 w/w; grey) versus respective spray dried forlation (1+10 w/w, pink).

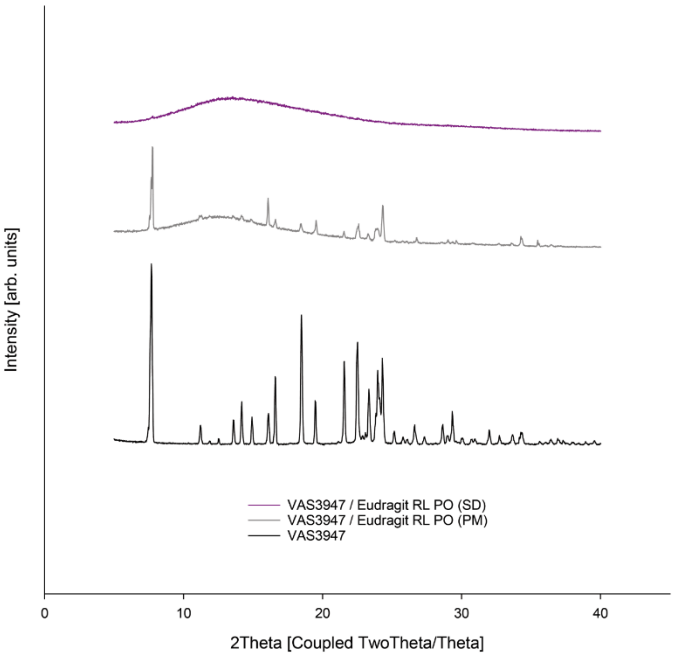


**Figure S3C**: X-ray diffraction pattern of VAS3947 (raw substance, black) and physical mixture of VAS3947 with Eudragit RL PO (1+10 w/w; grey) versus respective spray dried formulation (1+10 w/w, pink).

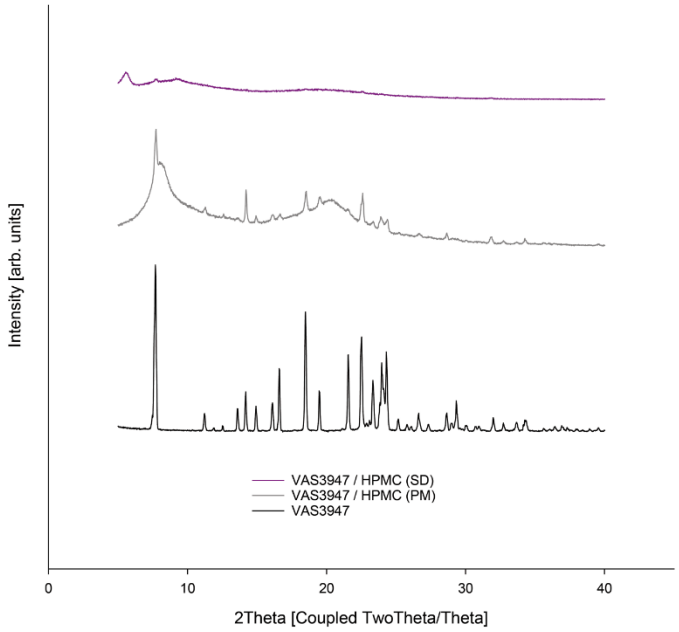


**Figure S3D**: X-ray diffraction pattern of VAS3947 (raw substance, black) and physical mixture of VAS3947 with HPMC (1+10 w/w; grey) versus respective spray dried formulation (1+10 w/w, pink).

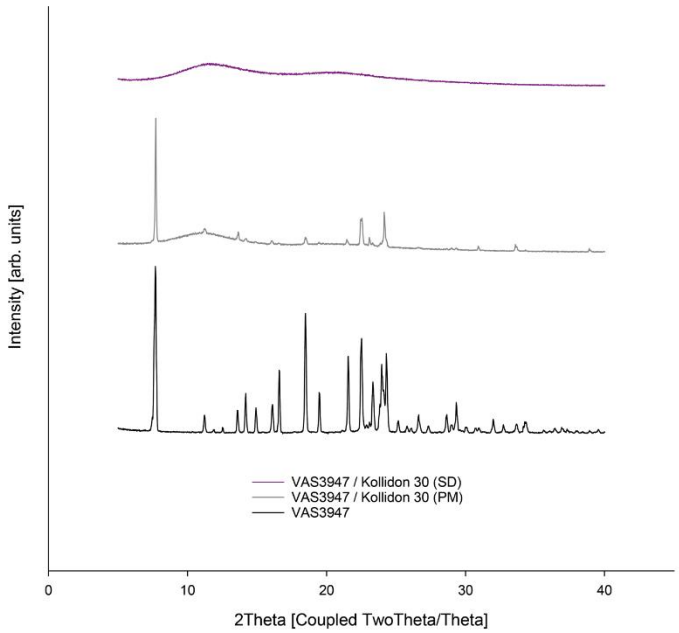


**Figure S3E**: X-ray diffraction pattern of VAS3947 (raw substance, black) and physical mixture of VAS3947 with Kollidon 30 (1+10 w/w; grey) versus respective spray dried formulation (1+10 w/w, pink).

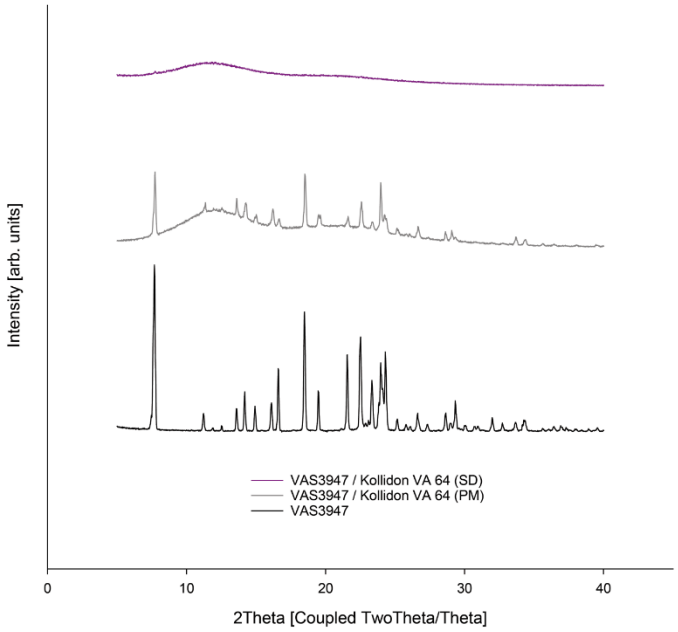


**Figure S3F**: X-ray diffraction pattern of VAS3947 (raw substance, black) and physical mixture of VAS3947 with Kollidon VA 64 (1+10 w/w; grey) versus respective spray dried formulation (1+10 w/w, pink).

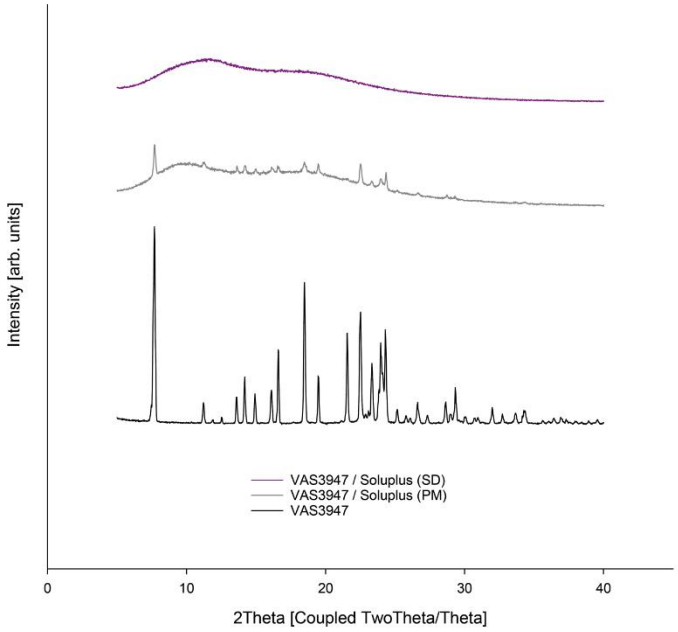


**Figure S3G**: X-ray diffraction pattern of VAS3947 (raw substance, black) and physical mixture of VAS3947 with Soluplus (1+10 w/w; grey) versus respective spray dried formulation (1+10 w/w, pink).

# CHAPTER IV

## STABILITY STUDIES ON THE TRIAZOLOPYRIMIDINE TYPE NOX INHIBITORS

Nils Terveer, Nina Hecht, Marcus Gutmann, Marco Saedtler, Lorenz Meinel, and Ulrike Holzgrabe*

Universität Würzburg, Institut für Pharmazie und Lebensmittelchemie, Am Hubland, Würzburg, Germany

*Unpublished manuscript.*

## Abstract

Triazolopyrimidine derivatives efficiently and selectively inhibit NADPH oxidases (NOX) with promising potential for the treatment of cardiovascular diseases. We addressed the pharmaceutical properties of an effective NADPH oxidase inhibitor with a particular focus on chemical stability in solution, plasma stability, transepithelial transport, and cytotoxicity. VAS3947 was found to be remarkably instable in buffer, when exposed to light, metabolic enzymes and human plasma. VAS3947 and all related compounds of the triazolopyrimidine substance class consist of an oxazol moiety linked with a thioether to the triazolopyrimidine skeleton which is essential for the pharmacological effect. This moiety is prone to hydrolysis leading to cleavage and further reactions. Hence, VAS3947 and the related compounds are neither appropriate as a tool for ROS studies nor suitable for preclinical studies.

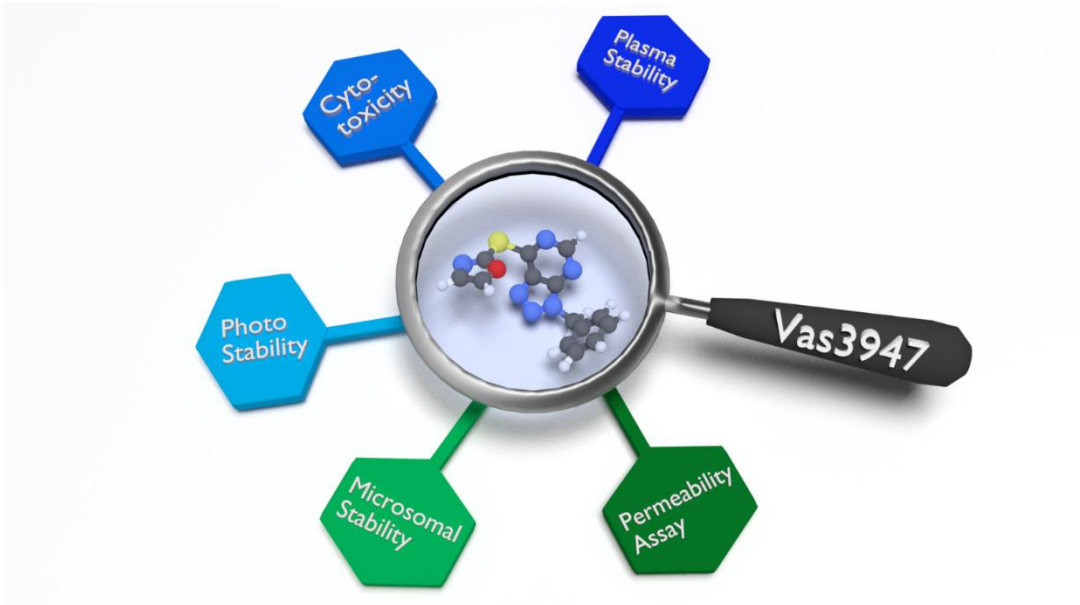

# 1. Introduction

Endothelial dysfunctions causing diseases such as hypercholesterolemia, atherosclerosis, hypertension, diabetes, and heart failure are one of the main causes of death for humans [1]. It has been well known for some decades that reactive oxygen species (ROS) are involved in the formation of cardiovascular diseases [2] and that an accelerated inactivation of nitrogen monoxide by ROS contributes to the formation of endothelial dysfunction [3]. Since NADPH oxidases are one of the predominant sources of ROS in vascular cells [4-6], selective inhibition of ROS production is one of the strategies for an effective therapy of cardiovascular diseases [2].

Triazolopyrimidine compounds such as VAS2870 and VAS3947 (**Figure 1**) [6, 7] are specific inhibitors of the NADPH oxidases [8]. During the last years, more than 50 publications have described the VAS compounds as effective NADPH oxidase inhibitors and hence promising for the treatment of cardiovascular diseases. Additionally, these VAS compounds have demonstrated biological effects in preliminary cell culture studies. VAS2870, one of the most active compounds of this library, was found to inhibit oxidized low-density lipoprotein (oxLDL)-mediated ROS formation in human endothelial cells [9]. Furthermore, VAS2870 was reported to suppress PDGF-mediated ROS liberation in vascular smooth muscle cells [6] and to blunt pro-vasculogenetic effects of PDGF-BB in mouse embryonic stem cells [10]. VAS2870 inhibited wound margin $H_2O_2$ production and leucocyte recruitment in zebrafish larvae [11].

VAS3947, a novel derivative of VAS2870 with a higher solubility, was introduced as an apparently specific inhibitor of the NADPH oxidase which did not interfere with commonly used ROS assays [8]. Using VAS3947, the pharmacological evidence of NADPH oxidases being indeed a relevant source of ROS formation was provided in the animal model of Spontaneously Hypertensive Rats (SHR) [8].

In view of planned preclinical studies, appropriate formulations of VAS3947 were recently presented [12]. The aim of this paper was to study the inherent stability of VAS3947 before translation into preclinical studies as all compounds from the VAS library carry an oxazol moiety linked with a thioether which is typically prone to hydrolysis, possibly jeopardizing the class's pharmaceutical properties.

To this end, VAS3947 was assessed for its stability against light exposure, and the degradation products were investigated. Additionally, a biopharmaceutical characterization of VAS3947 was performed, including microsomal stability, plasma stability, permeability assays, and cytotoxicity studies in human liver and human embryonic kidney cells.

# 2. Materials and Methods

## 2.1. Materials

VAS3947 was supplied by Vasopharm GmbH (Würzburg, Germany). Deionized water was taken from an in-house supply with a Milli-Q® system (Merck Millipore GmbH, Darmstadt, Germany), or purchased from Thermo Fisher Scientific GmbH (Schwerte, Germany). Male mice microsomes (CD-1) were purchased from Sigma Aldrich GmbH (Schnelldorf, Germany) and NADPH+$H^+$ was from AppliChem (Darmstadt, Germany). K2-EDTA and heparin plasma were obtained from Sera Laboratories International Ltd. (Haywards Heath, UK). 12-well plates and filter inserts were purchased from Greiner Bio-One GmbH (Frickenhausen, Germany). Penicillin G and streptomycin solutions were purchased from Biochrom AG (Berlin, Germany), and fetal bovine serum (FBS) from Thermo Fisher Scientific GmbH. Hank's balanced salt solution (HBSS), Dulbecco's modified eagle medium (DMEM), Minimum Essential Medium (MEM), and Non-essential Amino Acids solution 100x (NEAA) were purchased from Sigma Aldrich GmbH. Caco-2 cells, Hep-G2 cells, and HEK-293 cells were purchased from DSMZ GmbH (Braunschweig, Germany). CELLSTAR® tissue culture dishes (100 mm) and 96-well plates from Greiner Bio-One GmbH, and WST-1 Solution from Roche Diagnostics Deutschland GmbH (Mannheim, Germany). 5 mm NMR tubes (S-5-900-7) were bought from Norell Inc., (Marion, NC), deutero dimethylsulfoxide, and deutero chloroform from Deutero GmbH (Kastellaun, Germany). 2 mL Verex vials for HPLC analysis were purchased from Phenomenex Ltd. Deutschland (Aschaffenburg, Germany), petroleum ether and ethyl acetate as well as syringe filters (0.22 µm) from VWR International GmbH (Darmstadt, Germany), and POLYGRAM® SIL G/UV254 polyester sheets for thin layer chromatography from Macherey-Nagel GmbH & Co. KG (Düren, Germany). Acetonitrile and methanol (CHROMASOLV® gradient grade), trifluoroacetic acid (TFA), and formic acid were

purchased from Sigma Aldrich GmbH. All chemicals were at least of analytical or pharmaceutical grade and were used without further purification.

## 2.2. Methods

### 2.2.1. Stability Testing

A photostability testing of VAS3947 was performed according to Singh et al. [13] and to the guideline of the International Council on Harmonization Q1B [14]. The test substance was dissolved in a mixture of acetonitrile and water (60/40% v/v) at a concentration of 1 mg/mL. This solution was transferred into two 5 mL glass vials and exposed to light, providing an overall illumination of 1.2 million lux h and 6 million lux h, respectively, using near ultraviolet energy of 250 watt h/$m^2$ produced by the Suntester CPS+ instrument (Atlas Material Testing Technology GmbH, Linsengericht-Altenhaßlau, Germany).

Another set of two samples, wrapped in aluminium foil but apart from that treated likewise, was used as dark control to evaluate the thermally induced degradation in comparison to the totally observed decrease of drug content. Concentrations of drug in solutions were determined by HPLC. The samples were diluted in a mixture of acetonitrile/water (60/40% v/v) and the concentration was calculated using a regression line over the range of 1 µg/mL to 250 µg/mL. All experiments were carried out in triplicate.

### 2.2.2. Chromatographic Conditions for Stability Testing

An Agilent 1100 chromatographic system (Agilent Technologies GmbH, Waldbronn, Germany) equipped with an online degasser (G1322A), an autosampler (G1313A), a binary pump (G1312A), a thermostated column department, and a diode array UV/VIS detector (G1315B) was used for the investigation of photostability samples. The ChemStation® software package was used for data handling (Agilent Technologies GmbH). The chromatographic conditions were as follows: As a stationary phase a Phenomenex Synergi Max RP (50 × 4.6 mm; 4 µm particle size) analytical column was

used. The run time was 10 min followed by a post time of 5 min. A binary gradient was applied with a mixture of water and acetonitrile (90/10% v/v) adjusted with 0.05% TFA as mobile phase A and a mixture of water and acetonitrile (10/90% v/v) adjusted with 0.05% TFA as mobile phase B. The gradient profile was as follows: from 0 min to 8 min from 100% to 20% mobile phase A, from 8 min to 9 min at 20% mobile phase A, and from 9 min to 10 min from 20% to 100% mobile phase A. UV detection was performed at 254 nm and 280 nm. The column compartment was maintained at 23 °C, the flow rate was 1.5 mL/min, and 10 µL of sample was injected.

### 2.2.3. Production and Isolation of Degradation Products

For the investigation of degradation products the same Agilent 1100 chromatographic system as described for the stability testing was used. Additionally, an Agilent LC/MSD G2445D ESI ion trap (Agilent Technologies GmbH) with a syringe pump KDS100 (KD Scientific, Holliston, MA) coupled to the electro spray ionization (ESI) interface was used. Data handling was performed with the help of ChemStation® software package.

For the determination of degradation products 30 mg of VAS3947 were dissolved in 10 mL methanol. This solution was transferred into a glass vial and exposed to light, providing an overall illumination of 6 million lux h using near ultraviolet energy of 250 watt h/$m^2$ using Suntester CPS+ instrument to reach complete degradation of the API. The reaction was controlled by thin layer chromatography using petroleum ether and ethyl acetate (2/1 v/v) as the eluent and POLYGRAM® SIL G/UV254 polyester sheets as the stationary phase. Afterwards, the solvent was evaporated and the degradation products were separated by flash chromatography using a Puri Flash 430 instrument from Interchim S. A. (Montlucon, France) equipped with a 4 g silica column, UV detector, and automatic sampling of fractions. Petroleum ether and ethyl acetate were used as eluents (2/1 v/v) and a 4 g silica column was used as stationary phase.

After evaporation of the solvents the structure of the purified degradation products was elucidated by NMR spectroscopy and mass spectrometry.

### 2.2.4. Chromatographic Conditions for Elucidation of Degradants

The chromatographic conditions for mass analysis were as follows: As a stationary phase an Agilent Zorbax SB-CN (50 × 4.6 mm; 3.5 µm particle size) analytical column was used. The run time was 20 min followed by a post time of 5 min. A binary gradient was applied using water with 0.1% formic acid as mobile phase A and acetonitrile with 0.1% formic acid as mobile phase B.

The gradient profile was as follows: from 0 min to 5 min 5% mobile phase B, from 5 min to 10 min from 5% to 90% mobile phase B, from 10 min to 15 min 90% mobile phase B, and from 15 min to 20 min from 90% to 5% mobile phase B. UV detection was performed at 254 nm and 280 nm. The column compartment was maintained at 23 °C, the flow rate was 0.4 mL, and 10 µL of sample was injected.

The parameters for the ESI ion trap were as follows: The flow rate was 0.4 mL/min, the nebulizer pressure 15 psi, the dry gas flow 5 L/min, the dry temperature 325 °C, the capillary voltage 3500 V, and helium was used as collision gas.

### 2.2.5. Microsomal Assay

VAS3947 was subjected to an *in vitro* microsomal stability assay in order to simulate Phase-I metabolism. Liver enzymes were prepared from male mice microsomes and gently thawed on ice prior to use. A 10 mM stock solution of VAS3947 was prepared in dimethylsulfoxide. 5 µL of the stock solution were dissolved in a mixture of 445 µL potassium phosphate buffer (100 mM; pH 7.4), 50 µL of liver enzyme preparation (10 mg/mL), and 0.5 mg NADPH/$H^+$ (final volume: 500 µL). This resulted in final concentrations of 100 µM VAS3947, 1 mg/mL enzyme, and 1.2 mM NADPH/$H^+$. The solutions were incubated at 37 °C in a water bath and aliquots (50 µL) were taken at 0, 15, 30, 60, 90, 120, 150, 180, 210, 240, and 270 min. The samples were immediately diluted

with acetonitrile (1/1 v/v) to stop the enzymatic activity, vortex mixed for 30 seconds and centrifuged for 2 min at 10.000 rpm at a temperature of 4 °C. The clear supernatant was analysed on a Jasco-HPLC system (Groß-Umstadt, Germany) equipped with a degasser (DG-2080-53), a gradient unit (LG-2080-02), a pump (PU-1580), an autosampler (AS-2051Plus), and an UV/VIS detector (UV-2075Plus). The column oven was from Phenomenex (Thermasphere TS-130). The Galaxie chromatography software package was used for data handling (Version 1.9.3.2., Varian, Inc., CA). A Phenomenex Synergi Polar RP analytical column (80 Å, 40 x 4.6 mm, 4 µm) was used. Mobile phase A was $H_2O$/acetonitrile (90%/10% v/v) adjusted with 0.05% TFA, and mobile phase B was $H_2O$/acetonitrile (10%/90% v/v) adjusted with 0.05% TFA with a gradient from 0 min to 1.5 min at 80% to 60% for mobile phase A, and from 1.5 min to 4.0 min at 60% mobile phase A. Detection was at λ = 277 nm with an injection volume of 15 µL, a flow rate of 2.0 mL/min, and a column temperature at room temperature. 5 µL VAS3947 stock solution in 495 µL potassium phosphate buffer as well as 5 µL VAS3947 stock solution, 495 µL potassium phosphate buffer, and 0.5 mg NADPH/$H^+$ (negative control) were investigated under the same conditions.

### 2.2.6. Plasma Stability Assessment

The *in vitro* assessment of plasma stability of VAS3947 was performed in human K2-EDTA plasma and heparin plasma. 100 µL of a 100 µg/mL stock solution of VAS3947 in acetonitrile was added to 1000 µL pre-warmed plasma (final concentration of VAS3947: 9.09 µg/mL). Control samples were prepared likewise using water instead of plasma. Samples were incubated in a water bath at 37 °C and aliquots (110 µL) were taken after 0, 15, 30, and 60 min. After sampling, the aliquots were immediately diluted with 300 µL acetonitrile and centrifuged for 10 min at 10.000 rpm at a temperature of 4 °C. The clear supernatant was analysed on the HPLC system from Jasco using a Phenomenex Synergi Polar RP analytical column (80 Å, 40 x 4.6 mm, 4 µm). Mobile phase A was

$H_2O$/acetonitrile (90%/10% v/v) adjusted with 0.05% TFA, and mobile phase B was $H_2O$/acetonitrile (10%/90% v/v) adjusted with 0.05% TFA with a gradient from 0 min to 1.5 min at 70% to 40% for mobile phase A, from 1.5 min to 4.0 min at 40% mobile phase A, and from 4.0 min to 6.0 min at 40% to 0% mobile phase A. Detection was at λ = 280 nm with an injection volume of 15 µL, a flow rate of 2.0 mL/min, and a column temperature at room temperature. Additionally, the experiment was repeated with plasma spiked with 0.5% sodium fluoride and with heat inactivated plasma [15]. Furthermore, VAS3947 was investigated in the presence of the reducing agents acetylcysteine, glutathione and dithiothreitol (concentration (reducing agents) [µM] = concentration (VAS3947) [µM] * 1000) in water.

### 2.2.7. Permeability Assay

For Caco-2 cell assays a Neubauer improved hemocytometer from LO-Laboroptik Ltd. (Lancing, UK), a fluorescence spectrometer LS50B from Perkin Elmer (Waltham, MA), and a chopstick EVOM2 STX3 electrode connected to a EVOM2 epithelial voltammeter (World Precision Instruments, Sarasota, FL) were used. Caco-2 cell assays were performed as described by Hubatsch et al. [16]. In brief, Caco-2 cells were cultured in Dulbecco's modified Eagle's medium (DMEM) high glucose containing 10% heat inactivated fetal bovine serum, 100 U/mL penicillin G and 100 µg/mL streptomycin at 37 °C and 5% $CO_2$ as described before [16].

$2.6 \times 10^5$ cells / $cm^2$ were seeded on polycarbonate filter inserts (diameter 12 mm; 0.4 µm membrane pore size) on 12-well plates. Cells typically had at least three passages. The monolayer integrity was monitored by measuring the transepithelial electrical resistance (TER). TER measurements were performed for each cell-seeded filter using a chopstick electrode EVOM2 STX3 electrode connected to an EVOM2 epithelial voltammeter. Specifications for cell-seeded filters required TER values exceeding 400 $\Omega \times cm^2$.

On day 21 after sowing permeability assays were performed from the apical to the basolateral compartment. For the permeability experiment, 1200 µL of Hank's Balanced Salt Solution pH = 7.4 (HBSS) was provided in the basolateral compartment and 500 µL of a 100 µM solution of VAS3947 in HBSS, 500 µL of 100 µM solution of Lucifer Yellow in HBSS (negative control), and 500 µL of a 100 µM solution of Fluorescein sodium in HBSS (positive control), respectively, was added to the apical side (n=3). After 30 min, 60 min, and 120 min of incubation at 37 °C, 7% $CO_2$, and orbital shaking at 150 rpm, 100 µL of sample was taken from the basolateral side and the volume loss was compensated by adding fresh HBSS.

Additionally, 100 µL of the sample solution was taken from the apical side directly after adding the samples and after 120 min for the calculation of mass balance and $P_{app}$. The calculation of $P_{app}$ was conducted according to the following formula:

$$P_{app} = \left(\frac{dQ}{dt}\right)\left(\frac{1}{A \times c_0}\right)$$

with $P_{app}$ being the apparent permeability coefficient

$\left(\frac{dQ}{dt}\right)$ being the steady-state flux in µmol/sec,

A being the insert/filter surface area in $cm^2$, and

$c_0$ being the starting concentration in the apical (donor) chamber in µM.

The concentration of VAS3947 was analysed by HPLC using the method as described for the microsomal assay.

Lucifer Yellow (negative control) and Fluorescein sodium (positive control) were analysed using fluorescence detection. The following parameters were set for Lucifer Yellow (negative control): The excitation wavelength was 470 nm, the excitation slit was 2.5 nm, the emission wavelength was 535 nm, the emission slit was 2.5 nm, and the read time was 0.4 s.

The following parameters were set for Fluorescein sodium (positive control): The excitation wavelength was 490 nm, the excitation slit was 2.5 nm, the emission wavelength was 514 nm, the emission slit was 15 nm, and the read time was 0.4 s.

### 2.2.8. Cytotoxicity

For cytotoxicity assays a SPECTRAmax® 250 automated microtiter plate reader from Molecular Devices LLC. (Sunnyvale, CA) was used operating at 450 nm and at 650 nm. The assays were conducted in human liver cells (Hep-G2) and human embryonic kidney cells (HEK-293) according to ATCC protocols [17, 18]. In brief, cells were seeded on 96-well plates at a cell density of $3.2 \times 10^4$ cells/mL for HEK-293 and $1.0 \times 10^5$ cells/mL for Hep-G2 (using 125 µL per well).

For Hep-G2 cells, a stock solution of VAS3947 was prepared in dimethylsulfoxide and serially diluted with growth medium (MEM) containing 10% heat inactivated fetal bovine serum, 1% non-essential amino acids, 0.1 mM amino acid L-glutamine, 100 U/mL penicillin G, and 100 µg/mL streptomycin. The solutions of VAS3947 were prepared in the following concentrations: 2.5 µM, 5 µM, 7.5 µM, 10 µM, 25 µM, 50 µM, 75 µM, 100 µM, and 200 µM. The residual content of dimethylsulfoxide was 0.5%.

For HEK-293 cells, a dilution series was prepared from the same stock solution in growth medium (DMEM) containing 10% heat inactivated fetal bovine serum, 100 U/mL penicillin G and 100 µg/mL streptomycin. The solutions of VAS3947 were prepared in the following concentrations: 1 µM, 2.5 µM, 5 µM, 7.5 µM, 10 µM, 25 µM, 50 µM, 75 µM, and 100 µM. The residual content of DMSO was 0.5%.

VAS3947 solutions were incubated on cell layers for 24 h at 37 °C and 5% $CO_2$ (n=4). After the incubation period, water-soluble tetrazolium solution (WST-1) was added to each well according to the manufacturer's instructions. The absorption of formazan at 450 nm following from an enzymatic reaction of living cells with tetrazolium chloride was measured using a SPECTRAmax 250 automated microtiter plate reader. The positive controls

(Hep-G2/HEK-293 cells and respective medium including WST-1) and negative controls (respective medium and WST-1) were processed likewise. Finally, the percentage of surviving cells was calculated with the positive control normalized to 100% and the negative control normalized to 0% survival.

### 2.2.9. Structure Elucidation of the Degradants

$^{1}$H NMR spectra were measured using a Bruker Avance III spectrometer (Bruker Rheinstetten, Germany) operating at 400.13 MHz, equipped with a 5 mm BBO broadband observer with Z-gradient. Data processing was done with the TopSpin® 3.2 software.

$^{1}$H NMR spectra were recorded with a flip angle of 30°, spectral width of 20 ppm, transmitter offset of 6.15 ppm, acquisition time of 3.99 s followed by a relaxation delay of 1.00 s. 128 scans were collected to 64.000 data points, resulting in a digital resolution of 0.25 Hz. Processing parameters were set to an exponential line broadening window function of 0.3 Hz, an automatic baseline correction, and manual phasing.

Unless stated otherwise, 20 mg of sample was dissolved in 700 µL of $CDCl_3$ or DMSO-$d_6$ and transferred into a standard 5 mm NMR tube. The solvent signal served as the field frequency lock. The temperature was adjusted to 300 K.

# 3. Results

Since preclinical studies were planned for VAS3947 (**Figure 1**), the compound was investigated for its chemical and metabolic stability in addition to permeability and toxicity studies.

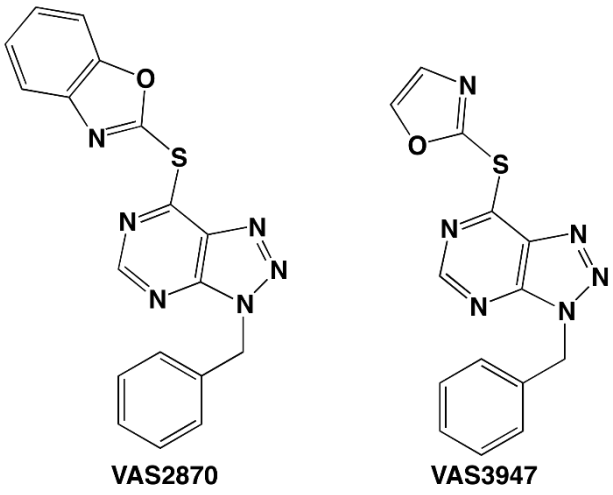


**Figure 1**: The chemical structures of VAS2870 and VAS3947.

### 3.1. Photostability

A photostability testing of VAS3947 was performed according to Singh et al. [13] and the ICH guideline Q1B [14]. A significant degradation of VAS3947 was observed upon light exposition (**Figure 2**). Whereas the content of the control samples (wrapped in aluminium foil) decreased to 97 ± 0.6% (1.2 Mio lux hours) and 92 ± 0.4% (6 Mio lux hours), the decrease was 47 ± 0.3% for the light exposed sample at 1.2 million and complete degradation was assessed after exposition to 6 million lux h, respectively.

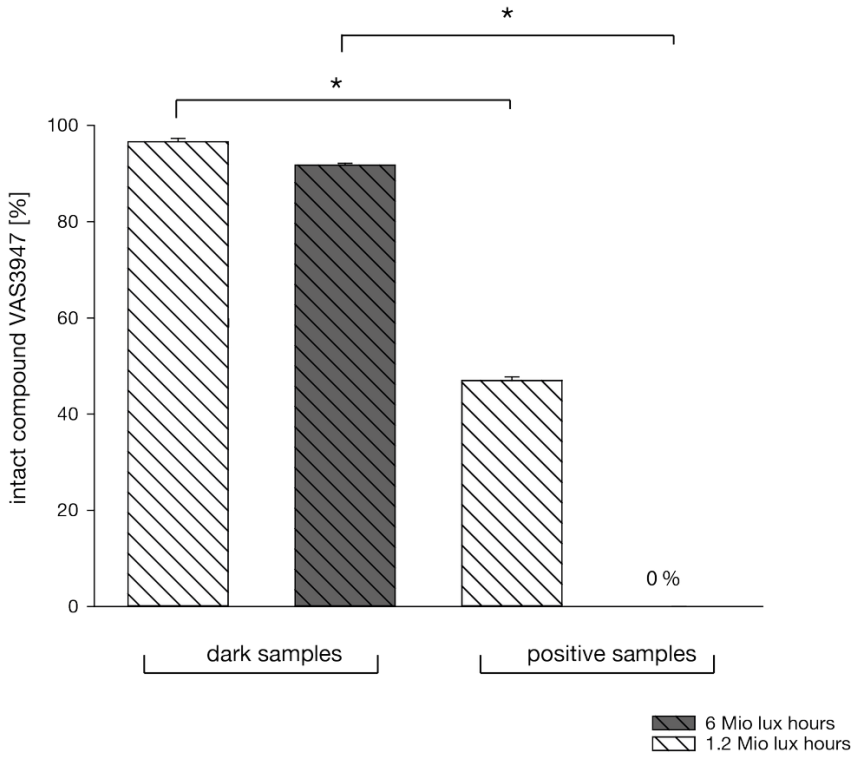


**Figure 2**: Photostability of VAS3947: Dark samples wrapped in aluminium foil versus positive samples exposed to light illumination. The samples were exposed to 1.2 million lux h and to 6 million lux h, respectively.

To identify the degradation products, a forced degradation experiment was conducted. A mixture containing three degradation products was obtained and the analytes were separated chromatographically. The comparison of the $^{1}$H NMR spectra of VAS3947 and its degradation products revealed the loss of two protons at δ = 7.96 ppm (H-11) and 7.44 to 7.38 (H-12) (**Figure 3**). Additionally, a new signal at δ = 4.26 ppm occurred attributed to a methyl group. All other signals were identical to the parent compound VAS3947 indicating the integrity of the triazolopyrimidine skeleton.

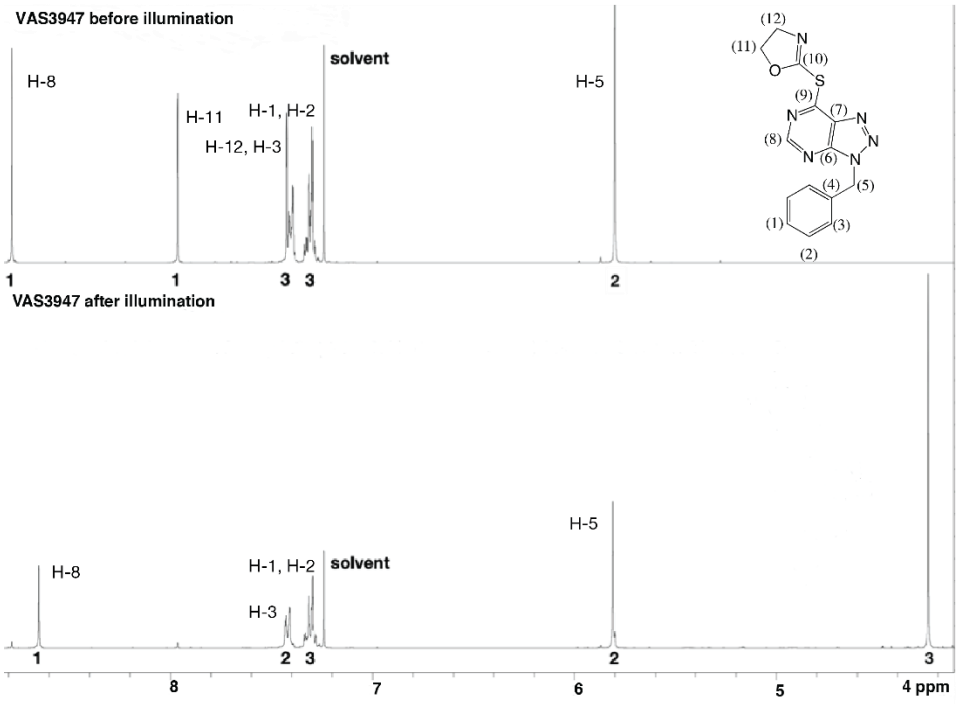


**Figure 3**: Comparison of the $^{1}H$ NMR spectra ($CDCl_3$) of VAS3947 before and after degradation by providing overall illumination of 6 million lux h.

The NMR spectrum of the degradation products (**Figure 3**) represents the mixture of the three degradation compounds. The degradation product with m/z = 242 g/mol may correspond to the methoxylated compound a (**Figure 4**). The degradation product with m/z = 260 g/mol, which also shows a methyl signal, might be in agreement with compound c. Again, the methylation (naturally irrelevant) resulted from methanol exposure. The degradation product with m/z = 243 g/mol did not exhibit any methyl signal and was assigned to compound b.

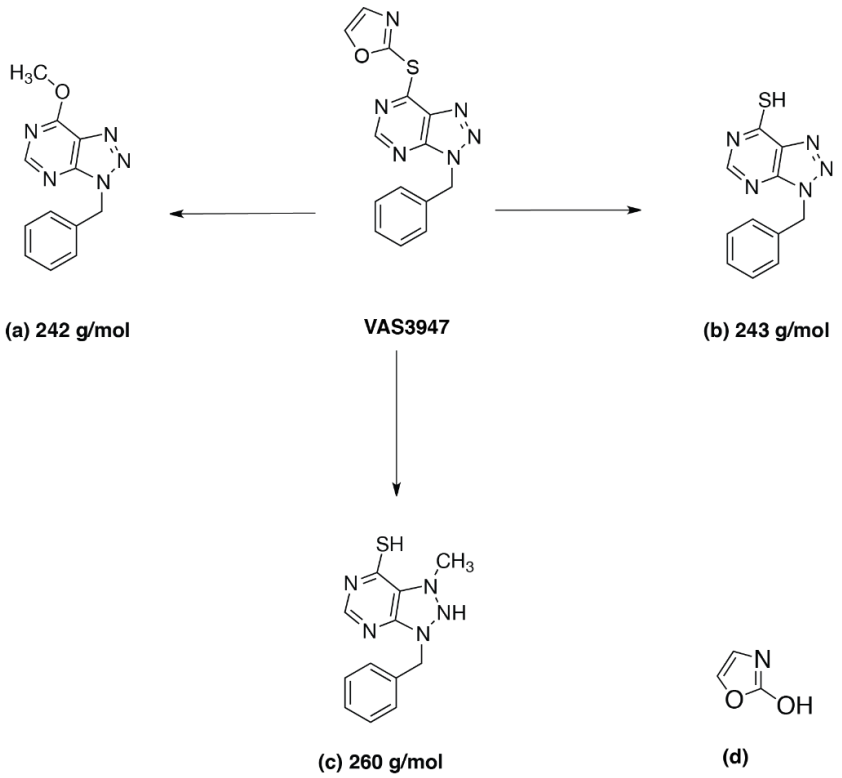


**Figure 4**: The structures of VAS3947 and the identified degradation products (**a-c**) after providing overall illumination of 6 million lux h. Structure (**d**) represents the hydroxylated oxazole moiety after separation from the skeleton.

### 3.2. Microsomal Stability

The assessment of microsomal stability was performed for the prediction of Phase-I metabolism. Firstly, the stability of VAS3947 was tested against phosphate buffer and secondly, against NADPH+$H^+$ dissolved in phosphate buffer (negative control). Already in buffer (without NADPH+$H^+$ and microsome exposure), VAS3947 proofed instability (90% ± 1% after 240 min). A minor degradation proportion was further related to the presence of NADPH+$H^+$ (negative control), and the content of VAS3947 decreased to 86% ± 2% after 240 min (**Figure 5A**). Following exposure to microsomes in this vehicle, the VAS3947 content rapidly decreased (71% ± 1% after 15 min) followed by a slower degradation phase. After 240 min, the amount of VAS3947 levelled off at 32% ± 3%, indicating a substantial metabolic liability of compound VAS3947.

### 3.3. Plasma Stability

VAS3947 was incubated in K2-EDTA plasma at 37 °C to study the stability against plasma. Control samples were incubated in water instead of plasma. After 30 min of incubation in plasma, VAS3947 was completely degraded whereas the compound was stable in the control group (97% after 360 min). The assay was repeated in heparinized plasma to assess a possible impact of EDTA. Furthermore, the investigation was conducted in heat inactivated K2-EDTA plasma and in K2-EDTA plasma containing 0.5% sodium fluoride to assess the impact of active proteins on VAS3947 stability, respectively. All three experiments resulted in complete VAS3947 degradation after 30 min. To further address the possible degradation mechanism, the effect of reducing agents was investigated by incubating the compound in water with acetylcysteine, glutathione, and dithiothreitol. Following incubation for 30 min, 59 ± 1% of VAS3947 were found in the presence of acetylcysteine, 30 ± 1% in the presence of glutathione and 11 ± 0% in the presence of glutathione and dithiothreitol, indicating the sensitivity of VAS3947 for redox reactions.

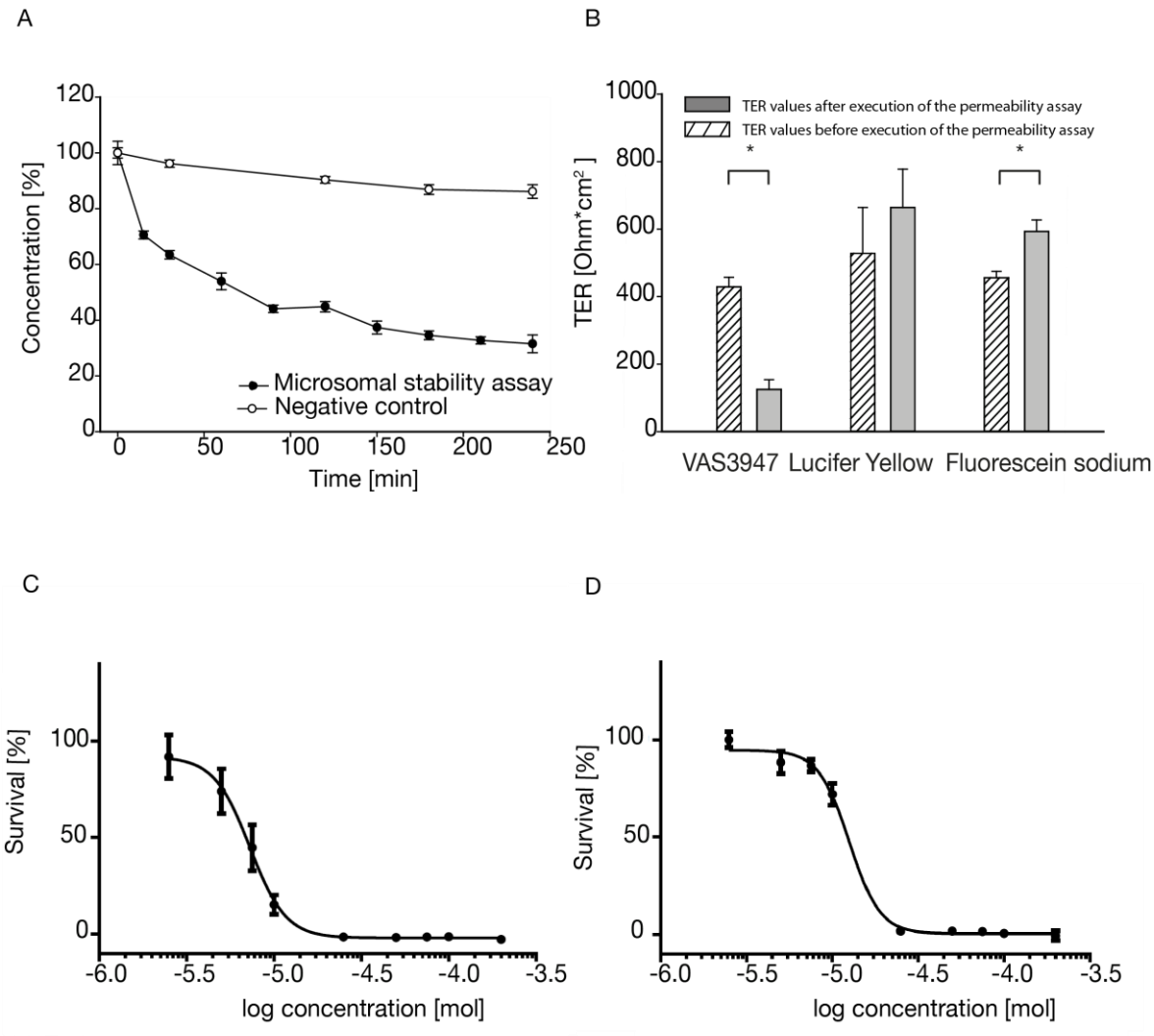


**Figure 5A**: The microsomal stability of VAS3947 in phosphate buffer / NADPH+H$^+$ (negative control) and in the respective medium including liver microsomes from mice**.**

**Figure 5B**: The transepithelial resistance (TER) of Caco-2 cell layers before the addition of the test compounds (shaded bars) and incubated with VAS3947, Lucifer Yellow (negative control) and Fluorescein sodium (positive control) for 120 min (grey bars).

**Figure 5C**: $IC_{50}$ of VAS3947 in HEK-293 cells.

**Figure 5D**: $IC_{50}$ of VAS3947 in Hep-G2 cells.

### 3.4. Permeability and cytotoxicity assay

The permeability of VAS3947 across physiological membranes was studied by Caco-2 cell assays with Lucifer Yellow serving as negative control and Fluorescein sodium as positive control [16]. The results for TER measurements are summarized in **Figure 5B**. Assay specifications included minimal TER values of 400 Ohm × $cm^2$ before and after the experiment. For Lucifer Yellow (negative control), TER results were assessed as 528 ± 136 Ohm × $cm^2$ prior to the experiment and 664 Ohm × $cm^2$ ± 114 Ohm × $cm^2$ after termination of the permeability experiment. The mass ratio was 99.4% ± 2.4% of the specified content after 120 min and $P_{app}$ was 0.26 ± 0.30 × $10^{-6}$ cm/s. For Fluorescein sodium (positive control), TER results were 456 ± 19 Ohm × $cm^2$ before and 596 Ohm × $cm^2$ ± 34 Ohm × $cm^2$ after the experiment. The mass ratio was 99.2% ± 6.8% of the specified content and $P_{app}$ was 1.11 ± 0.17 × $10^{-6}$ cm/s.

These results indicated intact cell monolayers throughout the experiment. For VAS3947, the transepithelial resistance decreased considerably from 429 ± 28 Ohm × $cm^2$ to 125 ± 29 Ohm × $cm^2$ after 120 min of incubation. In addition, a low mass ratio of 24.5 ± 11.2% of the specified content was found after 120 min. Firstly, these results indicate that VAS3947 leads to the destruction of cell monolayers and secondly, gets absorbed into the cells. Having no intact cell monolayer in place, the calculated $P_{app}$ result of 6.4 x $10^{-6}$ cm/s can be neglected.

A cytotoxicity assessment of VAS3947 was performed in kidney cells (HEK-293) and hepatocytes (Hep-G2) and resulted in $IC_{50}$ values of 7.3 ± 0.5 µM (**Figure 5C**) and 12.6 ± 1.0 µM (**Figure 5D**), respectively, indicating a substantial toxicity.

## 4. Discussion

Although cardiovascular diseases are a major cause of death in the majority of the developed countries [1], an effective therapy preventing the formation of cardiovascular diseases is still missing. Previously, the novel small molecule drug candidates developed by Vasopharm [6, 7] were described as specific inhibitors of the NADPH oxidases. They suppress the formation of ROS which is involved in the formation of cardiovascular diseases [2, 8]. Thus, the development of these novel NOX inhibitors seems to be a reasonable approach to inhibit NADPH oxidases and ROS, respectively, in the formation of endothelial dysfunctions.

Since instability of a drug candidate is always an issue, the VAS compound having the highest aqueous solubility, namely VAS3947, was subjected to stability assays and to a biopharmaceutical characterization. The compound was found to be highly labile in water, buffer, and plasma, and preliminary data suggest that degradation is not driven by enzymatic activity but by redox reactions.

The instabilities were linked to the chemical structure of VAS3947 (**Figure 2, 3**). The oxazol moiety of the molecule next to the thioether, which seems to be essential for a high pharmacological activity, is hydrolysis sensitive. Thus, the degradation reaction is likely to occur at the oxazol part of the molecule. Possibly, an intermediate hemiaminal is obtained from the hydrolysis which converts into the hydroxylated oxazol moiety d and the N-benzylated compounds a to c (**Figure 4**). The main degradation product potentially is compound b characterized by a thiol group in position 9 (**Figure 4**) which can also be found in compound c. The NMR and the mass spectra of compound c pointed to an additional methylation of one triazole nitrogen (**Figure 4**) possibly driven by a radical reaction with methanol occurring during the light-stress studies. In compound a, the thiol attached to position 9 of the triazolopyrimidine is possibly replaced by a methoxy group originating from methanol, which was used for the dissolution of the drug. Even when no reaction with methanol takes place, the oxazol is always cleaved by hydrolysis. Since the

oxazol ring, which is linked to the triazolopyrimidine via a thioether is a highly labile moiety, it is impossible to decide whether the degradation upon incubation with mice liver microsomes is due to simple chemical reactions or due to enzyme driven reactions.

In the Caco-2 assays, VAS3947 challenged cell membrane integrity. Furthermore, the cytotoxicity testing of VAS3947 conducted in HEK-293 and HEP-G2 cells resulted in $IC_{50}$ values of 7.3 µM and 12.6 µM, respectively, which are in the same order of magnitude reported for other cell lines or assessed in cell-free systems [6]. However, due to the high reactivity of the VAS drug it cannot be decided whether the membrane disintegration and the cytotoxicity are caused by the drug compound itself, or by its degradation products or by some intermediates of the degradation process.

**The following limitations apply to the stability study on the NOX inhibitors:**

From scientific point of view, the elucidation of the resulting intermediates and degradation products is fundamental. Preliminary data suggest an instability of the oxazol moiety / the thioether after light exposure. Further investigations (NMR, mass spectrometry) are of crucial importance to clarify the chemical structure of all decomposition products occurring in the stability and biopharmaceutical assays. Moreover, the respective degradation pathways will need to be investigated.

Following the elucidation of decomposition compounds, systematic attempts to stabilize VAS3947 in the relevant environments (e.g. in aqueous solutions, plasma) will need to be performed. In this regard, cyclodextrin and microemulsion formulations of VAS3947 proposed in a previous work [12] will further be investigated for their stabilizing properties to complement this set of experiments.

## 5. Conclusion

To the best of our knowledge stability studies of VAS3947 were conducted for the first time even though the compound was previously used in numerous assays. VAS3947 has limited chemical stability against buffers and light, in the presence of metabolic enzymes, reducing agents, and in human plasma, most likely due to the oxazol / thioether element. Furthermore, it harmed Caco-2 cell membranes and cytotoxicity data were found to be in the same concentration range as efficacy data published for different cell lines before. This fact is a major issue and hinders further drug development process of the triazolopyrimidine substance class. Since the results cannot currently be attributed to the drug compound itself rather than to the degradation products, VAS compounds studied here are not appropriate candidates for the investigation of ROS involvement in the formation of cardiovascular diseases. From this follows that the preclinical studies already carried out in the past have to be reassessed in light of the poor pharmaceutical properties of the triazolopyrimidine derivatives. Future formats for effective NOX inhibitors should deploy more stable skeletons. However, it is tempting to speculate whether one or more degradation products of VAS3947 and its analogues are responsible for the biological effects reported until now.

## Acknowledgements

This study was funded by the Bayerische Forschungsstiftung – BFS – within the project ‘Springs and Parachutes – New Formulations for Poorly Water Soluble Drugs’. We thank Vasopharm GmbH for financial support as well as for the input of scientific knowledge. We gratefully acknowledge ACC GmbH (Analytical Clinical Concepts GmbH, Leidersbach) for financial and instrumental support.

## References

[1] S. Sans, H. Kesteloot, D. Kromhout, The burden of cardiovascular diseases mortality in Europe. Eur. Heart J. 1997, 18 (8): 1231–1248.

[2] B.K. Rodiño-Janeiro, B. Paradela-Dobarro, M.I. Castineiras-Landeira, S. Raposeiras-Roubin, J.R. Gonzalez-Juanatey, E. Álvarez, Current status of NADPH oxidase research in cardiovascular pharmacology. Vasc. Health Risk Manag. 2013, 9: 401–428.

[3] H. Cai, D.G. Harrison, Endothelial dysfunction in cardiovascular diseases: The role of oxidant stress. Circulation Research. 2000, 87 (10): 840–844.

[4] S. Heumüller, S. Wind, E. Barbosa-Sicard, H.H. Schmidt, R. Busse, K. Schröder, R.P. Brandes, Apocynin is not an inhibitor of vascular NADPH oxidases but an antioxidant. Hypertension. 2008, 51 (2): 211–217.

[5] B. Lassegue, R.E. Clempus, Vascular NAD(P)H oxidases: specific features, expression, and regulation. Am. J. Physiol. Regul. Inte. Comp. Physiol. 2003, 285(2): R277–R297.

[6] H. ten Freyhaus, M. Huntgeburth, K. Wingler, J. Schnitker, A.T. Baumer, M. Vantler, M.M. Bekhite, M. Wartenberg, H. Sauer, S. Rosenkranz, Novel Nox inhibitor VAS2870 attenuates PDGF-dependent smooth muscle cell chemotaxis, but not proliferation. Cardiovasc. Res. 2006, 71 (2): 331–341.

[7] F. Tegtmeier, U. Walter, R. Schinzel, K. Wingler, P. Scheurer, H. Schmidt, Compounds containing a N-heteroaryl moiety linked to fused ring moieties for the inhibition of NAD(P)H oxidases and platelet activation, patent EP1598354, 2005.

[8] S. Wind, K. Beuerlein, T. Eucker, H. Müller, P. Scheurer, M. Armitage, H. Ho, H.H. Schmidt, K. Wingler, Comparative pharmacology of chemically distinct NADPH oxidase inhibitors. Br. J. Pharmacol. 2010, 161 (4): 885–898.

[9] C. Stielow, R.A. Catar, G. Muller, K. Wingler, P. Scheurer, H.H. Schmidt, H. Morawietz, Novel Nox inhibitor of oxLDL-induced reactive oxygen species

formation in human endothelial cells. Biochem. Biophys. Res Comun. 2006, 344 (1): 200–205.

[10] S. Lange, J. Heger, G. Euler, M. Wartenberg, H.M. Piper, H. Sauer, Platelet-derived growth factor BB stimulates vasculogenesis of embryonic stem cell-derived endothelial cells by calcium-mediated generation of reactive oxygen species. Cardiovasc. Res. 2009, 81 (1): 159–168.

[11] P. Niethammer, C. Grabher, A.T. Look, T.J. Mitchison, A tissue-scale gradient of hydrogen peroxide mediates rapid wound detection in zebrafish. Nature. 2009, 459 (7249): 996–999.

[12] N. Hecht, N. Terveer, C. Schollmayer, U. Holzgrabe, L. Meinel, Opening NADPH oxidase inhibitors for *in vivo* translation. Eur. J. Pharm. Biopharm. 2017, 115: 206–217.

[13] S. Singh, M. Bakshi, Guidance on Conduct of Stress Tests to Determine Inherent Stability of Drugs. Pharm. Tech. On-Line. 2000.

[14] International Council on Harmonisation, Stability Testing: Photostability Testing Of New Drug Substances And Products Q1B, 1996. http://www.ich.org/products/guidelines/quality/quality-single/article/stability-testing-photostability-testing-of-new-drug-substances-and-products.htmL. (access date: 23.06.2016).

[15] Montefiori Laboratory Duke University. Protocol for Heat-Inactivation of Serum and Plasma Samples. 2011.

[16] I. Hubatsch, E.G. Ragnarsson, P. Artursson, Determination of drug permeability and prediction of drug absorption in Caco-2 monolayers. Nat. Protoc. 2007, 2 (9): 2111–2119.

[17] ATCC (American Type Culture Collection). Hep G2 [Hep-G2] (ATTC® HB8065™).

[18] ATCC (American Type Culture Collection). 293 [HEK-293] (ATTC® CRL1573™).

# CONCLUSION AND OUTLOOK

Many drug candidates and marketed drugs suffer from high lipophilicity, probably resulting in poor aqueous solubility. Other drugs have a high molecular weight, likely to lead to poor membrane permeability. These unfavourable drug features ultimately prevent the exploitation of the full potential of drugs, driving the need for novel bioavailability enhancing technologies [1-4]. The strategies described and explored within this thesis address the drawbacks of poorly water soluble and poorly permeable drugs by chemical modification or by technological approaches, thereby allowing the optimization of the compound's physico-chemical, biopharmaceutical and toxicological properties.

As outlined in **chapter I**, "hydrophobic ion pairing" of BCS class III compounds with voluminous, lipophilic counterions is one of several promising strategies to overcome the challenging drug delivery of poorly permeable drugs [5-7]. Despite numerous studies demonstrating the beneficial effects of hydrophobic ion pairs, the mechanisms behind are incompletely understood and fundamental *in vitro* and *in vivo* studies need to provide further insight into the absorption and distribution processes [8]. Moreover, an increased understanding of the influence of counterion type, drug-to-counterion-ratio and steric configuration of the complex is pivotal for successful drug formulation and therefore requires systematic investigations. The ultimate goal might be a matrix guiding formulation scientists in dependency on the desired complex properties, i.e. in particular overall solubility and lipophilicity. The ion pairing of two active substances, as already demonstrated for ionic liquids, is a further strategy boost the activity of the complex [9]. Besides activity, counterion toxicity plays an important role on counterion selection as it directly influences the safety profile of the complex [10]. Ongoing screenings for safe and effective counterions ("GRAS") are required in order to develop a library of suitable lipophilic ion pairing agents facilitating successful drug formulation and delivery. However, toxicological evaluations are labour- and cost-intensive and complicated by regulatory

hurdles and may therefore prevent pharmaceutical industry from further research. In conclusion, drug transport of poorly permeable substances across membranes remains challenging, nevertheless, using the ion pairing technology, significant advances have been made towards the delivery of poorly permeable drugs on non-invasive routes.

An increasing number of novel pharmaceutical entities identified nowadays is characterized by poor aqueous solubility [11]. Accordingly, this disadvantageous property was assessed for the quinolone amide GHQ168, a very potent antitrypanosomal drug candidate developed for the treatment of HAT [12, 13] and introduced in **chapter II** [14]. Currently, only five drugs are commercially available for the treatment of this parasitic disease widespread in sub-saharian Africa, and due to emerging resistances and severe side effects, novel and safe drugs are in great demand [15-17]. Therefore, the aim of this research project was the solubility improvement of GHQ168 by means of chemical modification and by spray drying [18] in order to facilitate preclinical studies in mice for the first time. After intraperitoneal administration it turned out that GHQ168 significantly increased the MSD of infected mice as compared to the untreated control group (17 versus 9 days in the stringent model and 32 versus 7 days in the early-treatment model), demonstrating highly promising *in* vivo efficacy and even curing of mice in the latter model. Owing to this early preclinical stage, the number of animals included in the first *in vivo* studies was small (4 mice in the control groups, 4 mice treated with GHQ168 in the stringent model and 6 mice treated with GHQ168 in the early-treatment model, respectively). Therefore, statistics need to be interpreted with care and continuing studies with higher number of animals are essential to further confirm the positive results observed for GHQ168. During the *in vivo* studies, mice showed no signs of external toxicity, however, the toxicological features of the substance are unknown and toxicological studies are necessary to decide on the further development of GHQ168. Additionally, the collection of PK data after intravenous administration is crucial in order to provide further insight into ADME parameters and to support dose finding. Future works

can include additional chemical modifications (e.g. structural variations) or different salt forms to further optimize physico-chemical, biopharmaceutical and toxicological properties. Furthermore, the development of controlled release formulations exhibits great potential regarding the optimization of the drug's *in vivo* behaviour and may open up alternative administration routes. Besides, some efforts have yet been made to elucidate the mode of action of GHQ compounds, however, future studies will have to fully clarify on pharmacodynamics. The outcome might fuel the synthesis of even more active compounds or allow for the translation to related indications, such as other diseases caused by protozoa. Currently, there is evidence that the GHQ compounds affect the morphology of mitochondria [13]. Summarized, there is still potential for optimization of the quinolone amide skeleton and further data sets (*vide supra*) are required for GHQ168, however, the curing of *T. b. rhodesiense* infected mice after i.p. administration of GHQ168 is a valuable starting point towards novel treatment options against HAT. Just recently, *in vitro* antitrypanosomal activity of quinolone type compounds was reported against *Trypanosoma cruzi*, highlighting the ongoing interest in this compound class [19].

VAS3947, a BCS class II compound, was developed as NADPH oxidase (NOX) inhibitor for the treatment of elevated ROS levels that detrimentally promote the development of cardiovascular diseases [20]. Despite promising *in vitro* results observed for the VAS substance library [21-24], *in vivo* studies were still lacking due to insufficient aqueous solubility [22]. This drawback was addressed in **chapter III** with the ultimate aim to firstly open VAS3947 for parenteral and oral application in *in vivo* studies [25]. Apart from spray drying as also applied for GHQ168, the formulation of microemulsions [26] and the complexation with cyclodextrins [27] successfully improved the aqueous solubility of VAS3947. In view of preclinical studies, a stability profiling and toxicological evaluations were conducted as presented in **chapter IV**. VAS3947 was found to be instable in buffer, in human plasma, in the presence of metabolic enzymes and under light exposition. Furthermore it impaired cell membranes and depicted toxicity in the low micromolar

concentration range as equally observed in efficacy investigations. Due to these destructive findings, VAS3947 was classified as inappropriate candidate for further clinical development. Indeed, the inherent instability of the VAS compounds is related to their chemical structure, most likely to the oxazol and thioether moieties, which are simultaneously responsible for their efficacy. Initially, the detailed elucidation of the degradation pathways and the resulting decomposition products is of crucial importance in order to decide on suitable stabilizing strategies. Firstly, structural modifications of the skeleton should be considered, including for example the introduction of groups that sterically protect the labile elements from degradation. Additionally, structural variations are also required to broaden the therapeutic window of the substance class. Secondly, the spray-dried formulations, microemulsions and cyclodextrines as presented in chapter III will have to be evaluated for their potential to protect the drug from degradation caused by pH or by solvents. In this regard, the formulations should be considered as starting points with potential for optimization, e.g. concerning the excipients or drug/excipient ratio. Alternative approaches like the preparation of cocrystals may provide a further option for the fine-tuning of stability without altering the drug's molecular structure [28]. Lightproof packaging materials address stability limitations related to the light induced degradation. Overall, during the last decades, a plenty of smart strategies has been developed in academics and in pharmaceutical industry, possessing the potential to leverage even compounds with initially undesired solubility, permeability and stability properties. Consequently, the exceptional role of formulation scientists is obvious in supporting patients with safe and effective medicines.

## References

[1] A. Fahr, X. Liu, Drug delivery strategies for poorly water-soluble drugs, Expert Opin Drug Deliv, 4 (2007) 403-416.

[2] N.J. Yang, M.J. Hinner, Getting across the cell membrane: an overview for small molecules, peptides, and proteins, Methods Mol Biol, 1266 (2015) 29-53.

[3] H.D. Williams, N.L. Trevaskis, S.A. Charman, R.M. Shanker, W.N. Charman, C.W. Pouton, C.J.H. Porter, Strategies to Address Low Drug Solubility in Discovery and Development, Pharmacol. Rev., 65 (2013) 315-499.

[4] H. van de Waterbeemd, B. Testa, R. Mannhold, H. Kubinyi, G. Folkers, Drug Bioavailability: Estimation of Solubility, Permeability, Absorption and Bioavailability, 2008.

[5] V.S. Dave, D. Gupta, M. Yu, P. Nguyen, S. Varghese Gupta, Current and evolving approaches for improving the oral permeability of BCS Class III or analogous molecules, Drug Dev Ind Pharm, 43 (2017) 177-189.

[6] G.L. Amidon, H. Lennernas, V.P. Shah, J.R. Crison, A theoretical basis for a biopharmaceutic drug classification: the correlation of in vitro drug product dissolution and in vivo bioavailability, Pharm Res, 12 (1995) 413-420.

[7] J.D. Meyer, M.C. Manning, Hydrophobic ion pairing: altering the solubility properties of biomolecules, Pharm Res, 15 (1998) 188-193.

[8] P.K. Suresh, S.D. Paul, Ion-paired Drug Delivery: An Avenue for Bioavailability Improvement, Sierra Leone J Biomed Res, 3 (2011) 70-76.

[9] M.R. Cole, M. Li, B. El-Zahab, M.E. Janes, D. Hayes, I.M. Warner, Design, synthesis, and biological evaluation of beta-lactam antibiotic-based imidazolium- and pyridinium-type ionic liquids, Chem Biol Drug Des, 78 (2011) 33-41.

[10] B.J. Aungst, Intestinal Permeation Enhancers, J. Pharm. Sci., 89 (2000) 429-442.

[11] R.O. Williams III, A.B. Watts, D.A. Miller, Formulating Poorly Water Soluble Drugs, 2012.

[12] J.R. Franco, P.P. Simarro, A. Diarra, J.G. Jannin, Epidemiology of human African trypanosomiasis, Clin Epidemiol, 6 (2014) 257-275.

[13] G. Hiltensperger, N.G. Jones, S. Niedermeier, A. Stich, M. Kaiser, J. Jung, S. Puhl, A. Damme, H. Braunschweig, L. Meinel, M. Engstler, U. Holzgrabe, Synthesis and structure-activity relationships of new quinolone-type molecules against Trypanosoma brucei, J Med Chem, 55 (2012) 2538-2548.

[14] G. Hiltensperger, N. Hecht, M. Kaiser, J.C. Rybak, A. Hoerst, N. Dannenbauer, K. Müller-Buschbaum, H. Bruhn, H. Esch, L. Lehmann, L. Meinel, U. Holzgrabe, Quinolone Amides as Antitrypanosomal Lead Compounds with In Vivo Activity, Antimicrob Agents Chemother, 60 (2016) 4442-4452.

[15] V. Lejon, M. Bentivoglio, J.R. Franco, Human African trypanosomiasis, Handb Clin Neurol, 114 (2013) 169-181.

[16] E.M. Fevre, B.V. Wissmann, S.C. Welburn, P. Lutumba, The burden of human African trypanosomiasis, PLoS Negl Trop Dis, 2 (2008) e333.

[17] P.P. Simarro, J. Franco, A. Diarra, J.A. Postigo, J. Jannin, Update on field use of the available drugs for the chemotherapy of human African trypanosomiasis, Parasitology, 139 (2012) 842-846.

[18] W.L. Chiou, S. Riegelman, Pharmaceutical Applications of Solid Dispersion Systems, J. Pharm. Sci., 60 (1971) 1281-1302.

[19] D. Insuasty, S.M. Robledo, I.D. Velez, P. Cuervo, B. Insuasty, J. Quiroga, M. Nogueras, J. Cobo, R. Abonia, A Schmidt rearrangement-mediated synthesis of novel tetrahydro-benzo[1,4]diazepin-5-ones as potential anticancer and antiprotozoal agents, Eur J Med Chem, 141 (2017) 567-583.

[20] F. Tegtmeier, U. Walter, R. Schinzel, K. Wingler, P. Scheurer, H. Schmidt, Compounds containing a N-heteroaryl moiety linked to fused ring moieties for the inhibition of NAD(P)H oxidases and platelet activation, patent EP1598354, 2005.

[21] H. ten Freyhaus, M. Huntgeburth, K. Wingler, J. Schnitker, A.T. Baumer, M. Vantler, M.M. Bekhite, M. Wartenberg, H. Sauer, S. Rosenkranz, Novel Nox inhibitor VAS2870 attenuates PDGF-dependent smooth muscle cell chemotaxis, but not proliferation, Cardiovasc Res, 71 (2006) 331-341.

[22] S. Wind, K. Beuerlein, T. Eucker, H. Müller, P. Scheurer, M.E. Armitage, H. Ho, H.H. Schmidt, K. Wingler, Comparative pharmacology of chemically distinct NADPH oxidase inhibitors, Br J Pharmacol, 161 (2010) 885-898.

[23] C. Stielow, R.A. Catar, G. Muller, K. Wingler, P. Scheurer, H.H. Schmidt, H. Morawietz, Novel Nox inhibitor of oxLDL-induced reactive oxygen species formation in human endothelial cells, Biochem Biophys Res Commun, 344 (2006) 200-205.

[24] S. Altenhofer, P.W. Kleikers, K.A. Radermacher, P. Scheurer, J.J. Rob Hermans, P. Schiffers, H. Ho, K. Wingler, H.H. Schmidt, The NOX toolbox: validating the role of NADPH oxidases in physiology and disease, Cell Mol Life Sci, 69 (2012) 2327-2343.

[25] N. Hecht, N. Terveer, C. Schollmayer, U. Holzgrabe, L. Meinel, Opening NADPH oxidase inhibitors for in vivo translation, Eur J Pharm Biopharm, 115 (2017) 206-217.

[26] I. Danielsson, B. Lindman, The definition of microemulsion, Colloids and Surfaces, 3 (1981) 391-392.

[27] T. Loftsson, P. Jarho, M. Masson, T. Järvinen, Cyclodextrins in drug delivery, Expert opinion on drug delivery, 2 (2005) 335-351.

[28] G. Kuminek, F. Cao, A. Bahia de Oliveira da Rocha, S. Goncalves Cardoso, N. Rodriguez-Hornedo, Cocrystals to facilitate delivery of poorly soluble compounds beyond-rule-of-5, Adv Drug Deliv Rev, 101 (2016) 143-166.

# LIST OF ABBREVIATIONS

| | |
|---|---|
| ACN | Acetonitrile |
| ANOVA | Analysis of variance |
| API | Active pharmaceutical ingredient |
| ATCC | American type culture collection |
| AUC | Area under the curve |
| BCS | Biopharmaceutics classification system |
| b.i.d. | Twice a day (“bis in die” (lat.)) |
| BW | Body weight |
| $CC_{50}$ | 50% cytotoxic concentration |
| CD | Cyclodextrin |
| $CDCl_3$ | Deuterated chloroform |
| CHN | Carbon, Hydrogen, Nitrogen |
| CI | Confidence interval |
| CICS | Complexation induced chemical shifts |
| CL | Clearance |
| CV | Coefficient of variation |
| DCM | Dichloromethane |
| DIPEA | Diisopropylamine |
| $D_2O$ | Deuterated water |
| DLS | Dynamic light scattering |
| DMEM | Dulbecco's modified eagle medium |
| DMSO | Dimethyl sulfoxide |
| DSC | Differential scanning calorimetry |
| EA | Ethyl acetate |
| EDTA | Ethylenediaminetetraacetic acid |
| ESI | Electrospray ionization |
| FA | Formic acid |
| FaSSIF | Fasted state simulated intestinal fluid |
| FBS | Fetal bovine serum |
| FCS | Fetal calf serum |
| FDA | Food and drug administration |
| GRAS | Generally recognized as safe |
| HAT | Human African trypanosomiasis |
| HBSS | Hanks balanced salt solution |

| | |
|---|---|
| HEPES | 4-(2-hydroxyethyl)-1-piperazineethanesulfonic acid |
| HIP | Hydrophobic ion pairing |
| HPLC | High performance liquid chromatography |
| HPMC | Hydroxypropyl methylcellulose |
| HPRT | Hypoxanthine-guanine phosphoribosyltransferase |
| HSA | Human serum albumin |
| $IC_{50}$ | Half-maximal inhibitory concentration |
| ICH | International Council for Harmonisation of Technical Requirements for Pharmaceuticals for Human Use |
| i.p. | Intraperitoneal |
| i.v. | Intravenous |
| k′ | Capacity factor |
| $k_{el}$ | Elimination rate constant |
| LC | Liquid chromatography |
| LogP | Log partition coefficient |
| MEM | Minimum essential medium |
| MP | Melting point |
| MRD | Mean relapse duration |
| MS | Mass spectrometry |
| MSD | Mean survival duration<br>Mass selective detector |
| m/z | Mass-to-charge ratio |
| NADP | Nicotinamide adenine dinucleotide phosphate (oxidized form) |
| NADPH | Nicotinamide adenine dinucleotide phosphate (reduced form) |
| NEAA | Non-essential amino acids |
| NMM | *N*-methylmorpholine |
| NMR | Nuclear magnetic resonance |
| NMRI | Naval Medical Research Institute |
| NOX | NADPH oxidase |
| NQO | 4-nitroquinoline-*N*-oxide |
| ODS | Octadecylsilane |
| oxLDL | Oxidized Low-Density Lipoprotein |
| $Ph_2O$ | Diphenyl ether |
| $P_{app}$ | Apparent permeability coefficient |
| PBS | Phosphate-buffered saline |
| PD | Pharmacodynamic(s) |

| | |
|---|---|
| PDGF | Platelet derived growth factor |
| PDMS | Polydimethylsiloxane |
| PE | Plating efficiency |
| $P_{eff}$ | Effective permeability |
| PEG | Polyethylene glycol |
| PET | Polyethylene terephthalate |
| PLGA | Poly(lactic-co-glycolic acid) |
| PK | Pharmacokinetic(s) |
| PM | Physical mixtures |
| ROESY | Rotational nuclear Overhauser effect spectroscopy |
| ROS | Reactive Oxygen Species |
| RP | Reversed phase |
| RSD | Relative standard deviation |
| rt | Room temperature |
| sat | Saturated |
| SD | Standard deviation |
| | Spray dried |
| SDS | Sodium dodecyl sulfate |
| SEDDS | Self-emulsifying drug delivery system |
| SEM | Scanning electron microscopy |
| $t_0$ | Dead time |
| $t_{1/2}$ | Half-life |
| *T. b.* | Trypanosoma brucei |
| $t_R$ | Retention time |
| TER/TEER | Transepithelial electrical resistance |
| TFA | Trifluoroacetic acid |
| TSP | Trimethylsilylpropanoic acid |
| UV | Ultraviolet |
| V | Volume of distribution |
| VIS | Visible |
| WHO | World Health Organization |
| XRPD | X-ray powder diffraction |
| $\delta$ | Chemical shift |
| $\lambda$ | Wavelength |
| $\Omega$ | Electrical resistance |

# PUBLICATIONS AND PRESENTATIONS

## PUBLICATIONS

N. Hecht, N. Terveer, C. Schollmayer, U. Holzgrabe, L. Meinel, Opening NADPH oxidase inhibitors for *in vivo* translation, Eur J Pharm Biopharm, 115 (2017) 206-217.

G. Hiltensperger, N. Hecht, M. Kaiser, J.-C. Rybak, A. Hoerst, N. Dannenbauer, K. Müller-Buschbaum, H. Bruhn, H. Esch, L. Lehmann, L. Meinel, U. Holzgrabe, Quinolone amides as antitrypanosomal lead compounds with *in vivo* activity, Antimicrob Agents Chemother, 60 (2016) 4442-4452.

R. Firdessa, L. Good, M.C. Amstalden, K. Chindera, N.F. Kamaruzzaman, M. Schultheis, B. Röger, N. Hecht, T.A. Oelschlaeger, L. Meinel, T. Lühmann, H. Moll, Pathogen- and Host-Directed Antileishmanial Effects Mediated by Polyhexanide (PHMB), PLoS Negl Trop Dis, 9 (2015) e0004041.

## PRESENTATIONS

*Oral Presentation*

In silico optimization of *in vivo* efficacy study designs for new chemical entities, 8th Joined Ph.D. Students Meeting; New Trends in Infectious Disease Research, 2014, Retzbach, Germany

*Poster Presentation*

N. Hecht, G. Hiltensperger, H. Bruhn, L. Meinel, U. Holzgrabe, Improvement of Low Water Solubility of Potential New Drugs against Sleeping Sickness for the Assessment of their *in vivo* Efficacy, 3rd International Symposium, Novel Agents against Infectious Diseases - An Interdisciplinary Approach, 2013, Würzburg, Germany

# CURRICULUM VITAE

# ACKNOWLEDGEMENTS

I would like to express my sincere thanks to **Prof. Dr. Dr. Lorenz Meinel** for giving me the opportunity to be part of his research group and for his constant guidance and great support throughout my PhD thesis. Due to his excellent input and knowledge, he managed to inspire and motivate me independently of success or failure. Within the years of performing my thesis, I managed to increase my scientific knowledge enormously.

My sincere thanks extends to **Dr. Bernhard Scheidel**, CEO of ACC GmbH, who gave me the chance to perform my PhD thesis in parallel with working in his company. I am very grateful for his support and the trust in me to manage the high workload and to fulfill all requirements. I really appreciate this exceptional chance.

Moreover, I would like to thank **Prof. Dr. Ulrike Holzgrabe** for the fruitful collaboration and her frequent and helpful scientific input. That also applies for two of her former PhD students, with whom I cooperated closely during my dissertation works: **Dr. Georg Hiltensperger**, who supported me in getting started with my first project dealing with antitrypanosomal lead compounds. I really appreciate the time spent with him doing research, developing our project and discussing on results. I also thank **Dr. Nils Terveer**, with whom I successfully worked on NADPH oxidase inhibitors.

I am glad that I got the opportunity to work with all my PhD colleagues in the chair for Drug Formulation and Delivery, namely **Dr. Isabel Schulz, Dr. Gabriel Jones, Dr. Sebastian Puhl, Dr. Vera Werner, Dr. Marika Kutscher, Dr. Anja Balk, Eva Gador, Joel Wurzel, Alexandra Braun, Marcus Gutmann, Dr. Christoph Steiger, Cecilia Amstalden and Marco Saedtler.** I am thankful for their support in my scientific work, for many fruitful discussions and, last but not least, for their company.

Two postdocs, **Dr. Jens-Christoph Rybak** and **Dr. Johannes Wiest**, always took the time to support me and offer advice and therefore contributed to the success of this thesis. I am also thankful for the time spent with **PD Dr. Tessa Lühmann**, **Dr. Sascha Zügner, Dr. Jennifer Ritzer, Christine Schneider and Doris Moret** and for their assistance throughout my PhD time.

I am also thankful to my colleagues at ACC GmbH, especially to **Diane Ackermann**, for her always encouraging words. Many thanks also to **Martin Barkworth**, who supported me in experimental work (LC/MS/MS), always pretending that we would make it (which was true.).

Finally, I want to thank my **close friends** for their guidance and for their sympathy.

I would like to acknowledge with gratitude the constant assistance of my **family** that facilitated my studies and my thesis. I am grateful they supported me wherever possible throughout my life.

Furthermore, I am deeply thankful for the immeasurable patience and constant encouragement of my husband **Christian**.

# DOCUMENTATION OF AUTHORSHIP

This section contains a list of the individual contribution for each author to the publications reprinted in this thesis. Unpublished manuscripts are handled accordingly.

| | |
|---|---|
| **M1** | **N. Schüßler*, J. O. Morales*, L. Meinel**<br>Hydrophobic ion pairing to improve bioavailability of BCS class III compounds.<br>Unpublished manuscript. |

| **Author** | **1** | **2** | **3** |
|---|---|---|---|
| Study design / concept development | X | | X |
| Literature analysis and interpretation | X | X | X |
| Manuscript planning | X | | X |
| Manuscript writing | X | X | |
| Correction of manuscript | X | | X |
| Supervision of Nina Schüßler | | | X |

* The authors contributed equally to the work.

| | |
|---|---|
| **P1** | **G. Hiltensperger*, <u>N. Hecht</u>*, M. Kaiser, J.-C. Rybak, A. Hoerst, N. Dannenbauer, K. Müller-Buschbaum, H. Bruhn, H. Esch, L. Lehmann, L. Meinel, U. Holzgrabe**<br>Quinolone amides as antitrypanosomal lead compounds with *in vivo* activity, Antimicrob Agents Chemother, 60 (2016) 4442-4452 |

| **Author** | **1** | **2** | **3** | **4** | **5** | **6** | **7** | **8** | **9** | **10** | **11** | **12** |
|---|---|---|---|---|---|---|---|---|---|---|---|---|
| Synthesis | X | | | | | | | | | | | |
| Formulation | | X | | | | | | | | | | |
| Solubility | X | X | | | | | | | | | | |
| X-ray diffractometry | | X | | X | | X | X | | | | | |
| SEM | | X | | | | | | | | | | |
| Physico-chemical parameters (logP, $pK_a$) | X | X | | | | | | | | | | |
| DSC | | X | | | | | | | | | | |
| Serum albumin binding | | | | | X | | | | | | | |
| Permeation through Caco-2 cell monolayers | | X | | | | | | X | | | | |
| *In vitro* activity | | | X | | | | | X | | | | |
| Cytotoxicity | | | X | | | | | X | | | | |
| Metabolism and mutagenesis | | | | | | | | | X | X | | |
| Plasma Stability | X | | | | | | | X | | | | |
| PBPK modelling and pharmacokinetics | | X | | | | | | | | | | |
| *In vivo* efficacy studies | | | X | | | | | | | | | |
| Statistics | | X | | | | | | | X | X | | |
| Study design / concept development | X | X | | | | | | | | | X | X |
| Data analysis and interpretation | X | X | X | X | X | X | X | X | X | X | X | X |
| Manuscript planning | | | | | | | | | | | | X |
| Manuscript writing | | | | | | | | | | | | X |
| Responsible for text modules and context** | X | X | X | X | | X | | X | X | X | X | |
| Correction of manuscript | | | | | | | | | | | X | X |
| Supervision of Nina Hecht | | | | | | | | | | | X | X |

* The authors contributed equally to the work.

** The authors wrote the chapters corresponding to their experimental contributions.

| | |
|---|---|
| **P2** | **N. Hecht*, N. Terveer*, C. Schollmayer, U. Holzgrabe, L. Meinel**<br>Opening NADPH oxidase inhibitors for *in vivo* translation, Eur J Pharm Biopharm, 115 (2017) 206-217 |

| **Author** | **1** | **2** | **3** | **4** | **5** |
|---|---|---|---|---|---|
| Differential scanning calorimetry | X | | | | |
| log *P* assessment | | X | | | |
| Solubility assessment of the API | X | | | | |
| Preparation of spray dried formulations | X | | | | |
| X-ray powder diffractometry | X | | | | |
| Spray dried formulation studies | X | | | | |
| Determination of pH, particle size | X | | | | |
| Microemulsion formulation studies | X | | | | |
| Cyclodextrin formulation studies | | X | | | |
| $^{1}$H NMR investigation of CICS | | X | | | |
| ROESY measurements | | X | X | | |
| Cyclodextrin formulation for i.v. application | | X | | | |
| Study design / concept development | X | X | | X | X |
| Data analysis and interpretation | X | X | X | | |
| Manuscript planning | X | X | | X | X |
| Manuscript writing | X | X | | | |
| Correction of manuscript | | | | X | X |
| Supervision of Nina Hecht | | | | X | X |

* The authors contributed equally to the work.

This chapter or parts of its content is also published in the dissertation of Dr. Nils Terveer (title: *Springs and Parachutes* Development and Characterization of Novel Formulations for Poorly Water-Soluble Drugs; 2017, urn:nbn:de:bvb:20-opus-154311).

| | |
|---|---|
| **M2** | **N. Terveer*, N. Hecht*, M. Gutmann, M. Saedtler, L. Meinel, U. Holzgrabe**<br>Stability Studies on the Triazolopyrimidine Type NOX Inhibitors.<br>Unpublished manuscript. |

| **Author** | **1** | **2** | **3** | **4** | **5** | **6** |
|---|---|---|---|---|---|---|
| Stability testing | X | | | | | |
| Production and isolation of degradation products | X | | | | | |
| Microsomal assay | | X | | | | |
| Plasma stability assessment | | X | | | | |
| Caco-2 cell assay | | | X | X | | |
| Cytotoxicity cell assay | | | X | X | | |
| Chromatographic studies | X | X | | | | |
| NMR studies | X | | | | | |
| Study design / concept development | X | X | | | X | X |
| Data analysis and interpretation | X | X | | | | |
| Manuscript planning | X | X | | | X | X |
| Manuscript writing | X | X | | | | |
| Correction of manuscript | | | | | X | X |
| Supervision of Nina Hecht | | | | | X | X |

* The authors contributed equally to the work.

This chapter or parts of its content is also published in the dissertation of Dr. Nils Terveer (title: *Springs and Parachutes* Development and Characterization of Novel Formulations for Poorly Water-Soluble Drugs; 2017, urn:nbn:de:bvb:20-opus-154311).

## Erklärung zu den Eigenanteilen des Doktoranden sowie der weiteren Doktoranden als Koautoren an Publikationen und Zweitpublikationsrechten bei einer kumulativen Dissertation.

Für alle in dieser kumulativen Dissertation verwendeten Manuskripte liegen die notwendigen Genehmigungen der Verlage (‚reprint permission') für die Zweitpublikation vor, außer das betreffende Kapitel ist noch gar nicht publiziert. Dieser Umstand wird einerseits durch die genaue Angabe der Literaturstelle der Erstpublikation auf der ersten Seite des betreffenden Kapitels deutlich gemacht oder die bisherige Nichtveröffentlichung durch den Vermerk „unpublished" oder „nicht veröffentlicht" gekennzeichnet.

Die Mitautoren der in dieser kumulativen Dissertation verwendeten Manuskripte sind sowohl über die Nutzung als auch über die oben angegebenen Eigenanteile informiert und stimmen dem zu.

Die Anteile der Mitautoren an den Publikationen sind in den vorausgehenden Tabellen aufgeführt.

| | |
|---|---|
| _____ | _____ |
| Unterschrift | Unterschrift |
| Prof. Dr. Dr. Lorenz Meinel | Nina Schüßler |